USE OF INVESTOR-ACCEPTED REGIONAL-SCALE HYDRODYNAMIC MODELLING SOFTWARE TO ESTIMATE TIDAL STREAM ENERGY RESOURCES AND EFFECTS OF RESOURCE EXPLOITATION

by

SIMON MARK WALDMAN

Submitted for the degree of Doctor of Philosophy

Heriot-Watt University
School of Energy, Geoscience, Infrastructure & Society
International Centre for Island Technology

November 2017

Abstract

Regional-scale numerical hydrodynamic modelling is increasing in importance for estimating the tidal stream energy resource that is available in any given location, and for predicting the environmental effects of exploiting that resource. However, the state-of-the-art models that are commonly used in academia are not always trusted by investors or regulators, and are hence of limited value to commercial site developers.

In this work two commercially-available modelling suites that are widely used in industry — MIKE and Delft3D — are used to simulate the effects of tidal farms in the Pentland Firth, Scotland. The optimum methodology with each software package is explored, and their predictions compared. It is concluded that they are suitable for the broad-scale predictions for which they are intended, but should not be relied upon alone for fine detail.

A flaw is identified in the approach to tidal turbine representation at very high resolutions, relating to the estimation of upstream velocity, which leads to inaccuracy of up to 15%. A correction is implemented and tested.

A similar approach in a third model code, FVCOM, is used to estimate the power available from the Goto Islands, Japan, and to study the interactions of parallel channels when energy is extracted. It is found that the multiple channels in Goto do not behave in the same way as the multiple channels of the Pentland Firth, and a possible explanation for this is discussed.

Finally, the techniques developed in earlier chapters are combined in the development of a new MIKE 3 model of Lashy Sound, Orkney, and the use of this to estimate the maximum theoretical power yield from this channel.

Acknowledgements

I would like to acknowledge and thank the following people and organisations for their help, guidance and support throughout the years of my studentship:

- First and foremost, of course, my supervisors: Jon Side for planting the idea of a PhD with me, for securing funding, and for offering support while allowing me to develop my own interests. David Woolf for stepping in as primary supervisor at short notice when illness made this necessary, and for his mild-mannered, grounded, experienced advice since then. Susana Bastón for her viewpoint from the "coal face" of modelling, and in particular for helping me to realise that sometimes things don't work, and one just has to carry on. Lastly Rob Harris for his brief contribution, at short notice, to the supervisory team during staff illness. Without these people, nothing contained herein would have been possible.

- The rest of the staff and students at ICIT for friendship, assistance, and generally making the Orkney campus a good place to be. Special mention must go to Mike Bell for his kindness and occasional mentoring, as well as the example set by his work ethic; to Kate Pirie and the rest of the Professional Services team for making everything work; and to Sandy Kerr for his support as Director, and for his ability to keep disruption to a minimum while the Institute went through five heads of school (and three Schools) in four years!

- The various members of the EPSRC-funded TeraWatt and EcoWatt2050 consortia, with which I have been closely involved. They did not laugh at my naïve suggestions in early meetings, they did not look down upon me as the most junior researcher present, and they have been willing to help me whenever I have asked. Thanks in particular to Judith Wolf of the NOC, and to Rory O'Hara Murray and the rest of Marine Scotland Science's oceanography group.

- The MASTS organisation, in particular Mark James and the review panels who have approved the funding that I have benefited from on various occasions. It is their support that made my time in Japan possible. This was a memorable life experience that led to Chapter 5, to a journal publication, and hopefully

to future collaborations.

- The renewable energy community in Orkney including Neil Kermode of EMEC, Gareth Davies of Aquatera, Calum Miller of Scotrenewables, and many, many others, within and without the OREF group. Orkney has achieved remarkable things in this area, and will no doubt continue to do so, and this is entirely due to the people involved.
- Venki Venugopal of the University of Edinburgh, a collaborator throughout my studentship but most recently my part-time employer. Working with him while writing up enabled me to broaden my horizons into a different subject area and in a different university, as well as pay the bills.
- Heriot-Watt University itself, for the James Watt scholarship that allowed me to undertake this work.
- My family in the south of England, primarily for putting up with me being Far Away in Orkney and only seeing me once or twice a year, but supporting me anyway! My friends all over the country for similar reasons.

Acknowledgements specific to Chapter 3

- Reddy Nemalidinne and Venki Venugopal of the University of Edinburgh for the MIKE 3 model used in this chapter.
- Susana Bastón of Heriot-Watt University for the Delft3D model used.
- Rory O'Hara Murray of Marine Scotland Science for the turbine layouts.
- The Crown Estate and the UK Hydrographic Office for the provision of bathymetry and bathymetry-related data.

Acknowledgements specific to Chapter 4

- Guillaume Genet, undergraduate summer intern, for initial modelling work as described in the chapter.

Acknowledgements specific to Chapter 5

Japanese and Chinese names are given here in the Western convention, i.e. family name last.

- The MASTS pooling initiative (the Marine Alliance for Science and Technology for Scotland) for travel funding through its PECRE scheme. MASTS is funded by the Scottish Funding Council (grant reference HR09011) and contributing institutions.
- Kyushu University, and in particular Prof. Changhong Hu and Dr. Soichi Yamaguchi, for hosting me and providing office space and computing time.
- Patxi Novo Garcia and Alicia Murga, former and current PGR students at Kyushu University, for technical assistance, friendship, and help in navigating life in Japan.
- Prof. Yusaku Kyozuka of Kyushu University, for his advice and kindness.
- The Ministry of Environment of Japan, for permission to use observational data that was obtained through the "Promotion of Realization of Tidal Current Power Generation" project in 2014 and 2015.
- Dr. Huihui Sun, formerly of Kyushu University, who developed the base FVCOM model that was used.

Acknowledgements specific to Chapter 6

- Scotrenewables Ltd., for bathymetry and coastline data for Lashy Sound and for the ADCP records used for validation.
- The Crown Estate and the UK Hydrographic Office for the provision of bathymetry and bathymetry-related data.

Writing these acknowledgements has been an interesting, and surprisingly emotional, experience; a retrospective on 4+ years. A lot of people impact on one's life in such a timeframe, and I have undoubtedly missed off many who deserve my thanks. For this I apologise.

ACADEMIC REGISTRY
Research Thesis Submission

Name*:*	Simon Mark Waldman		
School:	EGIS		
Version: *(i.e. First, Resubmission, Final)*	Final	Degree Sought:	Doctor of Philosophy

Declaration

In accordance with the appropriate regulations I hereby submit my thesis and I declare that:

1) the thesis embodies the results of my own work and has been composed by myself
2) where appropriate, I have made acknowledgement of the work of others and have made reference to work carried out in collaboration with other persons
3) the thesis is the correct version of the thesis for submission and is the same version as any electronic versions submitted*.
4) my thesis for the award referred to, deposited in the Heriot-Watt University Library, should be made available for loan or photocopying and be available via the Institutional Repository, subject to such conditions as the Librarian may require
5) I understand that as a student of the University I am required to abide by the Regulations of the University and to conform to its discipline.
6) I confirm that the thesis has been verified against plagiarism via an approved plagiarism detection application e.g. Turnitin.

* *Please note that it is the responsibility of the candidate to ensure that the correct version of the thesis is submitted.*

Signature of Candidate*:*		Date:	

Submission

Submitted By *(name in capitals):*	SIMON MARK WALDMAN
Signature of Individual Submitting:	
Date Submitted:	

For Completion in the Student Service Centre (SSC)

Received in the SSC by *(name in capitals):*			
Method of Submission *(Handed in to SSC; posted through internal/external mail):*			
*E-thesis Submitted (**mandatory for final theses)***			
Signature:		Date:	

Please note this form should be bound into the submitted thesis.

Contents

Glossary of abbreviations

ADCP Acoustic Doppler Current Profiler

ADT Actuator Disc Theory

CFD Computational Fluid Dynamics

CSA Cross-Sectional Area

DHI Danish Hydraulics Institute. Developer of the MIKE software.

DNS Direct Numerical Simulation

EMEC European Marine Energy Centre

EWTEC European Wave & Tidal Energy Conference series.

FVCOM Finite Volume Community Ocean Model

GUI Graphical User Interface

IEC International Electrotechnical Commission

LES Large Eddy Simulation

MASTS Marine Alliance for Science & Technology in Scotland

MATLAB No longer an acronym, simply the name of software by Mathworks, conventionally written in capitals.

MBES Multi-Beam Echo Sounder

MIKE Software by DHI. It is not known whether this is an acronym, or simply a trademark that is written in capitals.

MSL Mean Sea Level

MTMC MIKE Turbine Mesh Correction

NOAA National Oceanic & Atmospheric Administration (US government body)

nRMSE Normalised Root Mean Square Error

PFOW Pentland Firth & Orkney Waters

RANS Reynolds-Averaged Navier-Stokes

RMSE Root Mean Square Error

SI Scatter Index

SIF Significant Impact Factor

TEC Tidal Energy Converter

TKE Turbulent Kinetic Energy

TOPEX/Poseidon Radar altimetry sattelite mission.

UTM Universal Transverse Mercator

Chapter 1

Introduction

This project studied, and improved upon, best practice for incorporating tidal stream energy extraction in regional-scale hydrodynamic models. It then used these methods to investigate the tidal energy resources available in three promising areas, and the effects on the flow of exploiting those resources.

This introductory chapter will briefly cover the background to and motivation for the work, and its context in relation to the TeraWatt and EcoWatt2050 projects. Following this is an explanation of its goals and an outline of the thesis, with an emphasis on highlighting the novel contributions that have been made.

1.1 Background

It is widely accepted that to avoid a potentially catastrophic rise in global temperatures, and other detrimental effects such as ocean acidification, humanity must reduce its emissions of greenhouse gases (GHG) (IPCC, 2014). Combustion of fuel for energy accounts for 68% of global anthropogenic GHG emissions, of which 42% is for the generation of electricity (IEA, 2016). There is, therefore, a need to develop forms of electricity generation that involve low or no emissions of greenhouse gas. A reduction in the use on fossil fuels is also desirable for energy security, since being dependant on imported hydrocarbons makes nations politically and economically vulnerable.

One potential source of low-GHG electricity is the tides. Earth's tides are best considered as a resonant wave system that is forced by the tractive forces of the Sun and Moon, together with the Coriolis force (Boon, 2004), with an input power of approximately 3.5 TW (Munk and Wunsch, 1998). Shallow water waves are created in the ocean basins, and these drive tidal dynamics on continental shelves and in connected smaller bodies of water.

Tidal electricity generation has generally been considered via two different modes, although at high levels of exploitation the dividing line between them can be unclear. "Tidal range" power consists of creating a difference in elevation between water on either side of a wall, and then allowing the water to return to equilibrium through a set of turbines, much as in a low-head hydroelectric scheme. It is usually proposed to create this height difference by means of a barrage across an estuary mouth (as per the constructed scheme at La Rance, France) or by enclosing a "lagoon" area on all sides (as per the proposed scheme at Swansea, Wales). A third approach is to build a long T- or L-shaped wall, joined to the coast at one end, and exploit the phase difference in the tidal wave either side of the wall.

"Tidal stream" power involves placing Tidal Energy Converters (TECs) in areas of fast flow and converting kinetic energy to electricity. All of the "first-generation" designs of TEC are rotating horizontal-axis turbines analogous to wind turbines, although other approaches have been suggested. It is this tidal stream approach, with horizontal-axis turbines, that will be considered in this work, but the majority of the methods and conclusions developed could be adapted easily to other device concepts.

Tidal steam energy has some significant advantages over other forms of renewable energy such as solar and wind: while inherently variable, it is periodic and can be accurately predicted far in advance, making it relatively easy to plan for its inclusion in a wider energy mix. It occupies little land, and is thus not in competition with crops, although in some locations there may be spatial conflict with fisheries. Depending on the design, it may be fully submerged and thus not represent any visual intrusion on landscapes. However, this does not mean that it is free of environmental impacts. Removing energy from a system must change it, and if regulators are to grant or deny consent for tidal energy developments in a rational way, conforming to applicable legislation, they and developers will require means of estimating those changes (Gallego *et al.*, 2016).

1.2 Context

My PhD project was conceived in support of the TeraWatt and EcoWatt2050 projects (EPSRC, 2012, 2014), and throughout my studentship I have been closely associated with them. Both of these were EPSRC-funded Grand Challenge endeavours with participants from a number of universities across Scotland and Wales, under the auspices of the Marine Alliance for Science & Technology for Scotland (MASTS).

TeraWatt was born from a realisation that numerical modelling will increasingly be used to inform regulators as to the environmental impacts of wave and tidal

models, and that it will be necessary to establish clear and consistent best practice methods to ensure that different submissions of modelled evidence are comparable. A significant output of the project was a book of position papers (MASTS, 2015) reviewing the state of the art, and I was a major contributor to one of these (Baston *et al.*, 2015).

EcoWatt2050 was a follow-on project, aiming to move beyond the then-planned developments and to use the methods developed in TeraWatt to predict the effects of very large-scale energy extraction as might, at the time, have been anticipated in the year 2050. Within the period of my studentship I was employed by the EcoWatt2050 project on two occasions: The first was for thirteen months in 2014/15 with Heriot-Watt University to cover PDRA maternity leave, working on tidal energy extraction. The second was for eight months in 2017 with the University of Edinburgh to produce deliverables in spectral wave modelling. During the first of these periods my doctoral studentship was suspended, and during the second I switched my studies to part time, whilst working at the University of Edinburgh for 4 days / week.

1.3 Motivation

1.3.1 Why use numerical models?

Regional-scale numerical modelling of flow is important, in the context of tidal energy, for two purposes: to understand the energy resource available in an area, and to estimate the effects of exploiting that resource. A very brief outline of these matters will be given here to establish the need for modelling; they will be returned to in greater detail in Chapter 2.

The methodology of early tidal resource assessments was based on that used for wind farms: a calculation was made of the power that could be produced by a single TEC placed in the undisturbed channel, based on the speed of the flow, and this was multiplied by the number of TECs planned. This is valid for wind farms, but it is less applicable to tidal arrays because a large tidal array can affect the flow in the channel as a whole, making the speed of the undisturbed channel a poor indicator of the power that can be extracted. In order to arrive at a credible estimate of the power available from a channel, it is therefore necessary to understand how the proposed TEC array will affect the flow in that channel — something which is also required if we wish to predict the environmental impacts of abstracting that power.

Direct analytical techniques such as those developed by Garrett and Cummins (2005, 2007) can be used to estimate the power available in simple channels with idealised

energy extraction, but for realistic TECs in real-world sea areas, the problem is too complex for analytical solution and a numerical modelling approach is required.

1.3.2 Why use commercial software?

At the outset of TeraWatt, strong guidance was received from industrial stakeholders that only unaltered, reputed and well-tested commercial software could be used for modelling work if the results were to be accepted by investors and, to a lesser extent, regulators. We were advised of a perception amongst investors that open source code cannot be trusted unless backed with the reputation of a trusted commercial organisation (personal communications with site developers under Chatham House rule, 2013–14).

The current IEC Technical Report on marine energy resource assessment notes that one of the factors in model selection should be (IEC Technical Committee PEL/114, 2015),

> *"acceptance of the code in the commercial domain; i.e. that the results will be acceptable for project financing decisions."*

Many of the academic modelling codes commonly used in research were deemed unsuitable on this basis, and based on guidance from industry two three-dimensional flow modelling systems were selected: MIKE 3 by DHI*, and Delft3D-Flow by Deltares†. Both of these packages are already in extensive use commercially.

FVCOM, used in Chapter 5, is not commercial software. However, it has benefited from considerable trust-building both through its use around the world and from its adoption by Marine Scotland Science for their modelling work. As such, it is very likely to be trusted by the regulator in Scotland (which is another part of the Scottish Government), and this will lend it further credence with investors.

1.4 Goals

The initial goals of this project were,

- To establish whether existing commercial software can be used to predict the regional-scale effects of tidal stream energy extraction, and what the best practice is for using such software for this purpose.
- To improve upon this state-of-the-art where practicable.

*`http://www.mikepoweredbydhi.com/`
†`https://www.deltares.nl/en/software`

- To test and demonstrate this best practice, and the improvement made, in a real-world scenario.

1.5 Outline of thesis

This work has four main elements of new investigative work, reported in chapters 3–6. After this introduction and the literature review, Chapter 3 relates work that was conducted as part of TeraWatt, demonstrating and testing the inclusion of energy extraction in MIKE 3 and Delft3D. Validated models were received from other project members and compared without energy extraction. Tidal turbines were then included, and a similar comparison performed with them present. The method of including tidal turbines in Delft3D is, to the best of my knowledge, new to the academic literature. The work in this chapter has recently been published in Ocean & Coastal Management (Waldman, Bastón *et al.*, 2017). New MATLAB code for efficiently placing large numbers of turbines in both models has been made publicly available. Due to a bug in this code some of the figures in the journal article were incorrect, and an erratum has been submitted, which is included in Appendix C. The figures shown in Chapter 3 are the corrected versions.

While studying MIKE's representation of tidal turbines, I identified a flaw — applicable not just to MIKE, but to most regional-scale models — that becomes significant at very high mesh resolutions and can cause the effects of tidal turbines to be underestimated by 10–15%. In Chapter 4 this error is investigated and a correction derived. The correction is implemented as a MATLAB script that is run externally to the model, and is tested extensively. This script is publicly available. The work in this chapter was presented at an early stage at the EWTEC conference in 2015 (Waldman *et al.*, 2015). Parts of the correction itself, and all of the implementation, are novel (see note in Chapter 4).

An area of personal interest during my studies has been the interactions between tidal arrays in separate, nearby channels. The Goto Islands in Japan are an area of planned tidal energy development that has such channels, and I identified an opportunity to collaborate with researchers at Kyushu University by applying the methods of energy extraction that had been studied in MIKE 3 to an existing model that they had produced in the FVCOM modelling suite. While FVCOM is not commercial software, it is still of interest for UK industry as it has recently been adopted by Marine Scotland Science for their Scottish Shelf Model (Wolf *et al.*, 2016). This work, presented in Chapter 5, provided the first resource assessment of the Goto Islands to take account of the effects of energy extraction, and generated new insight into the effects of the layout of multiple channels on the level of interaction

between them. An article on this work, co-authored with Japanese and Scottish collaborators, has recently been published in the International Journal Of Marine Energy (Waldman, Yamaguchi *et al.*, 2017).

In the final segment of this project (Chapter 6), nearly all of the techniques used in earlier sections were combined in a case study of Lashy Sound, Orkney. A new MIKE 3 model was built using the lessons learned in Chapters 3 & 5, and calibrated and validated with techniques from Section 2.2. An assessment of the maximum extractable power was conducted in a manner similar to that performed in the Goto Islands, and the far-field effects of both this scenario and a more realistic one were investigated. It was planned to test the model's predictions with and without the correction of Chapter 4, but unfortunately this was impractical in the time available. Some of the work in this chapter was presented at the EWTEC conference in 2017 (Waldman, Side *et al.*, 2017), and to the best of my knowledge it is the first academic study to look at Lashy Sound in detail.

Discussion and conclusions relating to each section of work are included in the relevant chapters, but Chapter 7 discusses broader points and conclusions that may be drawn from the project as a whole, as well as outlining some areas of followup work that might be worthwhile.

Appendices A and B detail specific techniques for modelling in MIKE that were established during my early experimentation with the MIKE software, including the development of approaches to preparing bathymetry, and some sensitivity testing to understand the effects of the input parameters. Finally, in Appendix C, selected peer reviewed articles produced during my studentship — including most of those referenced above — are bound into this thesis for the reader's convenience. A complete list of peer-reviewed outputs is also included here.

Chapter 2

Literature & theory

The work in this thesis is primarily concerned with using numerical flow models and their results, and not the development of the models themselves. However, it is important for the practical modeller to understand the principles behind the models that they use, in order to understand what effects the models do and do not include and hence apply appropriate judgement in interpreting their results. Therefore the mathematical underpinnings will be touched, but not dwelt upon, in this chapter.

The chapter has five sections: First is a short explanation of the principles of numerical flow modelling. Next is a review of the calibration and validation of such models — why these processes are necessary and how the skill of a model can be assessed. The third section examines how energy extraction is implemented in regional models, and touches on how these methods have been tested.

As established in the introduction, there are two primary uses of regional-scale modelling in connection with tidal energy: to estimate the energy resource that is available in an area, and to predict the environmental impacts of removing that energy. The final two sections give overviews of prior work and methodologies for both of these applications.

2.1 Numerical hydrodynamic modelling

> *"It is, as I understand it, quite candidly admitted by Mr. Froude that the regime contemplated by his theory is not capable of exact expression. This, however, is no obstacle to the application of any theory in real hydrodynamics; if it were necessary for the engineer to await the pleasure of the pure mathematician in these matters, the subject would have made scarcely perceptible progress since the time of Noah."*
>
> *— F.W. Lanchester, 1915, quoted by Garrett and Cummins (2007)*

In this section I shall first discuss some fundamentals of numerical modelling. Chief among these is the concept that models are *inaccurate* representations of the real world. There is usually a trade-off to be made between accuracy and performance, so to build a model it is necessary to decide what simplifications and assumptions may be used to provide useful results while running in a practical time on the available hardware.

Next is a brief explanation of the Navier-Stokes equations, followed by details of some of the simplifications that are relevant for the work in this thesis. Finally the available options for discretization and will be touched upon, and the approaches used by the three model codes used here (MIKE, Delft3D, and FVCOM) identified.

2.1.1 Fundamental aspects of numerical modelling

Why do we use numerical models? In most cases, we use them to solve problems that cannot be solved analytically — either because they are theoretically intractable or because they are impractical to solve that way.

Our use of a model is normally because we want it to provide a prediction; we want it to use quantities that we do know to predict quantities that we do not know. Dee (1995), citing Hodges and Dewar (1992), defines a prediction as

> *"a statement about a potentially observable quantity or event, supplemented with a claim about the accuracy of the statement as well as with an argument that backs up the claim".*

For a prediction to be worth anything it must be possible to justify it; without such justification, it is simply speculation. However, providing an argument that backs up a claim from a numerical model is not straightforward. The individual making the prediction (or, indeed, a reviewer) cannot simply work through the calculations themselves, because if this were practicable then the model would not have been required in the first place. In some cases it might be feasible to follow the *method*

used, and to justify the prediction on that basis, but (as will be discussed below) this is not always the case.

One solution is to use the model to make predictions that we can test against observations. If there is a good match, it is reasonable to assume that other similar predictions will be good as well. For example, if a tidal model correctly predicts the water levels at a tide gauge for a given month, it may be reasonable to believe that it will predict them similarly well for a different month or a different location (although care must be taken that the situations are sufficiently alike).

Sources of error in numerical hydrodynamic models

A model is a simplified, and hence degraded, expression of reality. It cannot represent real systems correctly in every way, because if it did then the model would be just as complex as reality. There is usually a trade-off to be made between accuracy and performance, so to build a model it is necessary to decide what simplifications and assumptions may be used to provide useful results while running in a practical time on the available hardware.

Statistician George Box famously encapsulated this concept in a section title "All models are wrong, but some are useful" (Box, 1979), going on to comment that,

> *"It would be very remarkable if any system existing in the real world could be exactly represented by any simple model. However, cunningly chosen parsimonious models often do provide remarkably useful approximations.*
>
> *For such a model there is no need to ask the question "Is the model true?"... The only question of interest is "Is the model illuminating and useful?"."*

Inherent in using a model, then, is accepting that it involves errors. Dee (1995) looked at the sources of these errors and proposed four levels of modelling, each of which is less true to reality than the one before.

1. **Natural system:** This level is the reality that the model is intended to represent. By definition, it has perfect fidelity.

2. **Conceptual model:** A description of the physics of the model. At this level the modeller has codified what variables are to be considered, and what assumptions are to be made about their behaviour and interrelationships. This might be expressed as a system of continuous differential equations. By defining what is to be included, the modeller has also determined the effects that are to be disregarded, and as such they have introduced the first differences between the model and reality.

3. **Algorithmic implementation:** The methods for computing the model. This step determines the approaches to discretization of the continuous equations, the numerical methods that are to be used, and so forth. While the conceptual model is a perfect representation of the simplified physics that are being included, the algorithmic implementation is an approximation to these, and as such it is a further source of error.

4. **Software implementation:** This level covers the conversion of the mathematical algorithms of level 3 to actual software code. Wheras steps 2 and 3 have intentionally made approximations as part of the modelling process, in an ideal world this stage should be exact. However, any software has bugs and so, in practice, additional errors may be introduced. Post and Votta (2005) mention that the defect rate in scientific programming is similar to that in other programming disciplines, and imply that hard-won lessons on quality control in general software development are not always applied in scientific project teams.

With modern model codes, which are applied to many different problems, a fifth level could be included in this list:

5. **Scenario specification:** The details of the specific scenario that the model code is being asked to simulate. In a flow model this includes the mesh that is used, the representations of coastlines and bathymetry, the open boundary conditions, the model parameters chosen, and so forth.

These inputs represent another source of errors that will affect the predictions made by the model. Hackett *et al.* (1995) note, on the importance of data quality, that,

> *"great care must be given to the specification of the model set-up, initial conditions, boundary conditions and forcing… At worst, the whole exercise may be rendered useless, if the model's performance was dominated by, e.g., faulty boundary forcing"*

The need for validation

From an idealised perspective, a reviewer should be able to follow through every stage in this process and verify it at each point. In many cases, however, this is not practical or even possible. For example, the MIKE software from DHI is closed-source, and while DHI do share the conceptual formulations used (DHI, 2012a), it is not possible to verify their code. Willmott (1981) saw this difficulty emerging some decades ago, stating that

> *"As models become ever more lengthy and complex, it will become increasingly important to have access to source programs in order to serve the guidelines of science, i.e. verification and reproducibility".*

Even where the code is available for public inspection, Post and Votta (2005) highlight the reality that some modern model codes are too complex for any one person to understand them in their entirety, especially if doing so is not their main job. While this observation was made in the context of significantly more complex models than those that we are dealing with here, a related point remains that an expert in the physics behind a simulation may not have the expertise to verify the mathematical methods or the software approaches used.

In many circumstances, then, step-by-step verification will not provide the confidence that is needed. Indeed, even if every step was subject to expert verification to avoid inadvertent errors, it would still be very difficult to predict the effects of *intentional* error sources, such as simplifications and discretizations, in this manner. An alternative (or additional) approach is to treat the model as a "black box" and to test it against known scenarios to see whether its outputs are as expected. Dee refers to this as "functional validation", while Post and Votta simply call it "validation".

2.1.2 The Navier-Stokes equations

The Navier-Stokes equations, also known as the momentum equations, are a set of partial differential equations that describe the accelerations of a parcel of fluid in the frame of the Earth's surface. Together with the continuity equation, they are the foundation of most numerical flow modelling. They can be derived from the principles of conservation of mass and momentum, together with Newton's second law, but will simply be stated here for brevity. For a clear derivation, see Stewart (2008).

$$\frac{\partial u}{\partial t} + u\frac{\partial u}{\partial x} + v\frac{\partial u}{\partial y} + w\frac{\partial u}{\partial z} = -\frac{1}{\rho}\frac{\partial p}{\partial x} + 2\Omega v \sin\varphi + F_x \tag{2.1a}$$

$$\frac{\partial v}{\partial t} + u\frac{\partial v}{\partial x} + v\frac{\partial v}{\partial y} + w\frac{\partial v}{\partial z} = -\frac{1}{\rho}\frac{\partial p}{\partial y} - 2\Omega u \sin\varphi + F_y \tag{2.1b}$$

$$\frac{\partial w}{\partial t} + u\frac{\partial w}{\partial x} + v\frac{\partial w}{\partial y} + w\frac{\partial w}{\partial z} = -\frac{1}{\rho}\frac{\partial p}{\partial z} + 2\Omega u \cos\varphi + F_z - g \tag{2.1c}$$

$$\frac{\partial u}{\partial x} + \frac{\partial v}{\partial y} + \frac{\partial w}{\partial z} = 0 \tag{2.2}$$

where u, v and w are components of velocity in the x, y and z directions where x, y and z are traditional Cartesian axes with z oriented normal to the geoid and pointing upwards. p is pressure, ρ is water density, Ω is the angular velocity of the

earth's spin, φ is latitude, and g the acceleration due to gravity. The first term on the right hand side represents any pressure gradient in the fluid (such as that caused by a change in surface elevation), the second accounts for Coriolis force, the third the drag from friction, and the fourth (in the equation for the z direction only) the acceleration due to gravity.

The form of the equations shown here assumes an incompressible fluid (see below on Bousinnesq assumption) with fixed temperature and salinity, and only considers advection (not diffusion). The equations are shown here for Cartesian axes, but because the surface of the Earth is not a plane this is in itself an approximation, analogous to a map projection. The same relations may be stated in spherical coordinates, but they then become more complex as terms relating to curvature and rotation enter each equation. It is therefore common to use the Cartesian form at small scales, where the planet's curvature is small compared to the scale of the model. This also simplifies postprocessing, as distances between points relate directly to differences in their grid coordinates. For most purposes this approach is acceptable for domains covering less than 1000 km (Cushman-Roisin and Beckers, 2011).

2.1.3 A range of simplification

Many different types of modelling are based on the Navier-Stokes equations, solving diverse problems in a huge number of fields. In nearly all cases, it is necessary for the modellers to make simplifications and assumptions to make the computational problems tractable while still retaining the features that are important for the intended application. The next few pages will explain a few types of model that are used for geophysical flows, starting with the most directly linked to the Navier-Stokes equations and proceeding through additional simplifications until reaching the shallow water solvers that are used here.

Direct numerical simulation

Solving the Navier-Stokes equations at the Kolmogorov scale — the scale at which turbulence dissipates and at which molecular viscosity applies — should yield a good description of fluid flow (Bakker, 2006b). This approach is indeed used for some specialist studies of small-scale turbulence, when it is referred to as Direct Numerical Simulation (DNS). However, the difference in scale between these studies and most problems in engineering and oceanography renders DNS infeasible for most uses; there is not sufficient computing power to work at the smallest scales across a domain of metres or kilometres (Moin and Mahesh, 1998). For the majority of applications, then, assumptions are applied to make the problem more tractable. These can be

thought of as a "spectrum" of methods, which trade accuracy for speed.

RANS and LES CFD

Reynolds-Averaged Navier-Stokes (RANS) models consider the velocity of a parcel of water as the sum of its average velocity $\langle \mathbf{u} \rangle$ and a random fluctuation, $\mathbf{u'}$, that represents turbulence:

$$\mathbf{u}_{\text{total}} = \langle \mathbf{u} \rangle + \mathbf{u'} \tag{2.3}$$

It is assumed that, since $\mathbf{u'}$ acts randomly in all directions, over a short time it will average to zero.

Ideally this would remove turbulence from the equations. However, the Navier-Stokes equations are non-linear, and the square of a mean is not the same as the mean of a square; therefore, additional terms are generated. For example, if we wanted to consider the average of a product of two velocity components, this expands as follows when (2.3) is applied (adapted from Cushman-Roisin and Beckers (2011):

$$\langle uv \rangle = \langle (\langle u \rangle + u') \times (\langle v \rangle + v') \rangle \tag{2.4}$$

$$= \langle \langle u \rangle \langle v \rangle \rangle + \langle \langle u \rangle v' \rangle + \langle \langle v \rangle u' \rangle + \langle u'v' \rangle \tag{2.5}$$

$\langle u' \rangle = \langle v' \rangle = 0$ by definition, so the middle two terms disappear, but we cannot say the same for $\langle u'v' \rangle$ so we are left with

$$\langle uv \rangle = \langle u \rangle \langle v \rangle + \langle u'v' \rangle \tag{2.6}$$

which gives us the desired product in terms of averaged components but also an additional term that depends upon the turbulent fluctuations. These extra terms are called "Reynolds stresses".

The point of separating out the short random fluctuations from the larger-scale flow is so that we do not have to resolve the turbulence in a numerical model. We must still consider the Reynolds stresses, though, and so an assumption is made that energy lost to these stresses can be treated in the same way as energy lost to the viscosity of the fluid. This is one of the concepts sometimes known as the Boussinesq assumptions, and the resulting term is known as "eddy viscosity". Turbulence is thus modelled separately as a subgrid process, appearing in the governing equations only as part of the overall drag.

Some formulation is required to estimate the magnitude of this eddy viscosity. Such schemes range from the very simple that use fixed values, through approaches such as Smagorinsky's (which relates the eddy viscosity to the change in velocity, *i.e.* shear,

between grid cells (Smagorinsky, 1963)), to more complex turbulence models such as the $k - \epsilon$ and Mellor-Yamada approaches (Launder and Spalding, 1974; Mellor and Yamada, 1982), which solve additional transport equation(s) for turbulent kinetic energy and, in the case of $k - \epsilon$, its dissipation.

Large Eddy Simulation (LES) is a compromise approach where turbulence down to a specific scale — usually chosen to include the most meaningful scales for the task at hand — is explicitly modelled, and turbulence below this scale is treated as eddy viscosity (Lesieur and Metais, 1996). This method usually yields more accurate results than RANS, but at a higher computational cost.

An illustration of the scales at which these methods operate, with respect to the scales at which large-scale eddies form and at which small-scale turbulence dissipates, may be seen in Figure 2.1. The typical resolution of RANS and LES models is in the orders of millimetres to metres, although they can be successfully employed on both larger and smaller meshes.

Regional scale shallow water models

The term "shallow water models" encompasses a variety of different formulations, including models of the type that are used throughout this project. A common theme is that they take the RANS approach and make a number of additional assumptions and simplifications to reduce the complexity of the problem and thus the computational expense. The higher computational speed of these models allows them to be run for large domains (from tens to thousands of kilometres) over significant time periods (days to months or years) on available hardware in practical timescales. The typical resolution of shallow water models is in the orders of tens of metres to tens of kilometres.

In shallow water models the scale of vertical motion is assumed to be much smaller than that of horizontal motion, and vertical accelerations are assumed to be small compared to the acceleration due to gravity. Momentum equations are only solved in the horizontal plane. In two-dimensional models the Navier-Stokes equations are depth-integrated for the entire water column, and are sometimes known as the Saint-Vernant equations. In three-dimensional models the horizontal equations are solved in multiple vertical layers, taking account of shear stress between them, and vertical velocity is retrieved from the continuity equation (Deltares, 2014; DHI, 2012a).

Models of this type commonly follow a further Boussinesq approximation: an assumption that density is constant, except in terms that are multipled by g. This implies that water is nearly incompressible, and that its density is constant except in terms

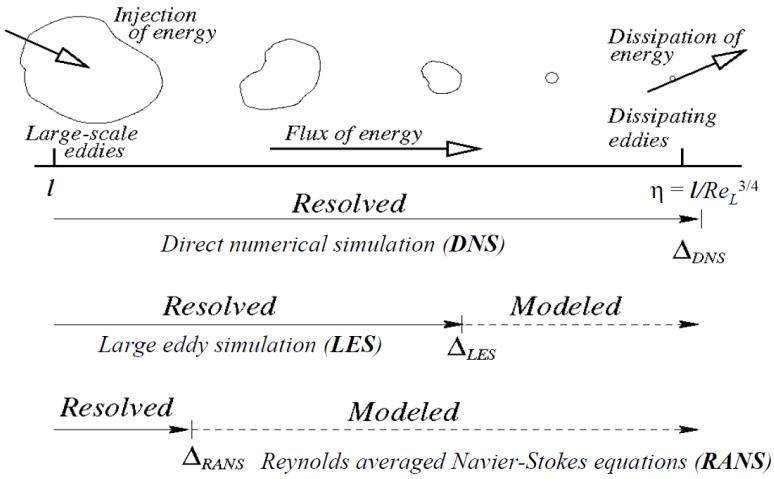

Figure 2.1: *Illustration depicting the scales of turbulence at which DNS, LES and RANS operate. Source: Bakker (2006a).*

relating to buoyancy — an assumption which is valid provided that velocities are small compared to the speed of sound, and greatly simplifies the continuity equation (Stewart, 2008). Relatedly, an assumption of hydrostatic pressure is usually made — *i.e.* that pressure changes only with depth (Deltares, 2014).

It is common for 3D shallow water models to use "sigma layers", whereby vertical layers relate not to an absolute z coordinate but to a relative vertical coordinate σ whose value varies between 0 at the seabed and 1 at the surface thus (*e.g.* DHI, 2012a):

$$\sigma = \frac{z - z_b}{h} \tag{2.7}$$

where z_b is the elevation of the seabed and h is the depth of water. The "vertical velocity" in the model then describes movement of water between layers, and actual vertical velocity is computed as a post-processing step. The number of layers remains constant regardless of the water depth, with the thickness of the layers scaling as necessary. This allows the representation of a smooth seabed without allowing steps to appear, as is common with the alternative absolute-coordinate approach (Figure 2.2).

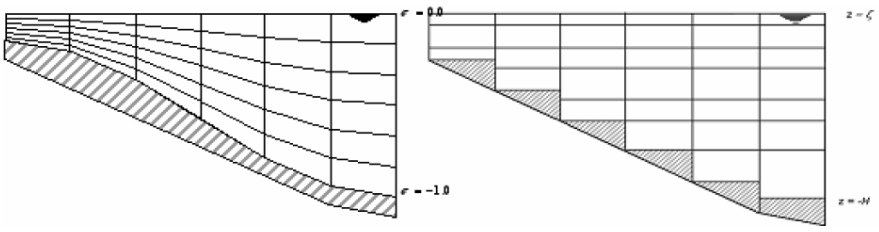

Figure 2.2: *Illustration of the difference between relative (σ) and absolute (z) vertical coordinate systems. Source: Deltares (2014).*

2.1.4 Discretization & numerical methods

To this point we have considered the continuous physics that are to be represented. Unfortunately, a general analytic solution of the Navier-Stokes equations has yet to be found.* It is therefore not possible to solve the continuous equations exactly; instead, it is necessary to discretize them in space and time, and use iterative numerical solvers. A wide variety of numerical methods has been used to represent geophysical flow. The the most common will be described here in conceptual terms. For further detail including more mathematical explanations, the reader is referred to Cushman-Roisin and Beckers (2011), except for finite element methods, for which Durran (2010) is suggested.

Finite difference methods

If time is discretized as $t_n = t_0 + n\Delta t$ where n is the timestep, and $u_n = u(t_n)$, then from the definition of differentiation,

$$\frac{du}{dt} = \lim_{\Delta t \to 0} \frac{u(t + \Delta t) - u(t)}{\Delta t} \tag{2.8}$$

Therefore we can write an approximation to the value of $\frac{du}{dt}$ at timestep n as

$$\left.\frac{du}{dt}\right|_{t_n} \approx \frac{u_{n+1} - u_n}{\Delta t} \tag{2.9}$$

We have replaced the infinitesimal timestep dt with the finite difference Δt. Doing the same in space allows us to solve the equation at a grid of discrete points.

The right hand side of (2.9) is the first term of a Taylor expansion of the continuous function. The sum of the remaining terms is known as the "truncation error" and represents the difference between this discretized approximation and the true value. Including additional terms can reduce the error but requires consideration of more points.

This is the simplest form of finite difference method, known as the Euler method. The approach is conceptually simple and, for a structured grid, it is relatively straightforward to implement and obtain good performance. However, it is difficult to implement on an unstructured grid without introducing unwanted complications, and it tells us nothing about the spaces between the discrete points.

*Showing that such a solution does or does not exist was identified by the Clay Mathematics Institute as one of its "Millennium Problems" for which a proof would win a million-dollar prize (Clay Mathematics Institute, 2000). The prize has yet to be claimed.

Finite volume methods

The finite volume approach is built upon Gauss's theorm, which tells us that for any vector, the volume integral of its divergence is equal to the integral of the flux over the surface area of that volume (Cushman-Roisin and Beckers, 2011). To put this in less formal terms, for the quantity of something in a given volume to change, there must be a flux of that thing across the surface of the volume. If we can evaluate the integral of the flux over the surface, we have an exact value for the change within the volume.

Discretization comes from the fact that the flux must be averaged over the duration of a timestep. While the true value at a single moment and position may not be represented exactly, the average flux leaving one volume during a timestep must be exactly equal to that entering another (or crossing the open boundary), meaning that this method is inherently conservative. This is an important advantage for modelling hydrodynamic flow, where a number of properties such as mass and momentum must be conserved.

Since we are concerned with a set of volumes that fill the model domain, rather than a set of discrete points, the volumes can have arbitrary shapes. This means that finite volume methods lend themselves well to unstructured meshes. In the models used here triangular mesh elements are mostly employed, but quadrilateral ones appear in Chapter 4 and are equally valid.

The finite volume approach tends to be more computationally expensive than finite difference ones.

Finite element methods

In the broader category of "series expansion methods" the continuous equations are replaced by a combination of a finite number of predetermined functions with a weight assigned to each. A familiar example is that of a Fourier series. Solving the system then becomes a problem of finding the set of weights that minimises the residual between the approximation (it must be an approximation in most cases because a finite number of functions is used) and the original governing equation. Different ways of minimising this residual exist, of which the most common for finite element techniques is the Galerkin method. For further details see Durran (2010).

This is a very general approach, and the finite difference method can be shown to be a special case of it (Durran, 2010).

The finite element method is a subset of this category where the weights are designed

such that each function has a weight > 0 in only one mesh element. It is very flexible, and can be applied to nearly any situation in any geometry (good for unstructured meshes). However, it is mathematically complex to fully describe and, often, expensive to solve. There is little obvious physical significance to the mathematics, which makes intuitive understanding harder (Autodesk, 2015).

Explicit *vs.* implicit schemes

The terms "implicit" and "explicit" in this context refer to the way in which a model is moved forward through time.

In an explicit scheme, the state at timestep $n + 1$ can be expressed as a function of the state at timestep n. In an implicit scheme, terms that are not time derivatives may be defined in terms of values at timestep $n + 1$ — *i.e.* unknowns defined by other unknowns.

Implicit methods are more difficult to implement and often more computationally expensive on a per-timestep basis, as additional iterative processes may be required to solve them. However, they also tend to be more numerically stable, which can permit the use of much longer timesteps — often enough to more than pay back the extra cost of each timestep and lower the computational effort per unit of model time. The tradeoff for using longer timesteps, *i.e.* a lower temporal resolution, is a certain level of smoothing, which may be undesirable if the model must resolve transient events.

2.1.5 Description of the models used herein

All of the models used in this thesis are shallow water models as described in Section 2.1.3 and use the Boussinesq and hydrostatic approximations (FVCOM has a non-hydrostatic option, but this was not used). All offer a choice of Cartesian or spherical coordinates. All are capable of baroclinic simulations, but in this work all were used in barotropic mode (*i.e.* temperature and salinity, and hence density, are fixed) because the waters being studied were known to be well-mixed. All use the Smagorinsky formulation for eddy viscosity in the horizontal, but offer a range of turbulence sub-models to estimate it in the vertical.

Delft3D-FLOW (used in Chapter 3) is a finite difference model on a structured, quadrilateral grid using implicit timestepping. Spherical (lon/lat) coordinates were used. A number of options are available for vertical eddy viscosity, but in this case the $k - \epsilon$ model was selected.

MIKE 3 (used in Chapters 3, 4, and 6) is a finite volume model, solved explicitly on an unstructured mesh. Triangular mesh elements are most commonly used, but quadrilateral ones are also supported and are used in Chapter 4. Cartesian coordinates were used. In Chapter 3 vertical eddy viscosity uses the $k - \epsilon$ method, while in later chapters a simple log law is employed.

FVCOM (the Finite Volume Community Ocean Model, used in Chapter 5) is, as per its name, also a finite volume model, although it uses slightly different grid arrangements to MIKE. Cartesian coordinates were chosen. It offers a choice of explicit or semi-implicit solution; explicit was used here. It uses an unstructured mesh of triangular elements. Vertical eddy viscosity is estimated by a Mellor-Yamada turbulence sub-model.

It is worth noting that a model can rarely be perfect for its intended application, becuase of the necessary simplifications that are described above. For example, the choice of a shallow water model is a sensible one for regional-scale modelling, because it makes useful results achievable on available hardware. However, the assumption that vertical motion is small, combined with the hydrostatic assumption, means that the models used here are unlikely to correctly represent the upwellings that are commonly seen in fast-flowing areas such as the Pentland Firth. This illustrates why it is important for the modeller to be aware of what choices and compromises have been made in model design, and bear these in mind when considering results.

2.2 Tidal model skill, tuning & validation

Section 2.1.1 established that in order to put trust in numerical models, we must first validate them by comparing their predictions to measurements. Below is a review of methods for performing this comparison, followed by a look at how these methods are used for tuning ("calibration") and validation.

2.2.1 Comparing models to observations

In order to calibrate or validate a model, it is necessary to compare its predictions to observations. When doing this, it is worth bearing in mind that the observations will not be perfectly accurate or reliable (Gerritsen *et al.*, 1995). Owen and Bryden (2007) note that much bathymetry and current data is based on surveys that are a hundred or more years old, and comment that

> *"The availability of data is… often much greater than its continuity or accuracy, and this fact must be borne in mind when modelling the*

resource"

It is also worth noting a fundamental difference between model predictions and most observations: that the values produced by a model represent the area of an entire grid cell over the length of a time step, while most observed values are instantaneous measurements taken at a single point (Gerritsen *et al.*, 1995). Interestingly, neither of these things is true for ADCPs. Spatially, their output represents the volume of their beams in each depth bin, but this will usually be much smaller than a grid cell (at least horizontally), and so can be considered as a single point. Temporally, however, ADCPs average over an 'ensemble' period (Teledyne RD Instruments, 2011) and this, often between ten and thirty minutes, is likely to be substantially longer than the time step of a coastal flow model.

A theme throughout this section will be that the best method for assessing the capability of a model depends upon the use that is planned for that model. Gerritsen *et al.* (1995) describe this as "application-driven skill assessment". The most obvious choice is whether water levels or velocities are most important for the intended application, but one can go further. Vested *et al.* (1995) gives an example of a storm surge model that was tested not for the accuracy of all of its water level predictions, but for the accuracy of its predictions of *peak* water levels.

There is no clear consensus in the literature on a single best way to evaluate the goodness of fit between a model and observations. However, there are a number of common methods.

Accuracy statistics

The simplest approach is to compare predictions and observations in the time domain using one of a number of statistical measures of accuracy. The most straightforward two measures are the Root Mean Square Error (RMSE) and the Mean Absolute Error (MAE):

$$\mathrm{RMSE}(S,O) = \sqrt{\frac{1}{N}\sum_{n=1}^{N}(s_n - o_n)^2} \tag{2.10}$$

$$\mathrm{MAE}(S,O) = \frac{1}{N}\sum_{n=1}^{N}|s_n - o_n| \tag{2.11}$$

where s_n is a prediction of the simulation, o_n is an observed value at the same point in time and space, and S and O are the sets of N of these values (adapted from Sutherland, Peet *et al.*, 2004). Mean Square Error (MSE) is also sometimes used, and is simply the RMSE without the square root.

Using relative rather than absolute values can make it more straightforward to compare one model to another. Scatter Index (SI, also known as normalised root mean square error or nRMSE) and Relative Mean Absolute Error (RMAE) accomplish this for RMSE and MAE respectively, in each case dividing the absolute statistic by the mean observed value. See Brière *et al.* (2007) for details.

Correlation statistics

Another approach to measuring goodness of fit is to use the linear correlation coefficient:

$$r_{XY} = \frac{\langle (Y - \langle Y \rangle)(X - \langle X \rangle) \rangle}{\sigma_X \sigma_Y} \tag{2.12}$$

where X and Y are two sets of values, $\langle\rangle$ denotes the mean of the set contained within, and σ_X is the standard deviation of X (adapted from Sutherland, Peet *et al.* (2004)). This is a measure of correlation rather than accuracy, and as such should not be used as the only measure of goodness of fit. This is because a model with a constant systematic error could give predictions that are perfectly correlated to measurements while still being wrong at every point (see Figure 2.3 for an example). However, the combination of a correlation statistic and a measure of accuracy can be useful.

Bias statistics

Accuracy statistics can tell us how much predictions differ from observations, and correlation statistics can tell us whether they change in the same way over time. Bias statistics serve to highlight systematic under- or over-predictions by the model.

The simplest approach is simply to report the mean error (ME), often also known as

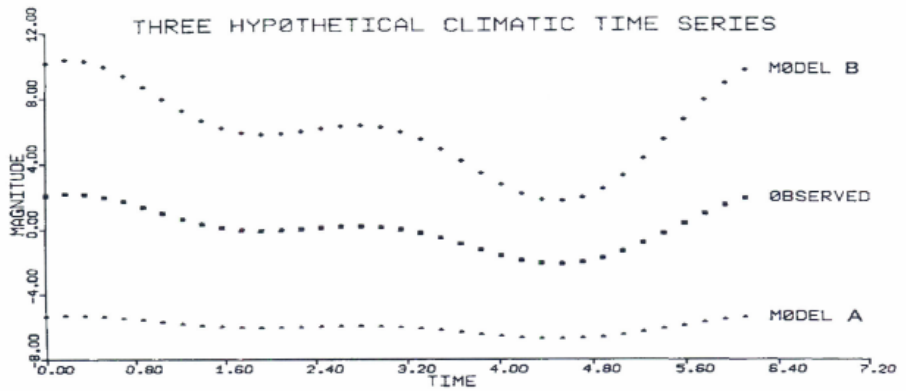

Figure 2.3: *Example of two sets of model outputs that would both have a perfect correlation with the observed values (i.e. $r = 1$), despite being inaccurate. Source: Willmott (1981).*

the bias:

$$\mathrm{ME}(S,O) = \frac{1}{N}\sum_{n=1}^{N} s_n - o_n \tag{2.13}$$

which is expected to be close to zero if errors are random, but will deviate from zero to indicate a systematic bias. An alternative is to report the gradient of the line of best fit to a scatter plot of predictions vs observations (see section on graphics below). This complements the correlation coefficient well, in that both are measures of fit between the scatter plot and a straight line.

Skill scores

A refinement, expounded by Sutherland, Peet *et al.* (2004), is "skill" measurements. These are non-dimensional quantities that represent how much better the predictions are than a set of "baseline predictions", and have been in use for assessing meteorological models for some time (Murphy, 1992). They can be used to provide a simple indicator of how much better or worse different models are than a baseline model, for instance when conducting a sensitivity analysis (*e.g.* Oke *et al.*, 2002) or a model calibration. Alternatively a "naïve" model may be adopted as the baseline, and all other models compared against it. For morphodynamic modelling and for meteorological applications, the naïve model is sometimes simply taken as being the mean measured value. It is not inmediately clear what an appropriate equivalent would be for a periodic quantity such as tidal elevation.

Skill measurements can be constructed using any of the accuracy statistics mentioned above. Sutherland, Peet *et al.* favour the Brier Skill Score (BSS), which is based on the MSE. Murphy refers to the same simply as the Skill Score.

$$\mathrm{BSS} = 1 - \frac{\mathrm{MSE}(S,O)}{\mathrm{MSE}(B,O)} \tag{2.14}$$

where S and O are sets of predictions and observations, as above, and B is the set of baseline predictions. A value of 1 represents a perfect model, a value of 0 means that the model is no better than the baseline prediction, and a negative value means that it it worse. For two skill values to be comparable the same baseline model must have been used for both, and so the baseline model that has been used should always be clearly stated.

There are two main advantages to the skill approach:

Firstly, that it provides a simple and easily-readable comparison between two models (the baseline and another); it is much easier to see at a glance whether a skill score is above or below zero than to compare two RMSE values presented in a table.

Secondly, that a raw measure of error such as MAE or RMSE can be lowered by expanding the domain to include "easy" areas in which the model performs well (*e.g.* areas far offshore) — thus "diluting" the errors. With a skill measurement, including these areas will have little effect if the baseline prediction performs well within them as well.

Gunn and Stock-Williams (2013) note that while skill scores are good for finding which of two models is the better, they do not provide any quantitative understanding of how well any model matches observations. Therefore, while they may be helpful for sensitivity studies or for calibration, they should not be used for validation of models.

Graphical representations

Whatever statistical measure one adopts, it is also important to visually inspect the comparison on a graph. Hackett *et al.* (1995) give an example of simulated and observed water level data that match closely, but exhibit a phase shift. Since there would be a difference in water level at nearly every moment that is compared, this results in a high RMSE, but a visual inspection clearly reveals that the model is predicting the right things at the wrong times. Where the results are to be used for statistical rather than predictive purposes, this may not be a problem. ABP Mer (2012), using absolute and relative RMSE statistics, state that,

> *"Under certain conditions, models can meet statistical calibration standards but appear to perform poorly in a visual comparison; conversely, seemingly accurate models judged visually can fall outside of statistical standards."*

Time series, such as that shown in Figure 2.4, are the most obvious means of graphical comparison. They make it easy to spot phase shifts, but suffer from only showing a short length of time (or becoming unreadable as the time axis is compressed). Willmott (1981) and Gunn and Stock-Williams (2013) recommend the use of scatter plots, as shown in Figure 2.5. These allow an overall impression of the model's behaviour throughout its runtime, and make it easy to spot, for instance, particular velocity ranges in which the model underperforms. A further development of this technique is to colour the points according to the phase of the tide (flood or ebb), as in the example.

Using linear regression to calculate a line of best fit to the scatter plot makes it possible to compute the proportion of the MSE attributable to systematic and to unsystematic error (Willmott, 1981; Gunn and Stock-Williams, 2013). If a significant systematic error is found, further refinement of the model may be called for.

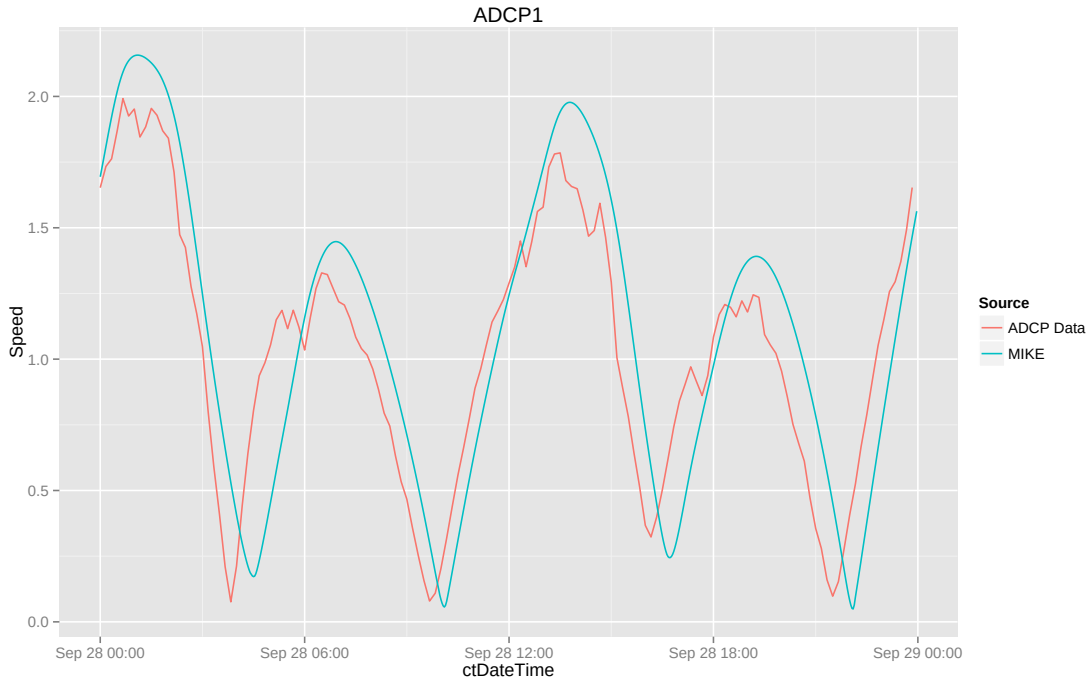

Figure 2.4: *Example of a time series plot of model predictions against observations. In this case a phase shift is clearly visible, as well as a small discrepancy in amplitude on these dates. Source: Author.*

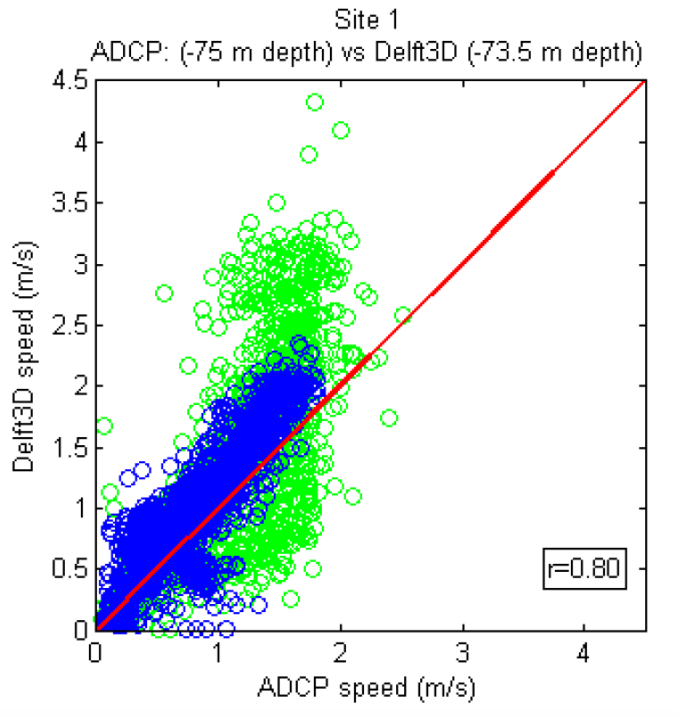

Figure 2.5: *Example of a scatter plot of predictions (on the vertical axis) vs observations (on the horizontal). In this case the points have been coloured according to the direction of flow: blue points for the flood and green for the ebb. The red line represents a perfect match. It is easy to see from this plot that the model overpredicts the higher speeds on the ebb. Source: Baston* et al. *(2013).*

For current velocity, the direction as well as the magnitude is important. Two scatter plots can be used for direction and speed. Alternatively a 2D scatter plot, also known as a hodograph, may be used to show the velocity in vector form from the origin, with the points coloured according to whether they are from predictions or observations. See Figure 2.6 for an example.

Taylor diagrams (Taylor, 2001) provide a means of plotting datasets according to their standard deviations and correlations with one another, such that the distance between them on the diagram is proportional to the RMSE (Figure 2.7). Note, however, that they do not show bias, and hence do not provide a "complete" picture of the quality of match between datasets. Taylor diagrams are common in climate science, where many different models are compared, but rarely seen in the literature around tidal energy.

3D models

For three-dimensional models, it is also necessary to test how well the variation in velocities with depth is predicted. One way is to use the measures above at a number of different depths. However, while this gives a numerical measure of the model's accuracy, it does not provide an intuitive understanding of any discrepancies in the the vertical velocity profiles (Gunn and Stock-Williams, 2013).

Davies and Gerritsen (1994, p.214) describe the ability to reproduce the vertical velocity profile as "the most sensitive test of a 3D model". This comparison of vertical profiles should be used in addition to, not instead of, comparisons of velocities over time when assessing a model's skill.

A useful graphical approach is to examine the profile of how velocity changes with depth at a given horizontal position at a given instant by the use of a profile plot (Figure 2.8), and compare this between model and measurements (*e.g.* Baston *et al.*, 2013). This introduces the risk that the instant chosen may not be typical. This risk can be mitigated by using not a single instant, but an average for that phase of the tide. For example, one might take the instants of maximum flow at a number of flood tides around springs and plot the mean profile, and do the same for ebbs at springs, floods at neaps, and ebbs at neaps (*e.g.* Warner *et al.*, 2005).

It is common practice to simply plot current speeds, and for some applications or in a strongly rectilinear flow this may be acceptable. However, some planned tidal energy sites are known to exhibit changes in flow direction with depth (known as "veer"), and so it is preferable to capture the direction of flow in some manner.

There are various ways of showing this graphically:

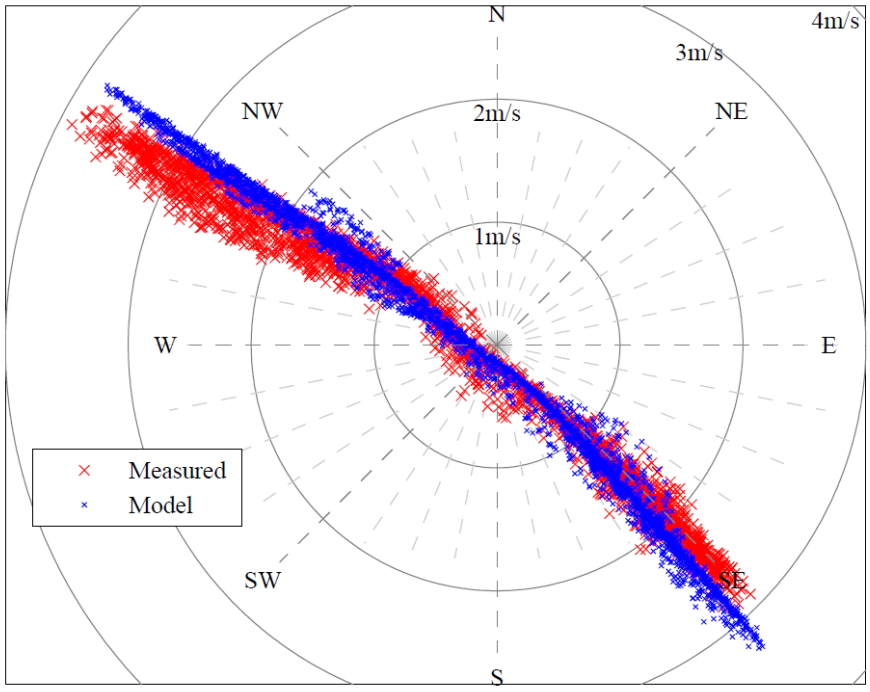

Figure 2.6: *Example of a hodograph showing flow velocity. The distance of a point from the centre represents the magnitude of its velocity, and its position on the circle represents the direction. The colours distinguish between predicted and observed values. Source: Gunn and Stock-Williams (2013).*

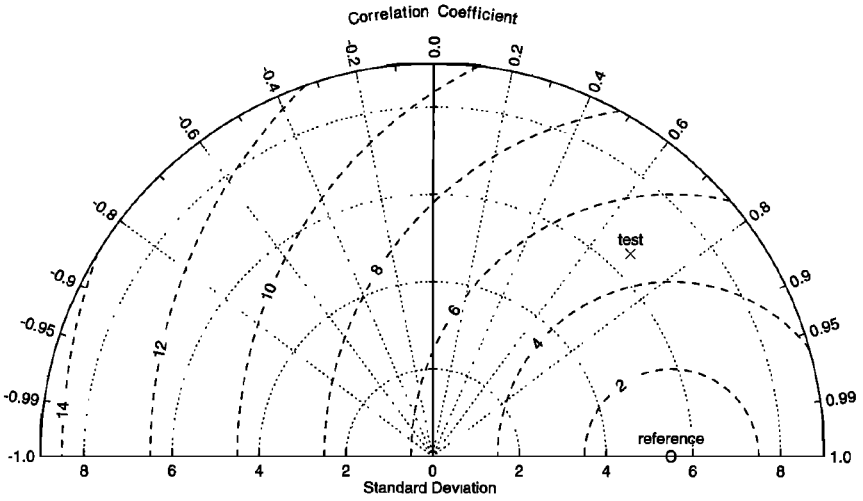

Figure 2.7: *Illustration of a Taylor Diagram. The contours marking distance from the "reference" dataset represent the root mean squared difference to any other dataset occupying that point on the diagram. Often only the right-hand quadrent is shown, as it is seldom necessary to compare datasets with negative correlations. Source: Taylor (2001).*

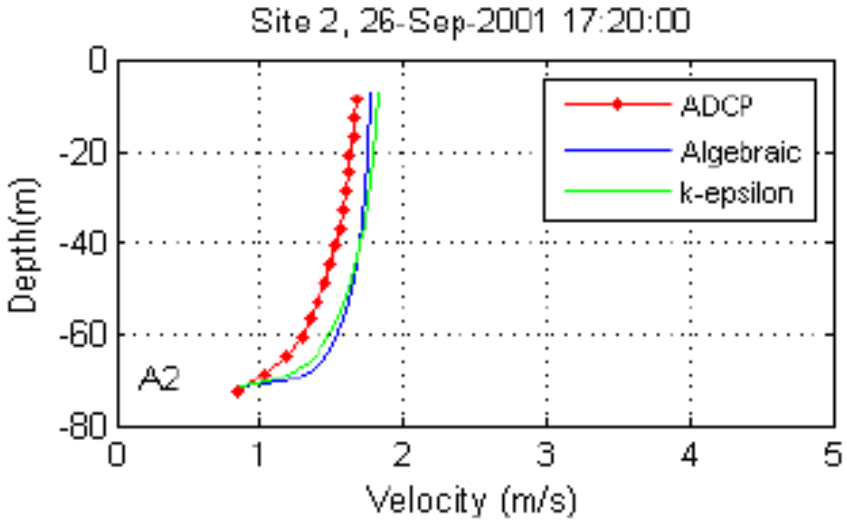

Figure 2.8: *Example of a vertical velocity profile for a given location at a given instant, comparing two different models against measurements. Source: Baston* et al. *(2013).*

- One straightforward approach is to plot the vertical profiles for u and v velocity components separately; if they differ in shape, there must be a change in direction with depth.
- Figure 2.9 shows the changes of direction very clearly for a given instant by using arrows, but does not make changes in magnitude visible and does not demonstrate changes over time.
- Figure 2.10 shows how things change over time, but still shows only direction and not velocity magnitudes.
- Figure 2.11 shows all three pieces of information, by colouring a set of velocity profiles by direction, but in this author's opinion is a relatively difficult plot to interpret.

While none of the figures shown actually compares a model to observations, in all cases two plots could be made side by side, and in some cases both could be shown on the same graph while remaining readable.

Frequency domain

The statistical techniques above are all applied to raw values of elevation and velocity. As already noted, they have a weakness when dealing with periodically varying results such as tidal effects: if a model has predicted the right result at a slightly wrong time, it will be awarded a high error score that may, depending on the objective of the exercise, be considered unfair (Sutherland, Walstra *et al.*, 2004). One way to address this is to evaluate the goodness of fit in the frequency domain.

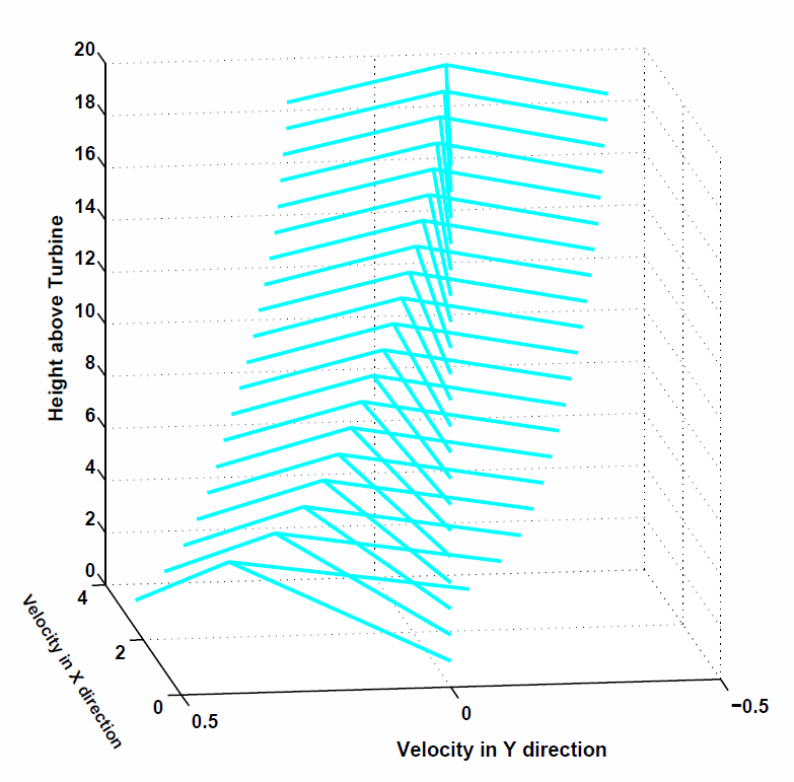

Figure 2.9: *Alternative method of showing veer in the water column, using arrows to show direction. Source: Sutherland* et al. *(2013).*

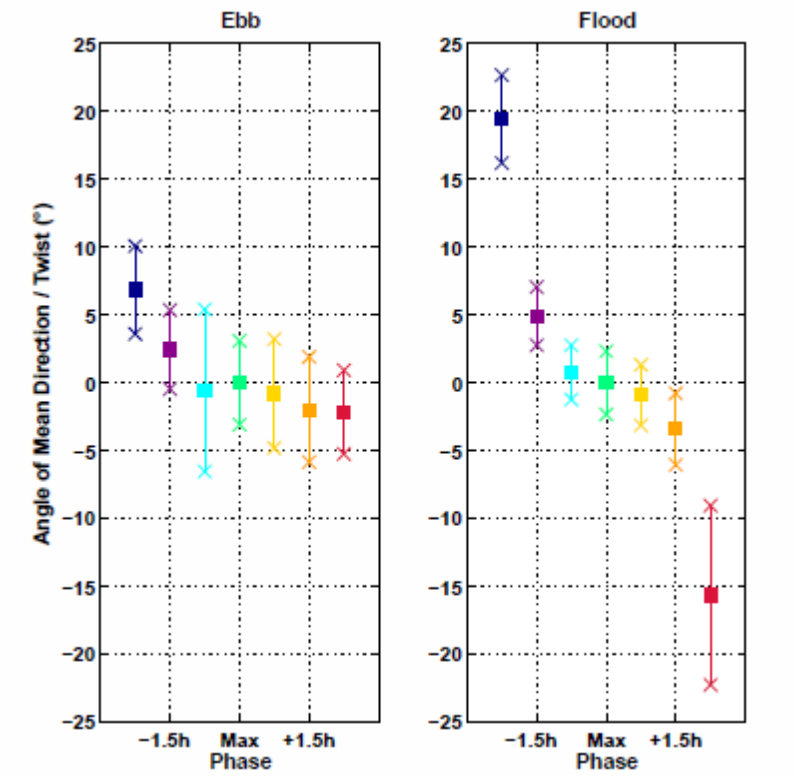

Figure 2.10: *Method of showing veer in the water column at different stages of the tide. The horizontal axes represent the phase of the tide (both graphs together making up 12 hours) and the vertical axis represents direction. The squares indicate the mean direction, and the "whiskers" represent the range of directions through the water column. Source: Sutherland* et al. *(2013).*

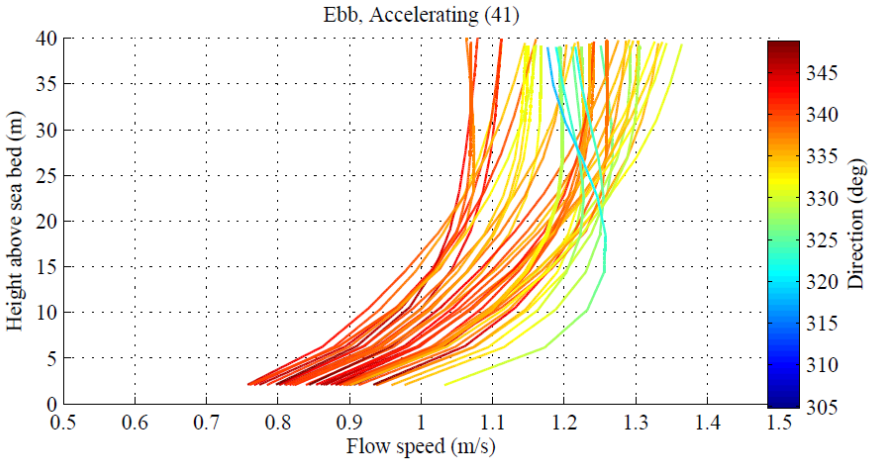

Figure 2.11: *Example of a set of velocity profiles, captured at different times during the same phase of the tide (in this case ebb), using colour to show the direction of flow. The change in colour with depth indicates veer, i.e. differences in flow direction according to depth. Source: Gunn and Stock-Williams (2013).*

The well-established technique of harmonic analysis (see *e.g.* Boon, 2004) can be used to express the periodic actions of tides as a series of sinusoidal constituents with specific astronomically-driven periods. If this technique is applied to both predictions and observations, then comparisons can be made between the phase and amplitude of each constituent. Gerritsen *et al.* (1995) extol the virtues of this approach, describing it as "quantitative and normed, reproducible and transferable". An additional advantage is that measurements and predictions may be taken at different times and the resulting tidal constituents still used together.

Easton *et al.* (2012) note that given a long enough data series, frequency-domain analysis removes meteorological effects and leaves only the tidal signal. However, if only a short time series is available for analysis, it can have the effect of "enshrining" these effects instead.

When harmonic analysis is applied to current speeds rather than surface elevations, it may not be able to capture all of the behaviour of the flow. This is because currents can include "aharmonic" components that do not correspond to the periods of any of the standard tidal constituents. These components can be produced by local topography and bathymetry, turbulence and eddies of all scales, and density-driven circulation in baroclininc models (Godin, 1983; Polagye *et al.*, 2010). Therefore, while frequency-domain analysis is a useful tool when used with currents, it should not be used alone.

Amplitude and phase results for water levels may be plotted graphically as pairs of scatter graphs. For velocities, a similar approach can be adopted of using a pair of scatter plots for u-velocity and another pair for v-velocity. Gunn and Stock-Williams (2013) show an alternative display where the same information is used to produce a

visualisation of the tidal ellipse for each constituent (see Figure 2.12).

2.2.2 Model setup and tuning

In the setup of a new hydrodynamic model, there are many variables that must be specified. These fall roughly into three categories:

- Some variables are based on physical properties that can be measured, such as bathymetry, and we want to get as close to the physical reality as possible given the limitations of measurement and of the model's discretization. Values of these parameters are likely to be fixed from the beginning of a model's life.
- Some variables do not relate to physical reality, but to the approximations made in the model. Examples include the density of the computational mesh, the positions of the boundaries, and the length of the time step used. Sensitivities to these will vary from one model to another, and the optimum values will depend on the purpose for which the model is intended, but in general there is a compromise between maximising the accuracy of the model and minimising the computing power or time needed to run it. Greater accuracy can always be obtained, at a cost, but for any given application there will be a point at which further fidelity is not useful. Vested *et al.* (1995) describe a situation in operational storm surge modelling where increasing the computation time beyond the required minimum would be not only wasteful but actively counterproductive, as a slower model would mean less warning of an impending flood.
- Some variables are based on properties that cannot be practically measured, such as bed resistance. The optimum value of these can only be arrived at by a tuning process, where the model is run with different values and the results compared to known observations.

The nature of model calibration

Parameters in the final category above can only be arrived at by an iterative process of trial and error. This tuning of the model is often referred to as "calibration"*.

When the value of a variable is established in this way, it no longer represents just the physical quantity that it is intended to embody, but also the influence of all of the effects that are not otherwise included in the model (Green and McCave, 1995). Despite this, it is important to bear in mind the physical parameters that calibration

*Strictly speaking this is, perhaps, not an accurate term, but it is generally used in the modelling community and so is adopted here.

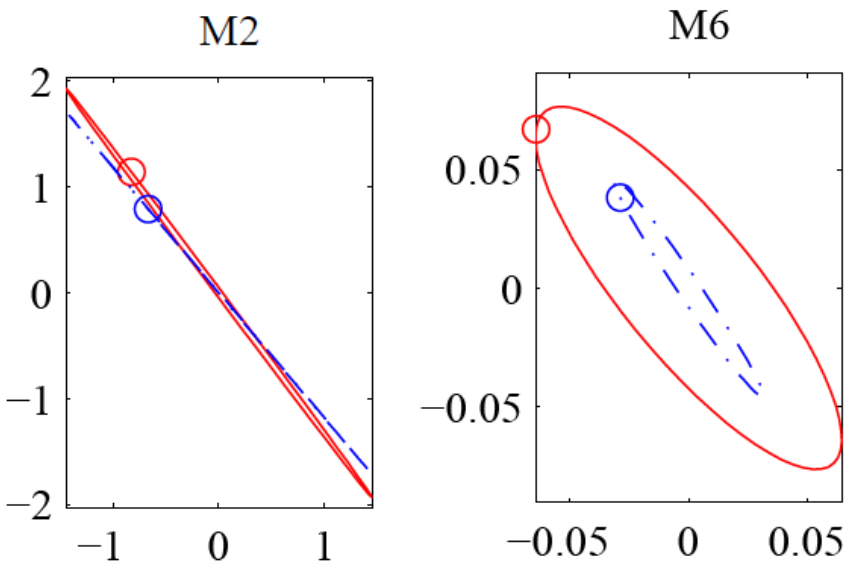

Figure 2.12: *Example plots showing tidal ellipses for the M2 and M6 constituents. Red shows the measured ellipse, and blue the modelled one. The small circle on each ellipse indicates the phase at a given time. In this example we can see that M2 is strongly rectilinear, and that the model gets both the phase and the direction very slightly wrong. For M6 the model correctly predicts a much wider ellipse than for M2, and gets the phase almost exactly right, but the direction is slightly wrong and the model substantially underpredicts the amplitude of this constituent. Source: Gunn and Stock-Williams (2013).*

variables are intended to represent, and to adjust the variables plausibly (Kurniawan *et al.*, 2010). Gerritsen *et al.* (1995) give an example of an automated calibration algorithm that was allowed to run too far, producing physically implausible changes in bed resistance from one subregion of their model to another. They describe this effect as "overcalibration" and note that in this scenario,

> *"the adjustments… may become fully unrealistic: The estimation may lead to pure data fitting and the model does then not retain its predictive properties for the subregion in question, let alone any predictive capability for the region as a whole."*

In this scenario, while predictions made at the calibration points will be excellent, those at any other location may be worse than if no tuning was attempted.

2.2.3 Model validation

As established in section 2.1.1, after a model has been tuned it is necessary to validate it to establish its predictive ability. This can be accomplished by using the model to make testable predictions and comparing them to observations. It is important that these not be the same observations that were used in calibration, as otherwise one is simply measuring how good the calibration has been — a "self-fulfilling

prophecy" (ASME, 2009). Instead they can be measurements taken at different locations and/or at different times. Ideally they should be in the area of interest for the model, because it is the model's predictive ability in this area that matters.

Validation is continuous, not binary. In other words, it is not correct to say that a model is or is not validated — instead we should report *how* well the model's predictions match observations. A threshold, determined in advance, may then be applied as to the goodness of fit that is acceptable for a particular application (Dee, 1995; Gunn and Stock-Williams, 2013). This threshold may be defined in the time or frequency domain, using any of the measures of goodness-of-fit that are discussed above. However, any validation exercise can only give quantitative results for the specific locations that are tested. While thresholds may be defined for these locations, confidence in the use of the model in areas away from validation points is a matter on which the modeller's judgement must be applied (ASME, 2009).

The United Kingdom Foundation for Water Research (cited in Easton *et al.* (2012)) have published standards that specify a maximum RMSE in tidal elevation of 10% at springs and 20% at neaps compared to measurements,* and a maximum RMSE in the timing of high water of 25 minutes. ABP Mer (2012) specifies similar, although slightly more complex, limits.

NOAA, in their standards for modelling (NOAA, 2003), have validation thresholds of an entirely different form. They measure, among other things, the frequency with which the model is wrong in each direction. This is a good example of validation criteria being set according to the application of the model. NOAA's primary application is for navigation and so, to take the example of water level, the critical statistic for them is the frequency with which the model overpredicts the water level — as this form of error could result in vessels running aground. An underprediction of water level, even of greater magnitude, is unlikely to be dangerous and so is of less import.

Kutney *et al.* (2013) briefly discuss the validation approach for tidal resource assessment, and they recommend validation metrics based on power density (*i.e.* the kinetic energy per unit cross-section of the flow) rather than current speed. However, assuming that water density is constant on the time and distance scales in question, power density is proportional to the cube of the speed (indeed, the measurements that predictions are compared against are likely to be derived by cubing measured speeds), and so it is effectively just a more sensitive measure of the same thing, and the same effect could be achieved by using speed with more stringent acceptance criteria.

*It is not clear, in the portion quoted by Easton *et al.* (2012), exactly what these are percentages *of*. It seems likely that these are actually nRMSE / Scatter Index values.

2.2.4 Recommendations for calibration & validation

For calibration, provided a suitable set of measurements is available which coincides with available forcing data, it is usually sufficient to work in the time domain. The skill score is a very useful way to compare the accuracy of a series of different variations on the model as they are compared to a baseline. This should be combined with a view of time series plots to allow systematic error to be diagnosed. Comparisons should ideally be made against both water level and current speed. There may be no set of parameters that optimises for both, and priority should be given to whichever predicted value is more important for the purposes of the model.

If effects that are not included in the model are thought likely to have a strong influence on the flow — *e.g.* surface winds in areas of very low current speed — then using the time domain alone for calibration may not be best advised. However, if effects not in the model are thought to be so important to the area, the modeller may ask whether those effects should be included.

For validation, numerical and visual comparisons should be made in both time and frequency domains. For validation, it is recommended to plot both short time series and scatter plots observations versus measurements.

Numerically, the RMSE should be used to describe accuracy. To examine systematic vs random error it is recommended to calculate the correlation coefficient, and the gradient and intersect of the line of best fit for the scatter plots mentioned above.

This approach is preferred over using standard deviation and bias because of the intuitive relationship between the numerical values and the scatter plot. However, they would be acceptable alternatives. An acceptable alternative to scatter plots for velocity is to plot hodographs, which can be more compact, but again have less intuitive connection to the numerical measures used.

It may be helpful to also calculate scatter index / nRMSE, if different models or different locations in the model are to be compared.

In the frequency domain, one of two approaches should be adopted for velocity measurements: Either to produce scatter plots of, and compare numerical values of, the phases and amplitudes of constituents in u and v separately; Or, to produce tidal ellipses and compare semi-major axis, semi-minor axis, inclination and phase. I think that the first approach is more intuitive, but both are valid.

This document is concerned with barotropic models, but if temperature and salinity have been included in a more sophisticated model then these should be compared to measurements by similar methods.

Mesh and time step sensitivity

In the field of computational fluid dynamics, it is normal practice to test for mesh sensitivity by running a simulation using a finer mesh than that which is intended to check that the results are not significantly different. This is less practical for regional-scale models, as some days or weeks of work may have gone into obtaining a mesh that is stable and performs well, and much of this work would have to be repeated for a general increase in resolution. Nevertheless, the modeller should always bear resolution in mind when developing a mesh, and if at this stage or later during testing they feel that a region may not be fully resolving the dynamics that are considered important, they may wish to test a local mesh refinement.

More practically, it is worth testing regional models for time step sensitivity by running using a shorter timestep than that intended and checking for any significant change to results.

2.3 Energy extraction from numerical models

Having covered the underlying mathematics of regional scale tidal models, and the means of assessing their skill, we now review how tidal energy extraction has been represented in them.

2.3.1 How turbines affect the flow

In operation, TEC rotors exert a retarding force on the flow, known as "thrust", as a result of the energy that is extracted. In regional models it is usual to follow an actuator disc approach, where the swept area of the rotor is considered as a disc and thrust is applied equally across its surface. This approach has been compared to Blade Element Momentum models (a more accurate and computationally demanding method that calculates the forces on each blade) and to a high-resolution, blade-resolving model, and shown to produce similar results except in the very near wake (Crammond *et al.*, 2013). Using the actuator disc approach, thrust (F) is defined as as

$$F = \tfrac{1}{2} C_T \rho A u^2 \tag{2.15}$$

where ρ is the density of the water, A is the cross-sectional swept area of the rotor, u is the component of the flow velocity that is parallel to the axis of the turbine, and C_T is the "thrust coefficient".

TECs cause a loss of energy from the flow in a number of locations (Vennell, 2012),

illustrated in Figure 2.13:

- From thrust at the rotor. Some of the power extracted here is converted to electricity, and some is lost in this converstion.
- In drag from the supporting structure.
- In turbulence caused by wake mixing, at at least two scales: the wake behind each turbine must mix into the general flow through the array, and the wake behind the array as a whole must mix into the surrounding flow. There may also be intermediate scales relating to "subgroups" of TECs (Garrett and Cummins, 2007).

Additional turbulence, not necessarily connected to wake mixing, is also generated at all scales; from trailing edge structures on individual turbine blades to vorticity generated in the flow behind a turbine, and so forth (Vennell *et al.*, 2015; Nishino and Willden, 2012b). It is important to note that the total power lost from the flow is greater than the power removed at the rotor.

In a regional-scale model, where a single cell is usually larger than a tidal turbine, most of these processes occur at a sub-grid scale and cannot be represented explicitly. Hence, there are two "macro" quantities that are relevant: the overall loss of momentum in each cell, including most of the effects above, and any overall effect on the level of turbulent kinetic energy (TKE). A third factor that may be of interest to researchers is the level of power absorbed by the rotor, as this can be used to calculate the electrical power produced. However, this is not of importance to operation of the model itself, being included as part of the overall loss of momentum.

Many researchers have investigated the loss of momentum in the cells containing turbines, and have implemented facilities for simulating this in models. Examples of these will be discussed below. A few have also modified turbulence models to account for increased TKE downstream of turbines — usually in models with a particularly high resolution. Losses to wake mixing beyond the cells with turbines will, to some extent, be handled by the model's standard mechanics for inter-cell shear. However, to the best of this author's knowledge, little testing has been done of the accuracy of this representation in regional models.

2.3.2 Representing energy extraction in the model

In early work the most common way of representing energy extraction in a regional model was simply to increase the drag of the seabed in the region containing turbines. Studies using this approach include Sutherland *et al.* (2007), Karsten *et al.* (2008) and Draper *et al.* (2014b), who used the TIDE2D, FVCOM and ADCIRC model

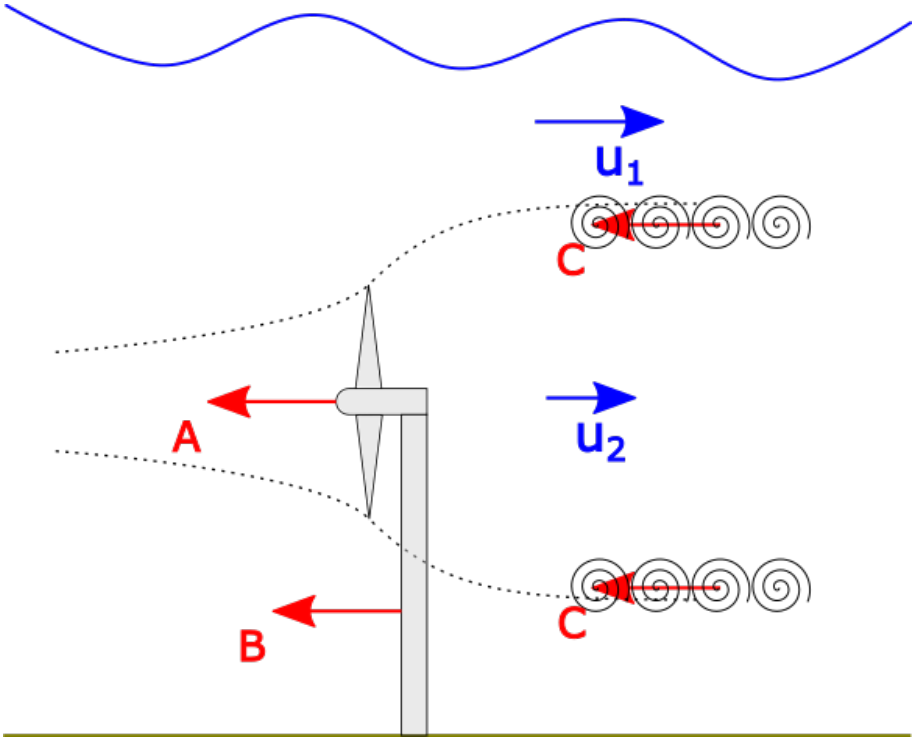

Figure 2.13: *Illustration of energy lost to the flow due to a turbine. A: thrust from the turbine rotor. Some of the power lost here will be converted to electricity. B: drag from the supporting structure. C: Energy lost through turbulence in wake mixing, as the faster bypass flow (u_1) mixes with the slower wake (u_2). Not shown on this diagram is wake mixing at larger scales, from the combined wakes of groups of turbines or the whole array.*

codes respectively. All of these models are two dimensional ones, where no distinction is possible between drag at the seabed and drag higher in the water column, and so it is sensible to use the mechanism of bed resistance that already exists in the model code. This approach would not be appropriate in a three dimensional model.

For a 3D model it is necessary to remove momentum from the vertical position of the TECs, by introducing a mid-water-column momentum sink. This approach can also be used in 2D models, where it may be convenient to be able to treat the turbines' thrust separately from other sources of drag. Researchers have added such a facility to various models, including Delft3D (Ramos *et al.*, 2013), TELEMAC (Haverson *et al.*, 2015), ROMS (Roc, Conley *et al.*, 2013), and FVCOM (Yang, Wang and Copping, 2013).

Modifications to turbulence models have, to the author's knowledge, only been made to two codes so far. Roc, Conley *et al.* (2013) made this addition first to ROMS and verified it against experimental data. Very recently Li *et al.* (2017) introduced similar code into FVCOM, and compared the results both to a (different) physical experiment and to a high-resolution RANS CFD simulation using a BEM theory model. In both cases the authors show that modifying TKE as well as removing momentum produces a more accurate result than using the momentum sink alone. Both of these studies use very high resolutions for their shallow water models (approx. 1/3 of a rotor diameter in ROMS, and 1/5 of a rotor diameter in FVCOM). It is not yet clear whether the TKE modifications made are beneficial or appropriate at lower resolutions.

2.3.3 Complications and complexities

Incorporating the concepts above into a real regional-scale model introduces a number of additional considerations, some of which are active research topics.

Flow is not always rectilinear

Many implementations of energy extraction in models make an assumption that the turbine is always oriented to face into the current. In areas of strong currents such as the Pentland Firth, complex flows tend to be generated including large eddies, and so the flow is often not simply bidirectional (Owen and Bryden, 2007). Some designs of tidal turbine can turn to face in any direction, and for these no additional difficulty is created for modellers. However, some designs are fixed in orientation and are designed to work optimally in flow from directly in front or directly behind. In this case consideration should ideally be made in the model of the angle between the flow and the turbine's heading.

Turbines do not have constant thrust coefficients

Much of the modelling work described above has assigned a fixed thrust or drag coefficient to a turbine. This treats the turbine as akin to any other fixed object in the flow, represented by a constant drag coefficient and removing a fixed proportion of the momentum in the flow. The reality is that tidal turbines have a cut-in speed below which they produce no electricity, and a rated capacity above which they produce no additional electricity, and they use active control methods (*e.g.* variable pitch blades). Therefore, the thrust coefficient will not be constant, but will vary with the speed of the flow through the rotor (Easton and Woolf, 2013). It should also be remembered that any turbine has a supporting structure with a fixed drag coefficient, in addition to the rotor with its variable thrust coefficient (Plew and Stevens, 2013).

Both of these studies found that allowing the drag coefficient to vary as a function of flow speed makes significant changes to the modelled effect of the turbines on the flow. This is especially noticeable at times of peak current speed, where the turbines are operating at their rated capacity and are thus "shedding" excess energy (see Figure 2.14).

Array effects

An array of turbines cannot simply be considered as a group of turbines that operate independently. Each turbine will affect each other turbine in a number of ways. For example, downstream turbines will experience reduced flow speeds as a result of upstream turbines (Stallard *et al.*, 2013) and increased turbulence if they interact with the upstream turbines' wakes. Mixing between turbine wakes and the surrounding flow removes energy from the system (Draper *et al.*, 2010). Pairs of turbines may accelerate flow between them to improve the efficacy of downstream ones (Myers and Bahaj, 2012). These effects, between turbines within an array, are difficult to represent in a regional-scale model as they occur below or on a similar scale to that of the mesh. One approach to mitigate this problem may be to apply a correction factor to account for array effects in general. Shives *et al.* (2013) propose a solution where a regional-scale hydrodynamic model and a high-resolution CFD model of a small group of turbines are coupled together, to allow each model to perform at the scale for which it is designed. They show an iterative approach where the regional model provides the flow velocity to the CFD model, and the CFD model returns turbine performance parameters to the regional model, which is computationally expensive.

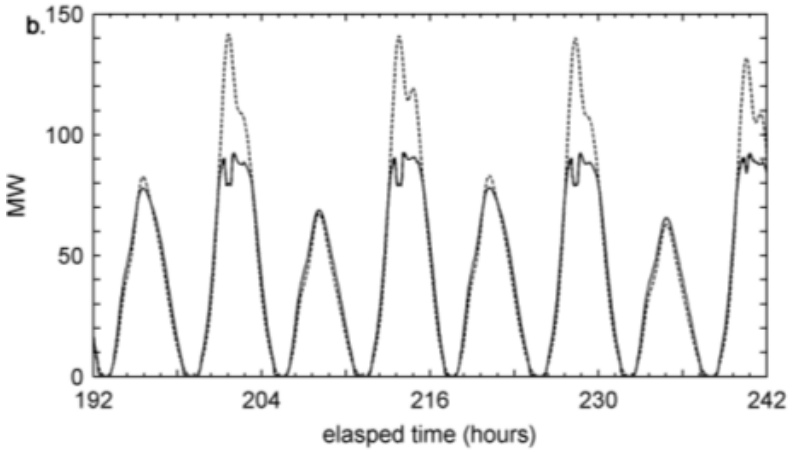

Figure 2.14: *Time series of energy dissipation by an array with (solid) and without (dashed) variable C_T. A variable thrust coefficient allows the model to reflect the capacity of the turbine, reducing the peaks in the output. Source: Easton and Woolf (2013).*

Grid scale issues

The question of grid size is closely linked to the array effects discussed above. If no correction for array effects is to be applied to the model, then it is desirable to make the mesh elements (or grid cells) small enough to have one element per turbine, ideally with an additional element in-between each turbine to allow for flow to pass between. While this can certainly not fully represent interactions between turbines, it does allow each device to experience a different flow velocity, influenced by other turbines in the array. For this reason, some recent works have used high resolution grids around turbines, as for example a regular grid with a resolution of 50m (*e.g.* Ramos *et al.*, 2013) or an unstructured grid with one third of the rotor diameter resolution (Roc, Conley *et al.*, 2013).

It would be computationally prohibitive to mesh an entire model domain at this scale, and so a local increase in resolution would be required. This can be achieved using a flexible mesh or by nesting multiple grids. However, the timestep required for a model to be stable tends to be determined by the smallest cells (Dix *et al.*, 2007, Appendix B), and so even if a local resolution increase only raises the number of elements by a small percentage it may dramatically increase the time required to run it. Additionally, a guarantee of one turbine per cell would often require the mesh to be adjusted if the array layout is changed. While this is the ideal, then, it is not always practical to achieve and so multi-turbine cells, and the resulting inaccuracies from neglecting array effects, must be accepted.

An additional consideration emerges with high-resolution models in that the standard method for representing tidal turbines, described above, develops an error as the scale of the grid reduces to approach that of the turbines. This matter is the focus

of Chapter 4, and the reader is referred there for further detail.

Open boundaries

Regional-scale hydrodynamic models are driven by their open boundary conditions. These are frequently "clamped" boundaries, in which time-varying water levels or velocities are specified either from observations, or from a wider-scale model that is itself driven by observations. Clamped boundaries are prescribed by the model setup, and cannot be affected by processes within the model.

When energy extraction is introduced in the model, it changes the hydrodynamics of the region around it. The energy extraction is not present in the observations from which the boundaries are taken, and so clamped boundary conditions cannot reflect the change. As such, the boundary conditions may constrain the response of the model to energy extraction. While well studied in other applications, the relevance of this issue to tidal energy extraction was first identified by Garrett and Greenberg (1977), who noted that the use of clamped boundaries is common and commented that

> *"The size of the region to be modelled is chosen… [such that] in the opinion of the modeller, it is large enough for the effect of the structure not to be felt at the open boundary. This assumption is obviously wrong in principle as the disturbance in the tidal regime introduced by the structure will propagate away from it and cause changes on the open boundary of the system, however far away they are."*

Kawase and Gedney (2013) demonstrated, with a numerical model of an idealised fjord and ocean basin,

> *"Changes in tidal energy flux due to extraction… throughout the ocean, indicating no discernible outer limit to the source region for the extracted energy… energy extraction in the fjord has a minute but global effect on the tides.*

Adcock *et al.* (2011) showed that the power captured by turbines can be sensitive to the locations of the boundaries, and hence that this matter requires attention for resource assessment purposes, and proposed two mitigating techniques:

Firstly, that the domain should be large enough that the "error wave" created by the tidal array is negligible by the time it reaches the boundary. This can be accomplished either by sheer distance, or by extending the domain beyond the continental shelf, where the sudden change in depth will tend to reflect the outgoing wave. Care should be taken to avoid excluding any reflecting features (*e.g.* sudden changes in channel

size or depth) that may cause a resonance effect.

Secondly, that transmissive or relaxing boundaries should be used that allow the outgoing "error wave" to pass out of the domain without reflecting at the open boundary. This problem has been well-studied in the context of ocean and coastal modelling, and a number of alternative boundary conditions have been proposed in the past; see Blayo and Debreu (2005), sections 1–3, for a review. Of the formulations mentioned, only that of Flather (1976) is available in the MIKE modelling suite used for the majority of this work. Use of this option requires that both the surface elevation and the velocity is specified at the boundary. Carter and Merrifield (2007) note that while elevations are readily available from global models based on satellite altimetry, the velocities given by these models can be unreliable in shallow waters. An alternative approach, suggested by Flather himself, is to initially run the model with clamped elevation boundaries (obtained from a global model) and from this predict the velocities at the boundaries, to be used in a second model run using Flather boundaries (Flather, 1987). This is clearly wrong in a theoretical sense, but may be better than the other available techniques; further testing would be required to establish the utility of this approach for tidal energy modelling.

Draper *et al.* (2014b) used two methods to check for constraint by the boundary conditions: Firstly, they specified the open boundaries by setting the water level and they compared the current flowing through the boundaries with and without turbines present. A significant difference would indicate that the effects of the energy extraction reached the boundary, and that unrealistic influences might arise. Secondly, they tested for resonance effects with the open boundary by re-running their simulation using a smaller computational domain and checking for significant differences in the available power. The first of these techniques is recommended by the recent IEC Technical Specification for tidal resource assessment (IEC Technical Committee PEL/114, 2015).

2.3.4 Validation of energy extraction

It is not currently possible to validate models' representations of large scale energy extraction using real-world measurements, because a tidal energy array of sufficient size has yet to be built in the sea. Two alternative approaches have been used. The first is to build models of idealised channels that can be analysed using analytic models and check the results against these "simple" models. Examples of this method are reported by Wan *et al.* (2015) and Pérez-Ortiz *et al.* (2017), although the latter probably tells us more about the limitations of the analytic model used than the strengths of the numerical one. This highlights a difficulty with this approach, that it is a comparison of one model to another.

The second approach is to compare numerical models directly to physical models (tank testing). Draper *et al.* (2013) reported such a test, comparing a physical experiment to a two-dimensional model, and concluded that "the numerical simulations reproduce the… measurements reasonably well across the full range of experiments", except in the area immediately behind the TEC. A similar test against ROMS, at very high resolution, was conducted by Roc *et al.* (2014).

Some work has been conducted to compare analytic models to tank tests, with mixed success in some areas (Whelan *et al.*, 2009; Cooke *et al.*, 2015). Li *et al.* (2017) compared the FVCOM model to a full RANS CFD system (Ansys Fluent) which, while helpful, again suffers from the difficulty of validating one numerical model with another.

2.4 Tidal resource assessment

For a developer or investor to assess the business case for a tidal energy development, they must be able to anticipate the amount of energy that it will produce. This section describes the development of how such resource assessments have been carried out in the nascent field of tidal energy. Only tidal stream resource will be considered, and not the energy available to tidal range schemes.

2.4.1 The Farm & Flux methods

Initial work on tidal resource assessment was based on a simple technique used for wind farms, known as the "farm method". This approach examines the undisturbed kinetic energy flux passing through each possible turbine location (or, sometimes, each cell in a grid) and assumes that a certain proportion of it can be extracted:

$$P = \frac{1}{2} C_p \rho A u^3 \tag{2.16}$$

where P is the power available, ρ the density of the water, A the swept area of the rotor, u the undisturbed speed of the flow at that point, and C_p a power coefficient representing the proportion of the kinetic energy of the flow that is converted to electricity.

A JOULE II project (European Commission, 1996) applied this method to EU waters in 1996, using Admiralty charts to provide velocities for UK waters and undisclosed sources for other areas. Approximately 64% of the total EU resource was estimated to lie in UK waters. ETSU (2003) performed a similar exercise for just the UK. Bahaj and Myers (2004) applied the farm method in greater detail to the Alderney

Race, and more recently ABP Mer (2007) used it, on a cell-by-cell basis, on a grid covering UK waters.

The farm method takes no account of the cumulative effects of TEC arrays, or the effects of one array on another. In the context of wind farms this is often reasonable, as appropriately-spaced wind turbines can be considered to exist in nearly unlimited open space (there being no boundary to the sides or above), and thus a full recovery of velocity can be assumed a sufficient distance downwind of a turbine as the kinetic energy is "replenished" from the surroundings. However, tidal flow is constrained above by the water's surface and often to one or both sides by coastlines. This means that there is little or no opportunity for additional kinetic energy to be added along the length of the channel. In a long channel it is possible for the farm method to arrive at an estimate for extractable power that is greater than the total kinetic energy flux through the channel, which is clearly unrealistic* (Owen and Bryden, 2007).

Whereas the farm method can be considered a "bottom-up" approach, in that it takes the power extractable by a single turbine and multiplies it by the number of turbines planned, the "flux method" adopts a "top-down" paradigm. An estimate is made of the total power of the tidal flow passing through a site — often from very limited information, as flow velocities are usually only known at a few points rather than across whole channels — and then an assumption is made that a certain proportion of this power can be extracted. Early proponents were Black & Veatch, who noted the flaws in the farm method and adopted the flux approach for a resource assessment for UK waters (Black & Veatch, 2005). They, and their academic collaborators (Couch and Bryden, 2006), postulated the idea of a "Significant Impact Factor" (SIF) which represented the proportion of the energy flux through the channel that could be removed without having a "significant impact" on the environment. Depending upon the cause of the high speeds in the channel this was estimated at between 10% and 50%, although these figures were not tested in any way. Note that the flux approach only provides information on the channel as a whole, and does not give any insight into the current speeds, and hence the energy available, at specific turbine locations.

In 2009 EMEC proposed a preliminary standard for resource assessment for tidal energy developments (EMEC, 2009), in which they combined both of these approaches and recommended that farm calculations be given an upper limit by the flux method.

The farm method is a straightforward approach for identifying potential areas for small tidal farms, before proceeding onto more detailed modelling or survey work.

*This is something that later research showed to be possible, through increasing head, but not in any way that the farm method could predict.

However, the nature of tidal arrays is to remove energy from the flow, and this must inevitably change the flow in the channel from its undisturbed state. When an array is large enough to have a significant effect on the flow in the channel as a whole, there is no longer any straightforward relationship between the undisturbed kinetic energy flux and the extractable power (Bryden and Couch, 2006; Polagye *et al.*, 2008), and the farm and flux methods cease to be useful.

Vennell *et al.* (2015) defined a "large array" as

> *"one which is able to influence channel-scale dynamics or one where the channel alters turbine performance via the duct-effect",*

and offered a rule of thumb that to be "large" in this sense, a TEC array must occupy more then 2–5% of the channel's cross-sectional area. Similarly, the IEC Technical Specification for tidal resource assessment (IEC Technical Committee PEL/114, 2015) permits direct measurements to be used for farms of less than 10 MW whose capacities are less than 2% of the undisturbed kinetic energy flux. Beyond this level, the use of models is required.

Karsten *et al.* (2008) reported that in the Minas Passage in Canada, theoretical and numerical modelling predicts that the extractable resource is more than three times greater than the figure given by an analysis based on the undisturbed kinetic energy. McMillan *et al.* (2013) gave an example of three adjacent channels where the one with the lowest undisturbed speed turned out, after modelling, to have the highest extractable resource. These differences between the actual resource and that indicated by undisturbed flow speeds in these studies are because adding impedance to the channel, in the form of tidal turbines, causes the driving hydraulic head to increase. In addition, Karsten *et al.* (2008) suggested that extracting the maximum possible power from the Minas Passage may move the M2 tide closer to resonance, further increasing its amplitude.

2.4.2 Use of modelling for resource assessment

It has been established above that some form of model is required to be able to accurately predict the resource of a tidal energy site. The "gold standard" here is to use numeric models of the type already discussed, well validated against measurements, but these are time-consuming to build and computationally expensive to run. There is thus scope for a simpler form of theoretical model, where the problem is reduced to a tractable one to solve either analytically or with a very simple iterative solver, which can give useful insights without the costs of the numerical approach. This section will first describe some of this latter type of model, and then look at *how* numerical models are best used to estimate tidal resource.

Theoretical models

The early seminal papers in this area were by Garrett and Cummins (2004, 2005) (hereafter GC04 & GC05), who took the one-dimensional momentum balance in a simple channel (effectively a simple form of the shallow water equations mentioned in Section 2.1.3) and used this to derive expressions for the maximum possible energy dissipation in either a channel linking a bay to a large sea, or a channel linking two large seas to one another. Blanchfield *et al.* (2008) combined these two models and showed that the GC05 formula could be applied to both situations, with modifications to constants according to the size and geometry of the bay*. The maximum available mean power from a tidal constituent can be approximately expressed in terms of the mean undisturbed volume transport and the driving amplitude across the channel.

These early papers noted that the maximum power calculated using their methods would apply if an unbroken, even tidal fence were to occupy the entire cross-section of the channel. To study the more likely scenario where gaps are left, Actuator Disc Theory (ADT) can be used.

> *"An actuator disk is defined... as an artificial device producing sudden discontinuities in flow properties." —Horlock (1978)*

Actuator disc theory was developed independently by both Lanchester and Betz in the early part of the 20th Century to describe propellers, but is now used for a variety of purposes wherever a thin disc effects a discontinuity in an otherwise continuous parameter of a flow. In this case the concept can be used to represent the removal of momentum by a TEC rotor, and the discontinuity in pressure that results. See Manwell (2009) for a clear mathematical explanation, as applied to wind turbines.

The first application of ADT to tidal energy was by Garrett and Cummins (2007) (hereafter GC07), studying a turbine that blocks only part of a channel. They considered the flow through the turbine, and the "bypass" flow around it, in terms of velocities and pressures. They arrived at expressions relating the thrust and power of the turbine to the ratios of speeds at various locations in the model, as well as the maximum proportion of the total energy in the channel that could be extracted, allowing for the diversion of flow around the turbine. Assumptions were made that the free surface was not distorted by the turbine and that the overall flow in the channel was not altered by the energy extracted (the latter being incompatible with GC05). Since this early work there has been a great deal of theoretical activity on the topic from a relatively small number of authors.

*The GC05 case of a channel linking two oceans is of course a special case of linking to a bay, where the bay is of very large size.

Whelan *et al.* (2009), Houlsby *et al.* (2008) and Draper *et al.* (2010) extended the theory to permit deformation of the free surface and to better consider wake mixing behind the turbine. A readable review is given by Houlsby and Vogel (2016). Nishino and Willden (2012b) proposed considering the problem at two scales — turbine scale and array scale — simultaneously using the same approach, and Vogel *et al.* (2016) applied this concept to study the optimum layout of a given number of turbines across a channel.

Vennell (2010, 2011) combined GC05 and GC07 differently to study the optimal tuning of the performance characteristics of tidal turbines, and noted that this would vary depending on channel blockage (and a number of other factors, including the phase of the tide). Vennell (2012) analysed the various losses of energy in a tidal channel, and in particular the relationship between extractable power and mixing losses behind the turbines.

The work above all considers flow through a channel, constrained by land on both sides. Flow around a headland has been much less studied, being visited from a theoretical perspective only by Garrett and Cummins (2013).

A third type of simple model has been proposed by some authors: that where a system of water bodies and the channels between them are represented, by analogy, as an electrical circuit. Channels have resistance and inductance, representing friction and inertia, while bays and harbours have capacitance. Surface elevation is analogous to voltage, as it provides a driving potential in a similar way. The most obvious limitation of this analogy is that resistance applies linearly in electrical circuits while drag in hydraulic flow is quadratic. However, this weakness is also a strength, as the use of linear drag can render complex hydraulic problems suddenly tractable, and there is existing software designed to analyse linear electrical circuits. The most commonly proposed use of this technique is to understand complex systems with multiple interacting channels. Proponents of the electrical circuit approach have included Woolf (2013), Draper *et al.* (2014a) and Cummins (2013).

Use of numerical models

For information on the mechanics of using numerical models and extracting energy from them, see Sections 2.1 to 2.3. The question remains, given the tools described above, how they can be best used to estimate the tidal resource of a channel or region. Three approaches have been used:

Undisturbed speeds: Here the undisturbed flow speed predicted by the model is used to calculate either the kinetic energy density or an estimated power output, using either the farm or flux method. As noted above, this approach

is theoretically wrong because it takes no account of the effects of energy extraction on the flow, and is wholly unreliable when looking at large scale development. However, it requires only a single model run and is the only method currently practical for evaluating many areas at once, for example when searching a whole country or region for promising areas for development. As such it has been used for many such "national resource assessments", *e.g.* Black & Veatch (2005) and ABP Mer (2008) for the UK and NEDO (2014) for Japan (in Japanese, described in English by Kinoshita (2012) and Hennequin (2016)). Sentchev and Thiébaut (2015) used this approach for a smaller area around Ushant.

Continuous lines of resistance: A continuous line momentum sink is placed across the channel(s), and its intensity is adjusted to find the greatest available power. This approach is concerned with what is theoretically available from the channel, and does not take into account practical considerations for real tidal farms such as water depth, navigational requirements, etc.. Examples of this approach include Hasegawa *et al.* (2011) and Draper *et al.* (2014b).

Realistic turbine layouts: Individual turbines are placed in the model in proposed locations, and the effects of the layout evaluated. Examples include Adcock *et al.* (2013) and Ramos *et al.* (2014). This approach initially only gives a prediction of the power of the array layout, and the turbine specification, that is tested, rather than the maximum available from the channel. From this starting position some level of optimisation is possible, either manually or using automated tools, although this will often be limited by the available computational resource. Optimisation of tidal array layouts in useful computing time is an active topic of research (Roc, Greaves, Conley *et al.*, 2013; Kramer *et al.*, 2015).

The first approach cannot be recommended except where there is no alternative, and then only with a great deal of caution. The second and third approaches mentioned are used to answer different questions: one is concerned with the maximum power that could theoretically be extracted from the channel, while the other predicts the power available from specific turbine types and layouts. The correct approach to choose depends, therefore, upon the task at hand — although with a dense enough array layout, a regional-scale model loses the ability to resolve individual turbines and the two methods become very similar.

2.4.3 Estimates of Pentland Firth tidal resource

The Pentland Firth is one of the most promising tidal energy sites in the world, and as such has been extensively studied. Table 2.1 lists some of the estimates that have been made of the available power and the methods used for these. As these studies have used very different methods, and have sought to answer slightly different questions, the figures given are rarely directly comparable. The table is intended to show the range of different approaches used and the resulting range in answers reached.

2.5 Environmental impacts of tidal power

Removing energy from an environment must change it, and hence it is inevitable that tidal energy extraction will have impacts. These fall into three categories:

- Direct physical effects on the flow, *e.g.* changes in speed or direction and the resulting alterations in bed stress, temperature, salinity, etc..
- Secondary physical effects caused by the above changes, such as changes to stratification or to sediment transport.
- Biological and ecological effects resulting from changes to any of the variables in the other two categories.

Each of these impact categories experiences two-way feedbacks with each of the others; for example, not only do changes to the flow effect benthic life, but changes to (*e.g.*) kelp beds can affect the flow. Only the first category, that of direct physical effects, is within the scope of this project, but it is the third category of biological and ecological impacts that is generally of concern for environmental impact assessments, etc., and prediction of these secondary and tertiary effects is an important use of the outputs of the modelling discussed here. This section is, therefore, not intended to be exhaustive, but is an overview of the potential impacts. Emphasis will be placed on the operational phase rather than construction or decommissioning.

2.5.1 Direct physical effects

A great many studies have considered the effects of energy extraction on the flow, as this is an essential byproduct of producing tidal power. Typically a reduction in speed, and hence in bed stress, is seen in line with the TECs, reflecting the momentum removed from the flow, and often an increase is seen to the sides as the flow takes a path of less resistance (*e.g.* Gillibrand *et al.*, 2016). In a 3D model, such

Authors & year	Method & notes	Power (MW)	
		Mean	Peak
European Commission (1996)	Farm method; PF sites as part of national survey	1167	3066
Black & Veatch, 2004 [1]	Flux method, SIF of 20%. PF sites as part of national survey.	1455	–
Black & Veatch (2005)	Refinement of 2004 work. SIFs changed, flux passing through multiple sites counted only once.	1005	–
ABP Mer (2007)	Plausible turbine locations & specifications, based on undisturbed velocities.	586	1824
Adcock *et al.* (2013)	2D numerical modelling. Rows of turbines placed across channel until marginal gain of next row is small. M2 & S2 only.	1900	–
Vennell (2013)	Theoretical analytic model in a simple channel "loosely resembling the PF". M2 only.	3100[2]	7400[2]
Draper *et al.* (2014b)	2D numerical modelling. Coast-to-coast line momentum sinks. M2 & S2.	4187	–
O'Hara Murray and Gallego (2016)	3D numerical modelling; turbines in lower 25 m of water column. M2 only.	1400	3000
De Dominicis *et al.* (2017)	3D modelling at national scale; individual turbines but at low resolution, many per cell	1640	–

[1] Report no longer available; information taken from 2005 document.

[2] Vennell's estimated powers are described as upper bounds which "do not include the effects of losses due to turbine support structure, nor electro-mechanical losses, power conversion or transmission losses".

Table 2.1: *Table showing a non-exhaustive list of resource estimates for the Pentland Firth (PF), using different methods, between 1996 and 2017.*

diversion may occur over and under the rotor as well. These changes to velocities result in changes to seabed stress (see Chapter 3 for more detail).

Such effects typically extend for some kilometres, but this does depend upon the scale of development. By including a very large level of energy extraction in the Pentland Firth and using a model with a large domain, De Dominicis *et al.* (2017) predicted a shifting of the amphidrome in the southern North Sea, with resulting small effects on tidal range along the British and Dutch coasts hundreds of kilometers from the tidal array.

Flow at many sites is not symmetrical, and because the processes affecting flow and energy extraction are non-linear, energy extraction can result in a change in the degree of asymmetry present (Defne *et al.*, 2011). This can result in a change in the residual current (the overall flow that remains when tidal cycles are averaged out). Ramos *et al.* (2014) noted a 10% change in residual current from their modelling of energy extraction in a Spanish estuary.

In the very far field, Kawase and Gedney (2013) showed very small basin-scale effects of energy extraction in an idealised numerical model, and Walkington (2014) used a 2D numerical model of the north Atlantic to predict that an extreme level of energy extraction in the Severn Estuary could cause small changes in the Bay of Fundy and the Hudson Strait, suggesting a possible disruption to basin-scale resonance. However, while illustrating well the global connectivity of the oceans, the effects shown in these studies are likely to be negligible in scale.

2.5.2 Secondary physical effects

Changes to velocities mean changes to turbulence intensities, and hence to vertical mixing. This can result in changes to the degree of stratification that is present in the water column. Only a modest amount of modelling work has studied stratification to date because representing it requires a baroclinic 3D model, which is computationally expensive to run.

Using an idealised model, Yang and Wang (2013) predicted a decrease in stratification as a result of energy extraction, presumably due to increased turbulence and the mixing that results. By contrast, De Dominicis *et al.* (2017) predicted small increases in stratification, using a large-scale model of the Scottish shelf, due to reduced mixing resulting from the reduction of velocities. The two scenarios are very different in scale and character, and it seems possible that effects may occur in either direction as a result of energy extraction.

Changes to bed stress may influence the pick-up of sediment by the flow, and changes

to flow speed will influence its carrying capacity. Changes to the residual current will have significant effects on sediment transport (Neill *et al.*, 2009).

Ahmadian *et al.* (2012) used a 2D model to predict changes to sediment patterns up to 15 km away from a large tidal array in the Bristol Channel. Fairley *et al.* (2015) used a 3D model to predict the effects on sediment of the planned Pentland Firth tidal developments, and found small effects which could cause the migration of a sandbank over time. Martin-Short *et al.* (2015) used a 2D model with a very high (18 m) resolution to study effects on sediment in the Inner Sound. They found little impact at low levels of exploitation, but when sufficient turbines were included, new gravel deposits started to form beneath the turbines. It is not clear whether this effect would apply in a 3D model that permitted the acceleration of bypass flow under the turbines.

2.5.3 Biological & ecological effects

Collision risks, noise and electromagnetic fields are disregarded here as the type of modelling under consideration can tell us nothing about them. A number of other potential routes to ecological impact have been identified, based on the changes to physical parameters outlined above.

Benthic species that live in high flow regions have adaptations for such environments, such as the ability to withstand large shear forces or the use of fast flow for transport of nutrients, food, waste products, larvae, etc. (Shields *et al.*, 2011). Consequently, a change in current speeds and seabed shear stress has the potential to alter this ecological niche.

There is evidence that megafauna use areas of fast tidal flow for foraging. This may be due to concentration or vulnerability of prey, or because benthic species are tranported to the surface by upwellings. Fish are known to use areas of rapid flow for travel, by inserting themselves into the stream in one direction and then moving to a slower part of the water column while the tide flows the other way (Benjamins *et al.*, 2015). A change in current speed could thus affect predator-prey relationships and might affect connectivity for swimming, as well as benthic, species.

Changes to tidal range resulting from energy extraction would alter the size of the intertidal zone, and hence the availability of such habitat. Movement of areas of sediment will clearly have impact on species which dwell or feed in sediment (Shields *et al.*, 2011). Changes in the concentration of organic suspended sediment may also affect oxygen levels in the water (Gill, 2005)

Changes to stratification — especially in estuary environments — may change the

temperature and/or salinity in particular parts of the water column or at the seabed. This represents a change to habitats (Yang, Wang, Copping and Geerlofs, 2013).

2.6 Chapter summary

The following are the main points from this chapter that are of relevance to future chapters:

- Regional flow models use the Navier-Stokes equations with a number of simplifications.
- Such models are not fully realistic. There are choices to be made as to which simplifications and assumptions are used, and which physical parameters are included in a model, which require judgement by the modeller. In general there is a tradeoff to be made between accuracy and computational effort.
- Such models are calibrated (tuned) and validated by comparison with measurements. Many methods have been reviewed.
- Energy extraction is implemented by increased bed resistance (2D models only) or with a momentum sink term. In the literature, most such work has been with academic models or with modifications to the code of models such as Delft3D, which may not be acceptable to investors (see Section 1.3.2). Means of doing energy extraction in trusted commercial models will be addressed in Chapter 3.
- The standard method of representing energy extraction in regional models develops an error at high resolutions. This will be addressed in Chapter 4.
- Available resource can be estimated, in ideal conditions, using theoretical models. For accurate predictions in complex flows numeric modelling is required, and can be used either by simulating realistic array layouts or by removing momentum from the whole width of the channel to understand the theoretical maximum that can be extracted. The latter approach is used in Chapters 5 and 6.
- Environmental impacts of energy extraction can be physical or ecological in form, *e.g.* by affecting sediment or habitats. A significant physical parameter that can be used to estimate further impacts is the bed stress.

Chapter 3

Implementation of tidal energy extraction in MIKE 3 & Delft3D models

The TeraWatt project, of which this work formed a part, aimed to identify best practice methods for predicting the regional-scale effects of tidal energy extraction which could be used by industry and regulators. As discussed in Section 1.3.2, the project received strong guidance from industrial stakeholders that only unaltered, reputed and well-tested commercial software could be used for this work if the results were to be accepted by investors. Based on guidance from industry two such three-dimensional modelling suites were selected: MIKE 3 by DHI*, and Delft3D-Flow by Deltares†. Both of these packages are already in extensive use commercially.

Orkney is an archipelago off the north coast of Scotland, and the Pentland Firth is the channel between Orkney and the Scottish mainland (see Figure 3.1). This region is of interest for its tidal energy potential. Demonstration models of the Pentland Firth and Orkney Waters (PFOW) area were developed separately in the two suites by different teams, according to the capabilities of each. No attempt was made to match parameters between the models, as this approach would be unavailable to a developer or consultancy with access to only one software package. Rather, an emphasis was placed upon evaluating the differences, in both methods and results, between the two systems.

The objective of the work described here was to start with the validated models from these teams, and,

- compare the predictions of the two models without energy extraction.

*http://www.mikepoweredbydhi.com/
†https://www.deltares.nl/en/software

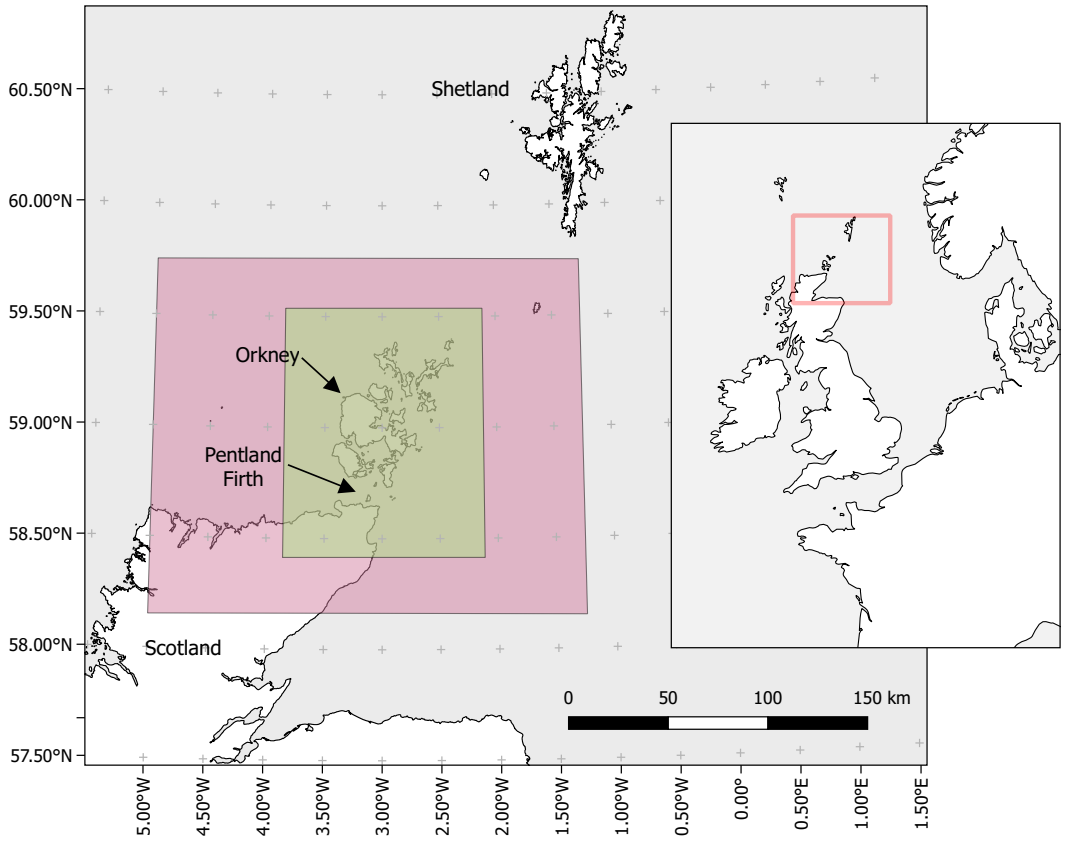

Figure 3.1: *Map showing the domains of the MIKE (inner green box) and Delft3D (outer red box) models. Inset map shows the location of the PFOW region on the north-west European shelf.*

- implement energy extraction in both models, as well as possible using the unaltered facilities of each.
- produce example predictions of the effects of energy extraction, which could be used by other project members to investigate methods for predicting ecological effects.

3.1 The models

Only a brief overview will be given here, as background, since these models were built by others. More detail on the supplied models, including calibration and validation, may be found in Waldman, Bastón *et al.* (2017) and Venugopal and Nemalidinne (2014). The versions of the model codes used were the 2012 edition of MIKE and the version of Delft3D with source control tag 3574.

The location of the study, and the domains of the models, can be seen in Figure 3.1.

There are no major river outflows in the Pentland Firth and Orkney area, and hence fresh water input from rivers was not included. Both models were run in barotropic mode, with no consideration of temperature or salinity and a fixed value for water density.

The open boundaries were driven using clamped time-varying water levels derived from global models based on TOPEX/POSEIDON satellite altimetry, although different models were used for each. It is acknowledged that the use of clamped boundaries is not ideal for the reasons discussed in Section 2.3.3, especially on relatively small model domains such as that of the MIKE model. Both MIKE 3 and Delft3D support more sophisticated radiative/transmissive boundaries, but in both cases they require external velocities, as well as elevations, to be provided. Accurate velocities over large spatial areas are not generally available in coastal areas, and so it would be unhelpful to suggest that commercial modellers should require this information. As noted in Section 2.3.3, it might be possible to use an initial clamped run to generate approximate open boundary velocities for further runs, but this has not been explored further in this work.

Both models use ten equally-spaced sigma layers in the vertical. For horizontal discretization the MIKE 3 model uses an unstructured triangular mesh, while Delft3D uses a regular, "rectangular" (in cylindrical coordinates), staggered Arakawa-C grid. In MIKE the timestep was automatically varied according to a target Courant number of 0.8, while in Delft3D it was fixed at 25 s. In both models the $k - \epsilon$ turbulence model was selected for vertical eddy viscosity (Launder and Spalding, 1974).

Both models were calibrated and validated against ADCP data in the Pentland Firth and the Fall of Warness. The locations of the ADCPs may be seen in Figure 3.7. The calibration and validation work was carried out by others, so for details the reader is referred to Waldman, Bastón *et al.* (2017). As a result of the calibration process, different values for bed resistance were used in each model. In the MIKE model bed resistance is defined as a quadratic drag coefficient (c_f) that is applied to the bottom layer of the model, and is set equal to 0.01. In the Delft3D model bed resistance is defined via a Chezy value C_{3D}, set to $50\,\mathrm{m}^{1/2}\mathrm{s}^{-1}$. Using the approximation $c_f \simeq g/C_{3D}^2$ (Soulsby, 1997), we can calculate that $c_f \simeq 0.004$ in Delft3D, meaning that the Delft3D model uses just under half the quadratic bed resistance of the MIKE one.

3.2 Variables of interest, and calculation of bed stress

Through discussion with other consortium members, the following variables were identified as being of interest for investigating the effects of tidal energy extraction on the benthic ecology of the area (M. Bell, personal communication):

- Depth-averaged current speed
- Current speed in the bottom layer
- Bed shear stress

The first two variables are outputs of the models, or trivially calculable from those outputs. Bed stress is less straightforward, as there is little consensus on the best method for deriving bed stress from information on velocity (Soulsby and Clarke, 2005). Wilcock (1996) identifies three approaches, all of which make use of the 'Law of the Wall' (von Karman, 1931):

$$\frac{u_z}{u_*} = \frac{1}{\kappa} \ln\left(\frac{z}{z_0}\right) \tag{3.1}$$

where u_z is the flow velocity at a distance z above the seabed, κ is Von Karman's constant (equal to 0.4), and z_0 is the hydraulic roughness length of the seabed. u_* is the friction velocity, defined as $u_* = \sqrt{\tau_b/\rho}$ where τ_b is the bed stress and ρ is the density of seawater. The Law of the Wall makes the assumption that the vertical variation in velocity follows a logarithmic profile.

The three methods for estimating the bed stress at a given horizontal location are as follows:

1. Use a single value of u_z, the closest available to the seabed (*i.e.* that from the bottom layer of the model) which we shall call u_b:

$$\boldsymbol{\tau_b} = \rho c_f |\mathbf{u_b}| \mathbf{u_b} \tag{3.2}$$

   This has the advantage that a logarithmic profile is only assumed between this location and the seabed. It makes full use of the ability of a 3D model to predict different vertical velocity profiles at different locations and timesteps, which need not all be logarithmic above the bottom layer. A disadvantage is that, due to the use of sigma coordinates, the distance between the seabed and the centre of the bottom layer of the model varies from point to point and timestep to timestep, so a temporal or spatial comparison using this approach is not necessarily comparing like with like.

2. Use the depth-averaged velocity, using a formulation given by Soulsby (1997):

$$\boldsymbol{\tau_b} = \rho \mathbf{U} |\mathbf{U}| \left(\frac{0.4}{1 + \ln(z_0/h)} \right)^2 \tag{3.3}$$

   where $\mathbf{U}$ is the depth-averaged velocity and h is the water depth.

   This is the only approach available for 2D models, and for 3D models it avoids the difficulty of varying layer thicknesses, but it does assume a logarithmic vertical velocity profile throughout the water column.

3. The Law of the Wall can be rearranged into the form of an equation of a straight line: $u_z = \frac{u_*}{\kappa} \ln(z) - \frac{u_*}{\kappa} \ln(z_0)$ (note that u_* and z_0 are constant). Consequently u_*, and hence τ_b, can be estimated by plotting $\ln(z)$ against u_z and finding the gradient of the line of best fit. This method assumes a logarithmic vertical profile, but also offers a means of assessing the validity of this assumption by looking at the quality of the fit. Unlike the other two methods, it does not require knowledge of the roughness length z_0 (which is related to the intercept, rather than the gradient, of the line of best fit).

Method 3 is in some respects the ideal approach because it is a more direct application of the Law Of The Wall than the other methods, and because the calculation of bed stress does not depend upon knowing the roughness length (or bed resistance), which has been used as a tuning parameter in the model. The computational requirements of performing a least-squares fit for the vertical profile of every horizontal element at every timestep makes it impractical for use alone. However, a short 6 h set of outputs from each model was analysed this way, and used to inspect how good the correlation is between the vertical profiles in the model and a log curve in order to inform the level of confidence that could be invested in the other methods (Figure 3.2). This

correlation was good in all areas in MIKE 3, except near slack water when current speeds (and hence bed stress) are low. In Delft3D some areas deviated from a log curve, but the correlation was still good ($R^2 > 0.85$) in the areas of interest in, and close to, tidal energy sites.

Since the areas of interest in both models showed a close fit to a logarithmic profile, Method 2 was adopted for the remainder of this chapter. The formulation in (3.3) can be applied to the output from both models once z_0 is known, but the method for finding z_0 differs due to the different ways in which the models define bed resistance.

For the MIKE 3 model, where bed resistance is a constant quadratic drag coefficient c_f applied to the bottom layer,

$$z_0 = \frac{z_b}{\exp\left(\frac{\kappa}{\sqrt{c_f}}\right)} \tag{3.4}$$

where z_b is the distance from the seabed to the centre of the bottom layer.

Delft3D uses a Chezy value C_{3D}, defined as

$$C_{3D} = \frac{\sqrt{g}}{\kappa} \ln\left(1 + \frac{z_b}{z_0}\right) \tag{3.5}$$

$z0$ can therefore be found using

$$z_0 = \frac{z_b}{\exp\left(\frac{\kappa C_{3D}}{\sqrt{g}}\right) - 1} \tag{3.6}$$

3.3 Predictions without turbines

From two numerical models of the same region it is reasonable to expect similar results, and that can help to build confidence in the models' predictive power. However, some differences are also expected because of the use of different boundary forcing, different grids and bathymetries, different numerical methods, etc.

3.3.1 Method of comparison

Each model was run for a period of 32 days starting from 01/02/2012. Output from the first four days, based on empirical observations, was discarded to allow for model spinup, leaving 28 days of predictions for use.

The two models use different grids, so in order to do any quantative comparison it was

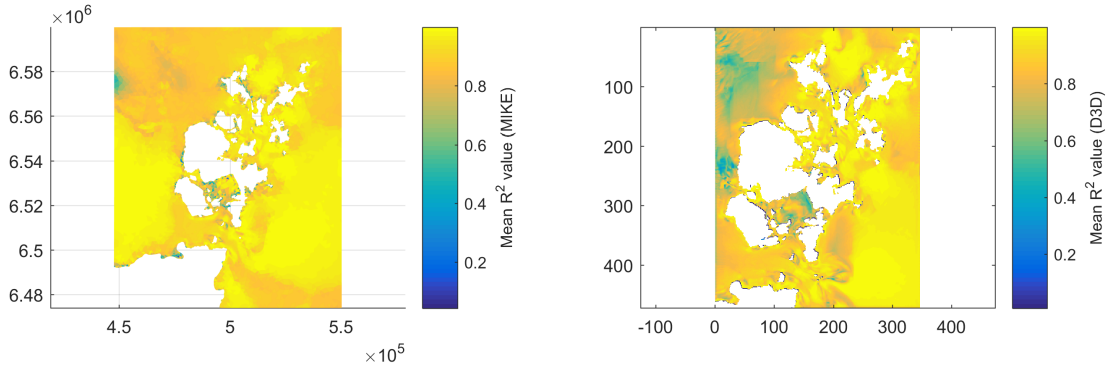

(a) **(b)**

Figure 3.2: *Maps showing the mean correlation over six hours between the vertical velocity profile and a logarithmic curve in each grid or mesh element in MIKE (a) and Delft3D (b).*

necessary to interpolate their outputs in the area of interest onto a common grid. A square grid (in UTM coordinates) was chosen with a resolution of 100×100 m, which is a higher resolution than either model's outputs, thus minimising loss of detail. Coordinate transform of the Delft3D data from lon/lat to UTM was performed using the MATLAB Mapping Toolbox, and interpolation of both data sets was completed using MATLAB's `scatteredInterpolant` function using the 'natural neighbour' technique*.

To compare the predictions of the models without turbines, the following plots and statistics were produced for each parameter of interest:

- False colour maps showing the mean value, over the full 28 days, in each grid or mesh element without interpolation. Presented side-by-side, these allow a qualitative comparison of the two models' predictions on their original meshes.
- Root mean square difference and mean difference between the models taken over similar maps (not shown) on the interpolated grid, to give a quantitative equivalent to this view.
- A scatter plot with MIKE values on one axis and Delft3D values on the other, with each point representing the predicted mean values for one cell on the interpolated grid. This provides an easy visual impression of the spatial correlation between the two models, and any difference in the magnitudes of their mean predictions.
- The R^2 correlation coefficient between the points in the scatter plot and the line of best fit, and the gradient of that line. This gives a quantitative backing to the correlation observed in the scatter plot, and puts a value to any scaling factor that is present between the two models: if the models match perfectly

*See Appendix B for a description of natural neighbour interpolation.

the gradient will be 1, but if one predicts higher values than the other then the gradient will show this.

3.3.2 Results

Comparison of the two models' predictions without turbines showed that they gave very similar spatial distributions of all the measured parameters, when viewed at a regional scale (Figure 3.3).

Mean depth-averaged speeds are very closely matched between the models. The interpolated scatter plot (Figure 3.4a) gives a line of best fit of gradient 0.97, which suggests that Delft3D tends to predict speeds 3% lower than MIKE 3.

Mean bottom speeds were slightly higher in Delft3D than in MIKE, maintaining the good correlation but with a gradient of 1.15.

Delft3D predicts dramatically lower mean bed stress magnitude than MIKE, with a gradient of 0.47, although once again the variation over the spatial domain is very similar.

3.3.3 Discussion

Some match in depth-averaged speeds between the two models is expected, because both were calibrated against the same measurements. However, this does not guarantee uniformity of their predictions away from the measurement locations, and so their agreement on the variation of depth-averaged current speed across the spatial domain is pleasing.

The small difference in bottom layer current speeds and the large difference in bed stress magnitudes are consistent with the fact that the MIKE model uses over twice the bed resistance of the Delft3D one. The scaling factor of 0.47 between MIKE and Delft3D's bed stress is consistent with the difference in bed resistance between the models and the small difference in depth averaged speed, using (3.3) and (3.4).

Some time was spent investigating this difference in bed stress, by use of the other two methods of calculating it discussed in Section 3.2. Using (3.2) to give $\tau_b \propto c_f u_b^2$, we can estimate that had bottom speed rather than depth-averaged speed been used to calculate bed stress, Delft3D would have approximately 0.53 times the bed stress of MIKE rather than 0.47. The curve fitting approach was used over a short 6 h period near springs*, and by this method Delft3D was estimated to have approximately

*6 h being the minimum period to include peak flow in both directions, although not a full semidiurnal cycle.

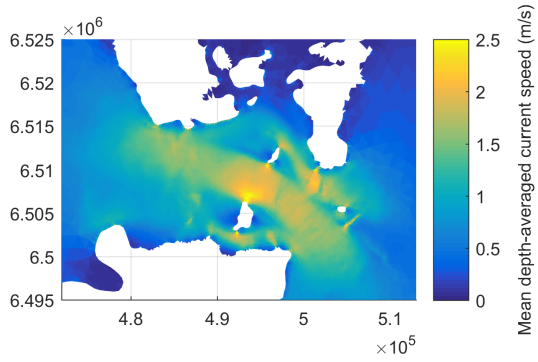

(a) *Depth-averaged current speed in MIKE 3*

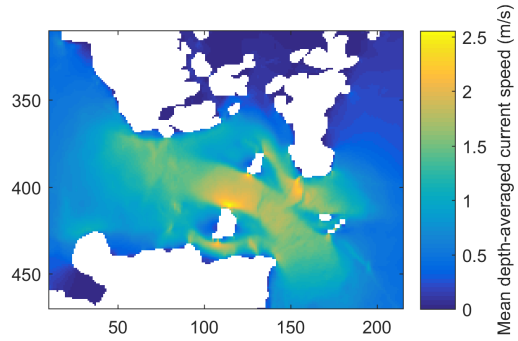

(b) *Depth-averaged current speed in Delft3D*

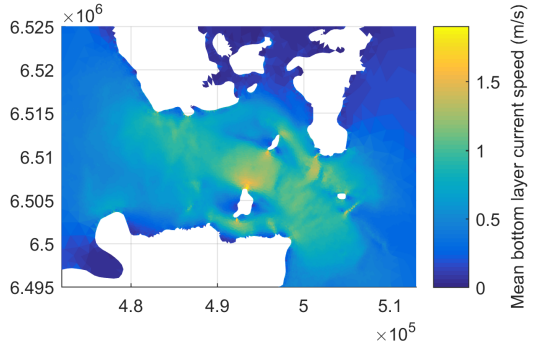

(c) *Bottom layer current speed in MIKE 3*

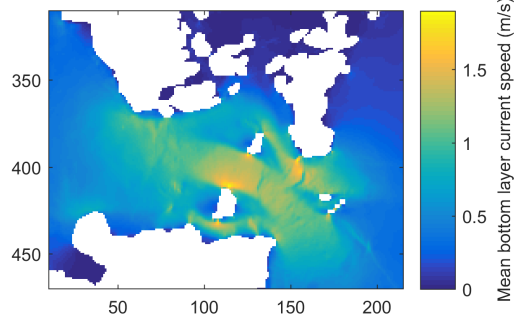

(d) *Bottom layer current speed in Delft3D*

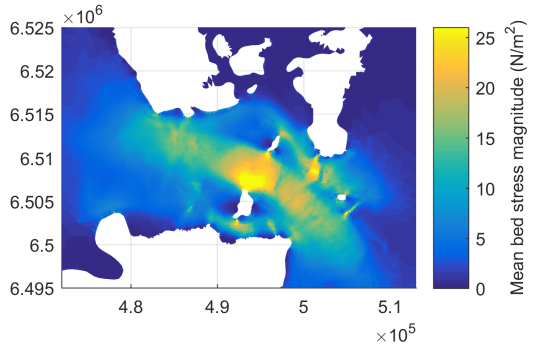

(e) *Mean bed stress magnitude in MIKE 3*

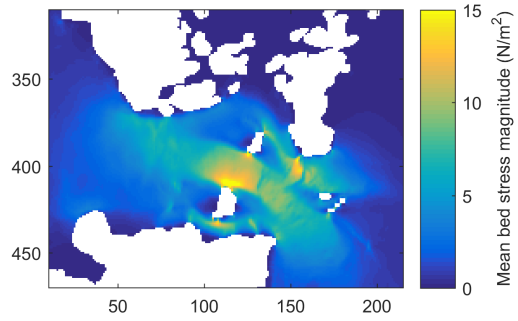

(f) *Mean bed stress magnitude in Delft3D*

Figure 3.3: *Comparison of mean depth-averaged current speed (magnitude), bottom layer current speed, and bed stress magnitude, over 28 days, predicted by the MIKE 3 and Delft3D models. Note the difference in colour scales between sub-figures (e) & (f).*

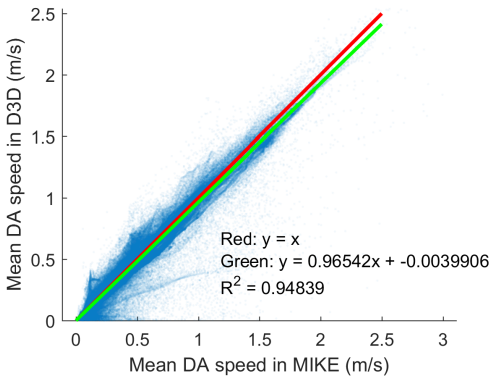

(a) *Depth-averaged current speed*

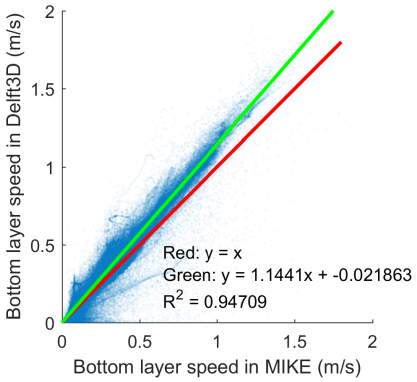

(b) *Bottom layer current speed*

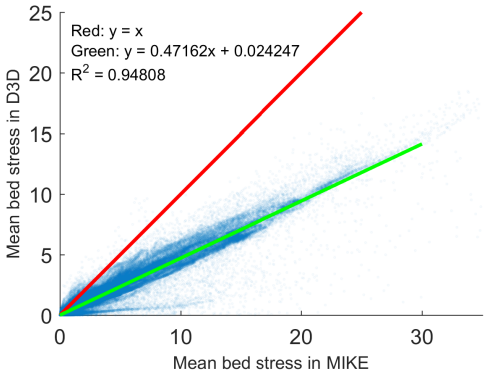

(c) *Bed stress magnitude*

Figure 3.4: *Scatter plots comparing mean predictions of three parameters, over 28 days, by the two models without turbines. Plots include points from the area covered by the inner domain of the Delft3D model. Points are partially transparent to emphasise regions of high point density. Red lines indicate 1:1 relationships, while green lines show lines of best fit.*

0.39 times the bed stress of MIKE (albeit with a poorer correlation than the other methods). See Figure 3.5 for detailed results of the curve-fitting test.

These results are close enough to reasonably conclude that the difference in bed stress in the models is "real" and not, for example, the result of an erroneous understanding of the input parameters. Both models produce vertical velocity profiles that follow a logarithmic curve, but that which emerges in Delft3D has a steeper gradient. Since the models have been calibrated to have equal depth-averaged speeds, this is consistent with the bottom layer speed being higher. However, if the bottom speed is 3% higher and the bed stress 47% lower in Delft3D, this implies 45% less energy dissipation in Delft3D*.

If MIKE is losing more energy while water flows through the channel at a similar speed, this would suggest that the change in surface elevation across the channel — the head, or potential, driving the flow — should be greater in MIKE in order to provide this energy. To investigate this, the amplitude of the difference in surface elevation between the ends of the Pentland Firth was "measured" over the same arbitrary 24-hour period in both models. The points used and the amplitudes found are shown in Table 3.1. This check showed that the Delft3D model has a driving amplitude of approximately 7% less than the MIKE model, which is too far from the 45% difference in energy dissipation to explain matters satisfactorily.

No further investigation was carried out on this discrepancy, but it remains troubling. Two factors may offer some explanation:

- As noted in Section 2.2.2, although a parameter that is tuned for calibration purposes nominally represents a particular physical variable — in this case bed resistance — it also implicitly represents the influence of all other effects that are not captured by the model, as well as errors that are introduced in the modelling process. While the physical scenarios represented by these two models are very similar, they do use different numerical methods, different meshes/grids and discretization approaches. One might, therefore, expect some small variation in the value of "bed resistance" that must be used to achieve the same results in flow rates.

- It is possible that one or both of the models was not perfectly calibrated. As noted at the start of the chapter, these models were calibrated by others, independently and (importantly) using different measurement locations (see Waldman, Bastón *et al.* (2017) for more detail). An example calibration, by me, of a MIKE model is described in Appendix A. The parameter controlled there is k_s rather than the drag coefficient c_f, but if one performs a conversion based on a typical 50 m depth, the range of values tested corresponds to more

*$1.03 \times 0.53 = 0.55$

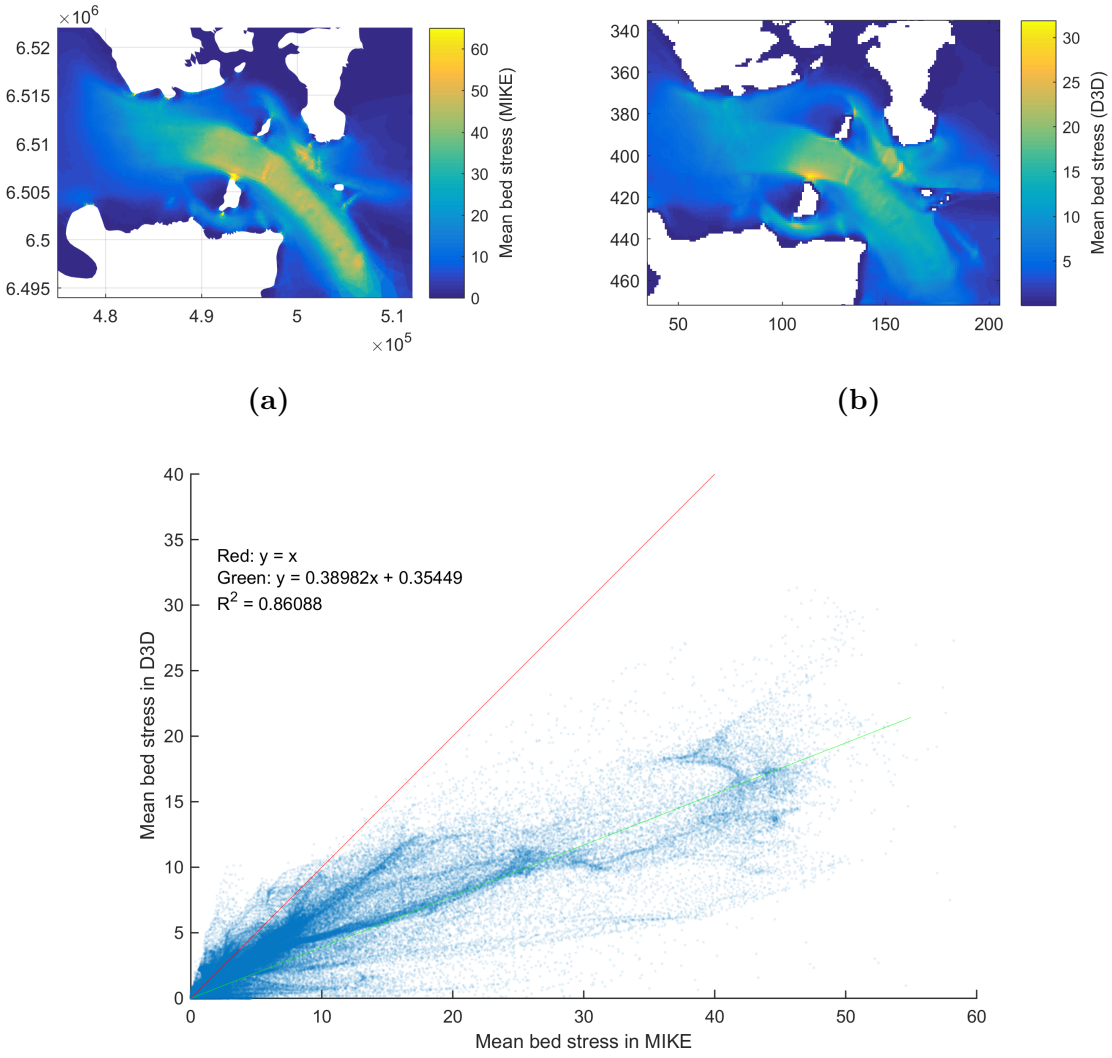

Figure 3.5: *Estimates of mean bed stress from a 6 hour period by curve fitting from MIKE 3 (a) and Delft3D (b), and element-by-element comparison of them on the whole of the common interpolated grid (c). Note the different colour scales in (a) & (b).*

than factor of 2 in c_f (*i.e.* more than the difference between the two models in this chapter), and the change in peak current speeds is only approx. $0.5\,\mathrm{m\,s^{-1}}$. In other words, flow speed is rather insensitive to bed stress.

We can conclude from the latter point that adjusting the bed resistance to match a flow speed to measurements is a poor method for determining bed resistance. Finding a method for measuring bed resistance or for estimating it from known factors, such as bathymetry, may be an important topic for future research.

3.4 Implementation of energy extraction

In both models, energy was extracted based on designated locations of individual TECs — although neither model had the resolution to resolve the actual devices. This was thought to represent an approach that could be readily adopted by site developers, who would know the specifications for their turbine and have a proposed layout. Since no real turbine or proposed layout existed for this project, it was necessary to arrive at plausible examples.

In February 2014, Marine Scotland Science held a workshop for wave and tidal developers under the Chatham House rule*, in which the parameters for a suitable generic TEC were discussed. By liaising with device developers following this event, parameters were agreed for a generic device that was acceptable to all concerned as being appropriate for use in the Pentland Firth, yet not infringing on commercial confidentiality. The agreed parameters are shown in Table 3.2 and Figure 3.6.

Example layouts for TEC arrays within five Crown Estate round 1 lease zones (see Figure 3.7), containing a total of 1000 rotors, were developed by Marine Scotland Science based on Environmental Statements submitted by developers. For details of their methodology, see O'Hara Murray (2015). The layouts were provided as lists of

*The Chatham House rule states that those present at a discussion may relate what was said, but not who said it.

	MIKE 3	Delft3D
Western point	(479257, 6510323)	(-3.335936, 58.73007)
Eastern point	(501747, 6502651)	(-2.970657, 58.66363)
Amplitude	1.375 m	1.283 m

Table 3.1: *Table showing "measurement" of the driving amplitude across the Pentland Firth in both models, without TECs. The western point is situated approximately half way between Dunnet Head and the south-western coast of Hoy. The eastern point is approximately half way between Duncansby Head and the Pentland Skerries. MIKE 3 coordinates are given in UTM30, and Delft3D ones as lon/lat.*

Device type	Unducted horizontal axis turbine.
Rotor diameter	20.0 m
Cut-in speed	$1.0\,\mathrm{m\,s^{-1}}$
Cut-out speed	$4.0\,\mathrm{m\,s^{-1}}$
Rated speed	$2.5\,\mathrm{m\,s^{-1}}$
Thrust curve	$C_T = 0.85$ from cut-in to rated speed, decreasing above this so as to maintain constant power.
Supporting structure	Monopile of 2.5 m diameter

Table 3.2: *Parameters for a generic TEC, as agreed with stakeholders. See Figure 3.6 for the agreed thrust curve.*

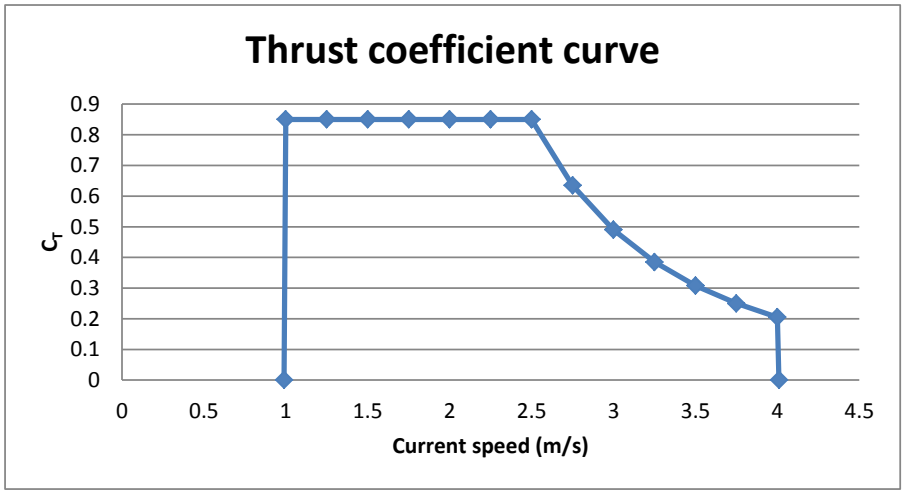

Figure 3.6: *Thrust curve for the generic TEC, as agreed with stakeholders. Strictly speaking, although the thrust would be minimised outside the operating range, it would not be zero, due to drag from the stationary rotor.*

coordinates in text files, with information on the distance above the seabed at which the rotors should be positioned. An example layout may be seen in Figure 3.8.

A brief investigation was made into the frequency distribution of tidal speeds and directions in each of the sites, based on the depth-averaged predictions of the MIKE 3 model. Tidal roses showing the outcome of this work may be seen in Figure 3.9. Note that while Westray South and Cantick Head have flows that reverse direction by 180° as the tide changes, the other sites have more complex cycles where the direction of the ebb does not exactly reciprocate that of the flood. Detailed examination of MIKE's predictions for the Brough Ness site indicated that parts of the zone, including the point from which the rose was generated, are affected by an eddy that causes them to experience strong tidal flow in only one direction. In a commercial situation, it is unlikely that TECs would be placed in this location.

3.4.1 Implementation of turbines in MIKE 3

Information below on the MIKE software is derived from the software's manual (DHI, 2012c) and scientific documentation (DHI, 2012a) and from personal communications with representatives of DHI. Except where information comes from a different source to these, detailed referencing has been omitted in the interests of readability.

The MIKE Hydrodynamic module allows the user to incorporate a number of sub-grid structures in the model, and one of the pre-defined types is "turbine". This option provides a basic actuator disc implementation of a horizontal axis tidal turbine, allowing the user to specify,

- Horizontal location of the turbine.
- Vertical position of the centre of the turbine, as an absolute elevation. There is no provision for relating this to water level, so floating turbines would be difficult to represent accurately.
- Horizontal orientation of the turbine (*i.e.* its heading).
- Diameter of the rotor.
- A lookup table of "lift" and "drag" coefficients representing the components of the force exerted by the turbine that are parallel and orthogonal to the flow, respectively. These vary according to the current speed at the turbine and the angle between the axis of the rotor and the flow direction, as per Figure 3.10. For conditions in-between those specified in the table, linear interpolation is used. For conditions outside those specified, there is no extrapolation — instead, the nearest value is used. This allows for cut-in and cut-out speeds.

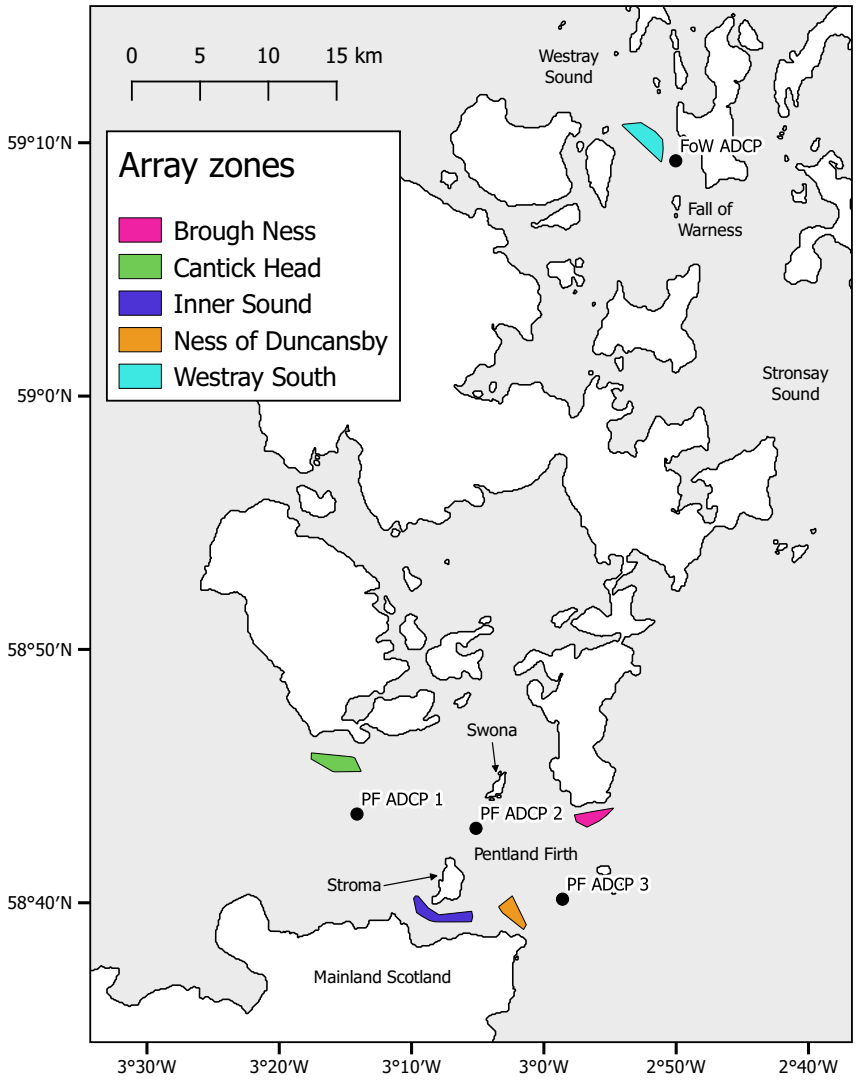

Figure 3.7: *Map showing part of the Pentland Firth and Orkney Waters. Black points show the locations of the five ADCPs used for calibration & validation: three in the centre of the Pentland Firth (labelled PF), one in the Inner Sound (labelled IS) and one in the Fall of Warness (labelled FoW). Coloured polygons show the areas in which tidal turbines were simulated.*

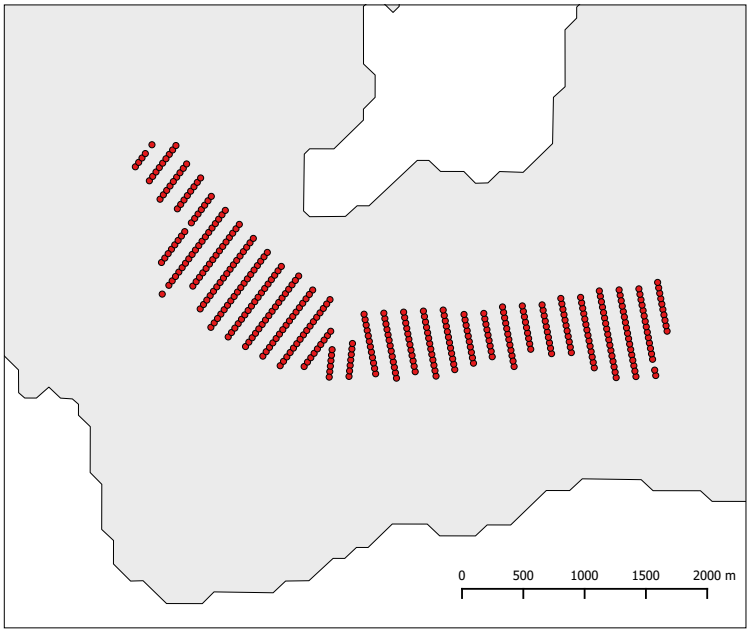

Figure 3.8: *Map showing the array layout provided for the Inner Sound zone, showing 400 TECs. Each red dot represents one device.*

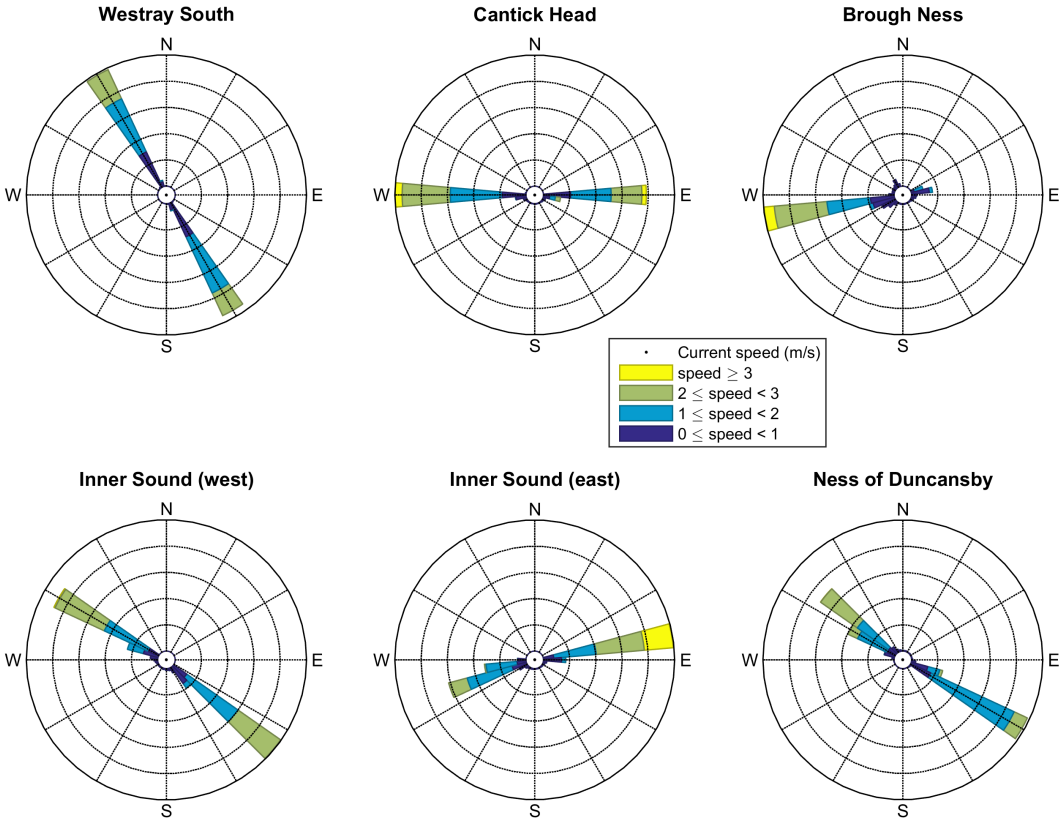

Figure 3.9: *Tidal roses as predicted by the MIKE model from the central areas of the arrays, using depth-averaged velocities over 28 days. The distance that sectors extend from the centre of each circle indicates the frequency of flow in that direction, while colours indicate the distribution of current speed in that direction. Two roses are shown for the Inner Sound array as there is a significant change in the flow direction within the exploited area.*

The drag and lift forces are calculated as follows:

$$F_D = \frac{1}{2}\rho\alpha C_D A_e u^2 \tag{3.7}$$

$$F_L = \frac{1}{2}\rho\alpha C_L A_e u^2 \tag{3.8}$$

where F_D and F_L are the forces parallel and orthogonal to the flow direction respectively, ρ is the density of water, C_D and C_L are the drag and lift coefficients, A_e is the 'effective area' of the rotor (after any angle between the turbine axis and the flow is taken into account), u is the current speed, and α is an arbitrary user-specified coefficient that defaults to 1.

The current speed used to look up the lift and drag coefficients, and thence to calculate the force applied, is the mean speed from all the layers that are intersected by the turbine; vertical shear over the turbine's disc is neglected. Similarly, the force applied by the turbine is equally distributed between all vertical layers that intersect the rotor, taking no account of differences in the area of the rotor that is in each layer.

These existing facilities were used to implement the agreed TECs. It was assumed that the turbines would rotate to face the flow (sometimes known as "weathervaning"). This was achieved by setting the lift and drag coefficents to the same values for every angle of incidence (see Figure 3.10). This allowed a single axial thrust coefficient to be used instead of lift and drag; *i.e.* $C_D = C_T$ and $C_L = 0$.

The supporting monopiles were included by use of MIKE's "pier" structure type. This facility is intended for modelling of bridge piers, but they can be specified as finishing short of the water's surface, and hence effectively emulate monopiles. Circular piles were inserted at the TEC locations, extending from the seabed to the hub height of the turbines.

The MIKE GUI requires all of the parameters that are used to define a turbine or a pier to be entered for each turbine, which is impractical when a thousand rotors are to be included. Consequently, a MATLAB script was produced to read coordinates from a text file and insert turbines with specified parameters at those locations in a MIKE model by modifying the model definition file. This script is publicly available (see Section 3.7).

3.4.2 Implementation of turbines in Delft3D

Unlike MIKE 3, the current version of Delft3D does not have any dedicated provision for tidal turbines built in. Other studies have modified its code to incorporate TECs as momentum sinks (*e.g.* Ramos *et al.*, 2013) in a similar manner to MIKE's

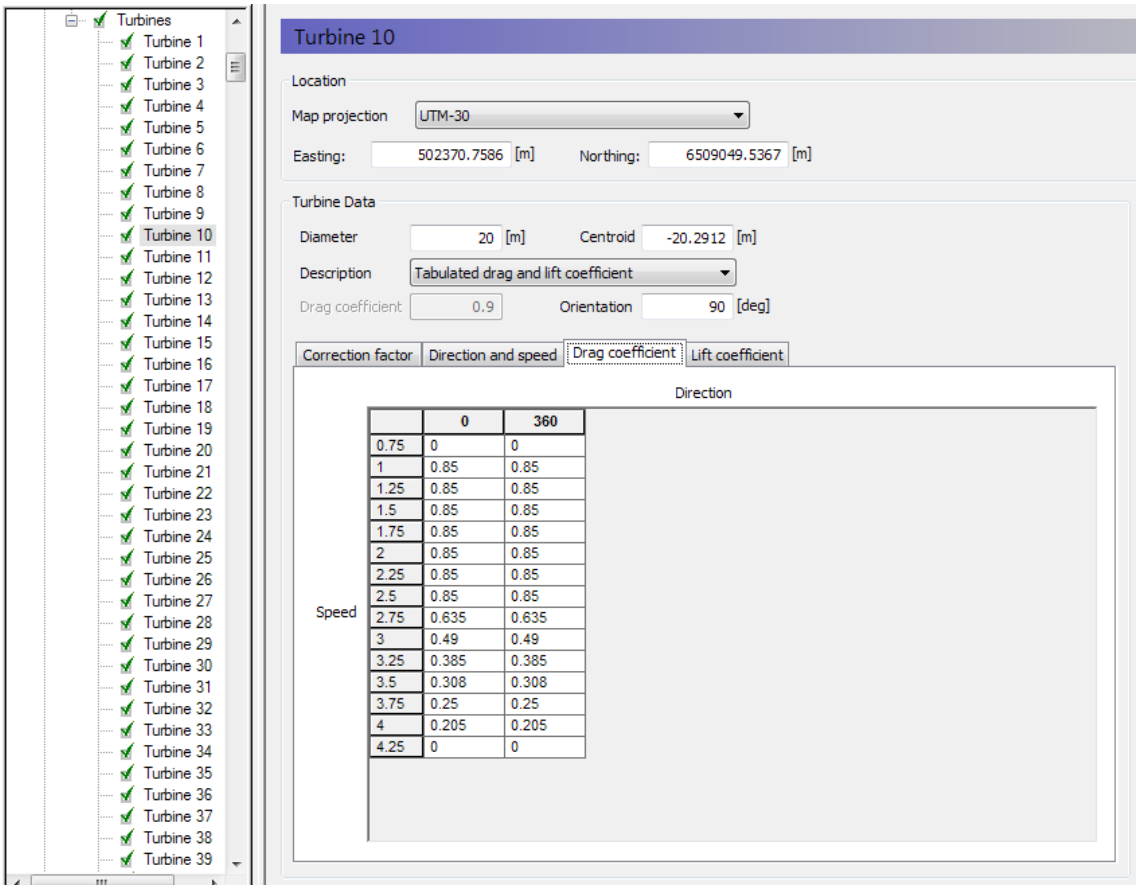

Figure 3.10: *Thrust curve for a weathervaning turbine entered in the MIKE GUI.*

implementation, and this approach would be preferable, but for the TeraWatt project a restriction was introduced to use unmodified commercial software (see Section 1.3.2). Consequently, this work focused on incorporating TECs into Delft3D as well as could be accomplished using the unmodified code.

Delft3D includes a built-in hydraulic structure called a 'porous plate'. Porous plates apply a retarding force on the flow based on a parameter c_{loss}, a quadratic drag coefficient which is applied to the layers that the plate occupies. The approach adopted was to calculate the equivalent porous plates to represent tidal turbines. The porous plates for an example TEC array are shown in Figure 3.11b.

Theory for determining c_{loss}

From the Delft3D manual (Deltares, 2014), equation 10.87 (shown as scalars for simplicity) describes a porous plate aligned with the y-axis (so affecting flow in an east-west direction):

$$M = \frac{c_{loss\text{-}u}}{\Delta x} u^2 \tag{3.9}$$

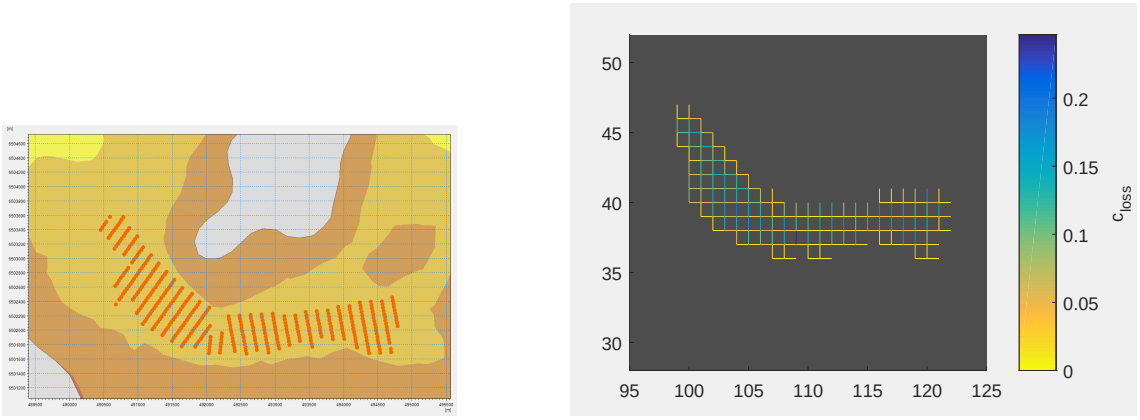

(a) **(b)**

Figure 3.11: *(a) 400 turbines in the Inner Sound, viewed through the MIKE GUI; (b) The same 400 turbines represented as porous plates for Delft3D. Higher values of the c_{loss} parameter, shown by bluer colours, indicate plates with higher drag.*

where M is the change of momentum per second per unit mass, Δx is the x-dimension of the cell, and u is the current speed.

Assuming for now a 2D model, the drag force of N turbines is the sum of thier individual drag forces:

$$F = N\frac{1}{2}C_D\rho A_t u^2 \tag{3.10}$$

where A_t is the area of a single turbine rotor.

Force is equal to change in momentum per second, while (3.9) refers to change in momentum per second per unit mass. Therefore, by dividing (3.10) by the mass of one grid cell we can equate the two:

$$M = \frac{c_{loss\text{-}u}}{\Delta x}u^2 = \frac{N\frac{1}{2}C_D\rho A_t u^2}{\rho \Delta x \Delta y h} \tag{3.11}$$

where h is the water depth. Cancelling,

$$c_{loss} = \frac{C_D N A_t}{2\Delta y h} \tag{3.12}$$

which allows the calculation of c_{loss} from known quantities.

Practical implementation

This approach was implemented in a MATLAB script (publicly available, see Section 3.7) which reads a set of turbine information and the model grid, and outputs a set of porous plate specifications in Delft3D's "PPL" format. Two elaborations are required upon the theoretical approach above: firstly, accounting for flow directions

that are not along a grid axis, and secondly, for turbines that occupy more than one vertical layer in the 3D model.

Delft3D requires that porous plates align with grid axes, or are at exactly 45° to them. In order to be able to represent turbines at arbitrary angles, two porous plates were inserted at right angles for each cell containing one or more turbines, and the required force decomposed into components parallel to the grid axes. Instead of using an area per turbine and the number of turbines, as in (3.12), we calculate the total effective area of rotor, from all the turbines in that cell, that is "visible" when viewed along the relevant grid axis. See Figure 3.12 for an illustration.

Delft3D requires a constant c_{loss} value for each porous plate (*i.e.* it cannot vary with time). C_D was therefore set equal to the value at the turbine's rated velocity, in this case 0.85.

The immutability of porous plates, combined with the approach of using two plates at right angles to represent arbitrarily-angled turbines, means that the orientation of the turbines must remain fixed throughout the model run. It is therefore not possible to accurately model weathervaning (yawing) machines. In commercial use, a site developer using fixed-angle turbines would supply the modeller with device orientations as well as positions. For the purposes of this work, the orientation of each turbine was determined by aligning it with the direction from which the highest undisturbed speed in a month was predicted. A more sophisticated approach would be to use the direction from which the greatest total power was received over that period.

In a 3D Delft3D model, a porous plate must occupy a whole number of vertical layers. Because the position of the plate is specified in terms of sigma layers, and cannot change which layers it occupies between timesteps, the rotor will effectively move up and down and expand and contract as the water depth changes through the tidal cycle. This is a limitation to this approach for incorporating energy extraction. In this implementation, the layers occupied by the rotor are determined from the mean elevations of the layers.

Thus for the u direction (parallel to the x-axis),

$$c_{loss\text{-}u} = \frac{C_D A_u / n}{2\Delta y \Delta z} \tag{3.13}$$

where n is the number of layers that the porous plate intersects, Δz is the vertical height of a layer, and

$$A_u = \sum A_t |\sin\theta| \tag{3.14}$$

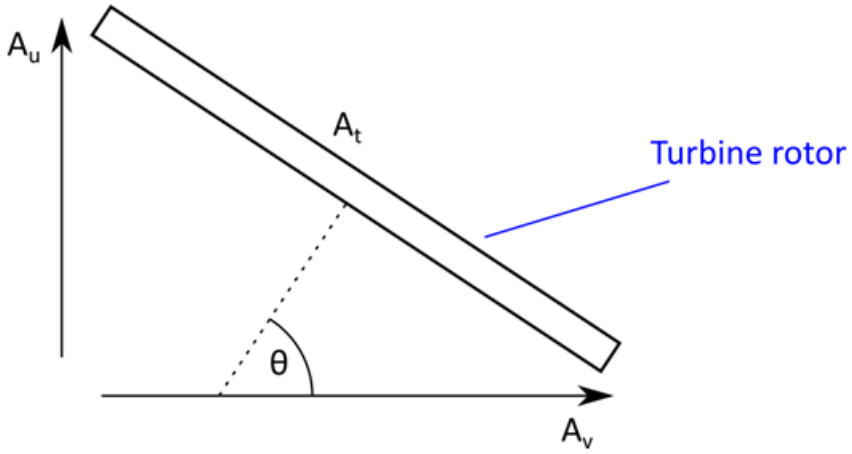

Figure 3.12: *Calculation of components of rotor area for each cell. The rotor has area A_t with an arbitrary angle θ between the x-axis and the axis of the turbine. The area A_u represents the total area of rotor that is represented by the porous plate aligned perpendicular to the x-axis (i.e. impeding flow in the u direction). The area A_v represents the total area of rotor that is represented by the porous plate aligned perpendicular to the y-axis.*

where θ is the angle between the u direction and the turbine's axis and the summation is over all turbines in that cell. Similarly for the v direction,

$$c_{loss\text{-}v} = \frac{C_D A_v / n}{2\Delta y \Delta z} \tag{3.15}$$

$$A_v = \sum A_t |\cos\theta| \tag{3.16}$$

Supporting structures were not included in the Delft3D model. It would be possible to make some approximation to their effects by increasing C_D by an appropriate amount, but is not clear how this amount should be calculated.

3.4.3 Discussion

There are some differences between the implementations of TECs in the two models that should be highlighted from the sections above. A number of these stem from limitations in using porous plates to represent TECs in Delft3D. In some cases the MIKE model could have been designed to have the same limitations as the Delft3D one, but the approach taken was to create the best possible representation using each code, as would be done in a commercial setting, rather than to limit one to match the other.

- Both models use sigma layers in the vertical, which move and expand and contract as the water level rises and falls. TEC elevations are fixed, and do not move with the layers (disregarding floating turbines, which would move

differently to sigma layers). MIKE recalculates the vertical position of its turbines on every time step, changing which model layers they fall within to maintain the correct absolute elevation. Delft3D requires porous plates to be fixed with respect to its sigma layers, and the plates therefore rise and fall, and change height, over time. This is unrealistic for TECs, and is a limitation of using porous plates to represent tidal energy extraction in Delft3D.

- When turbines were inserted into the MIKE model, it was assumed that they would "weathervane", or yaw to face the oncoming current at any given moment. In Delft3D, TEC orientation must be fixed.
- MIKE allows the thrust coefficient to be a function of the current speed. The porous plate approach in Delft3D requires that it is constant. As shown by Easton and Woolf (2013), modelling a realistic thrust curve makes a significant difference to simulated TEC performance. This is a further limitation of the porous plate approach to energy extraction.
- In MIKE, supporting structures were included. In Delft3D they were not.

3.5 Predictions of effects of energy extraction

In order to show the effects of energy extraction, each model was run with and without turbines present. The predictions with turbines were subtracted from those without on a per-element, per-timestep basis, to produce maps of the mean changes that result.

The same general features are present in the predicted effects on depth-averaged current speed from both models (Figures 3.13a & 3.13b): both show decreases in average speed in line with TEC arrays, and increases to either side. These effects are particularly strong in the Inner Sound, where the concentration of turbines is greatest and where the flow is tightly constrained by land boundaries on either side. Speeds in regions of the Pentland Firth distant from energy extraction are affected slightly ($< 0.1\,\mathrm{m\,s^{-1}}$), but in some areas the models disagree on whether this is a slight increase or a slight decrease.

At all of the energy extraction sites (including Westray South, not shown in plots) the magnitude of the effect of energy extraction is slightly greater in Delft3D than MIKE. In regions distant from energy extraction, the general effects on the flow are also greater in Delft3D. In the Inner Sound there are minor differences in the spatial distributions of the predicted effects.

The models predict similar effects on bottom layer current speed as on depth averaged

current speed, although slightly smaller in magnitude (Figures 3.13c & 3.13d).

Because of the large difference in the level of bed stress predicted by each model, there is little benefit in using the absolute changes with energy extraction as a comparison. Figure 3.14 compares the effect of adding TECs on bed stress as a proportion of the bed stress without TECs, calculated on a per-timestep basis and then averaged over 28 days. When viewed in this way, the spatial distribution of effects is similar to that for depth-averaged speed and the (proportional) magnitude of them is similar between the two models. Note that increases in bed stress are greater in magnitude than decreases. The proportional changes in bed stress that are predicted are substantial, with decreases of 45% and increases of 100% in some areas.

3.5.1 Discussion

The greater magnitude of the effect of energy extraction in Delft3D is consistent with the lower bed resistance in this model. Thanks to the lower natural resistance in the channel, the additional resistance of the TECs is a greater proportionate change to the overall impedance in that area.

In the western part of the Inner Sound, both models predict eddies at a scale which can only just be resolved by the meshes used. It is possible, therefore, that the different computational meshes and the different numerical methods in the two models are predicting these eddys in slightly different locations, such that they affect the turbines differently in the two models. This might explain the small differences in the locations of effects. Without any velocity measurements in these areas (or without a higher-resolution local study), it is not possible to know which model provides the better predictions.

The fact that increases in speed lead to larger changes in bed stress than decreases do is expected, and relates to the square relationship between the two parameters (the difference between x^2 and $(x+1)^2$ being greater than that between x^2 and $(x-1)^2$, for positive x). One implication of this is that the areas that experience the greatest change in bed stress (and associated environmental impact) due to energy extraction may not be the regions in line with the turbines, where the effect on speed is the strongest, but the areas to either side where flow is accelerated.

It is noteworthy that although the absolute values predicted for bed stress vary greatly between the two models, because of the different levels of bed resistance, their proportional changes with the addition of energy extraction are remarkably consistent. In the absence of measurements of bed resistance or bed stress (or the detailed velocity and surface elevation records that would be needed to empirically estimate them) it

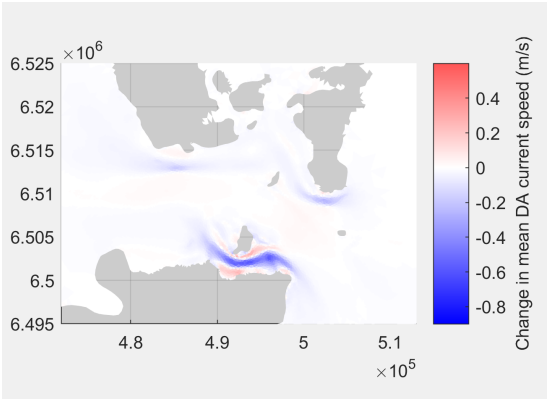

(a) *Depth-averaged current speed in MIKE*

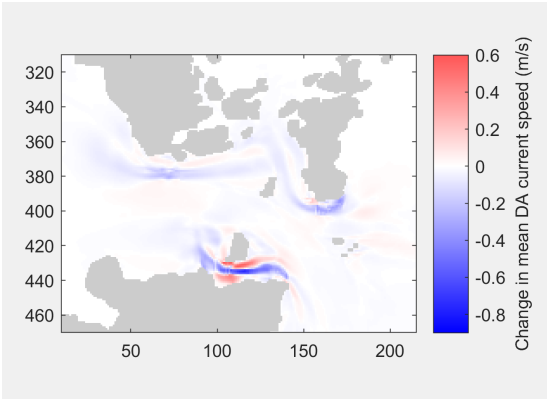

(b) *Depth-averaged current speed in Delft3D*

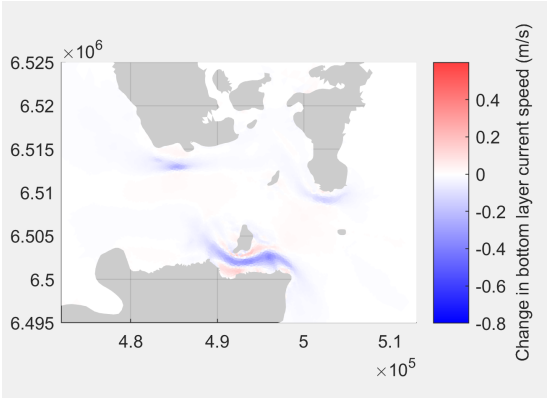

(c) *Bottom layer current speed in MIKE*

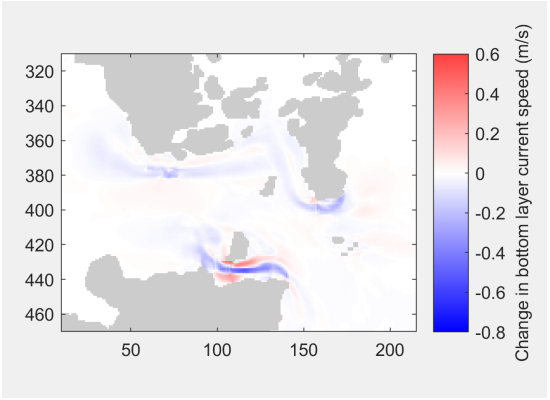

(d) *Bottom layer current speed in Delft3D*

Figure 3.13: *Changes in mean current speeds over 28 days as a result of adding turbines. See Fig. 3.7 for locations of energy extraction.*

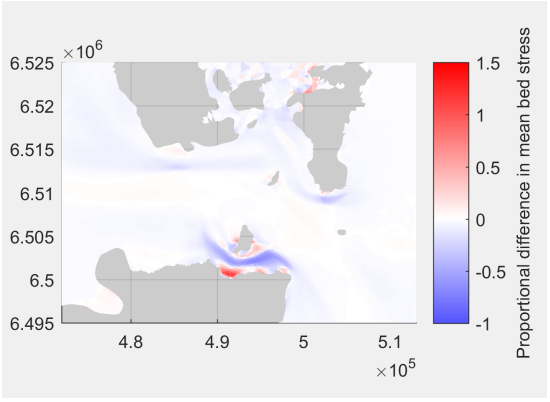

(a) *MIKE*

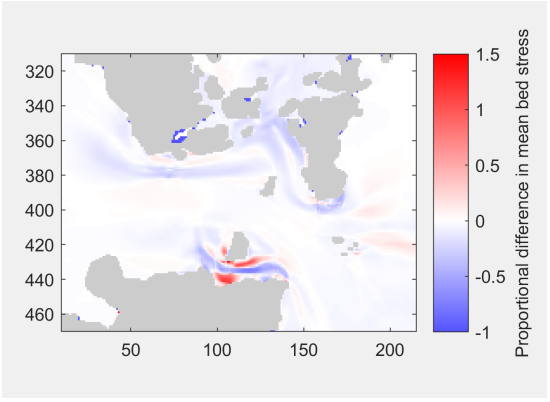

(b) *Delft3D*

Figure 3.14: *Change in mean bed stress magnitude over 28 days as a result of adding turbines, expressed as a proportion of the value without turbines. See Fig. 3.7 for locations of energy extraction.*

is not possible to make any assertion as to which, if either, model is closer to the true values. However, for many purposes it will suffice to understand which regions of the model will experience the greatest changes, and for that information the consistency between the models allows us some confidence.

Upstream velocity

To be strictly correct in calculating the thrust in MIKE, or c_{loss} in Delft3D, one should bear in mind the difference between the free-stream velocity when the flow is unaffected by energy extraction (u in (3.10)), and the velocity at the porous plate (u in (3.9)). With this consideration, (3.12) becomes

$$c_{loss} = \frac{C_D N A_t}{2\Delta y h} \cdot \frac{u_{fs}^2}{u_{cell}^2} \tag{3.17}$$

where u_{fs} is the free-stream velocity and u_{cell} is the cell velocity. This correction has not been used in this chapter's work with Delft3D, and is also not allowed for by the version of the MIKE software used. It will be discussed in detail, in the context of MIKE 3, in the next chapter. The uncorrected predictions of the effects of turbines given here are likely to be slight underestimates.

3.6 Further discussion & chapter conclusions

For discussion of the results of these specific models without and with turbines, see Sections 3.3.3 and 3.5.1 respectively. The aim of this work was not to develop the best possible tidal energy extraction models of the region of interest, but to determine how to best use existing industry-standard tools for this purpose, given their capabilities and limitations. Therefore, the emphasis of this final section is not on the specific models that were developed, but on observations of a broader scope.

3.6.1 Observations on model capabilities

Based on the work presented here, both MIKE 3 and Delft3D are suitable for modelling channels with strong currents at a regional scale, and for predicting the regional effects of energy extraction. These models cannot offer certainty regarding effects at specific locations at a scale that is similar to the resolution of the grid. For applications where such predictions are important, validation data should be

collected at the points of interest. In some cases, the use of a finer-scale model (backed up by this data) may be warranted.

At the time that this work was carried out, it is clear that MIKE 3 offered superior facilities for representing horizontal-axis tidal turbines. The porous plate approach used in Delft3D has been shown to be a good approximation, but requires that turbines are represented with a constant thrust coefficient and constant orientation, and causes their vertical position to vary over time in an unrealistic way. Both DHI and Deltares have recently released new versions of their respective software suites, and it is believed that the new version of Delft3D offers a dedicated tidal turbine module. No evaluation of these new versions has been attempted here.

For some users it will be notable that MIKE is a commercial software pack- age that must be licensed at considerable cost, while Delft3D is open source and available without payment. However, given the the perception of open source software mentioned in Section 1.3.2, if a user is aiming to satisfy an investor that the model code is trustworthy it is probable that they will use the commercial version of Delft3D, which attracts a license fee. This version uses the same underlying model code as the open source one, but benefits from the full support of Deltares.

Both models, operating as they do at a regional scale where the turbine is unresolved, can only deal in terms of the power removed from the flow by TECs. This will be greater than the power available for conversion to electricity, due to energy that is lost in mixing turbulence between the turbine wakes and the surrounding flow (Vennell, 2010). The power removed from the flow is the correct quantity to study when interested in environmental impacts, but it is interesting to note this discrepancy between the quantity being studied and the quantity that is controlled by the consenting process.

3.6.2 Observations on model performance & methods

Following calibration the two models made very similar predictions of current speed across all areas of the domain (including those not used for calibration), with an R^2 value of 0.95 when comparing the two models' predictions at each point of a common interpolated grid, and a ratio of Delft3D predictions to MIKE 3 predictions of 0.97 (see Figure 3.4). This suggests that we can have some confidence in the models' predictions of current speeds without energy extraction.

Achieving this calibration required the seabed resistance, which was used as a tuning parameter, to be set to markedly different values in the two models. This resulted in the prediction of different values for bed stress, although these values were highly correlated between the models due to similarity in their spatial distributions. This

finding underlines the importance of developing means of setting model bed resistance values from theory or measurement, rather than using it as an empirical tuning parameter, and this could be a focus for future work. In the meantime, models of this type should only be used for *relative* comparisons of bed stress (in this case, with and without turbines) and not as a means of estimating the absolute values.

The models predict broadly similar effects from energy extraction, and it is reasonable to conclude that their results may be used to inform policy as to regional-scale effects. There is some small disagreement on the magnitude of the effects on velocities, which is likely to be largely due to the difference in bed resistance mentioned above. There are minor differences in the models' predictions at a finer scale, which indicate that a model of this type should not be used for studying the effects of turbines within an array or at specific fine-scale locations elsewhere. In the case of changes in bed stress, where different absolute magnitudes are predicted, the spatial variation — which was the primary measure of interest for the prediction of environmental impact within the TeraWatt project — was similar between the models.

It is noteworthy that, because of the square relationship between velocity and bed stress — which means that increases in velocity have a stronger effect on bed stress than decreases do — the greatest changes in bed stress in this example scenario occur not in the immediate vicinity of any TEC array but to either side of one, where the flow is accelerated. This finding may be of relevance when considering the morphodynamic or ecological effects of energy extraction, for example in environmental impact assessments for tidal energy developments.

3.7 Source code availability

The MATLAB scripts for the insertion of tidal turbines into MIKE 3 models and for automating the calculation of equivalent porous plates in Delft3D models are publicly available at `https://github.com/TeraWatt-EcoWatt2050`.

Chapter 4

Correcting for the difference between free-stream and cell velocity

Historically, regional hydrodynamic models have used cell sizes that are much larger than the diameter of a tidal turbine. In recent years, for applications related to tidal energy, the resolution of these models has increased such that the cross-sectional area of a cell in the model approaches that of a turbine rotor (*e.g.* Ramos *et al.*, 2014; Martin-Short *et al.*, 2015). This increase in resolution is desirable as it permits more accurate representation of a channel and/or turbine array, which can make a significant difference to predicted current speeds (Culina and Karsten, 2011).

While studying the means by which tidal turbines are represented in regional scale models, it became clear that a mesh dependency in the calculation of thrust ought to exist when the scale of a model cell approaches the scale of a turbine. This error is unusual in that it becomes more severe as the resolution increases, which is the reverse of most inaccuracies in discretized models. Correcting for it improves the accuracy of the representation of tidal energy extraction in models of this type, and allows further improvements by permitting higher resolutions to be used without difficulty.

In this chapter the cause of the error will initially be explained in intuitive terms, and then demonstrated through a series of simple MIKE 3 models. Following this demonstration a correction will be derived from theory, and then its implementation for MIKE and MATLAB will be related in stages, starting with a very simple correction and then allowing for more of the variables that would be encountered in a real-world model. While testing was performed at each stage of this work, lastly overall testing in a taxing model will be documented.

A simplifying assumption will be made that the tidal turbines being considered are yawing types that are always aligned with the flow. This is realistic for some, but not all, of the technologies currently being developed.

A note on timing and originality

I had identified that the mesh dependency detailed here should exist, and that a correction should be possible through actuator disc theory, by the time that Kramer *et al.* (2014) was presented at the EIMR conference, relating work by a team at Imperial College. This demonstrated the error and gave a formula for the correction in two dimensions, but gave no information on the derivation for the correction or its implementation. Consequently, having derived the formula to my own satisfaction, I shifted the focus of my work to implementing this correction for MIKE users so as to make it useful for "real world" modelling.

Waldman *et al.* (2015) presented a basic working implementation, adapted for a three-dimensional model and a triangular mesh. This peer-reviewed conference paper was accepted prior to the availability of Kramer and Piggott (2016), which covers similar ground in more detail, on the arXiv preprint server. The remaining work in this chapter, which covers implementation details, has little in common with the work of the team at Imperial College.

In this chapter, therefore, the reasoning behind the error (Section 4.1) and the derivation of the correction (Section 4.3), although not the form of the correction itself, were arrived at independently. The implementation (Section 4.4 onwards) is original and novel to the best of my knowledge.

A draft of Waldman *et al.* (2015) was sent to DHI prior to publication, and this may have contributed to their decision to build a correction of this form into the 2016 edition of the MIKE software — although it is Kramer *et al.* (2014) that is cited in the user manual.

4.1 Explaining the error

MIKE 3's built-in Turbine module represents a tidal turbine as a sub-grid object. It calculates the retarding force that is exerted on the flow as a function of the flow velocity, the turbine's thrust coefficient, and the area of the rotor:

$$F = \frac{1}{2}\rho\alpha C_T A u^2 \tag{4.1}$$

where ρ is the density of the water, C_T is the thrust coefficient, A is the area of the rotor, u is the flow speed and α is a user-defined coefficient that is equal to 1 by default (simplified from DHI (2012c), assuming that the turbine is aligned with the flow).

As water approaches a tidal turbine, it slows from its "free stream" velocity u_0 to that at the turbine, u_t. By convention, and as specified in standards documents (IEC, 2013), the thrust coefficient is defined in terms of the free-stream velocity u_0. It is, therefore, u_0 that should be used in (4.1). However, the free stream velocity is not known in the model. The only velocity available is u_{cell}, representing the whole of the cell that contains the turbine, and so this is what is used in (4.1) to calculate the thrust.

When the model cell is large compared to the turbine, most of its cross-section is unobstructed and $u_{cell} \simeq u_0$, so a reasonably accurate result will be obtained. However, as the size of the cell is reduced to approach the scale of the turbine, an increasingly large proportion of its cross-section is occupied by the rotor and the reduction in speed due to the turbine has a significant effect on the cell as a whole, so that $u_{cell} < u_0$. This results in an underestimate of the turbine's thrust, which will lead to an error in any prediction of either the energy that can be harvested by the turbine or the environmental effects of its energy extraction.

4.2 Demonstrating the error

The modelling work in this section was conducted by an undergraduate summer intern under the guidance of the author.

To demonstrate this effect four simple models were built in MIKE 3, identical except for their meshes. The scenario chosen was a channel 5 km in length and 1 km in width, with a rectangular cross-section and a constant depth of 50 m. Bed roughness height was set to a constant value of $k_s = 0.05$ m and vertical eddy viscosity was by a simple log law formulation. Two open boundaries were specified at the ends of the channel, and were given clamped elevations such that there was a difference in water level of 0.083 m (an arbitrary value) from one end of the channel to the other, resulting in a steady undisturbed flow of 2.1 ms^{-1}.

All four meshes used ten equally spaced vertical layers. The MIKE Mesh Generator tool was used to create a computational mesh with a target triangle face length of approximately 250 m. The same base mesh was used for all four models, but for three of them an area of approximately 500 m square was refined to higher resolution, as shown in Figure 4.1.

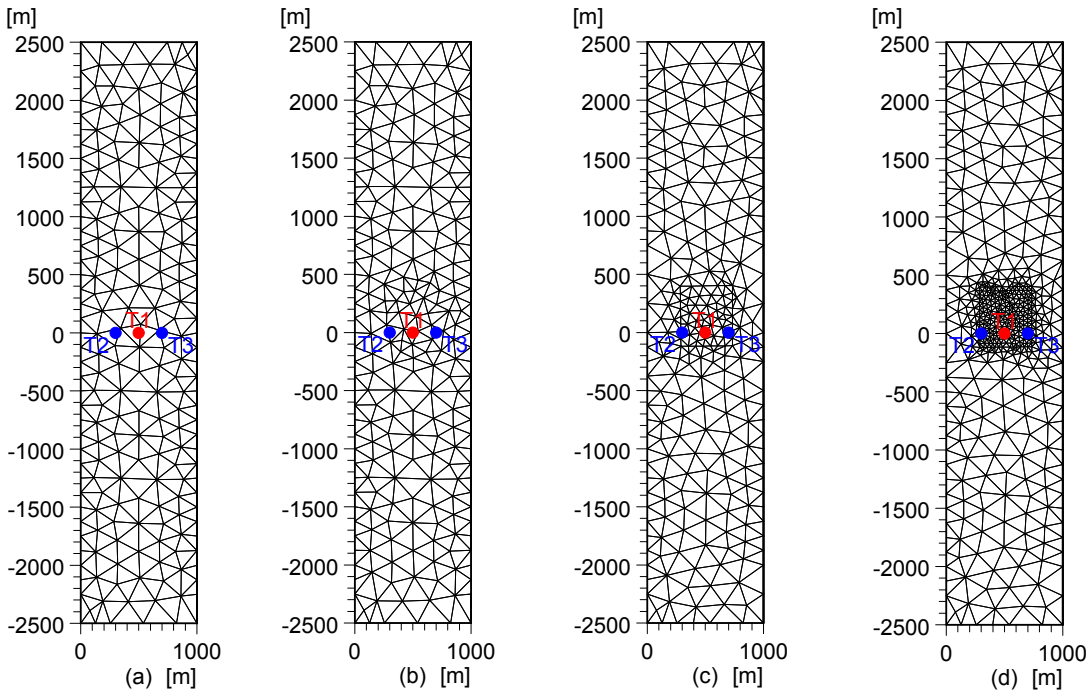

Figure 4.1: *The four meshes used for demonstrating the error and testing the initial MATLAB correction. Nominal element widths were (a)* 250 m*, (b)* 150 m*, (c)* 100 m*, and (d)* 50 m*. Turbine position T1, described in Section 4.2, is shown in red. Turbine positions T2 & T3, referenced in Section 4.4.2, are shown in blue. The direction of current flow is from the bottom to the top of the figure.*

For each mesh the model was run for 25 hours, which was more than sufficient for a steady flow to be reached. Initially they were run without any turbines in place, in order to test for any mesh sensitivity unrelated to the turbine implementation.

A single turbine was then added at the centre of each channel, close to the upstream end of the refined mesh region and oriented to face into the direction of flow. The diameter of the turbine was set to 20 m, and its hub elevation to −37 m. A constant thrust coefficient of 0.9 was specified. The force experienced by the turbine on the final time step was recorded and plotted against the width of the mesh element in Figure 4.2.

4.2.1 Result & discussion

In the test without turbines, all four meshes predicted the same flow speed at the planned turbine location to four significant figures (see Table 4.1). Thus, it is reasonable to conclude that the model is insensitive to mesh size when there are no turbines present.

With the turbine included, it can be clearly seen in Table 4.1 and Figure 4.2 that the force experienced by the turbine decreases with the size of the cell, indicating

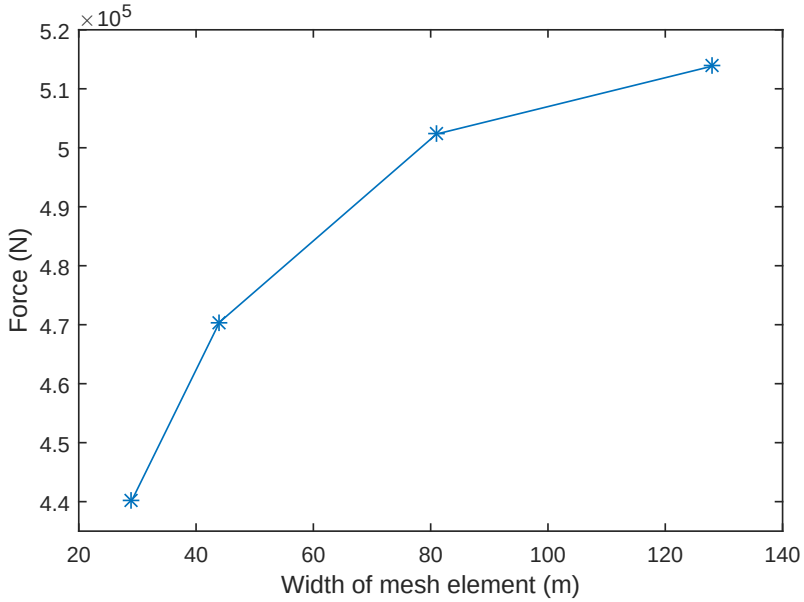

Figure 4.2: *Initial results, demonstrating the existence of the hypothesised mesh dependency. The value for 'width' used here is determined by the centroid method explained in Section 4.5.2.*

Table 4.1: *Predicted flow speeds in the four meshes without and with a turbine. The nominal element width, used for mesh generation, may not reflect the size of the actual triangle in which the turbine sits.*

Nominal element width (m)	Speed without turbine (m/s)	Speed with turbine (m/s)	Force on turbine (kN)
250	2.109	1.897	514
150	2.109	1.876	502
100	2.109	1.815	470
50	2.109	1.756	440

that the result depends on the mesh. The loss of apparent force from the coarsest to the finest mesh trialled was approximately 14%.

This result qualitatively matches those presented in Kramer *et al.* (2014) from larger, but two-dimensional, models in both MIKE 21 and Fluidity.

4.3 Theory behind a correction

The problem facing us is that the velocity being used in (4.1) is u_{cell}, while it should be u_0. What is needed is a way to estimate u_0 from the information available to the model.

The free stream velocity u_0 is frequently described as the velocity far upstream, before the flow has started to feel the effects of the turbine. In the simple case of a single turbine in a simple, wide, channel, the most straightforward way to determine u_0 would be simply to take the velocity from some distance upstream of the turbine. However, in the second or subsequent row of an array, or in a heavily blocked channel where the tidal farm affects the overall flow through the channel as a whole, the meaning of this description becomes unclear.

If we assume that no single turbine can affect the flow in the channel as a whole, then a better definition is that u_0 for a turbine is the velocity at the turbine's location when *only that turbine* is not present. It would be possible to discover u_0 for n turbines by running the model an additional n times, with a single turbine removed in each case, but the computational effort required would make this impractical for more than a very small value of n.

The approach adopted here is to use a relationship between C_T and the ratio of $\frac{u_0}{u_t}$ that is given by actuator disc theory, and extend this to provide the ratio $\frac{u_0}{u_{cell}}$.

The first part of this derivation, to (4.12), is a well-known approach from actuator disc theory and is based on Manwell (2009).

Consider a streamtube from far upstream to far downstream of a turbine, illustrated in Figure 4.3. We define u_k, p_k and A_k to be the velocity, the pressure, and the cross-sectional area of the streamtube, respectively, at location k. k may refer to any of four locations, denoted by numerals in Figure 4.3: 0 is far upstream of the turbine, 1 is immediately upstream of it, 2 is immediately downstream, and 3 is far downstream. Additionally, from continuity, $u_t = u_1 = u_2$ and $A_t = A_1 = A_2$, where t denotes the turbine location. Assume a single device in an infinitely wide channel with incompressible, steady flow. These assumptions mean that the pressure far upstream and far downstream of the rotor can be assumed to be equal to each

other and to the undisturbed pressure. The turbine rotor is represented by an "actuator disc", which is a thin circle at which there is a discontinuity in the flow — in this case, a discontinuity in pressure. Individual blades are not resolved, and the pressure difference across the disc (hence also the thrust) is assumed to be evenly distributed.

From conservation of momentum, the thrust of the turbine must be equal and opposite to the rate of change of momentum of the flow:

$$F = u_0(\rho A_0 u_0) - u_3(\rho A_3 u_3) \tag{4.2}$$

where ρ is the density of water. For steady flow (a good enough approximation for tidal devices at these scales, since the time for a parcel of water to pass the turbine is much less than the time scale of the tidal wave), conservation of mass indicates that $\rho A_0 u_0 = \rho A_3 u_3 = \rho A_t u_t$, and so

$$F = \rho A_t u_t (u_0 - u_3) \tag{4.3}$$

Applying the Bernoulli equation upstream and downstream of the turbine gives,

$$p_0 + \tfrac{1}{2}\rho u_0^2 = p_1 + \tfrac{1}{2}\rho u_1^2 \tag{4.4}$$

$$p_2 + \tfrac{1}{2}\rho u_2^2 = p_3 + \tfrac{1}{2}\rho u_3^2 \tag{4.5}$$

and since $p_0 = p_3$ and $u_1 = u_2$, we can solve these to give

$$p_1 - p_2 = \tfrac{1}{2}\rho(u_0^2 - u_3^2) \tag{4.6}$$

From the definition of pressure as force / area, we can say that $F = A_t(p_1 - p_2)$. Substituting in (4.6),

$$F = \tfrac{1}{2}\rho A_t(u_0^2 - u_3^2) \tag{4.7}$$

and equating this to (4.3) and solving for u_t simplifies to

$$u_t = \frac{u_0 + u_3}{2} \tag{4.8}$$

i.e. the velocity at the turbine is half way between the velocities far upstream and far downstream.

The "axial induction factor" a is conventionally defined as the proportional loss of velocity from the free stream (far upstream) to the rotor:

$$a = 1 - \frac{u_t}{u_0} \tag{4.9}$$

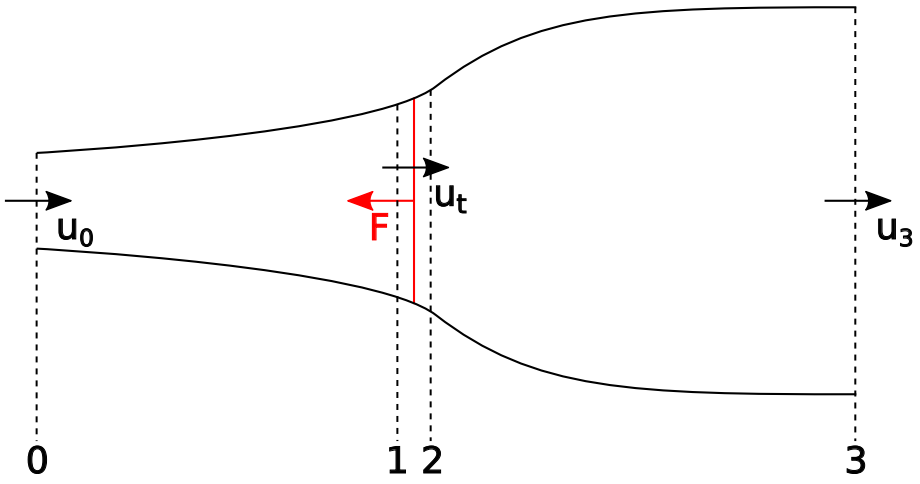

Figure 4.3: *Section through a streamtube around the turbine rotor, after Manwell (2009). The actuator disc and its thrust are shown in red. Numerals 0 & 3 denote positions far upstream and far downstream of the rotor, while 1 & 2 are immediately upstream and immediately downstream of the rotor.*

thus

$$u_3 = u_0(1 - 2a) \tag{4.10}$$

Returning to (4.7) and substituting in (4.10),

$$F = \tfrac{1}{2}\rho A_t u_0^2 4a(1 - a) \tag{4.11}$$

Comparing to the standard thrust equation (4.1), this means that

$$C_T = 4a(1 - a) \tag{4.12}$$

which is a well-known result (see *e.g.* Manwell (2009)). Solving this quadratic for a, substituting in (4.9), and then squaring both sides, gives

$$u_0^2 = \frac{4}{(1 + \sqrt{1 - C_T})^2} u_t^2 \tag{4.13}$$

which provides a relationship between the thrust coefficient and the ratio of u_0 and u_t. This is used by some high-resolution implementations of tidal turbines (*e.g.* Roc *et al.*, 2014) to solve the problem that we are addressing. However, it does require knowledge of u_t, and the models used here do not have a sufficiently small grid to resolve the turbine.

The thrust coefficient represents the proportion of the momentum passing through the rotor that is removed. If we define an analogous coefficient ν to represent the proportion of the momentum passing through the whole cell that is removed as a

result of the presence of the turbine, then

$$u_0^2 = \frac{4}{(1+\sqrt{1-\nu})^2} u_{cell}^2 \tag{4.14}$$

As an approximation for the value of ν (neglecting turbulence, supporting structures, or other losses of momentum caused by the turbine's presence), we can scale the turbine's thrust coefficient by the proportion of the cross-sectional area of the cell that the rotor occupies. In a three-dimensional model, where the rotor may intersect one or more vertical layers and where (as in MIKE 3) the thrust is split equally between l such layers,

$$\nu = C_T \frac{A_t/l}{\Delta x \Delta z} \tag{4.15}$$

where $\Delta x \Delta z$ is the cross-sectional area of the cell.

We now have a means of estimating u_0^2 from u_{cell}^2 and C_T, both of which are known to the model, and thus of correcting the thrust calculation to use u_0 in (4.1). Let us define η as this correction factor, where $\eta = \frac{u_0^2}{u_{cell}^2}$.

4.3.1 A note on applicability

The theory above is only applicable in a "Betz scenario", *i.e.* for a single turbine in an infinitely wide, unconstrained channel — or to put it another way, in a scenario where the channel blockage is negligible and hence the overall flow in the channel is not affected by the turbine. This is not a good match to the real scenarios that have been simulated in other chapters.

However, the correction can be used in more complex scenarios, because the channel for which the theory must be applicable is not that which we are simulating, but rather the channel (whether physical or virtual) in which the thrust curve was originally measured or calculated by the turbine manufacturer.

4.3.2 Verification

The simplest way to verify whether the correct correction is being arrived at is to plot the corrected thrust predictions from a number of different meshes, as per Figure 4.2, and check that a horizontal line is produced. When cyclic currents are used, thus making more than the final time step relevant, a similar assessment can be made by calculating the RMSE between the values predicted on the largest mesh and on each of the others. Both of these techniques provide evidence that mesh-independence is achieved, but do not show that it is achieved at the correct magnitude.

Evidence that the correct values are produced can be obtained by fitting a curve to the uncorrected points in Figure 4.2 and checking whether the corrected points align to the asymptote of this curve at large cell size (see Figure 4.4 for an example from an early experiment).

While this approach is straightforward and useful in simple test scenarios, it ceases to be appropriate in complex models with many turbines, because other mesh dependencies (*e.g.* in the representation of turbine wakes) will influence cell velocities and thus turbine thrust. An alternative, more direct, method is explained below.

The purpose of the correction is to estimate the unknown u_0 from the known u_{cell}. As noted above, one definition of u_0 for a turbine is that it is the velocity at the turbine's location when the turbine is not present. Therefore, by running the simulation with a given turbine removed, the correct value for u_0 can be discerned*. Let us refer to this value "measured" from a modified model as u_0'. A value for u_0 can also be calculated from the corrected simulation by $u_0 = u_{cell}\sqrt{\eta}$, where η is the correction factor. A comparison of the measured u_0' to the calculated u_0 can reveal whether the correct correction is being applied and permit the technique to be tested in any given scenario.

4.4 Initial implementation of a correction

In realistic scenarios the speed and direction of flow in a mesh element may change on each time step, as may the water level. C_T (a function of flow speed) and Δx (a function of flow direction) may therefore change from one time step to another, as may both the value of Δz and the number of layers that the rotor intersects, due to the use of sigma coordinates in the vertical. Therefore, it would become necessary to calculate a correction for each turbine in each time step, and would necessitate automation. Eventually a MATLAB package would be developed to perform the necessary corrections with a minimum of human input, but initially a manual test was conducted.

4.4.1 Manual tests on a mixed square and triangular grid

It was intended that the manual test should be conducted using a square grid, so that the question of triangle width (see Section 4.5.2) would be avoided. A model

*For a simple scenario where blockage is low and turbines do not affect one another, it is sufficient to perform a simulation with no turbines to find u_0. Where turbines are not independent of one another, or where the array significantly affects the flow in the channel as a whole, it is necessary to perform a seperate simulation for each turbine to be tested, where only that turbine is removed.

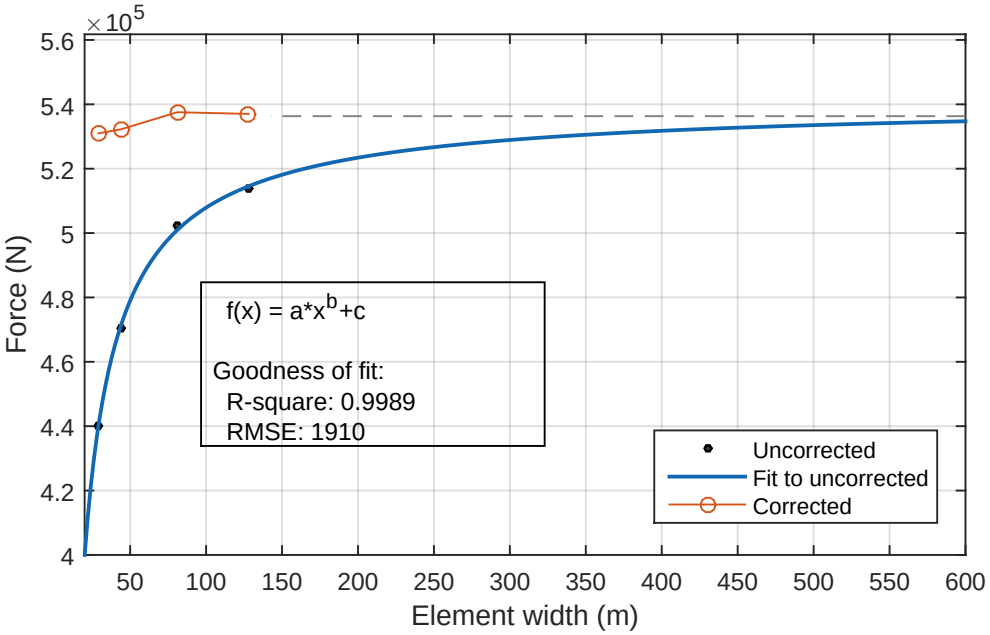

Figure 4.4: *The corrected and uncorrected values predicted in an early test are shown here, with a curve fitted to the uncorrected values and the x-axis extended to extrapolate to its asymptotic value. As illustrated by the dashed line, this is close to the corrected values.*

was constructed using MIKE 3's quadrilateral grid feature representing a channel 5 km long, 1 km wide and 50 m deep. Five different meshes were constructed, using square cells of sides 50, 100, 125, 200 & 250 metres, chosen to allow a whole number of cells to fit in the width of the channel. The eastern and western boundaries were specified as land with zero normal velocity (*i.e.* a conventional "slip" condition). The southern and northern boundaries were set as fixed elevations of 0.05 m and −0.05 m respectively, giving a hydraulic head of 0.1 m and thus a steady flow of 2.26 m s^{-1} from south to north in the absence of turbines. The bottom roughness was set to the default value of 0.05 m. Coriolis effects were turned off.

When a turbine was added to this model, its effect on the flow turned out to be highly unrealistic, with the resulting velocity deficit largely confined to one cell in a cross-flow direction and continuning to the edge of the domain to the north and south. There appeared to be little or no mixing between the wake and the surrounding flow (see Figure 4.5a). Adjustments were made to the model's horizontal eddy viscosity module, but these had no effect. After considerable experimentation, it was eventually concluded that there is a problem with MIKE's quadrilateral mesh option when a grid is perfectly aligned to a simple channel, and the flow aligns perfectly to this grid.

New meshes were constructed which used triangular elements for the majority of the domain but included three rows of quadrilaterals: the one containing the turbine, one upstream, and one downstream (Figure 4.6). The maximum triangle area for the

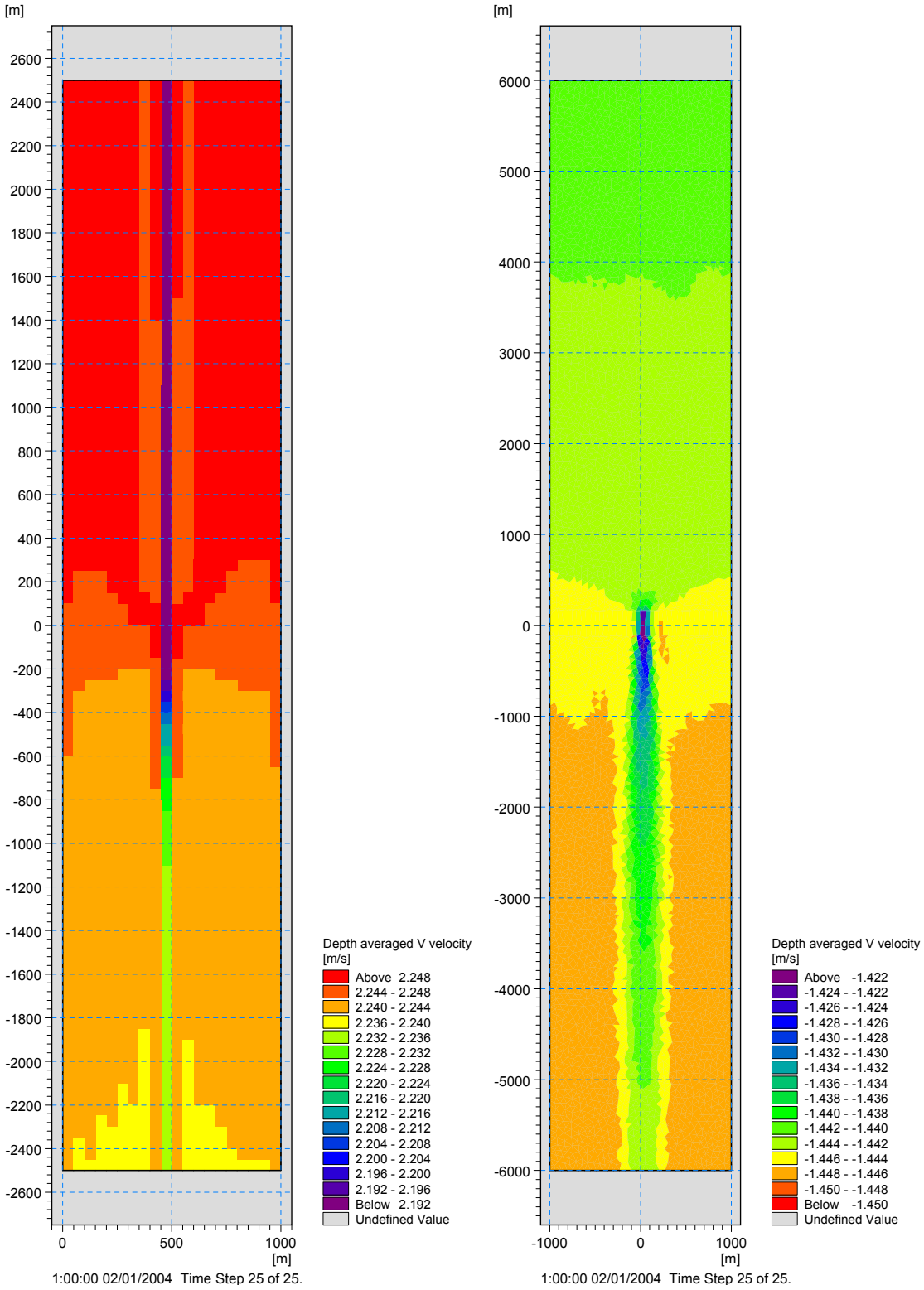

Figure 4.5: *Unsmoothed depth-averaged v-velocities from final time step on two meshes. (a) shows the* 50 m *square grid, whose results were thought to be erroneous. (b) shows the finest mixed triangular/quadrilateral mesh eventually used, as shown on the right-hand side of Figure 4.6. Note that the two subfigures show meshes of different dimensions, use different colour scales, and have flow in opposite directions — so they should not be directly compared! Subfigure (b) is included to give an idea of what (a) was expected to look like.*

triangular parts of the mesh was specified to give the triangles approximately the same area as the squares. In fact the triangles had somewhat smaller areas, because the mesh generator tends to produce triangles of smaller than the maximum allowed area.

The length of the channel was increased to allow for better wake mixing, but the difference in elevation between the ends was not changed. This resulted in a decreased speed in the centre, without a turbine, of approximately $1.49\,\mathrm{m\,s^{-1}}$. The length of the quadrilateral area was different between different meshes (as it was always three cells, regardless of the cells' size), and this introduced a small amount of mesh dependency to the speed without a turbine. This variation was judged to be acceptable, as it was at least an order of magnitude smaller than the effect of interest.

Manually calculating the correction for this mixed square & triangular mesh gave excellent results, which may be seen graphically in Figures 4.7 & 4.8. The difference in thrust between the largest and smallest meshes, expressed as $\frac{F_{\max}-F_{\min}}{F_{\max}}$, was reduced from 8% to 0.4%. Calculating the free-stream speed from the corrected speed ($u_0 = u_{cell}\sqrt{\eta}$) produced values very similar to the speed without a turbine present.

4.4.2 Initial MATLAB implementation

A MATLAB package was developed with the intent of minimising the level of manual intervention that was required, in order to allow its use as part of a practical modelling workflow by others. To this end, all of the required input data is parsed from various MIKE model files — some from the model input files, and some from the outputs of an uncorrected run of the model. The package was called "MTMC" for "MIKE Turbine Mesh Correction".

The initial implementation, which was described in Waldman *et al.* (2015), produced a series of time-varying values for α in (4.1) for each turbine, and modified the model input files so that these corrections would be applied on the next run of the model. The flow of information and calculations in this version may be seen in Figure 4.9.

This version was tested using the meshes shown in Figure 4.1 and produced promising results in a simple scenario involving a single turbine at position T1, with a fixed thrust coefficient in steady flow (see Figure 4.4). While perfect mesh-independence was not achieved, the range in forces amongst the four meshes tested was reduced from 14% of the maximum to just 1%, a worthwhile improvement. Further tests were conducted with turbines at different depths and different horizontal locations on the same mesh (positions T2 & T3 in Figure 4.1). In order to avoid inter-turbine interactions at this stage, only one turbine was modelled, and its location was changed

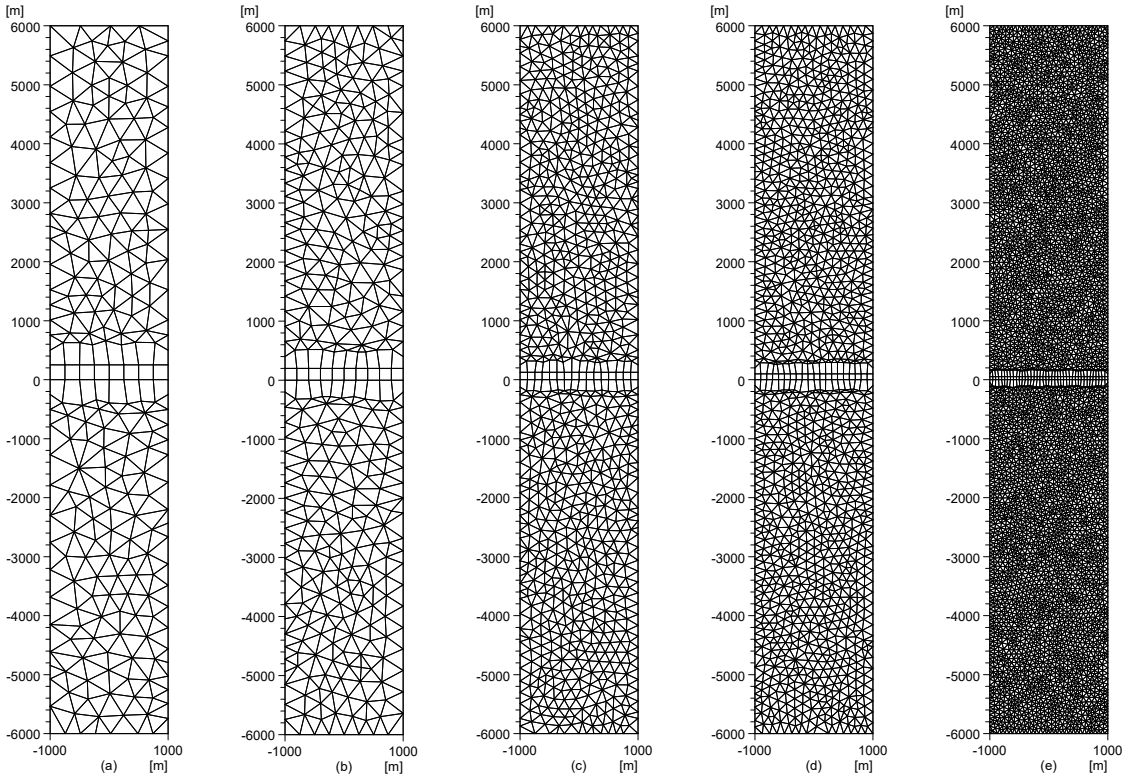

Figure 4.6: *Five mixed meshes used for manual testing of the correction.*

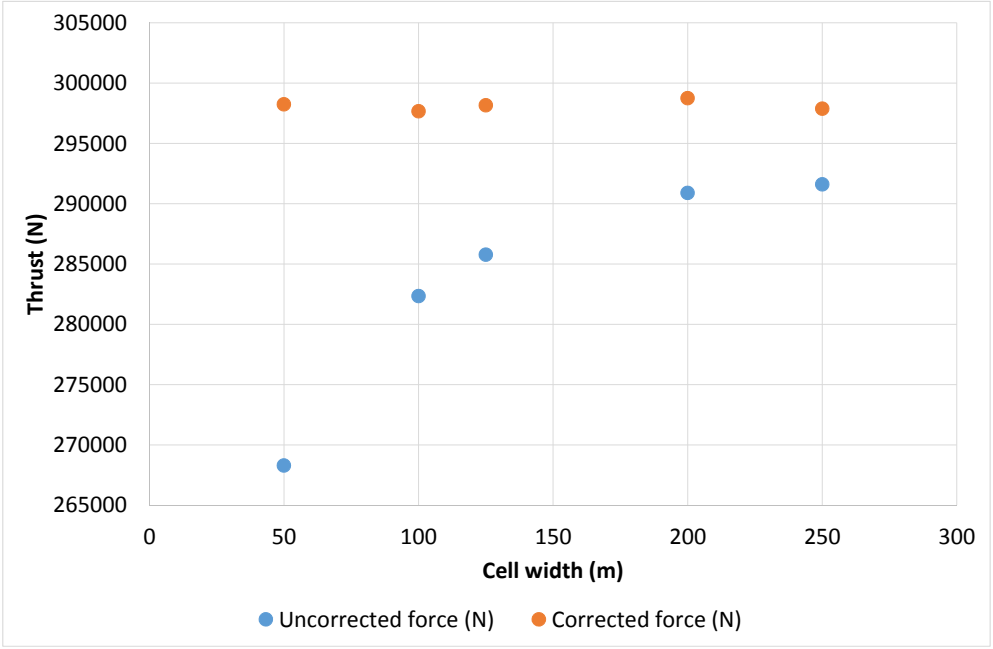

Figure 4.7: *Comparison of turbine thrust, predicted on five meshes with mixed quadrilateral and triangular elements, with and without the correction.*

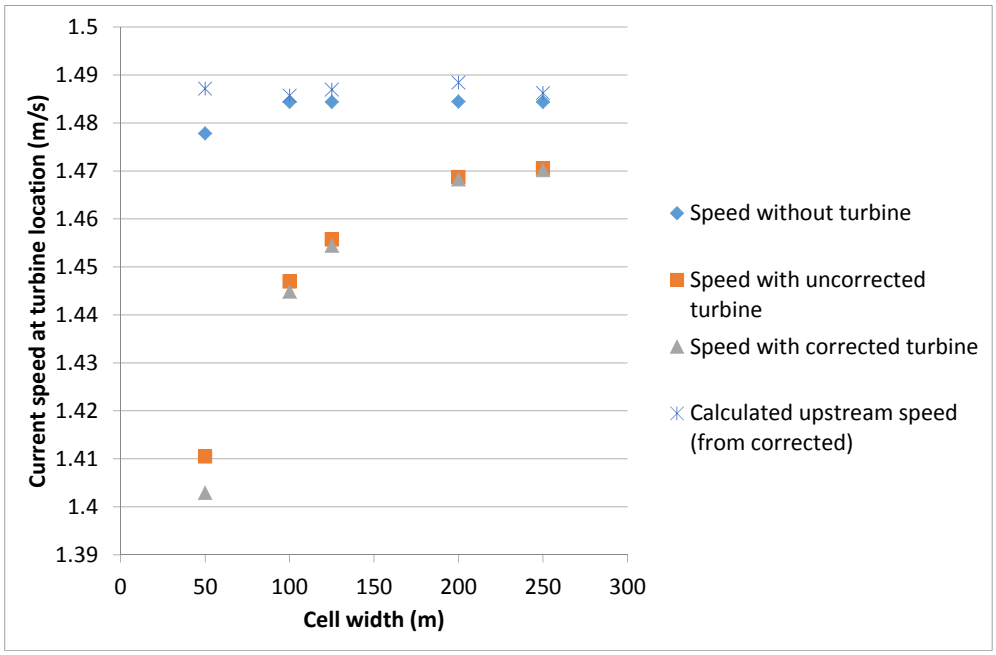

Figure 4.8: *Comparison of current speed at the turbine location, predicted on mixed quadrilateral & triangular meshes, (a) without any turbine; (b) with turbine, uncorrected; (c) with turbine, corrected; (d) free-stream velocity calculated from corrected speed by* $u_0 = u_{cell}\sqrt{\eta}$.

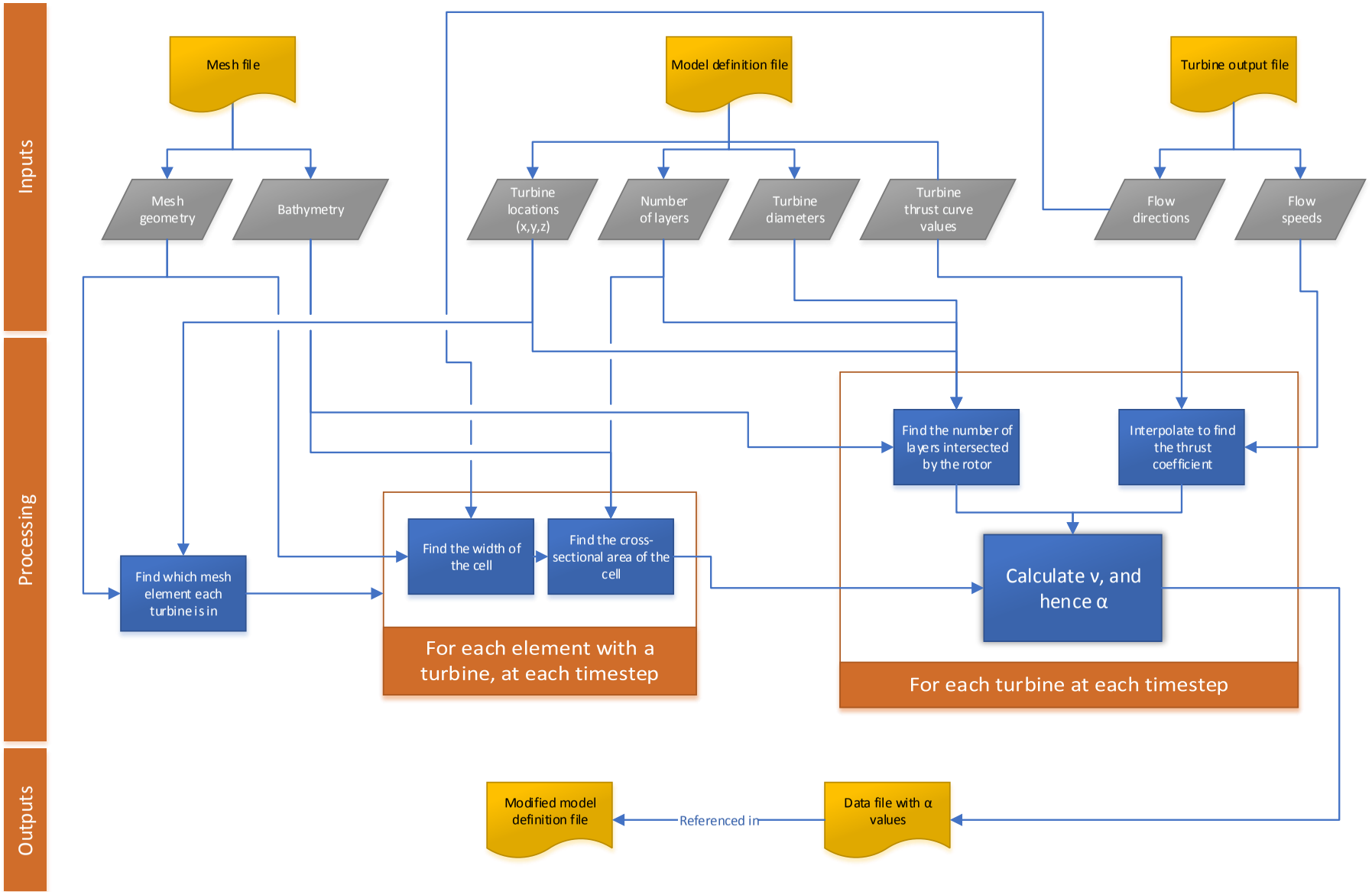

Figure 4.9: *Flow of information & calculations in the initial MATLAB package.*

for each set of simulations.

For different depths at the same horizontal location (Figure 4.10a), while the absolute force values vary with depth due to vertical velocity shear, the proportional change in force with mesh size is near-identical. This is as expected, because the turbine lies within the same horizontal triangle on each mesh at any depth. When the turbine was placed in different horizontal locations (Figure 4.10b), in each case the corrected result shows a reduction in sensitivity to mesh size compared to the uncorrected result. However, some mesh dependency clearly remained, and this varied in magnitude between different locations on the mesh. This variation is likely to be related to the interpretation of mesh geometry, which will be discussed further in Section 4.5.2.

4.5 Elaborations for non-idealised models

The work in the previous section provided the material for Waldman *et al.* (2015). It demonstrated the feasibility of a correction of this type, but was applicable only to a single turbine in a simple channel with constant flow. This section describes the improvements that made it appropriate for "real world" use.

4.5.1 New triangular meshes for testing

A new set of all-triangular test meshes was developed, using a larger domain than before and with better mesh characteristics (smoothness, triangle angles, etc.), based on the mixed square/triangular meshes shown in Figure 4.6. The new meshes were 12 km long by 2 km wide, and incorporated a sloping bottom to the channel with the same gradient as the undisturbed free surface. This was to avoid a slight acceleration of flow towards the outflow that was visible in previous models due to the reduction in water depth.

Five nominal element widths were chosen (250 m, 200 m, 150 m, 100 m & 50 m — although these should be treated simply as labels rather than accurate measurements), and the area of them was determined by $A = \frac{3}{4}w^2$, where w is the nominal width*. To keep computation times low, only an inner area of 2 km up- and downstream of the turbine location was given the full mesh resolution (see Table 4.2 & Figure 4.11). For the 50 m mesh an additional buffer zone between the fine and coarse mesh areas was

*There is no mathematically rigorous reason for using $\frac{3}{4}$ rather than $\frac{1}{2}$ in this formula; this was done because it is a *maximum* area that is specified, and the actual elements generated are often smaller. Additionally, most elements will not show their widest aspect to the flow. Ultimately the nominal width is only a label; the real cross-sectional area of elements is measured by the script.

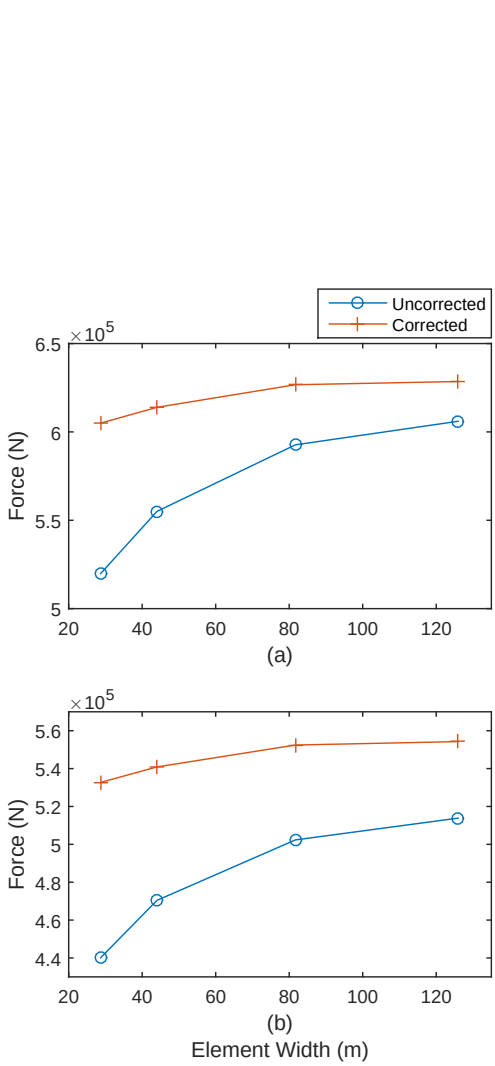

(a) *Initial correction applied to a turbine at the same horizontal location (T1), at depths (a) 25m, (b) 37m.*

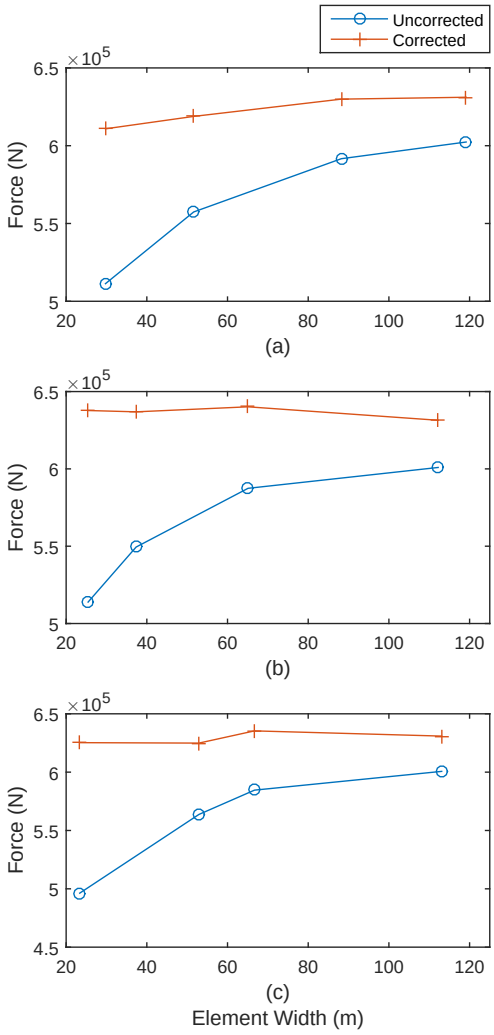

(b) *Initial correction applied to a turbine at the three horizontal locations (a) T1, (b) T2, (c) T3, shown in Figure 4.1. In each case the turbine was at 26m depth.*

Figure 4.10

included to prevent the change in mesh sizes from being too abrupt. The procedure used to generate the meshes in the MIKE Mesh Generator was as follows:

1. Set up the desired maximum element areas.
2. Run the "Generate Mesh" command.
3. Use the "Smooth Mesh" command with 500 iterations, with nodes not constrained to arcs. This allows the boundaries between mesh sizes to be softened.
4. Apply the desired bathymetry to the mesh.

With a difference in surface elevation between the two ends of 0.1 m, the current speed at the turbine location in these meshes (in the absence of any turbine) was consistent to four significant figures at $1.484\,\mathrm{m\,s^{-1}}$.

4.5.2 Approaches to triangle width

The parameter Δx in (4.15) refers to the width of the mesh element in which the turbine lies, from which the cross-sectional area (CSA) of the element is calculated. The value of Δx is clear when using a rectangular grid that is aligned to the flow, but in other circumstances it becomes non-obvious, and leads to a question "how to define the width of a triangle?".

The correct answer to this question depends on the numerical methods used within MIKE 3, and without access to the source code or information on its detailed functioning it must remain unknown. An empirical approach was therefore adopted. A number of methods were tried; unsuccessful ones included:

- The mean width as "perceived" by a parcel of water moving through the triangle.
- The maximum width at any point during this journey.

Nominal Width (m)	Area (inner, m^2)	Area (outer, m^2)
250	46,875	46,875
200	30,000	30,000
150	16,875	30,000
100	7,500	30,000
50	1,875	7,500 / 30,000

Table 4.2: *Maximum element areas specified the MIKE Mesh Generator when constructing the new test meshes. For the* 50 m *mesh a third zone of intermediate resolution was included to smooth the transition between the inner and outer zones.*

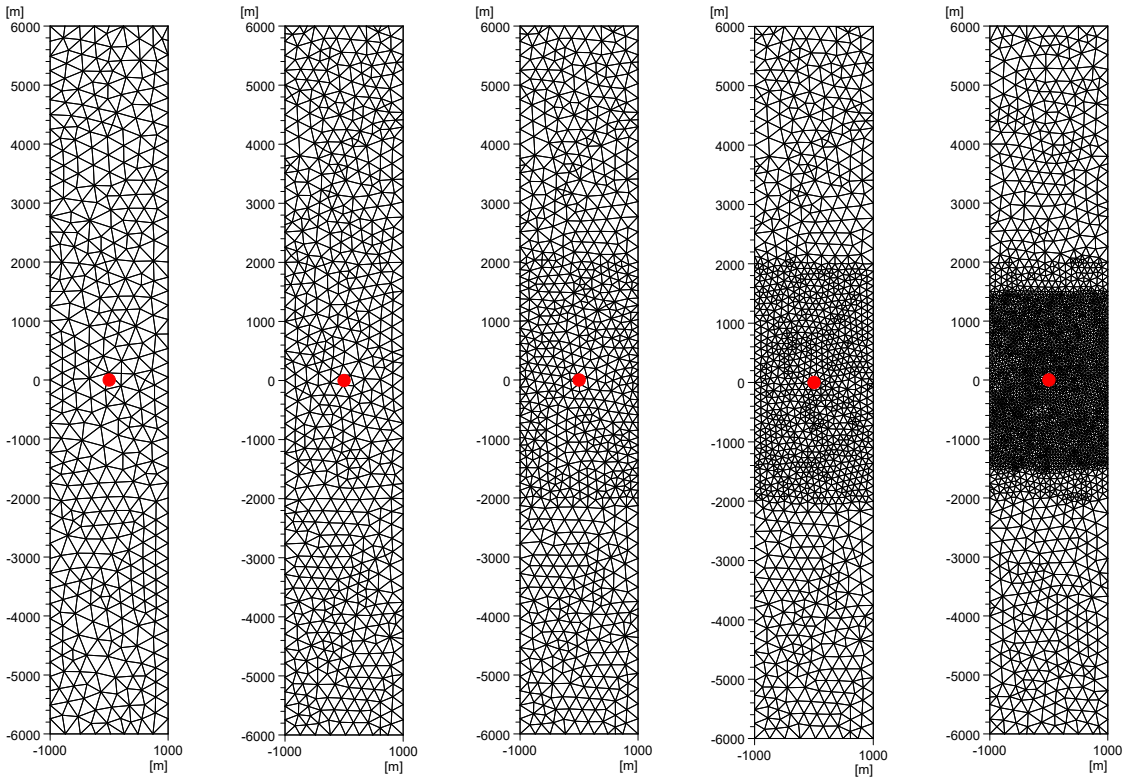

Figure 4.11: *Set of five test meshes described in Section 4.5.1. The red dot shows (0,0), which was the location used for a turbine except where specified otherwise.*

- The (larger) value given by projecting the triangle's vertices onto a line perpendicular to the flow and measuring the distance between the two outermost.

Two methods gave good results in use:

One approach, hereafter referred to as the "centroid method", was to use the distance between two faces of the triangular element along a line that passes through the centroid of the triangle and is perpendicular to the direction of current flow (Figure 4.12a). It is this method that was used for the initial testing described above.

The second approach, hereafter the "weighted average method", was to measure the length between faces of a large number of lines (typically 100) perpendicular to the direction of flow and evenly spaced throughout the element, and to take a weighted mean of these lengths where the weight assigned to each line was proportional to its length (Figure 4.12b):

$$w = \frac{\sum_{1}^{n} w_i^2}{\sum_{1}^{n} w_i} \tag{4.16}$$

Two ways of considering this approach are that the length of each line is weighted by the proportion of the flow through the element that would pass through that line, or that the triangle is divided into rectangular areas, and the width is the area-weighted mean. Although triangular meshes were used for the remainder of this work, the weighted average method should also be applicable to other element shapes.

In order to test these two approaches, turbines were specified at three locations on the new meshes, as detailed in Table 4.3. The script was run, and then MIKE run with the corrections, with each of the two possible width approaches. Results were evaluated by comparing the maximum and minumum values for thrust across five meshes, normalised by the maximum value ($\frac{F_{\max}-F_{\min}}{F_{\max}}$). These results may be seen in Table 4.4.

A second test was conducted using the method of comparing predicted and "measured" u_0 and u_0' values described in Section 4.3.2. Results of this are shown in Table 4.5.

It is clear that both methods provide a substantial improvement in inter-mesh consistency over the uncorrected scenario. Using the inter-mesh comparison of thrust predictions the weighted average method gives slightly better mean results, but the centroid method is more consistent. Using the comparison of u_0 values, this situation is reversed: the centroid method gives the lowest mean nRMSE, while the weighted average method gives more consistent results. It is not possible to determine a "winning" method without extensive further testing on more than three points. Since

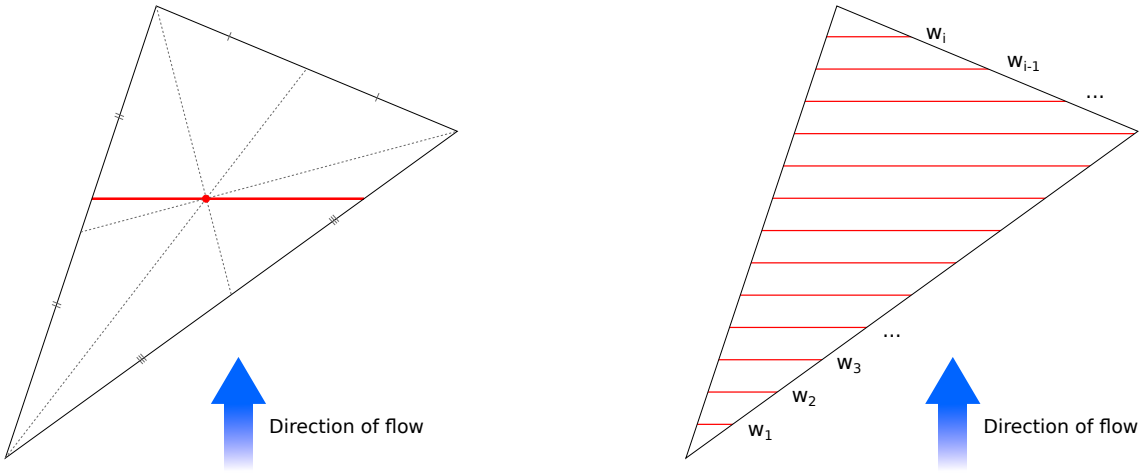

Figure 4.12: *Illustration of the two candidate methods of determining the "width" of an element, using: (a) centroid method; (b) weighted average method (see text).*

	x	y	z
T1	0	0	-26
T2	-400	250	-18
T3	350	-200	-30

Table 4.3: *Locations of simulated turbines for testing width methods. $z = 0$ at mean sea level. All units are metres. T1 is at the same central location as used for single-turbine simulations.*

	Uncorrected	Centroid	W. Avg
T1	12%	2%	1%
T2	11%	3%	4%
T3	10%	2%	1%
Mean	11%	3%	2%

Table 4.4: $\frac{F_{\max}-F_{\min}}{F_{\max}}$ *values showing variation of thrust between meshes at three locations, with two different methods of determining triangle width.*

	Cent. RMSE (ms^{-1})	W. avg RMSE (ms^{-1})	Cent. nRMSE	W. avg nRMSE
T1	0.0021	0.0102	0.17%	0.81%
T2	0.0159	0.0113	1.23%	0.87%
T3	0.0124	0.0114	1.01%	0.93%
Mean	0.0101	0.0110	0.80%	0.87%

Table 4.5: *RMSE and normalised RMSE (nRMSE) between u_0 (calculated) and u_0' (measured) values. nRMSE values are normalised by dividing by the mean value of u_0'. Cent. = centroid method, W. avg = weighted average method.*

both methods appear to perform reasonably well — although the remaining errors suggest that neither is quite correct — it was decided to proceed with the weighted average approach for the remainder of the work described in this chapter.

4.5.3 Allowing for variable C_T

Until this point, a constant value of the thrust coefficient had been assumed. To represent realistic turbines a thrust curve must be applied, such that C_T is a function of velocity. MIKE allows the user to specify a table of C_T values according to velocity, and this table can be read from the MIKE input files. The thrust curve discussed in Section 3.4 was applied to the simulated turbine. This curve is reproduced in this section as Figure 4.13 for convenience.

The early version of the MTMC script used for Waldman *et al.* (2015) included code to read the C_T table from the MIKE input file and perform a similar interpolation to that conducted by MIKE to arrive at an appropriate value for each timestep. However, using a realistic thrust curve with this code produced a perverse result, where a reduction in mesh scale caused an *increase* in thrust. This was because, while that version of the script corrected for the difference between u_{cell} and u_0 when calculating thrust, it did not have any effect on the speed value used to look up the thrust coefficient; a table of u_0 vs C_T was specified, but u_{cell} was used to look up values in it. Consequently, if the simulated speeds were in the part of the thrust curve between the rated and cut-out speeds (in our case between $2.5\,\mathrm{m\,s^{-1}}$ and $4\,\mathrm{m\,s^{-1}}$), the lower u_{cell} that arises from a smaller mesh would cause a higher value of C_T to be selected and hence a greater thrust predicted.

To cope with a variable $C_T(u_0)$, it was thus clearly necessary not only to correct the actual thrust calculation, but also to correct the velocity values in the table of thrust coefficients. These are specified as u_0, but need to be converted to u_{cell} since this is the information available to MIKE. This conversion can be done using the same correction (4.14 & 4.15) as is used elsewhere in this chapter. However, the conversion itself depends on the thrust coefficient, cell cross-sectional area (CSA) and number of layers intersected, which complicates matters.

Four possible approaches, of increasing accuracy and complexity, were identified, with advantages (+) and disadvantages (-). These methods are summarised below in text form, and are detailed in flowcharts in Figure 4.16. All of these methods require a prior, uncorrected, simulation to provide information.

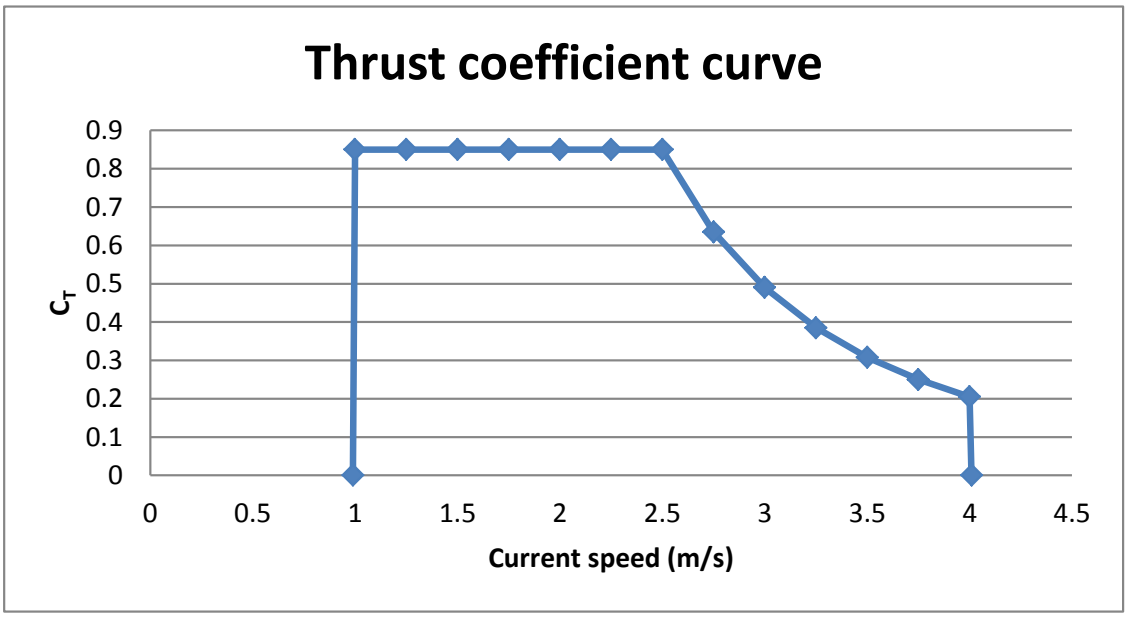

Figure 4.13: *Thrust curve for a generic tidal turbine, agreed by industrial partners in the TeraWatt project and used for testing. See Section 3.4 for further details.*

Method A

Produce a u_{cell}/C_T table, using mean and modal values of CSA and number of layers for calculating u_{cell}, then proceed as before with individual corrections on a per-timestep basis.

- + Simple.
- + The correction is still calculated accurately on a per-timestep basis.
- - Since C_T is a function of u_{cell}, which is itself affected by the thrust determined by C_T, iteration between the model and the correction will be required to obtain correct results in a non-horitzontal part of the thrust curve.
- - Since the u_0 to u_{cell} conversion has been done based on mean and modal values, there will be an effective distortion of the thrust curve when CSA, number of layers, etc., are far from their means and modes.

Method B

Precalculate the correction and produce a table of u_{cell}/C'_T, where $C'_T = C_T\eta$. The time-varying correction factor is not used. This is the approach suggested by Shives and Crawford (2015) (who use a CFD sub-model to arrive at a correction) and Kramer and Piggott (2016) (who take the same analytical approach used here).

- + Simple.

- + Because the correction is included in the thrust table, no iteration is required to deal with changes in current speed caused by the correction.
- - Because there is no time-varying correction, things must be approximated by mean and modal values, and (importantly) there is no way to respond to changes in surface elevation or current direction during the tidal cycle.

Method C

Produce both u_{cell}/C_T and u_{cell}/C'_T tables using mean and modal values. For each timestep, use the first of these tables to determine C_T, compare the correction indicated against the value of $\frac{C'_T}{C_T}$, and apply a time-varying 2nd-order correction to resolve the difference. These differences may arise through changes in cross-sectional area or number of layers away from the mean (due to changes in surface elevation or current direction), but can also appear because of the linear interpolation that is applied by MIKE to the thrust curve, especially around vertical cut-offs.

- + No iteration required.
- + Allows varying surface elevation (and other effects) to influence the correction on a per-timestep basis.
- - Not strictly correct, as the values for u_{cell} were still calculated using mean and modal values.

Method D

As Method C, but calculate a new u_{cell}/C_T table for each timestep and use this when determining the desired correction.

- + Should be the most accurate method available without iteration.
- - Complicated, and potentially slow when dealing with many turbines and many timesteps.

Method B was tested with a steady flow and achieved $\frac{F_{\max}-F_{\min}}{F_{\max}}$ of 0.2%, a record for this work (see Figure 4.14). Methods C and D were not tested at this stage, as without a varying surface elevation they would be unlikely to show any noticable difference.

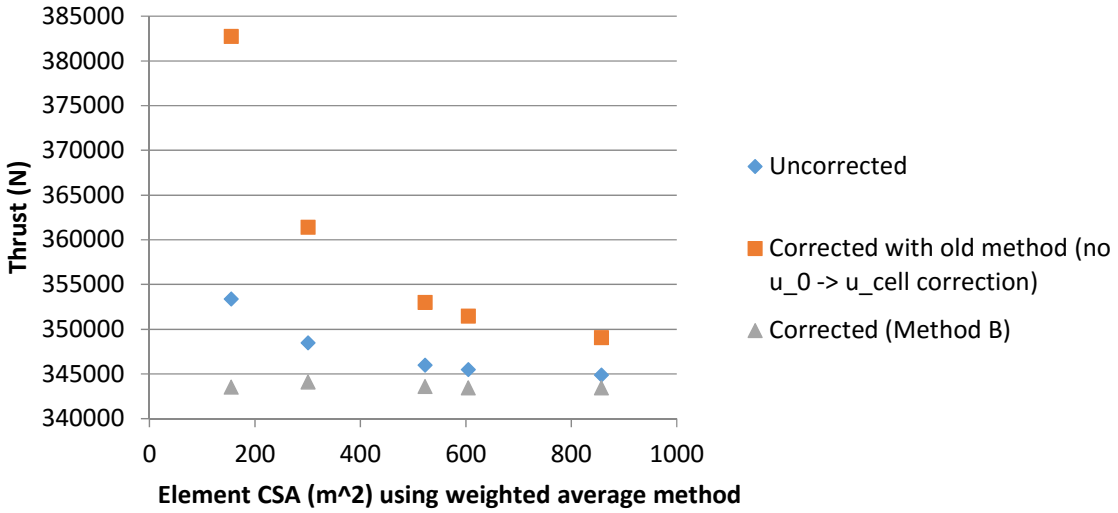

Figure 4.14: *Comparison of force predictions in a steady flow between the old approach used for fixed values of C_T (which did not correct the velocity side of the thrust table) and Method B. The old method produces a perverse result, with thrust sharply rising with decreasing CSA, because the part of the thrust curve that this simulation is operating in causes a reduced velocity to indicate a higher value for C_T.*

4.5.4 Allowing for changing surface elevation

With the use of sigma layers in the model, a change in surface elevation will result in a change in the height of each layer (Δz) and hence a change in the required correction factor. To perform corrections on realistic scenarios where sea level rises and falls with the tidal cycle, this effect must be accounted for.

An additional input file was added to those required by the correction script: a 2D MIKE output file containing predictions of surface elevation from a prior, uncorrected, run of the model. This additional information is used to recalculate Δz and the positions of layer boundaries on a per-timestep basis.

Strictly speaking, surface elevation and the correction factor both depend on each other. However, iteration would only be required if the *correction* to thrust, rather than the uncorrected thrust itself, were to result in a significant change to surface elevation, and so for most scenarios iteration is not necessary.

In order to test the response to changing surface elevation, it was necessary to move away from steady flow test scenarios and introduce tidal cycles into the channel. Initially one end of the modelled channel was changed to a land boundary, and an M2 signal applied to the other end, in order to convert the channel into a bay. However, the small dimensions of the channel, and hence the small volume of water contained within it, meant that elevation changes at one end propagated very rapidly to the other. As a result no significant hydraulic head could be developed, and thus no strong currents produced. The maximum speed obtainable at the turbine

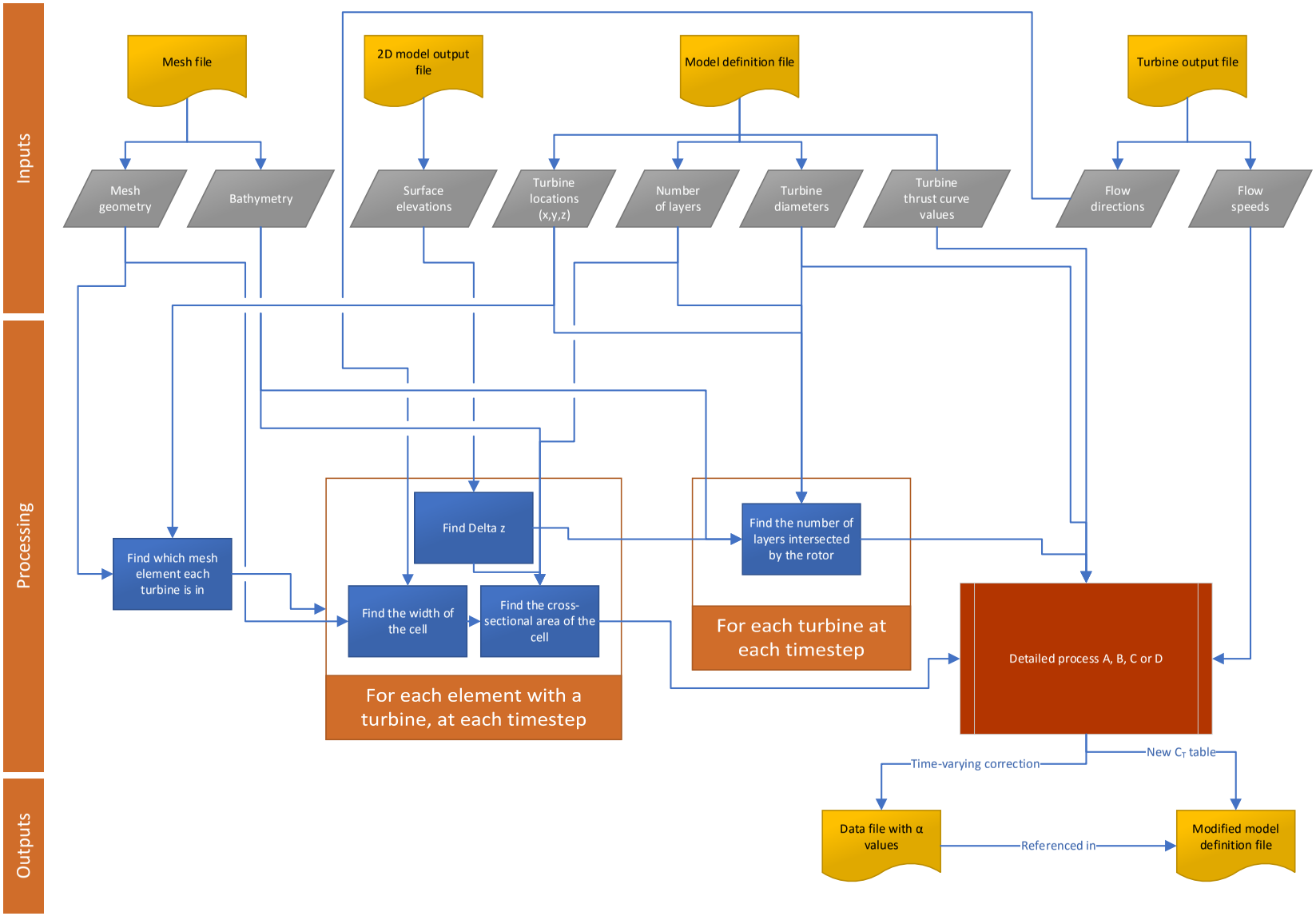

Figure 4.15: *Flow of information & calculations in the latest version of the MATLAB package. The detailed methods inside the red box are shown in Figure 4.16.*

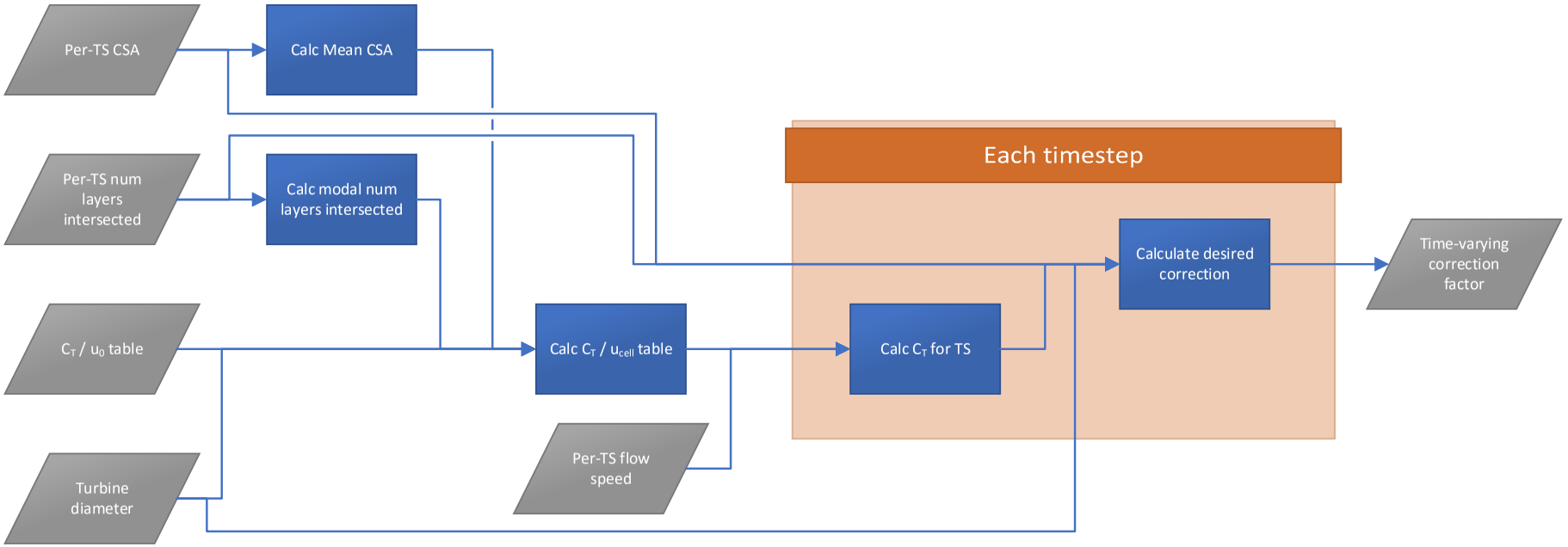

(a) *Method A*

Figure 4.16: *This and subsequent pages show different methods, described textually in Section 4.5.3, that operate within the red box in Figure 4.15.*

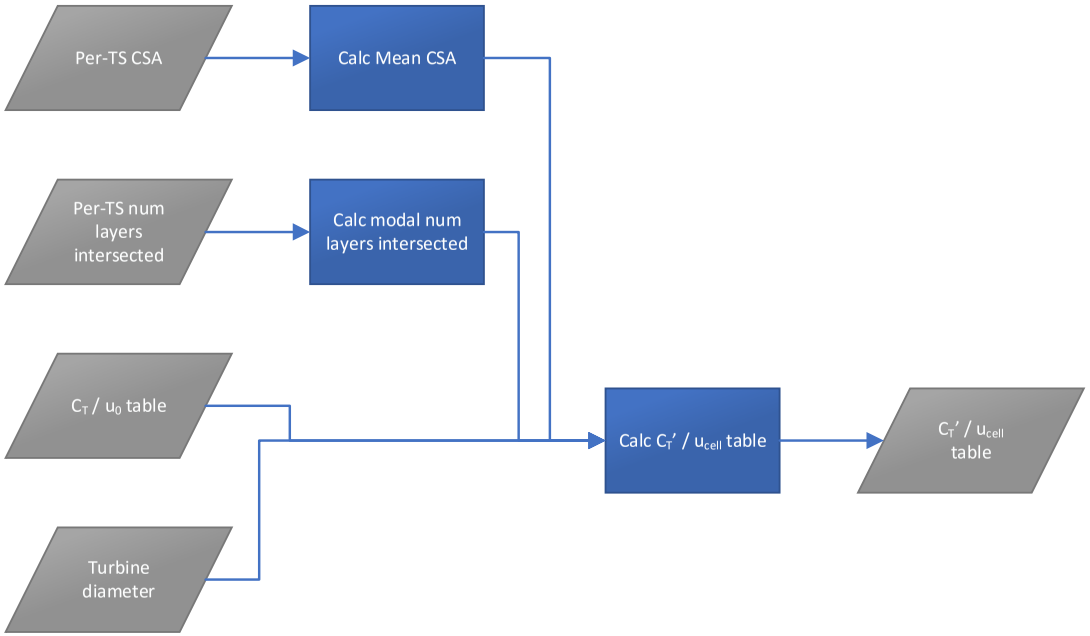

(b) *Method B*

Figure 4.16: *cont...*

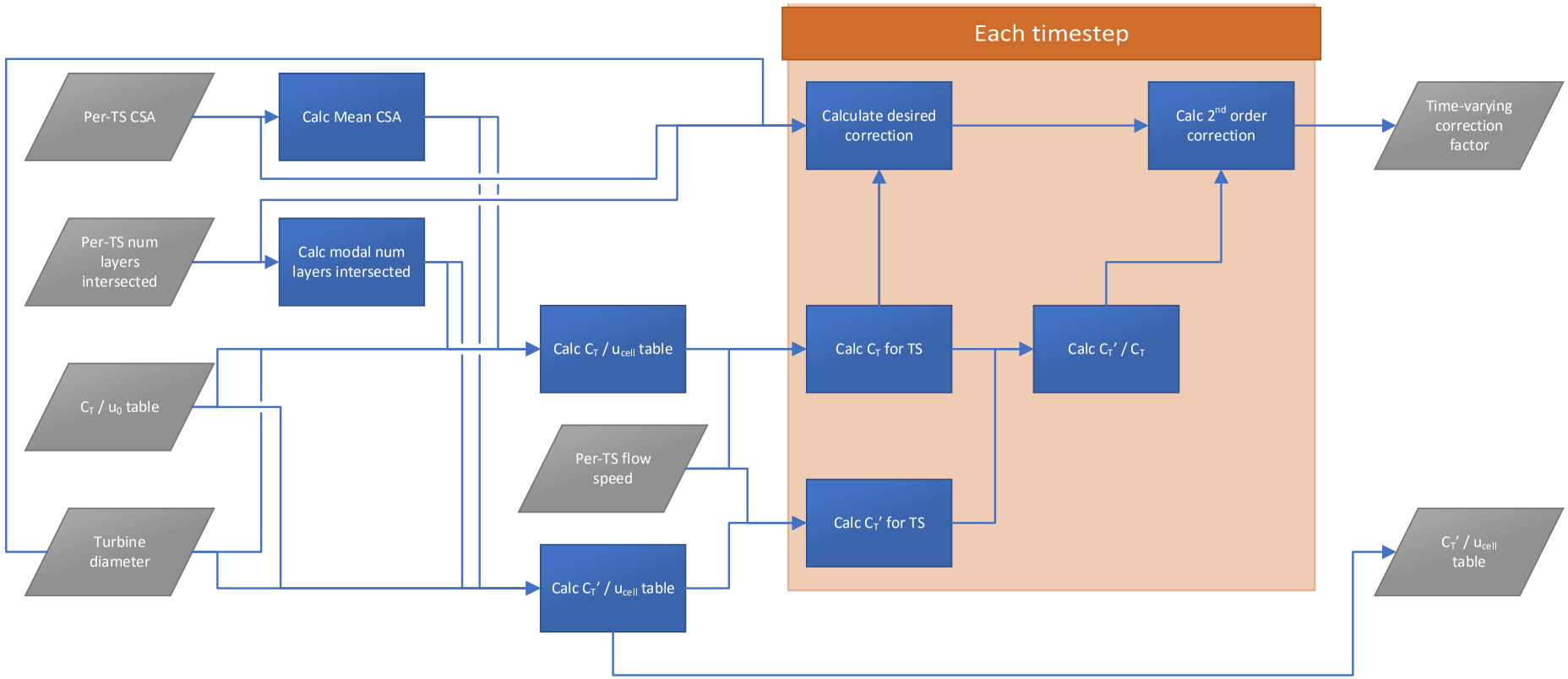

(c) *Method C*

Figure 4.16: *cont...*

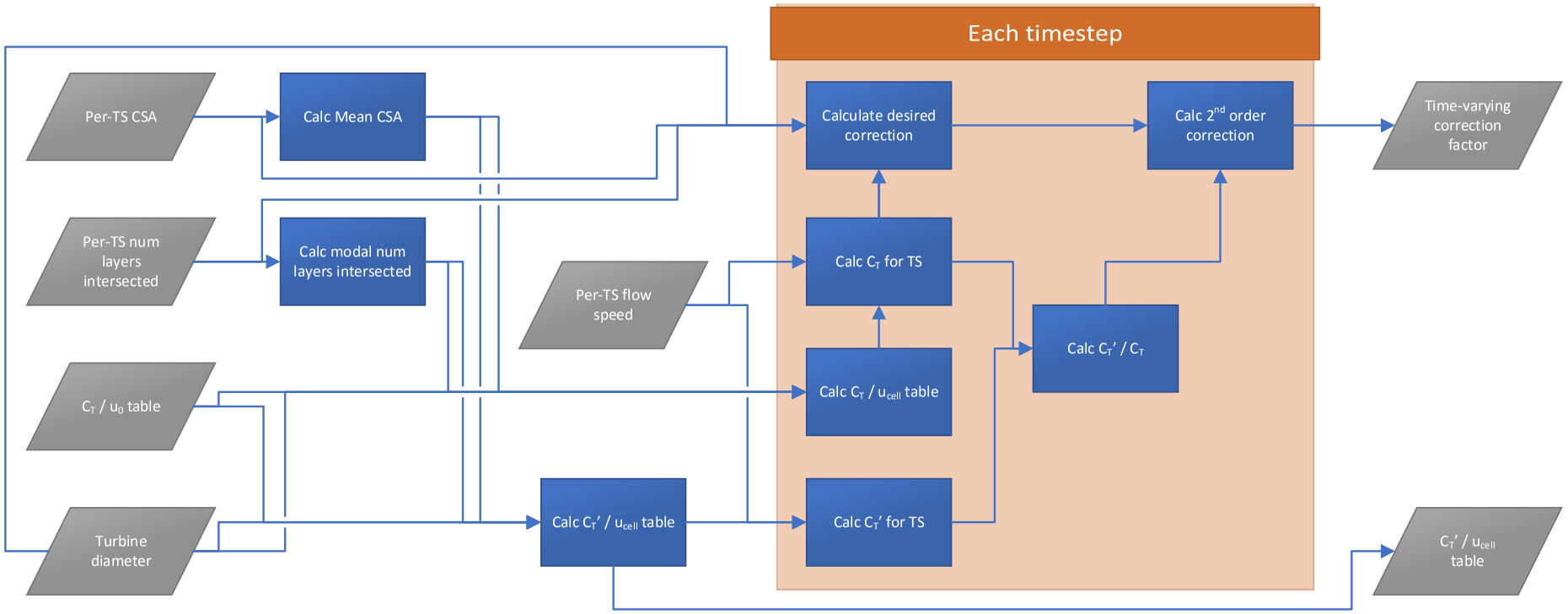

(d) *Method D (selected method)*

Figure 4.16: *cont...*

location using this approach was less than $0.1\,\mathrm{m\,s^{-1}}$, which was clearly not useful for testing.

Instead, an M2 cyclic elevation was applied at one end and the other end was clamped to zero elevation, with free flow of water permitted through both ends. This is unrealistic, and does not match any obvious natural scenario. However, it does provide a convenient means to establish oscillatory flows with high current speeds at the turbine location while using a small model domain, and without the need to calculate the correct phase offsets for varying the elevation at both ends. Since the purpose of this work is to evaluate the behavior of a modelled turbine in a given flow, and not to simulate a realistic channel, this was judged to be appropriate.

The behavior of the resulting channel is illustrated in Figure 4.17. The phase difference between elevation and flow speed is approximately 42°, indicating that friction and inertia have similar levels of influence on the oscillating flow.

The capability to allow for changing surface elevation was implemented and tested in parallel with that of allowing for variable C_T. Three of the methods described above were tested. Method A would not allow for feedback from changes in speed as a result of the correction to changes in C_T, and so was rejected. Method B lacks a time-varying element to the correction and so would not allow for the effects of changing surface elevation. It was included in tests for comparison purposes. Method D is the most "correct" approach, and was anticipated to be the most accurate possible without iterating between script and model. Method C is a simplification of this with fewer steps, which might offer a performance benefit.

An M2 signal with an amplitude of 0.8 m was applied at one end of the channel, for a tidal range of 1.6 m at the boundary and aproximately half of this at the turbine location. Methods B, C and D were applied to this scenario. Since we were now dealing with a time-varying driving force, the results could no longer be meaningfully expressed in terms of the thrust forces at the final timestep. Instead, results are shown in Table 4.6 as the root mean square difference between the largest (250 m) mesh and the other mesh scales.

Mesh size (m)	Uncorrected	Method B	Method C	Method D
50	38 646	8691.3	8687.0	8642.6
100	16 334	5874.4	6185.7	5873.8
150	5429.7	2757.7	2761.0	2750.1
200	3453.9	2148.6	2169.2	2143.4

Table 4.6: *Comparison of the RMSE of predicted forces (in N) for the given mesh sizes compared to those from the* 250 m *mesh, using three correction methods with an M2 amplitude of* 0.8 m *at the channel mouth.*

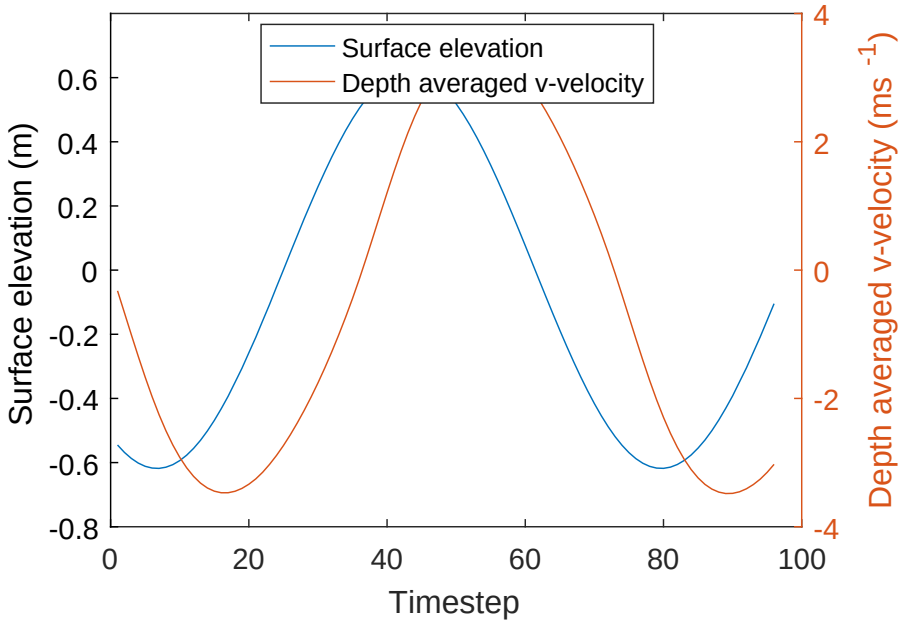

Figure 4.17: *Plot showing the phase difference between surface elevation and v-velocity at the centre of the test channel with no turbine.*

All of the corrected values are quite different to the uncorrected ones, but differences between the different correction methods are small. Method D consistently represents a small improvement on Method B. Method C is worse than either B or D, and as such should not be used. As Method B makes no allowance for changing surface elevation — which may become a more important factor in real scenarios where the tidal range is somewhat greater than that in this model — Method D was selected for future use. While it is more complex than the others, no difference in the performance of the script was discernable in timing tests, suggesting that even with multiple turbines and many timesteps, the speed of this calculation step will not be important*.

4.6 Overall testing

All tests to this point had concerned a single turbine operating in undisturbed flow. In order for the correction technique to be widely applicable, it was necessary to demonstrate that it produced the right results in less ideal conditions. Two further tests were carried out: one with a tightly packed array, where downstream turbines were within the wakes of upstream turbines, and one with a high channel blockage. Only the finest ("50 m") grid was used for these tests, because this was the most sensitive to the error in question and because only the finer grids allowed the desired

*The runtime of the correction script is currently dominated by the time taken to calculate cell widths / cross-sectional areas from mesh geometry, and so any future optimisation effort should focus there.

multi-turbine tests to be performed while maintaining a maximum of one turbine per mesh element.

The use of just a single mesh size meant that it was not possible to verify the correction by comparing multiple mesh scales. Instead, the corrected model was run an additional three times with a different turbine removed each time, and verification for these three turbine locations was performed by comparing the values of u_0 calculated from the corrected model to values of u_0' "measured" from a model with just that turbine removed, as described in Section 4.3.2. Results are reported numerically as the root mean square error between these two values over all timesteps, and are shown graphically as scatter plots.

4.6.1 Array test

Five turbines were placed in the usual channel, as shown in Figure 4.18. A 45×160m spacing was used, as suggested by O'Hara Murray (2015) based on environmental statements for real developments. From viewing the outputs of the uncorrected simulation (Figure 4.19) it is clear that all five turbines are within the single "blob" of decreased velocity that they cause, so the downstream pair are certainly affected by the wakes of the upstream ones.

Three out of the five turbines were removed, one at a time, to allow their free-stream speeds to be tested, and the results are shown in Table 4.7. In all three locations the normalised RMSE between the calculated and "measured" values of u_0 was 0.65% or less, and this was judged to be acceptable.

4.6.2 High blockage test

A single row of turbines was evenly spaced across the 2 km width of the channel, as close as was achievable without exceeding one turbine per mesh element. This

Turbine #	RMSE (ms^{-1})	nRMSE
1	0.0142	0.63%
3	0.0148	0.65%
5	0.0146	0.64%
Mean	0.0145	0.64%

Table 4.7: *RMSE between u_0 values measured from model run without that turbine versus calculated from model run with corrected turbines, in a scenario with a two-row array. nRMSE values are normalised by dividing by the mean value from the run without the turbine.*

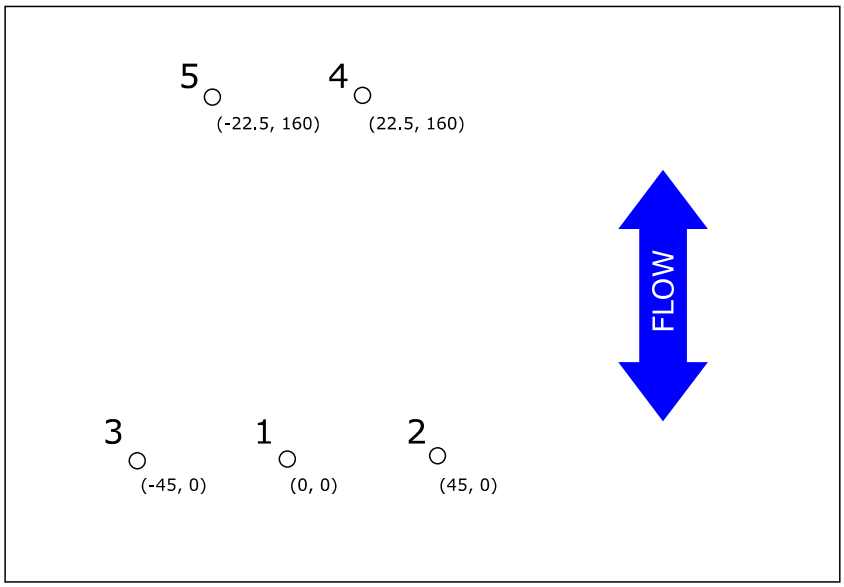

Figure 4.18: *Layout of five simulated turbines in the centre of the channel used for testing in an array. Not to scale.*

transpired to be 39 turbines at 50 m hub-to-hub spacings, equal to a blockage of 12.6% of the total cross-sectional area of the channel. Such a tight spacing, which would give a distance between blade tips of only 1.5 rotor diameters, is unlikely to be realistically simulated by MIKE on this mesh, as the channels between turbines will not be well resolved. However, the purpose of the test is to evaluate the performance of the correction script and not the ability of MIKE to accurately simulate the scenario.

Once again, three sample turbines were removed one at a time, and the corrected model rerun without each one, to allow the calculated value of u_0 to be verified at these locations. The three sample turbines are shown in Figure 4.20 and consisted of one adjacent to the channel wall, one in the middle of the channel, and one 3/4 of the way across.

Results of this test are shown in Table 4.8, and suggest that the correction applies in channels with significant blockage. A graphical illustration of the results, in the form of a scatter plot, may be seen in Figure 4.21.

Figure 4.22 shows a time series of total thrust, with and without the correction, from the high blockage scenario. This figure demonstrates the importance of using a realistic thrust curve: for much of the time the flow speed is above the rated speed of the turbine and so the thrust is reduced to avoid capturing more than the rated power. This means that the effect of the correction is to reach the maximum thrust at slightly lower speeds, which would result in the rated power being produced for a longer period on each tidal cycle.

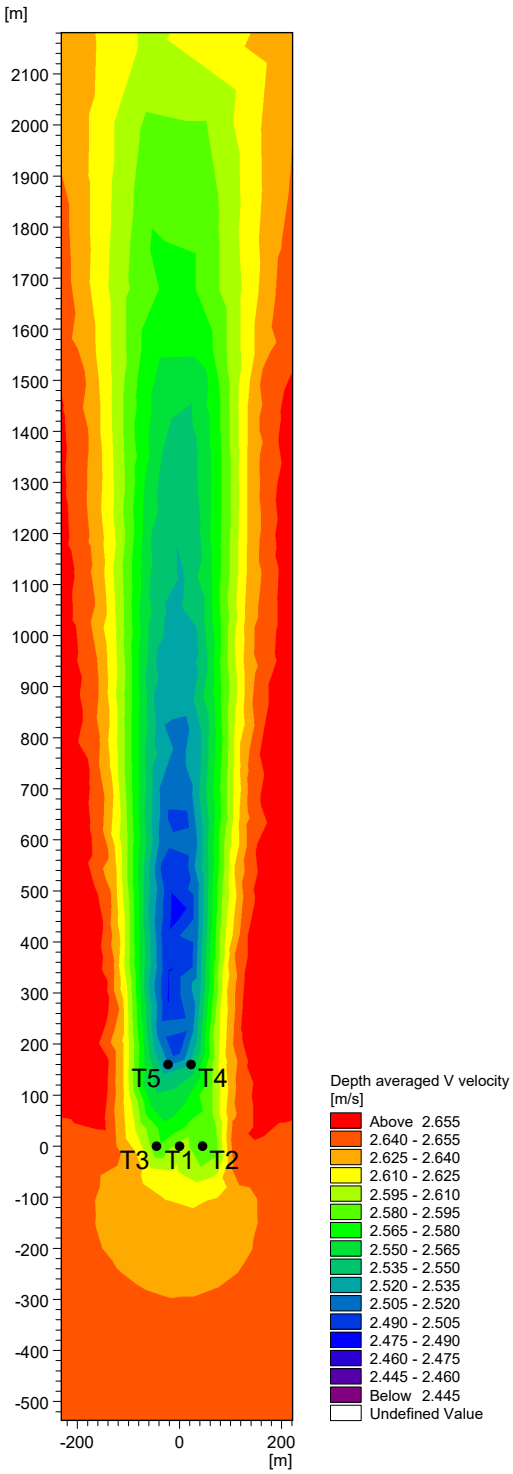

Figure 4.19: *"Snapshot" of a sample time step (with northwards flow) from uncorrected array test run, showing depth-averaged v-velocity and turbine locations.*

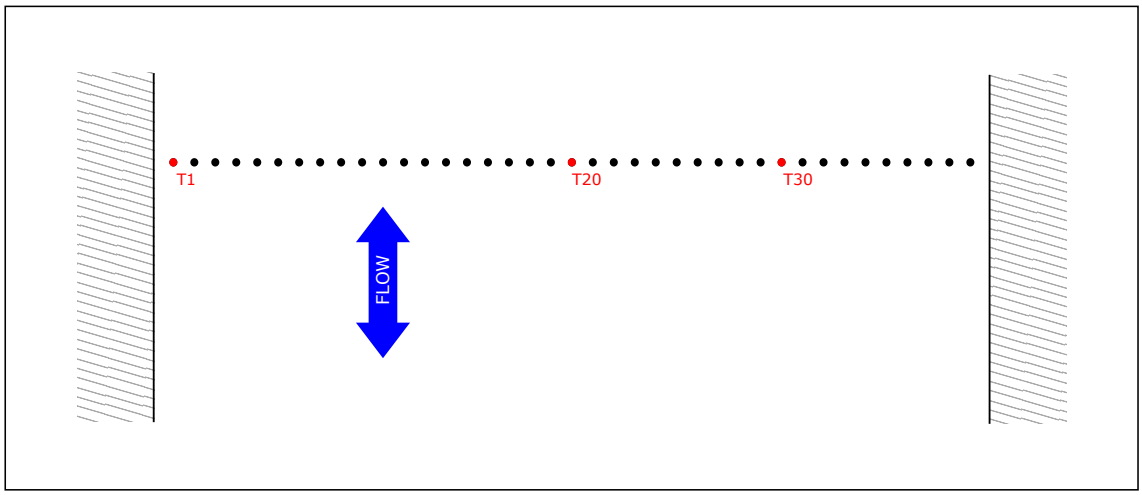

Figure 4.20: *Layout of 39 simulated turbines across the channel used for testing a high blockage scenario, highlighting the three locations used for verification.*

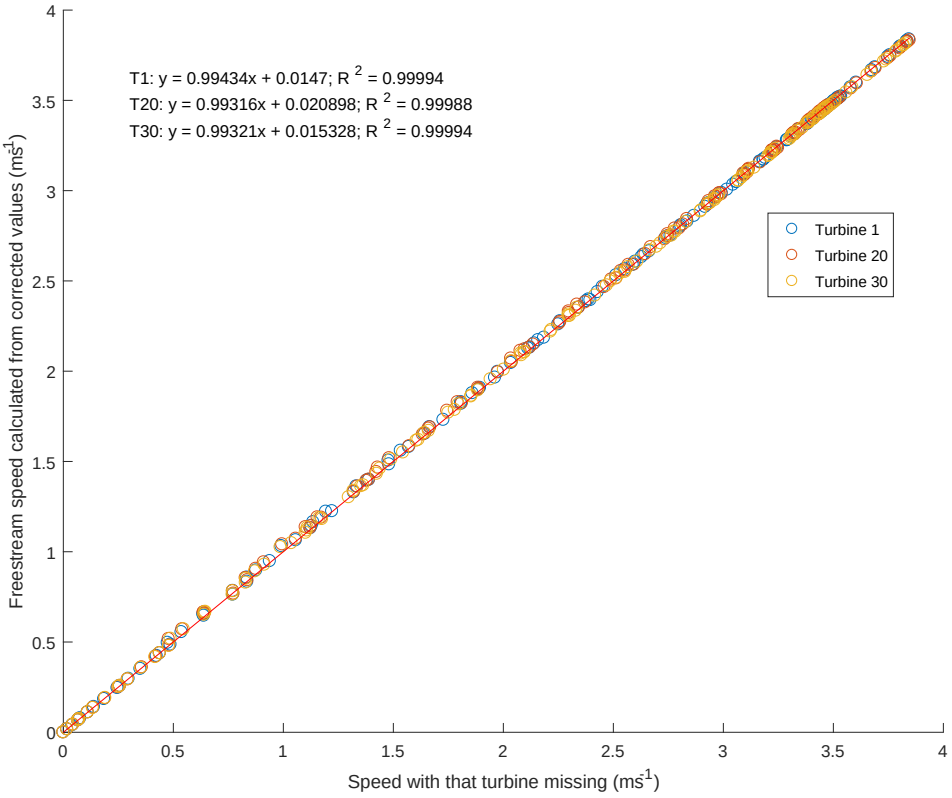

Figure 4.21: *Scatter plot showing calculated values of the upstream velocity against those measured at the same locations without turbines.*

Turbine #	RMSE (ms^{-1})	nRMSE
1 (by wall)	0.0115	0.50%
20 (middle)	0.0157	0.69%
30 (half way to far wall)	0.0117	0.51%
Mean	0.0130	0.57%

Table 4.8: *RMSE between u_0 values measured from model run without that turbine versus calculated from model run with corrected turbines, in a scenario with significant channel blockage. nRMSE values are normalised by dividing by the mean value from the run without the turbine.*

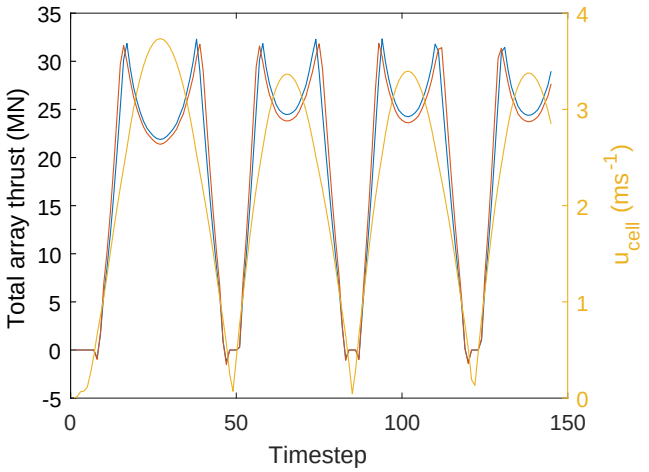

Figure 4.22: *Time series showing total array thrust in the high blockage scenario without (blue) and with (red) the correction. Yellow line shows uncorrected u_{cell}, averaged across all turbines. The brief excursions into negative thrust are the result of a bug in MIKE, possibly relating to "overshoot" where there is a step change in the thrust curve.*

4.7 Discussion & chapter conclusions

A correction has been implemented to allow for the error identified and all testing so far suggests that it works accurately, with a normalised RMSE between calculated and "measured" values of the free-stream velocity of less than 1%, such that it could be used for real modelling problems.

It is possible that greater accuracy could be achieved by using a more sophisticated sub-grid model. For example, the approach in Whelan *et al.* (2009) takes account of free-surface distortion by turbines, which might have a significant effect in shallow channels with high vertical blockage. Consideration of losses of momentum to in-cell turbulence might also be fruitful. However, at least in the scenarios examined here, the accuracy is already high enought that the potential benefits from further refinements are small compared to other uncertainties in regional flow modelling.

The following limitations apply to the current implementation:

- A maximum of one turbine per mesh element is permitted. Correcting for multiple turbines in a single element will require further thought, development, and testing.
- Turbines are assumed to lie on-axis to the flow at all times. This is realistic for some of the current designs, which yaw to face the current, but not for others, which are fixed or bi-directional. Off-axis turbines are well catered for in MIKE, which breaks the thrust coefficient down into components termed as "drag" and "lift" for forces parallel and orthogonal, respectively, to the turbine's axis*. However, it is not clear from the documentation how MIKE calculates the thrust for such turbines internally, and experimentation would be required to determine this in order to apply the same correction.

The emphasis of this work has been on correctly predicting turbine thrust, as it is this that affects the functioning of a regional-scale hydrodynamic model. One use of this type of model is estimating the power that may be produced by a TEC, and so it is relevant to briefly consider how the error referred to here will affect power. The power of a turbine would usually be described in terms of a power coefficient C_P, but in this case it is more helpful to consider it in terms of force and velocity. The power available at the rotor for conversion to electricity is equal to the thrust multiplied by the speed at the rotor, *i.e.*

$$P_{rotor} = F u_t = \tfrac{1}{2}\rho C_T A_t u_0^2 u_t \tag{4.17}$$

*For avoidance of confusion, note that drag and lift are not used here in their correct hydrodynamic sense of forces on individual blades.

u_t is not known to the model, but it could be estimated as a post-processing step using (4.12), (4.9) and $u_0 = u_{cell}\sqrt{\eta}$, where u_{cell} is taken from a corrected run of the model and η is the correction that was applied.

The power that is removed from the flow is greater than that available for conversion, partly due to the energy lost to turbulent mixing between the turbine wake and the surrounding flow (see Section 2.3.1). Some of this mixing will occur within the mesh element containing the turbine and some, at a larger scale, without it. Due to conservation of momentum, the total power lost to the flow within the element must be equal to the thrust multiplied by the overall speed in the cell, *i.e.*

$$P_{total} = Fu_{cell} = \tfrac{1}{2}\rho C_T A_t u_0^2 u_{cell} \tag{4.18}$$

where u_{cell} is taken from a corrected run of the model. The portion of mixing losses that occur outside the turbine's mesh element should be dealt with by the model's standard turbulence scheme. Vogel *et al.* (2013) make a similar argument, only they assume that all wake mixing happens within a single model cell and hence use u_0 in place of u_{cell}.

This calculation can be made as a post-processing step, using information that is available in or derived from outputs of the corrected model, provided that the total correction applied for each timestep have been saved. The total correction is recorded by the MTMC script in the `.mat` file that it produces.

4.8 Source code availability

The MATLAB code developed in this chapter is publicly available at `https://github.com/TeraWatt-EcoWatt2050/MTMC`. Development was continuous while the work in this chapter was conducted, but the version on which the final testing was performed is tagged "`Thesis`".

Chapter 5

Resource assessment and interactions between channels in the Goto Islands, Japan

It was originally planned that the methods developed in the last chapter should be applied to a MIKE model of Lashy Sound in Orkney, and that work is indeed shown later. However, an opportunity arose to collaborate with Kyushu University in Japan to perform similar work on a group of islands there. The model used was FVCOM, which is an open source academic code and thus not ideal according to the discussion in Section 1.3.2. However, FVCOM was the system chosen by Marine Scotland Science for their recently-commissioned Scottish Shelf Model (Wolf *et al.*, 2016). It is thus trusted and accepted by a regulator, and hence still of relevance to this project.

The Goto Islands in Nagasaki Prefecture, Japan, contain three parallel channels that are suitable for tidal energy development. Two of them are the planned location for a tidal energy test centre. Multiple channels are a common occurrence at tidal sites around the world, giving the findings here wider relevance than the location being studied. The work described in this chapter had two goals: Firstly, to provide an initial tidal resource assessment for the Goto Islands, and secondly to explore the behaviour of the parallel channels when energy is extracted.

Kyushu University provided a pre-existing 3D FVCOM model of the region, office space, computing facilities, advice and supervision. The research described here was conducted by the author. In this chapter, after describing the background to Japan's energy situation, the Goto archipeligo itself, and some theoretical background, Section 5.4 describes the numerical model that was used. Sections 5.5–5.7 relate simulations using realistic TEC representations, aimed at estimating the available resource. In Section 5.8 the realistic TEC parameters are put aside in an effort to

explore the maximum possible extractable power in one of the channels and its effect on the other straits. Section 5.9 discusses findings and compares the behaviour of the Goto Islands to that of the Pentland Firth.

5.1 Background

In 2010 nuclear power provided 25% of Japan's electricity (Statistics Japan, 2016), making Japan the third-largest producer of nuclear energy in the world (US Energy Information Administration, 2015). Following the tsunami of 2011 and the subsequent events at the Fukushima Daiichi nuclear power plant this figure reduced to less than 2% (in 2012) as the nation's reactors were taken offline, and most of the shortfall was replaced by fossil fuels. Lacking substantial fossil resources of its own, by 2015 Japan had become one of the world's greatest importers of fossil fuels, and in addition to the environmental implications this represents a significant drain on economic resources (US Energy Information Administration, 2015). While there has been some limited resumption of nuclear generation, this is deeply unpopular with sections of the public (Bricker *et al.*, 2016). As part of a strategy to increase domestic energy supply, the Japanese government plans for 22–24% of electricity to be generated by renewables in 2030 (Japanese Ministry of Economy, Trade and Industry, 2015). Work is in progress to set up a marine energy test centre, similar to the European Marine Energy Centre in Orkney, in the Goto Islands of Nagasaki Prefecture (Iwata, 2015).

5.2 Geographic & hydrodynamic situation

The Goto Islands form an archipelago approximately 80 km to the west of Nagasaki city and, at their closest point, separated from the Japanese mainland by approximately 20 km of sea (Fig. 5.1a). To the north is the Korea Strait, the main southern entrance to the Sea of Japan, while to the south lies part of the East China Sea and the Pacific Ocean. A portion of flow between these large bodies of water must pass through or around the archipelago.

Within the islands there are four channels running from north-west to south-east, three of which are approximately parallel and of similar dimensions: 7–8 km in length, 1–3 km in width, and 50–60 m deep in mid-channel. These are the Tanoura, Naru and Takigawara Straits (Fig. 5.1b). The first two have been designated by the Japanese government as an area for tidal energy development, and the first tidal energy convertor (TEC) is due to be installed by OpenHydro in the Naru Strait in 2018 (OpenHydro, 2016). The fourth channel, the Wakamatsu Strait, is less

than 30 m deep for most of its length and is hence unsuitable for the TEC design considered here.

The region experiences mixed diurnal / semi-diurnal tides. When compared to European seas, less of the energy is to be found in the M2 constituent and a greater proportion (approx. 15% of the total) is in K1 and O1. Table 5.1 shows the most important constituents.

5.3 Theoretical background & prior work

To extract tidal stream energy, a porous obstruction is placed in the flow in the form of a TEC. A proportion of the kinetic energy passing through the TEC is removed for conversion to electricity and a retarding force is applied to the flow, usually resulting in a reduction in its speed. For a given array in a given channel there exists an optimum proportion of energy removed, beyond which the flow is retarded to such an extent that the available power diminishes. In an idealised channel, this optimum is given by the theoretical model of Garrett and Cummins (2005) (see Section 2.4.2).

The exportable power available from the turbines cannot exceed the power extracted from the flow, and will usually be less. Where the array does not fill the cross-section of a channel, some flow will divert around it. The kinetic energy of this bypass flow is clearly not available for conversion, but some of it will still be lost from the channel in turbulent mixing when the bypass flow meets the slower wake behind the turbine (Vennell, 2012). Thus, so long as financial limitations on the number of turbines do not apply, a tidal stream array occupying the entire cross-section of a channel will always be optimal. This was demonstrated with theoretical models by Garrett and

Constituent	Proportion of total energy (%)	
	Goto	Fall of Warness
M2	65.2	79.3
S2	13.2	11.2
K1	9.2	1.9
O1	6.0	1.0
N2	2.7	3.3

Table 5.1: *Table showing the five most energetic tidal constituents in the Goto islands, based on a 29 day time series of surface elevation from a combined pressure sensor and ADCP deployment in the Naru Strait (Sun* et al.*, 2014). For comparison purposes the same information is presented for the Fall of Warness, Orkney, using pressure sensor data from four weeks of EMEC ADCP records. Harmonic analysis was conducted using the U-Tide software.*

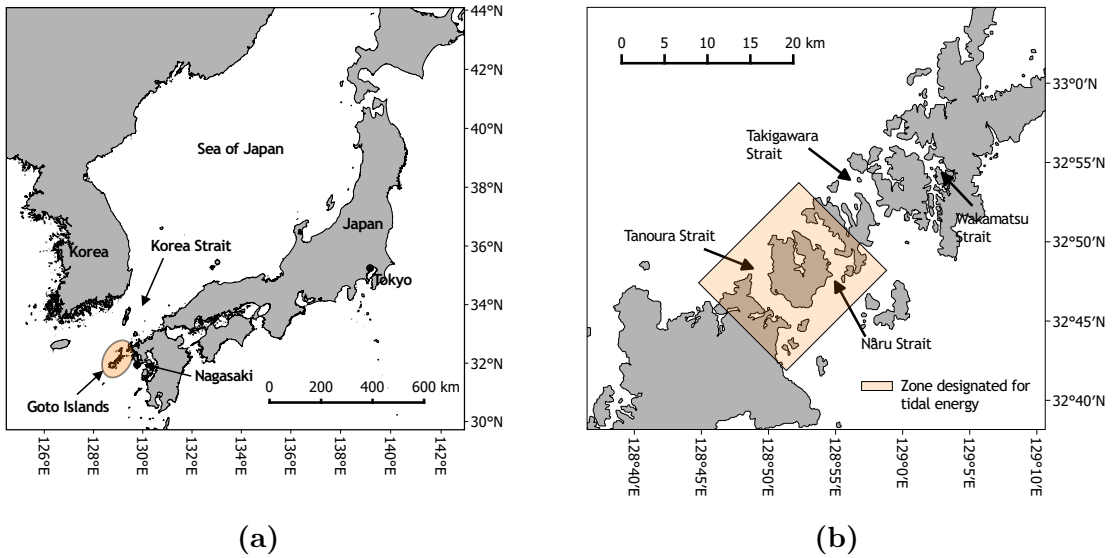

(a) **(b)**

Figure 5.1: *Maps showing (a) the situation of the Goto Islands with respect to Japan, and (b) the four channels running through the middle of the archipelago.*

Cummins (2007) and Houlsby *et al.* (2008).

The behaviour of multiple channels has been studied from a theoretical perspective by Atwater and Lawrence (2010), who considered the available power in terms of head loss, and Cummins (2013), who used the analogy of an electical circuit. Practical modelling investigations of the multiple channels in the Pentland Firth, Scotland, have been conducted by Draper *et al.* (2014b) (in two dimensions) and O'Hara Murray and Gallego (2016) (in three dimensions, using FVCOM). In all of these studies, where there are parallel sub-channels, there is a tendency for exploitation of one channel to cause flow to be diverted into unexploited sub-channels, reducing the yield.

The author is unaware of any prior resource assessments of the Goto Islands that account for the effects of energy extraction, and hence the estimates made here (also recently published as Waldman, Yamaguchi *et al.* (2017)) may be the first available.

5.4 Description of the model

Numerical simulations were conducted using the Finite Volume Community Ocean Model (FVCOM) (Chen *et al.*, 2003). The model used in this work was developed by others at Kyushu University using FVCOM version 2.8. It will be summarised here, but is described more fully in Sun *et al.* (2014).

An unstructured triangular mesh was used in a relatively small computational domain, the full extent of which is shown in Fig. 5.2. The mesh had a typical element size

of 50 m around the three narrow channels in the Goto islands (Fig. 5.3), gradually increasing to 5000 m toward the open boundary. Twenty sigma layers were used in the vertical. The small size of the domain is a potential cause for concern, as per Section 2.3.3. As the model was provided by others in a validated condition it was not practical to test different domain sizes. However, the mean changes in speed at the boundary, in the scenario with the maximum energy extraction, were occasionally an order of magnitude lower than those in the tidal channels and usually much less.

The model bathymetry (Fig. 5.2) was produced from data supplied by the Hydrographic and Oceanographic Department, Japan Coast Guard. Eight major tidal constituents (M2, S2, K2, N2, K1, O1, P1, Q1) were forced using a clamped open boundary, using amplitudes based on the NAO.99Jb regional tide model (Matsumoto *et al.*, 2000) and phases arrived at during the calibration process. The modified Mellor and Yamada level 2.5 turbulence closure scheme built into FVCOM (Mellor and Yamada, 1982) was used for vertical eddy viscosity. The model was run in barotropic mode with no freshwater inputs or meteorological effects.

The model was provided by its creators for FVCOM version 2.8, but the code that was to be used for energy extraction (see below) required a more recent version. An early task was therefore to update it to run under version 3.2.2 (the latest at the time). This required converting or remaking some of the input files, often changing from text to NetCDF format. Primary validation of this model had been conducted by others (Sun *et al.*, 2014), but because of the scope of these changes, and because of the possibility of changes to the physics algorithms in the new version, some further testing was conducted to ensure that the new version still produced plausible results, by comparing a two-week simulation to observations in the Naru and Takigawara straits (see Figure 5.3 for locations). The results of this comparison are illustrated in Figure 5.4, and were judged to be acceptable.

5.4.1 Energy extraction

Energy extraction was simulated by introduction of momentum sinks at the relevant locations, an approach first reported with FVCOM by Yang, Wang and Copping (2013). This method was implemented and enhanced by O'Hara Murray and Gallego (2016), who kindly provided their code. In summary, additional terms in the relevant momentum equations simulate a retarding force, where the total thrust is determined by

$$F = \tfrac{1}{2}\rho C_T A|\mathbf{u}|\mathbf{u} \tag{5.1}$$

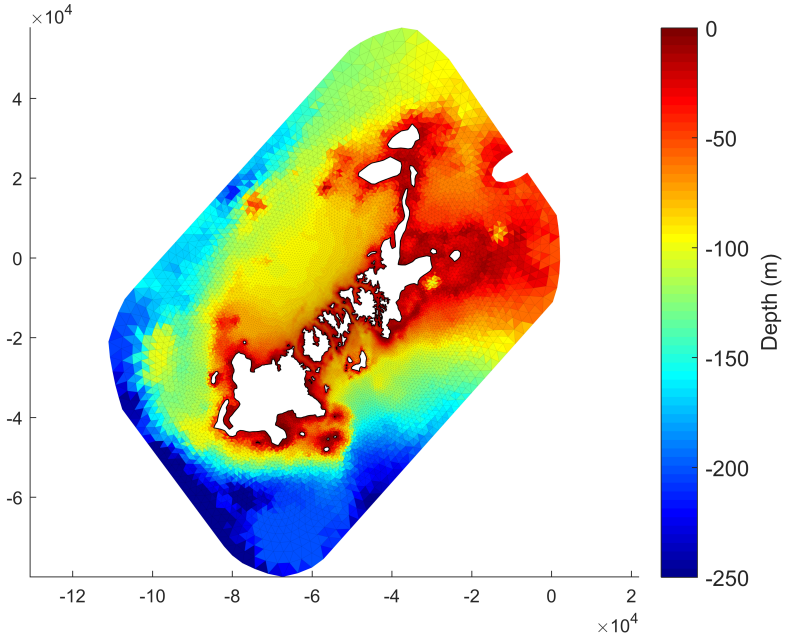

Figure 5.2: *Plot showing the model domain and bathymetry. The spatial coordinates are in metres, referring to the "Japan Plane Rectangular" coordinate system zone CS1, EPSG ref 2443.*

and this total is divided amongst the layers occupied by the rotor at mean sea level according to the proportion of the rotor's area that lies within each layer. ρ refers to the water density, C_T to the thrust coefficient of the turbine, A to the area of the rotor facing the flow, and $\mathbf{u}$ to the water's velocity. The thrust coefficient is determined at each timestep by the value of $|\mathbf{u}|$, using a lookup table and linear interpolation. The value of $\mathbf{u}$ is one that applies to the entire cell, as the correction discussed in Chapter 4 has not been implemented for FVCOM. The thrust is therefore likely to be slightly higher than the correct value for most of the tidal cycle.

The simulated TEC was based on the OpenHydro device that has been proposed for the Naru Strait. This is a seabed-mounted design with a diameter of 16 m, a hub height of 19 m above the seabed, and a rated capacity of 2 MW (OpenHydro, personal communication with Kyushu University collaborators). A realistic thrust curve was applied, based on that established in Chapter 3 but scaled to use a cut-in speed of $1\,\mathrm{m\,s^{-1}}$ and a rated speed of $3\,\mathrm{m\,s^{-1}}$. This rated speed was adopted because it is a speed that is regularly encountered during spring tides in the area of interest; the turbine's rated capacity of 2 MW would imply a rated speed of over $3.5\,\mathrm{m\,s^{-1}}$, but it is unlikely that this would ever be reached. The thrust coefficient between the cut-in and rated speeds is 0.85, while above the rated speed it is scaled to provide a constant power output.

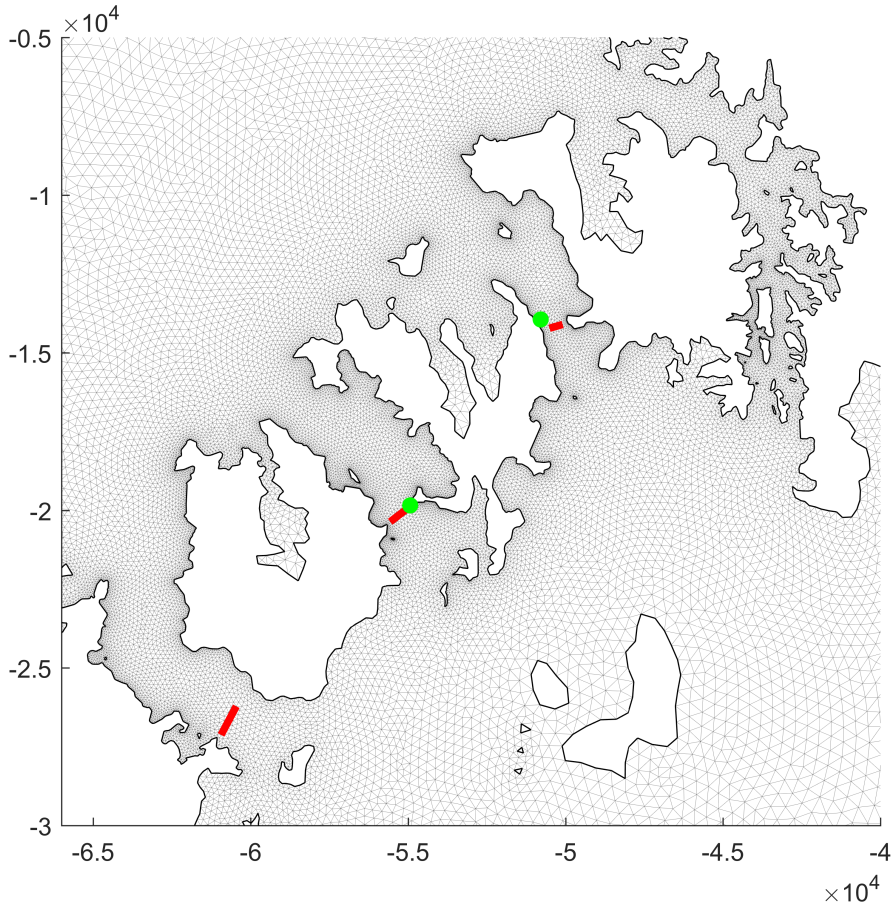

Figure 5.3: *Plot showing the inner part of the computational mesh. Thick red lines show the locations used for tidal turbines, as described in Section 5.5. Green points show ADCP locations, used for re-validation. Spatial coordinates are in metres, referring to the "Japan Plane Rectangular" coordinate system zone CS1, EPSG ref 2443.*

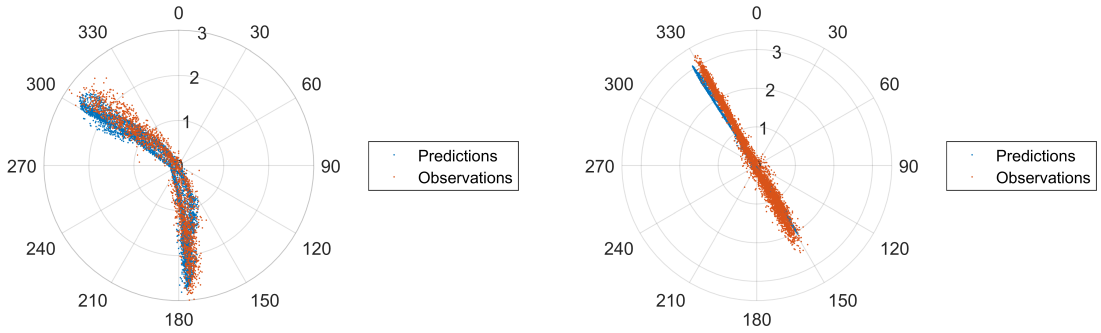

(a) *Naru strait* **(b)** *Takigawara strait*

Figure 5.4: *Hodographs showing current velocity in the updated model compared to measurements, for a one month period. Radial axis is speed in* m/s.

5.4.2 Calculation of power

Electrical power was calculated from simulated current speeds as a post-processing step. Initially, thrust was determined using (5.1). Power was then estimated using

$$P = C_C F |\mathbf{u}| \tag{5.2}$$

where C_C is a coefficient that represents the conversion losses between kinetic energy in the flow and electricity. This is, again, not entirely correct, as the value of $|\mathbf{u}|$ that is used represents an entire mesh element, while it should be the speed at the turbine. A value of 0.5 was assigned to C_C based on experimental results with a Schottel turbine reported by Jeffcoate *et al.* (2015). This two-stage approach is equivalent, below the rated speed, to a power coefficient of 0.425, which is within the range shown by Bahaj *et al.* (2007) from tank testing.

5.5 Single-channel scenarios

A transect across each strait between the 30 m depth contours was identified to hold TECs. This depth limitation allowed for the full height of the TEC (27 m from base to blade tip) to remain submerged throughout the tidal cycle. Simulated turbines were placed, evenly spaced, along these lines, and the number of turbines lying inside each intersected mesh element was provided to the FVCOM model. The transects were located by inspection of the areas of highest speeds without turbines on both flood and ebb, which were usually at or near to the narrowest parts of the channels. Their locations can be seen in Fig. 5.3.

A wide range of turbine numbers was tested in each channel, from the conservative to the implausible. In the more heavily exploited scenarios a single row of turbines is unrealistic, as they would be placed very close together and even overlap and collide. However, this approach allowed the level of energy extraction in a channel to be reduced to a single parameter, which is convenient and, in the event of performing an optimisation across multiple channels, reduces the number of degrees of freedom. Since the purpose of this work was not to study realistic array layouts but to examine the behaviour of the channel as a whole, this was judged to be acceptable.

In order to minimise computation time, initial simulations were driven only by the M2 tidal constituent. This allows the use of just 12.4 hours of output — a single M2 cycle — as a representative time period. It was determined empirically that the model required 3 days of spinup time before its output became fully periodic, so each scenario was run for 4 days of model time and the output data taken from the final 12.4 hours.

Fig. 5.5 shows the maximum and mean power output for each channel with scenarios between 5 and 1000 turbines. The use of M2 only means that results in this section show unrealistically low levels of power, so limited attention should be paid to the absolute power levels; of interest instead are the differences in output between different scenarios. It is clear that even with modest numbers of TECs, additional machines offer diminishing returns. The mean power available in each strait peaks at implausibly high levels of exploitation, ranging from 270 to 446 TECs; beyond this point, adding additional turbines gives a negative marginal return. The maximum power also peaks in each channel, but at even higher numbers of TECs than the mean.

O'Hara Murray and Gallego (2016) noted that when simulating turbines in their correct vertical locations, a portion of the flow would divert over and under the turbine rotors instead of passing through them (although in reality, or in a more detailed simulation, some of the flow under the rotor would be impeded by the device's base structure). This behaviour appears to be replicated in the Goto channels, as suggested by Fig. 5.6. Vertical diversion limits the power output that can be achieved, but is unavoidable while using bottom-mounted turbines and while, in some areas, preserving clear water above for navigation.

The use of realistic TEC arrangements will be continued for the next two sections to arrive at realistic resource estimates. In Section 5.8 the TEC description will be modified to explore the maximum power that can be extracted without engineering or navigational constraints.

5.6 Interactions between channels

Fig. 5.7 shows the effect on mean current speeds of placing 100 TECs in the Naru Strait. A reduction in mean speed of up to $0.15\,\mathrm{m\,s^{-1}}$ through the TECs is seen, as expected, and an increase of $0.1\,\mathrm{m\,s^{-1}}$ occurs at the sides of the channel around the array. Adding impedence to the Naru Strait has only small effects on the other channels; mean speeds in the Tanoura Strait are affected by less than $0.02\,\mathrm{m\,s^{-1}}$, and those in the Takigawara Strait by slightly more.

There are substantial areas of change to the north and south of the islands. These appear to be caused by changes in the positions of eddy structures that form at the downstream ends of the channels (see Figure 5.8).

The equivalent maps for the other two channels are not shown, but the qualitative results are similar: reductions in mean speed in the exploited channel, but only small changes in other channels.

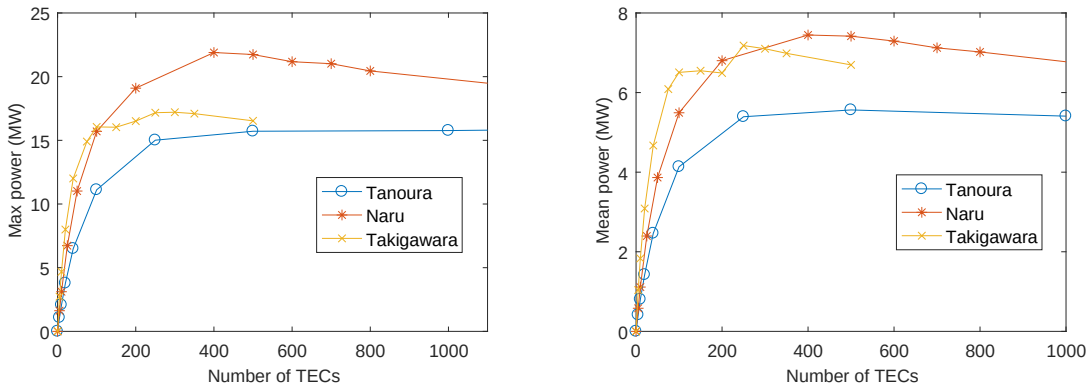

(a) **(b)**

Figure 5.5: *Plots showing (a) maximum and (b) mean power output from the three channels with varying numbers of realistic TECs, using M2 tides only. The maximum power in the Tanoura strait peaks at approximately 2400 TECs, beyond the limits of this plot.*

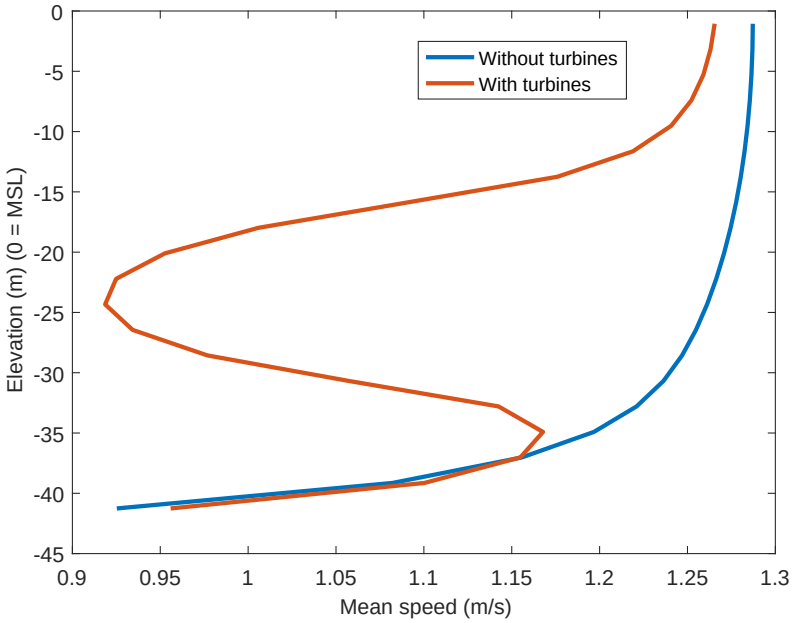

Figure 5.6: *Vertical speed profiles showing mean current speed over 24 hours with and without TECs. The scenario used for "with turbines" is that of 100 TECs in the Naru strait, and the mesh element used is that with the greatest number of TECs in this scenario.*

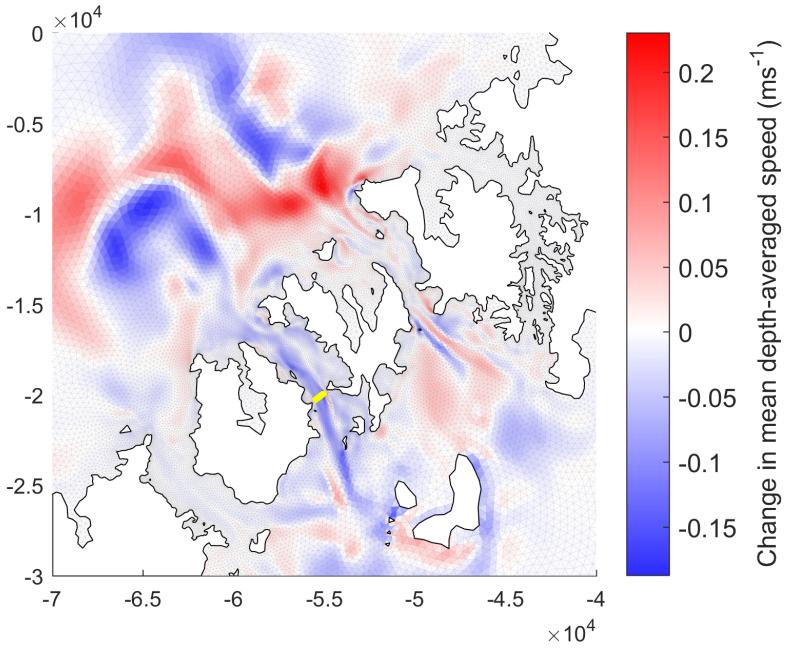

Figure 5.7: *Map showing the change in mean current speed over an M2 cycle in each mesh element as a result of adding 100 TECs to the Naru Strait. Yellow line shows location of turbines. Spatial coordinates are in metres in the "Japan Plane Rectangular" coordinate system zone CS1, EPSG ref 2443.*

In order to provide a quantitative perspective on inter-channel effects a series of simulations was conducted, using only the M2 constituent, with 60 TECs in each channel and in each combination of channels. Comparisons were made between the maximum and mean power outputs of these channels, and in particular between the power provided by a scenario with two or three channels together and the sum of the powers provided by each of those channels alone; interactions between the channels whould result in differences between these values.

The results of these simulations are shown in Table 5.2, and show an increase in mean power of the order of 1% from using two channels together, indicating that some interaction does exist but that it is weak. The reason why "all 3 together" has a lower maximum power, but a higher mean power, than the sum of 3 separately, is unclear. It may relate to slight phase differences in the progress of the tide through the channels.

The low level of interaction between channels in Goto contrasts with the findings of Draper *et al.* (2014b) in the Pentland Firth, where the power available in each subchannel depended markedly upon the level of exploitation in the others.

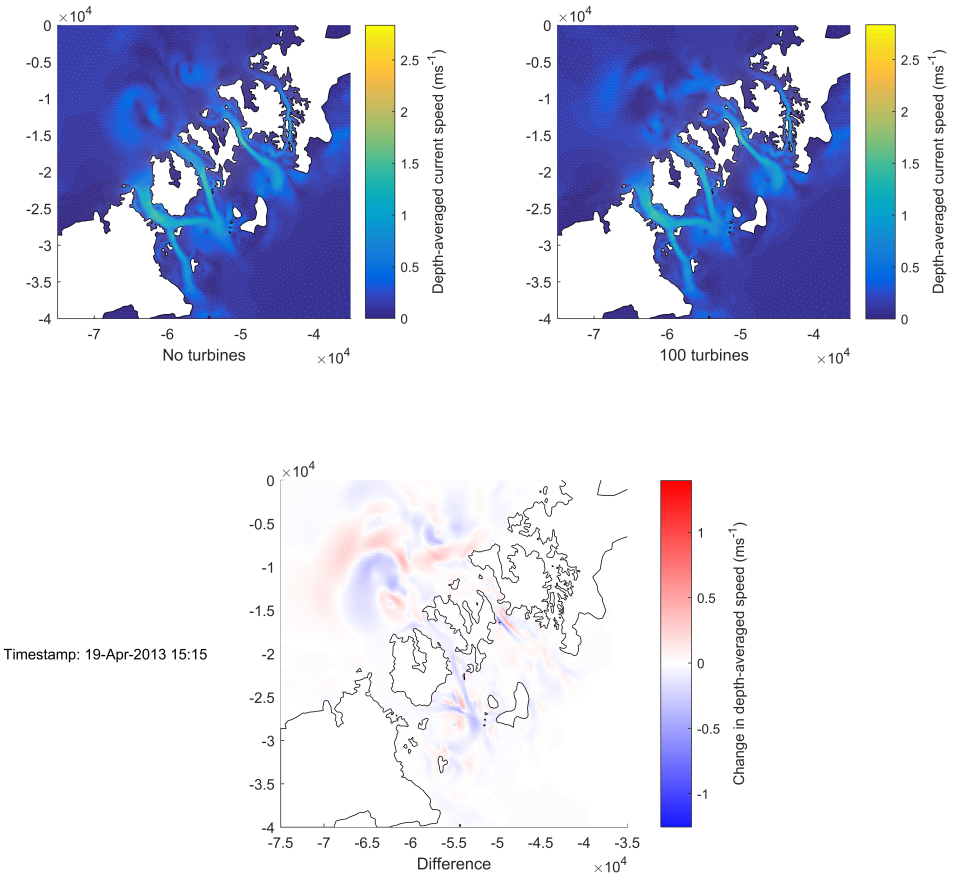

Figure 5.8: *Snapshot of a single timestep showing flow without turbines (top left), with 100 turbines in the Naru strait (top right), and difference (bottom). Note the differences in the eddies to the north of the channels.*

Channels exploited	Mean power (MW)	Max power (MW)
Tanoura alone	3.2	8.4
Naru alone	4.3	12.3
Takigawara alone	5.6	13.8
Sum of Tanoura & Naru separately	7.4	20.3
Tanoura & Naru together	7.5	20.5
Sum of Naru & Takigawara separately	9.9	25.2
Naru & Takigawara together	10.0	25.2
Sum of all 3 separately	13.1	32.7
All 3 together	13.2	32.3

Table 5.2: *Table showing mean and maximum outputs from different combinations of channels. 60 turbines were used in the exploited channels. Sums are on a per-timestep basis. The models were forced with M2 only, so the power estimates will be unrealistically low.*

5.7 Estimating the resource

Thus far, simulations have been driven only by the M2 constituent in order to minimise computation time. However, only 65% of tidal energy in this region is in M2 (see Table 5.1), and so this does not give a useful estimate of the available power.

Four "candidate scenarios" were identified to be run for 28 days (plus spinup) with eight constituents. Three corresponded to low, medium and high levels of development, where for each scenario the turbines of each channel had the same capacity factor. This was intended to represent a similar level of return on investment in each channel. The actual values of the capacity factors are not meaningful due to both the unrealistic array layouts and the use of M2 only, and so are not reported here. In the fourth scenario, termed "optimum", each channel had the number of turbines that corresponded to the greatest mean power output attainable over an M2 cycle. This "optimum" number of TECs may be different with more constituents than with M2 only, and indeed might change with realistic array layouts, but the number established here is used as an approximation that is available while keeping computing times low. The optimum number of TECs was estimated using simple parabolic interpolation between the highest-power scenario in Section 5.5 and the two either side of it.

It should be noted that this approach, where each channel is optimised independently and then the indicated level of deployment for each is combined in a single model, is not generally applicable; it is appropriate in situations such as this one where the channels do not interact significantly with one another, and avoids the need for a more difficult simultaneous optimisation of all channels.

Each of the four scenarios was simulated with all three channels active and with turbines in the Takigawara Strait removed, thus including only the channels currently designated for development. Table 5.3 shows the mean and maximum power outputs of each scenario, as well as the ratio of mean to maximum power output.

It is notable that at low levels of exploitation, the Takigawara Strait is predicted to give the most power at a given capacity factor, offering more than the other two channels combined in the "Low" scenario. At higher levels of development the Naru strait has more potential, as with the M2-only predictions in Fig. 5.5. In all scenarios, the ratio of mean:max power is higher when the Takigawara Strait is included than when it is not.

Level of development	Number of turbines				Power (MW)		Mean / Max
	Tanoura	Naru	Takigawara	Total	Mean	Max	
Low (A)	5	42	0	47	4.70	23.50	20%
Medium (A)	46	88	0	134	9.67	48.38	20%
High (A)	130	190	0	320	14.08	69.01	20%
Optimum (A)	414	446	0	860	16.25	79.30	20%
Low (B)	5	42	73	120	11.93	49.49	24%
Medium (B)	46	88	112	246	17.73	75.16	24%
High (B)	130	190	182	502	22.34	97.35	23%
Optimum (B)	414	446	270	1130	24.53	106.78	23%

Table 5.3: *Table showing the number of turbines allocated to each channel in each scenario, and the predicted power outputs. Scenarios marked "A" use only the two channels designated for tidal development, while those marked "B" use all three.*

5.8 Exploring the maximum power in the Naru Strait

In earlier sections a realistic representation of a bottom-mounted TEC was used. As noted in Section 5.5, this only occupies a portion of the water column and allows the flow to divert over and under the rotor. Additionally, the limitation of not placing TECs in water shallower than 30 m allows large regions of horizontal diversion in some channels. In this section these restrictions are discarded in an effort to maximise the energy available in one channel — the Naru Strait — and look for any response in the other channels.

Three changes were made from earlier scenarios:

1. Instead of extracting momentum from the vertical layers intersected by the rotor, the same thrust was applied evenly across all layers. This simulates the way that energy extraction would appear in a two-dimensional model, and approximates a possible future scenario where a large number of smaller TECs, with lower individual thrust, are deployed at different depths throughout the water column. Such a deployment might be possible through designs such as the Triton device (Black Rock Tidal Power, n.d.) that is planned for deployment in the Bay of Fundy. The same approach of "smearing" thrust throughout the water column was used by O'Hara Murray and Gallego (2016) for some scenarios in their modelling of the Pentland Firth.

2. Instead of placing turbines along a line between the 30 m contours, the line was extended to run from coast to coast. This is unrealistic with a natural coastline, but could be achieved through civil engineering works (*e.g.* dredging

or channelisation) to provide a minimum depth.

3. The thrust curve, previously a function of the current speed, was changed to a constant value of $C_T = 0.85$. This is because the presence of a cut-in speed would otherwise set a limit on how far the TECs could reduce the transport through the channel. This constant thrust coefficient is probably unrealistic, but it is certainly possible that future TECs will have cut-in speeds below the $1\,\mathrm{m\,s^{-1}}$ that was used to this point.

The M2-only simulations of the Naru Strait were repeated with these modifications. Additionally, transport through the northern mouth of the strait was recorded for each scenario. This was calculated by taking 200 sample points along a straight line from coast to coast, extracting mean depths and depth-averaged velocities normal to this line at each point, and using simple trapezoidal integration. The number of TECs was increased far beyond commercially realistic levels until a maximum power output was found past which the marginal change in power for extra TECs was negative. Fig. 5.9 shows the power output as a function of the number of turbines, and Fig. 5.10 relates it to the reduction in transport through the channel.

The maximum power available from the Naru Strait (M2 only) under these artificial conditions is predicted as approximately 36 MW, with between 600 and 800 turbines. This maximum occurs when transport through the channel is reduced by 36%; additional impedance, and further reductions in transport, beyond this point result in decreased power output.

Fig. 5.11 shows the effect on mean current speeds of 700 turbines across the full height and width of the Naru Strait. The effects in the exploited strait are unsurprisingly much greater than those with 100 turbines in Fig. 5.7. Once again, it is clear that there is minimal effect on the other channels through the archipelago.

5.9 Discussion

5.9.1 Capacity of Naru Strait

When pushing the simulated Naru Strait to its limit of available power, through unrealistic array layouts and turbine parameters, the maximum power of 36 MW was predicted with a reduction in transport through the channel of 36%. This may be compared against similar values found in modelling the Pentland Firth of 38% (O'Hara Murray and Gallego, 2016) and 42% (Draper *et al.*, 2014b), and is within the range of 29–42% that is given from theory by Garrett and Cummins (2005).

The maximum power that can be removed from this channel can be compared to

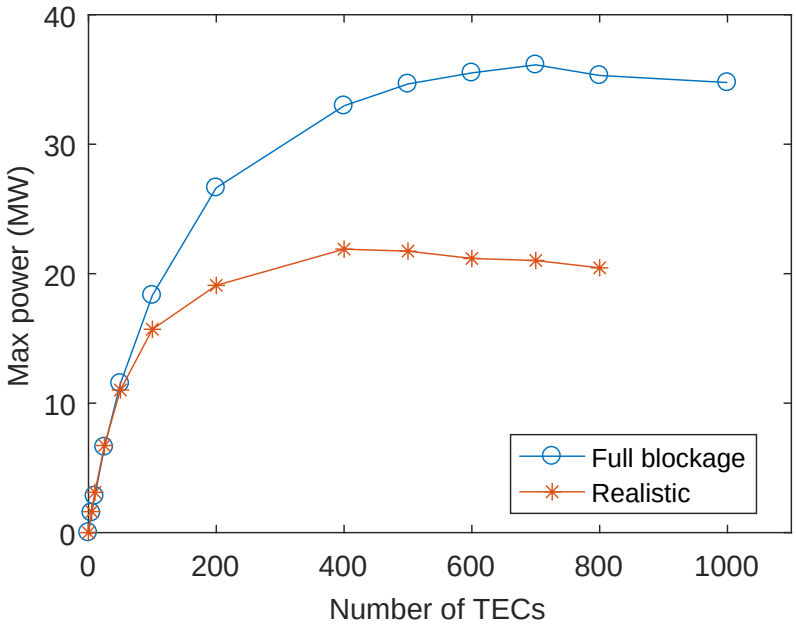

Figure 5.9: *Maximum output during a tidal cycle from M2 only with turbines evenly spread across full channel height and width, with no cut-in speed, compared to the realistic circumstances of Section 5.5.*

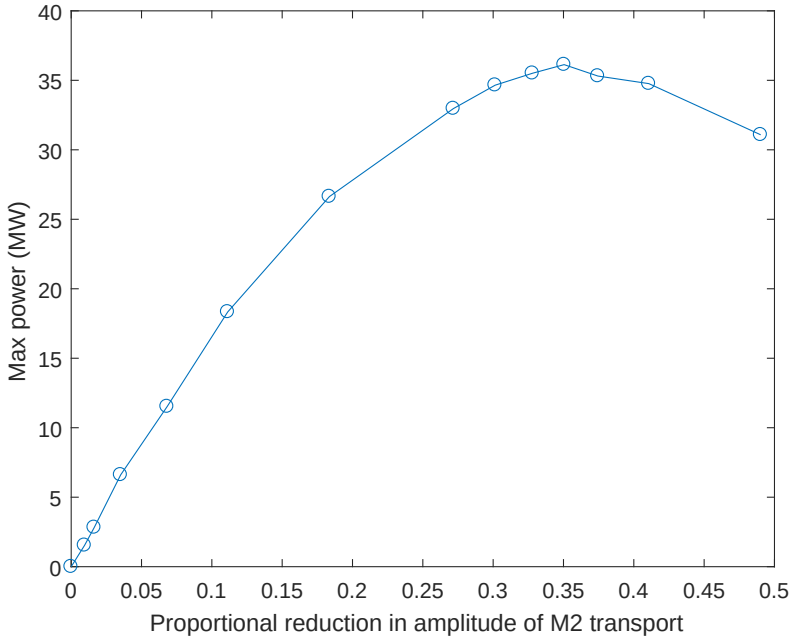

Figure 5.10: *Maximum power output during a tidal cycle from M2 only with turbines evenly spread across full channel height and width, with no cut-in speed, plotted against proportional reduction in the maximum transport.*

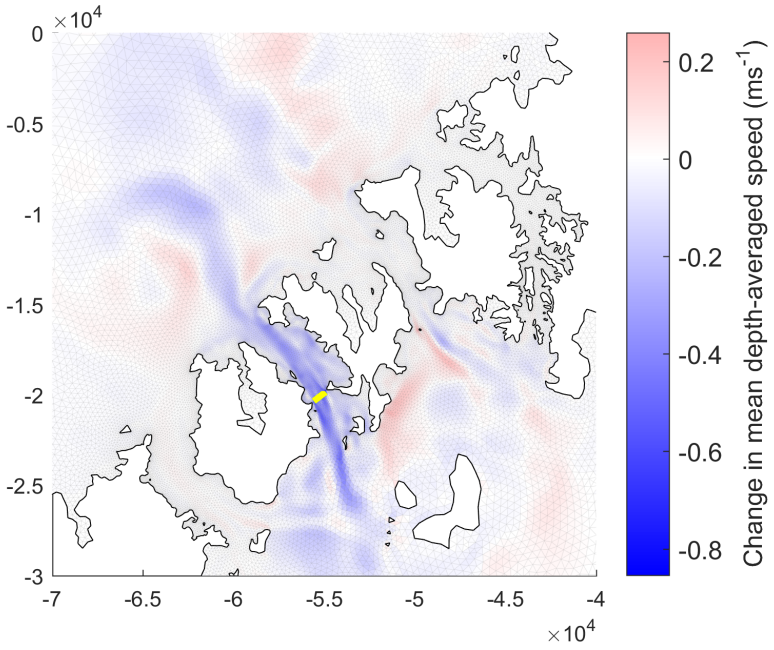

Figure 5.11: *Map showing the change in mean current speed over an M2 cycle in each mesh element as a result of adding 700 TECs to the Naru Strait, covering the full cross-section of the channel. Yellow line shows the location of turbines. Spatial coordinates are in metres in the "Japan Plane Rectangular" coordinate system zone CS1, EPSG ref 2443.*

that predicted by the Garrett & Cummins model:

$$P_{lost} = \gamma \rho g a Q_{\max} \tag{5.3}$$

where γ is determined according to the balance between frictional and inertial domination of the channel's dynamics. This balance can be estimated by measuring the phase lag between head and transport and referring to Figure 4 of Garrett and Cummins (2005). In this case (see Figure 5.12) γ is set to 0.20 based on a phase lag, measured from the model, of 24°. Using values for $Q_{\max}$ and a from the model, this predicts a maximum power of 65 MW.

Garrett and Cummins noted that an assumption in their model was that there was no "back effect", *i.e.* the height difference between the ends of the channel is not increased by the imposition of the turbines. As shown in Fig. 5.13, there is a small but noticeable back effect in the case of the Naru Strait at optimal yield, which should cause an increase in both flow and yield. The calculation of power here includes an efficiency factor of 0.5 in (5.2), and once this is taken into account the value of 36 MW is indeed slightly greater than that suggested by the simple model. The level of agreement between these values is encouraging.

Comparison with the realistic turbine setup used in earlier sections (Fig. 5.9) shows, as mentioned with respect to theory in Section 5.3, that spreading a given thrust

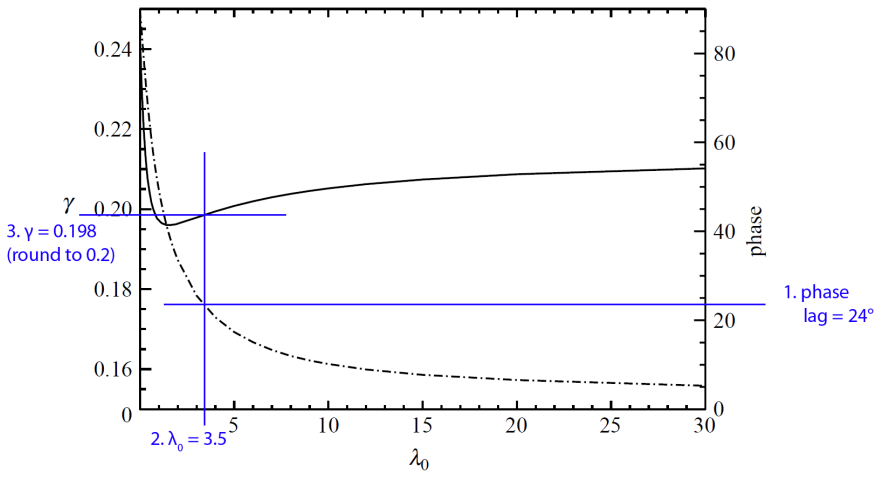

Figure 5.12: *Reproduction of Figure 4 of Garrett and Cummins (2005), showing its use to convert a phase difference to a value for λ_0 and thence γ.*

evenly across a channel will maximise the available power. This is difficult to realise with bottom-mounted TECs while allowing room for navigation, but it is possible to design tidal energy projects to get as close to this ideal as possible given the available technology and constraints. It is likely that some of the benefit of filling the channel cross-section with TECs could be realised by using a lesser quantity of TECs and reducing the channel cross-section, or increasing the impedance of bypass areas, with passive civil engineering measures. However, this option has not been studied here and it may have severe environmental impacts.

The difference between the realistic and non-realistic scenarios, in terms of the vertical distribution of thrust, highlights the importance of using three-dimensional models for detailed resource assessment work.

5.9.2 Interaction between channels

In the Pentland Firth, Scotland, Draper *et al.* (2014b) found strong connections between subchannels;* exploiting one led to flow diversion into others, and exploiting all together gave more power than the sum of each channel alone. This does not appear to be the case in the Goto Islands. While in some respects the channel systems of the Goto Islands and the Pentland Firth are quite similar, there are notable differences in the connectivity between their channels.

Both the Pentland Firth and the Goto channels run between large bodies of water that are strongly connected by other routes, and hence whose surface elevations

*The subchannels being the Inner Sound between the mainland and Stroma, the Outer Sound between Stroma and Swona, and the channel between Swona and South Ronaldsay to the east. See Figure 3.7 for a map with these islands labelled.

cannot be altered by changes to the transport through the channels in question (although local changes around the channel mouth(s) are possible). Thus the head over the archipelago as a whole is approximately fixed, but the distribution of the head loss within the isles may be altered by the addition of TECs.

In the Pentland Firth, the three sub-channels merge at either end into a single main channel. If a single channel is exploited, then (assuming low impedance in unexploited channels) the maximum head available for generation is slightly greater than the undisturbed elevation change over the length of the divided subchannel. This is because once the head reaches this level it also affects the other subchannels and causes flow to divert into them, resulting in the strong interactions that are predicted in that region. The full potential of the elevation difference between the Atlantic and the North Sea is thus only available if all three subchannels are exploited together.

In Goto, by contrast, the three main channels are almost entirely distinct, opening directly into the large bodies of water that they link without an intervening combined channel. As a result the full potential drop across the islands is available for energy extraction in any or all of the channels independently. Because there is no combined channel, and because the channel mouths are separated by significant distances, local elevation changes at one channel mouth are greatly diminished before they reach other channels. This results in very weak interactions between the straits.

Fig. 5.13 shows the changes in surface elevations as a result of adding 700 turbines to the Naru Strait. It is clear that the elevation gradient of that channel is dramatically altered — with water level upstream of the TECs increased and that downstream decreased, and most of the potential drop concentrated on the line of turbines. This effect does propagate weakly beyond the ends of the channel, in particular to the south, and this is probably because the bay-like shape of the archipelago here acts as a buffer between the Naru Strait and the South China Sea. However, this wider effect is small (generally <1 cm) and and there is almost no change in the elevation drop across the other straits.

As further work, it would be interesting to better understand the factors that influence whether channels are independent. In particular, it is not obvious how close the channel mouths must be to interact through local effects on surface elevation. This is likely to relate to both the distance between the channel mouths and the volume transport through each channel. The Rossby radius for 50 m water depth at a latitude of 33° is approximately 280 km, so rotational effects are unlikely to be significant in this case, but for shallower channels at high latitudes they should be considered.

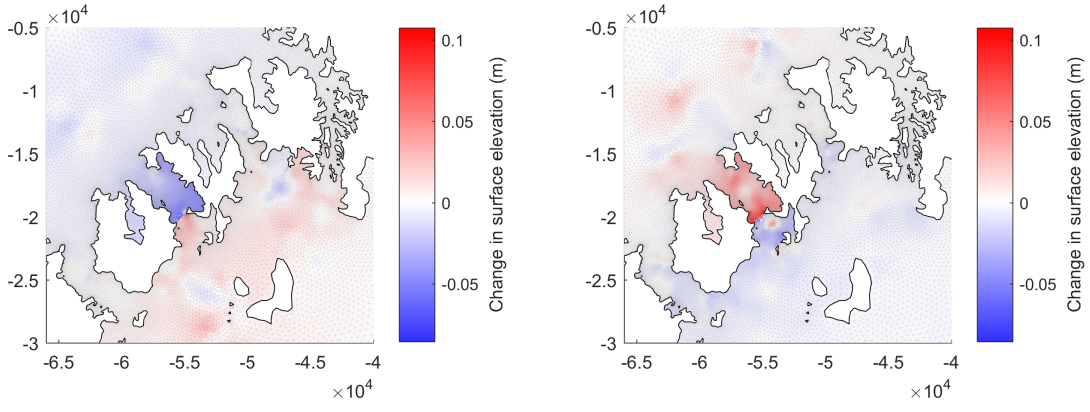

Figure 5.13: *Maps showing the change in surface elevations at single timesteps during (a) flood and (b) ebb, as a result of adding 700 turbines to the Naru Strait with full horizontal and vertical blockage. Spatial coordinates are in metres, referring to the "Japan Plane Rectangular" coordinate system zone CS1, EPSG ref 2443.*

5.9.3 Resource estimation

Estimating resource in the channels of Goto is more straightforward than in some areas because the channels do not significantly affect one another. In other areas it would be necessary to perform a difficult optimisation with at least as many degrees of freedom as there are channels, but in Goto one can simply arrive at a resource estimate for each channel and sum them.

In this case the number of turbines required to obtain the greatest possible mean output from each channel is very high, and unlikely to be commercially viable. Therefore, in addition to optimising for mean power, three arbitrary scenarios were simulated with lower levels of exploitation. The total available power from the three channels reaches maxima of 49.5, 75.2, and 97.4 MW at low, medium and high levels of exploitation respectively. The mean power in each scenario is consistently 23–24% of the maximum. There is a greater difference between mean and maximum here than is common in European waters, which may make development slightly less economically attractive. The relatively high variation in this study area can be attributed to its mixed diurnal and semidiurnal tides.

The maximum available resource in just the Tanoura and Naru straits, which are those designated for tidal energy development, is 23.5, 48.4, or 69.0 MW for the three scenarios. It is interesting to note that the channel with the greatest output in the low deployment scenario (probably the most economically attractive scenario) is the Takigawara Strait, which is not within the designated development area. Omitting the Takigawara Strait also reduces the Mean:Max power ratio to 20%.

The relatively modest capacities of these channels means that, even at quite low

levels of development, TECs' performances within any single channel will not be independent of one another. This will have implications for the management of the planned marine energy test centre, where a number of device developers might be testing different technologies within the same channel and may be affected by each others' activities.

5.10 Chapter conclusions

Methods similar to those discussed in earlier chapters have been used to predict the effects of tidal energy extraction from the Tanoura, Naru and Takigawara Straits in the Goto Islands using tidal energy converters (TECs) of the type planned by OpenHydro for deployment in the region. It is estimated that between 24 and 79 MW of power is available, depending on the level of development, from the designated tidal energy zone, and that between 50 and 107 MW is available from all three channels together, using the currently proposed bottom-mounted turbines (Table 5.3). The channel with the greatest potential at early stages of development (the Takigawara Strait) is not in the designated area.

As the level of energy extraction increases the marginal gain from adding additional turbines decreases, both because of a reduction in transport through the channel as a result of the increased impedance and because flow tends to divert over and under the rotors. TECs occupying more of the water column can use the same total rotor area more efficiently, which may be achievable in future using a larger number of smaller rotors.

Because modest levels of exploitation have noticeable effects on transport, managers and clients of the planned tidal energy test centre will need to be aware that the performance of a given device or array may be influenced by other test activities occurring in the same channel.

The maximum power that could, in principle, be generated from the Naru strait from M2 only is estimated to be 36 MW, in contrast with 22 MW using realistic technology. The necessary conditions for this higher output are unrealistic and undoubtedly uneconomical, but it is possible that civil engineering works to modify the channel, together with different designs of TEC, could permit a closer approach to this maximum.

There is little interaction between the channels in the Goto Islands, meaning that any or all of them can be exploited independently of the others. This may increase the attractiveness of the area for development, as — unlike Scotland's Pentland Firth — it is not necessary to develop all channels to realise the full potential of one. The

interaction of parallel channels is sensitive to their geometry, and it would be useful to understand this more fully.

Chapter 6

Case study : Lashy Sound

Much research effort has been put into studying the Pentland Firth (because it promises a great deal of tidal energy in the long term) and the large northern channel that includes the Fall of Warness (because it is the location of the EMEC test centre). Relatively little attention has been paid to the smaller channels within Orkney, what power may be available from them, and whether their exploitation could affect the major sites. In this chapter, the approach to resource assessment developed in the Goto islands is used to examine one of these smaller channels, Lashy Sound, which has tidal energy development planned but has been largely uncovered in the academic literature.

In this chapter a new MIKE 3 model of the Orkney area is created for the study of Lashy Sound as a case study of the methods developed to this point, intended to answer three questions,

1. How much energy is available, at the physical limit, from Lashy Sound?
2. What can this tell us about the feasibility of the planned 30 MW capacity array?
3. What would be the changes in current speeds and sea level resulting from energy extraction, and would there be any significant effect on the nearby tidal energy site in the Fall of Warness?

The development of the model is described in some detail, including mesh generation, calibration, and validation. Following this the approach to resource assessment will be explained, drawing upon lessons learned from the Goto Islands project. Results will be shown and then discussed, both as to the energy resource and regarding the effects of removing that energy.

It was originally intended to apply the "MTMC" correction developed in Chapter 4 to this model, but this was not possible because the implementation of the correction

does not currently permit multiple turbines in a single mesh element.

6.1 About Lashy Sound

Lashy Sound lies in the northern part of the Orkney archipelago, situated between the isles of Eday to the west and Sanday to the east. At the southern end it becomes Eday Sound, which links to the large channel through Orkney that includes the Fall of Warness. Eday Sound also has a shallow and partially-obstructed exit to the east which sustains rapid flows at some states of the tide. To the north, Lashy Sound opens into open sea. For a labelled map of these channels, see Figure 6.2.

It is notable that Lashy Sound has a north-south orientation, while the dominant tidal flow across the archipelago as a whole is between east and west. Strong currents in Lashy Sound must, therefore, stem not directly from the hydraulic forcing between the Atlantic and the North Sea, but from these links to other channels.

Lashy Sound itself is approximately 5 km long (measuring to the southern end of Sanday), between 3.5 and 1.5 km in width, and between 10 and 30 m deep. At the northern end a smaller subchannel of <0.5 km width and approx. 10 m depth branches off the main stream and passes to the other side of a small island known as the Calf of Eday. Between the Calf of Eday and Sanday, which is the narrowest part of the main channel, is a narrow constriction in the deep channel with shallow water to either side.

The channel is of interest for commercial tidal energy generation, and developer Scotrenewables Ltd. has received an "agreement for lease" from The Crown Estate for a project of up to 30 MW capacity (Scotrenewables, 2012).

6.2 Model development

A new hydrodynamic model was built in MIKE 3 for the purposes of this investigation. For a description of MIKE 3 itself, see Chapter 3. This section will describe the techniques adopted for development of the model.

6.2.1 Coastlines and bathymetry

In the inner part of Lashy Sound, coastline data supplied by Scotrenewables was used. Elsewhere, coastline shapes were sourced from the GSHHS global dataset (Wessel and Smith, 1996) at the highest available resolution, and then adjusted. The MIKE

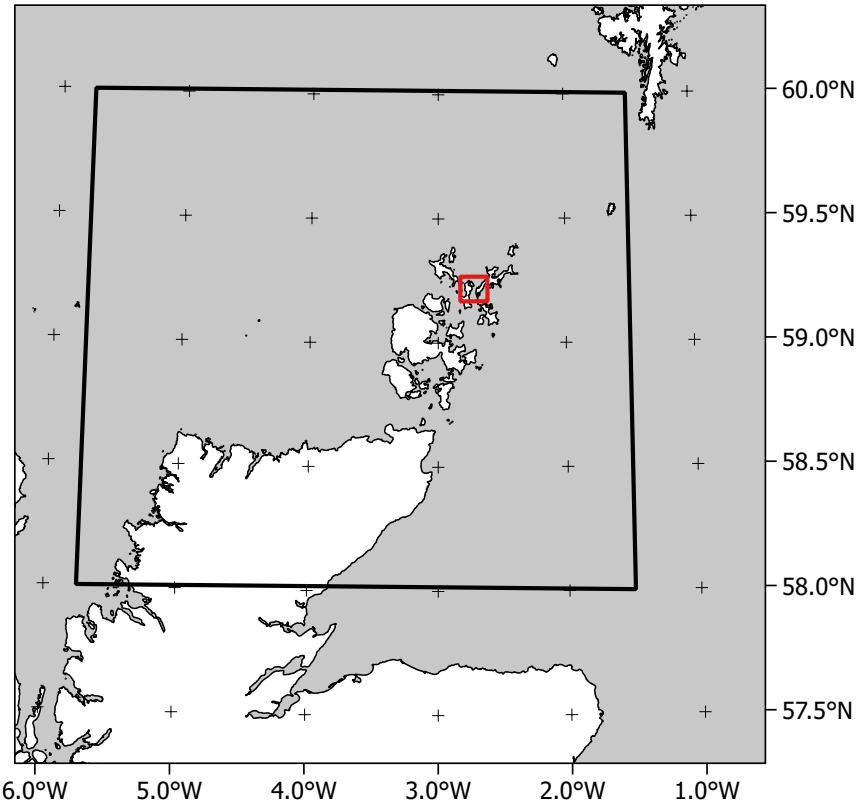

Figure 6.1: *Situation of Lashy Sound with respect to the Orkney archipeligo and the north of Scotland. The black box shows the extent of the model domain, and the red box highlights the location of Lashy Sound.*

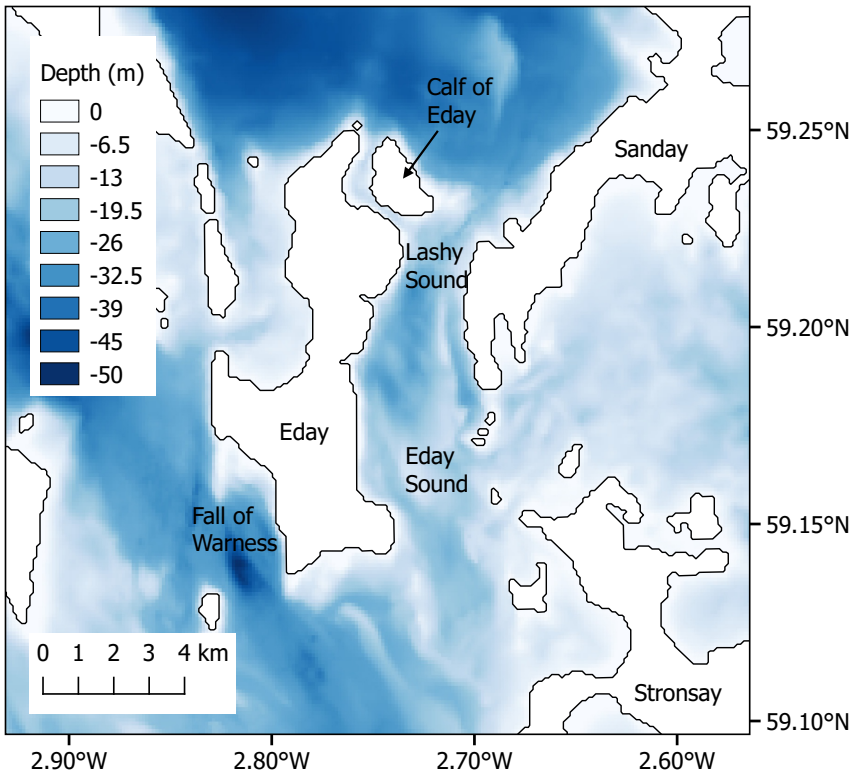

Figure 6.2: *Map showing the layout of Lashy Sound and the surrounding islands and channels. Colours show bathymetry with respect to mean sea level.*

mesh generator places a mesh node at each vertex of the coastline, so the density of points on the coast has an impact on the eventual resolution of the mesh. In the area of interest points were kept at approx. 100 m spacing (and closer where necessary to preserve important detail), while outside Lashy Sound the line was smoothed to use fewer nodes. In areas away from those of interest, the coast was further simplified by hand to remove details such as small river estuaries, which would require a fine mesh but would be unlikely to affect tidal flow far from their mouth. These variations in node spacing can be seen in Figure 6.3.

Bathymetry was obtained from a variety of sources, detailed in Table 6.1. The primary dataset used was a gridded product of 20 m resolution that was created by ABPmer under contract to The Crown Estate, and kindly made available to the project by the latter (ABPmer, 2012). A description of the inputs to this dataset is given in O'Hara Murray and Gallego (2017). In outer areas not covered by this product, the SeaZone bathymetry product was used (SeaZone Solutions Ltd., obtained via EDINA Marine Digimap Service, 2008). The Seazone bathymetry was smoothed using a gaussian filter along the model boundary, as this was found to improve numerical stability. In the inner area of Lashy and Eday Sounds these sources were supplemented by multibeam echo sounder data supplied by Scotrenewables. The bathymetry sources used for each area can be seen in Figure 6.3.

Some of these bathymetry data sets used Chart Datum for their vertical datum, while some referred to the local mean sea level (MSL). To correct between these the Vertical Offshore Reference Framework (VORF) dataset, produced by the UK Hydrographic Office, was used (Ziebart and Iliffe, 2009; University College London, 2012). This provided a spatial grid of offsets between chart datum and mean sea level, which was used to convert all bathymetry to MSL. Most of the datasets were reduced in resolution prior to use in MIKE, in order to fit within MIKE's limitations on the number of data points (see Appendix B). In all areas the linear resolution of the bathymetry was kept at least three times greater than that of the mesh.

Source	Supplied resolution	Intermediate resolution	Datum
Scotrenewables MBES	20 m	20 m	CD
ABPMer	20 m	40 m, 100 m and 1000 m	MSL
SeaZone	1 arc minute	1 arc minute	CD

Table 6.1: *Table detailing the sources of bathymetry used. "Intermediate resolution" is the resolution to which the bathymetry was reduced before being provided to MIKE (see Appendix B for more details). ABPMer data was reduced by different amounts according to mesh density in that area. CD = Chart Datum; MSL = Mean Sea Level.*

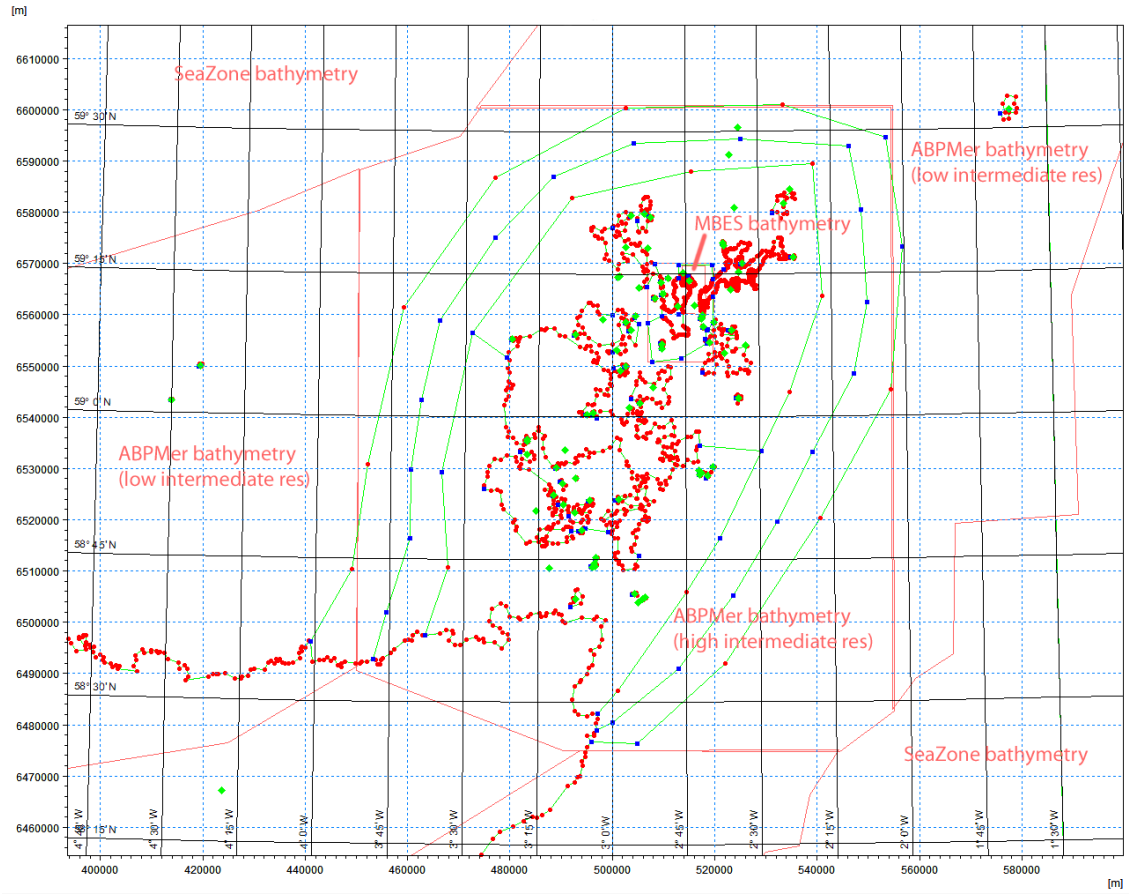

Figure 6.3: *View of the model setup prior to mesh generation. Red dots show coastline nodes; note the higher density around the isles of Sanday and Eday than elsewhere. Pink lines represent the zones in which different sources of bathymetry were used, as per the text labels and Table 6.1. Green lines show zones of different mesh density, as described in Table 6.2.*

6.2.2 Mesh generation

MIKE uses an unstructured horizontal mesh, described by "nodes" (or vertices) and "elements" (the triangles that the nodes form). The model is described as "element-centred", which means that while depths are held at the nodes, all other values are considered to represent the elements. For example, a node has a depth, but a triangle has a velocity.

In order to get a high resolution in the area of interest while keeping computational times reasonable, a number of different mesh scales were adopted. The MIKE mesh generator allows one to specify the maximum element area that is permissible in a zone, rather than the inter-node spacing. However, one can gain an approximate idea of the spacing by assuming equilateral triangles and applying the standard formula for the area of a triangle, resulting in:

$$\text{node spacing} \simeq \sqrt{2A} \tag{6.1}$$

where A is the element area. In practice this tends to overestimate node spacing, because not all triangles are generated at the maximum permitted size.

The element sizes for this mesh are shown in Table 6.2, and the zones to which they apply marked on Figure 6.3 with green lines. This scheme is approximately guided by the rule of thumb that element areas should not change by more than a factor of ten in one step, although it falls slightly short of this standard at some transitions.

Vertically, ten sigma layers were used.

Mesh optimisation

Optimisation of the computational mesh can result in a many-fold increase in model speed, because it enables longer timesteps to be used.

Region	Max element area (m^2)	Approx. node spacing (m)
Lashy Sound & Fall of Warness	5000	100
Inner (North)	60 000	346
Inner (South)	400 000	632
Mid	600 000	775
Outer	5 000 000	2236
Remainder of grid	57 000 000	7550

Table 6.2: *Maximum element areas specified for the mesh, according to zone. The boundaries of these zones can be seen in green on Figure 6.3.*

The Courant-Friedrichs-Lewy number (also known as the "CFL number" or "Courant number") describes the ratio between the maximum distance that information in a model can travel in a single timestep and the size of a mesh element. The formulation used by MIKE (DHI, 2012b) allows for the speed of a shallow water gravity wave in addition to the speed of the current:

$$C = \left(\sqrt{gh} + |u|\right) \frac{\Delta t}{\Delta x} + \left(\sqrt{gh} + |v|\right) \frac{\Delta t}{\Delta y} \tag{6.2}$$

where g is the acceleration due to gravity, h is the depth of water at that location, Δt is the timestep, u and v are the eastward and northward components of the velocity respectively, and Δx and Δy are the size of the mesh element in eastward and northward directions. For a model that uses explicit timestepping, such as MIKE's flexible mesh system, $C < 1$ is necessary (although not always sufficient) for numerical stability. This is often known as the "CFL condition". Effectively, it is a requirement that information cannot "skip" between non-contiguous mesh elements in a single timestep.

A consequence of the CFL condition is that the timestep of a model will usually be determined by a few triangles that are smaller than others, that are highly skewed (far from equilateral — hence small in one direction) or experience faster flow, and hence have a higher CFL number than the majority. Triangle shape is also important for numerical stability, as highly skewed triangles can increase the risk of numerical divergence (Pointwise, 2012).

Mesh optimisation is a process of removing small elements where they are not required, and improving the triangles to remove small angles. MIKE's Mesh Generator includes an an "Analyse Mesh" tool which shows the elements with the smallest areas and the narrowest angles at their vertices. It also includes a "Smooth Mesh" tool which attempts to iteratively improve the quality of the mesh by moving nodes to increase small angles. It is noted by Dix *et al.* (2007, Appendix B) that while the smoothing tool is generally successful at improving the mean statistics of the triangles, it tends to create a small number that are worse than it started with. The following process was therefore adopted for mesh optimisation:

1. The MIKE Mesh Generator's "Smooth mesh" tool was run for 20 iterations. Both of the options "Smoothing constrained by mesh criterion" and' "Leave mesh nodes at arcs untouched" were unchecked, allowing the software to soften the boundaries between areas of different mesh densities.

2. The "Analyse Mesh" tool was used to identify the cells with the narrowest angles and the cells with the smallest areas. The mesh was modified manually, by moving nodes and — where necessary — merging triangles, to improve these. In particular the minimum internal angle of any triangle was increased

to be over 25°.

3. The "Smooth mesh" tool was run again for another 20 iterations. No significant changes were seen, indicating that it had converged on at least a local optimum, and hence the best mesh that would be reached by this method.

4. The model was run for a short period of a few days around spring tides. One of the outputs specified was information on the CFL number for each mesh element in each time step in the area of densest mesh around Lashy Sound and the Fall of Warness. A mid-layer was processed* to produce a plot of the maximum CFL value that was reached during the run in each mesh element (Figure 6.4). Using this plot, the "hot spots" with the highest max CFL were identified and the mesh was improved by hand in these areas.

Through this process a significant speedup was obtained; the final step alone increased the average timestep by 15%†.

The finished mesh is shown in Figures 6.5 & 6.6. This was found to run at approximately 1.75 times speed (*i.e.* it takes 1 day to simulate 1.75 days of model time) on a 3.3 GHz 8-core Intel Xeon workstation.

6.2.3 Model physics

MIKE includes high and low order versions of its numerical implementation. DHI recommend that the "high order equations" option should be used in areas with strong currents. A test was made of the low order version. The low-order simulation ran approximately four times faster than the high-order version. A comparison was made between the results of the two formulations in short test runs. The maximum difference in speeds in the area of interest was more than $0.5\,\mathrm{ms}^{-1}$, and so it was decided to continue with the high-order version.

Eddy viscosity was determined in the horizontal by the Smagorinsky formulation (Smagorinsky, 1963) and in the vertical by a simple log law. The simulation was run in barotropic mode without wind forcing. Open boundaries were specified as clamped time-varying water levels, generated using the DHI global tidal model database (Cheng and Andersen, 2010). This database is derived from TOPEX/POSEIDON altimetry and provides twelve tidal constituents at a spatial resolution of 0.125° — although only a single constituent was used for much of the work in this chapter.

*The results of this appeared to be similar for all layers that were not at the top or bottom of the water column, and the top and bottom ones had lower CFL values.

†MIKE does not require the user to specify the timestep. Instead, the user gives a target CFL number, usually $C = 0.8$, and MIKE dynamically adjusts the length of its timestep during a simulation to maintain this. This allows longer timesteps to be used during periods of low flow speeds, such as slack water in a tidal model, while retaining for stability at other times.

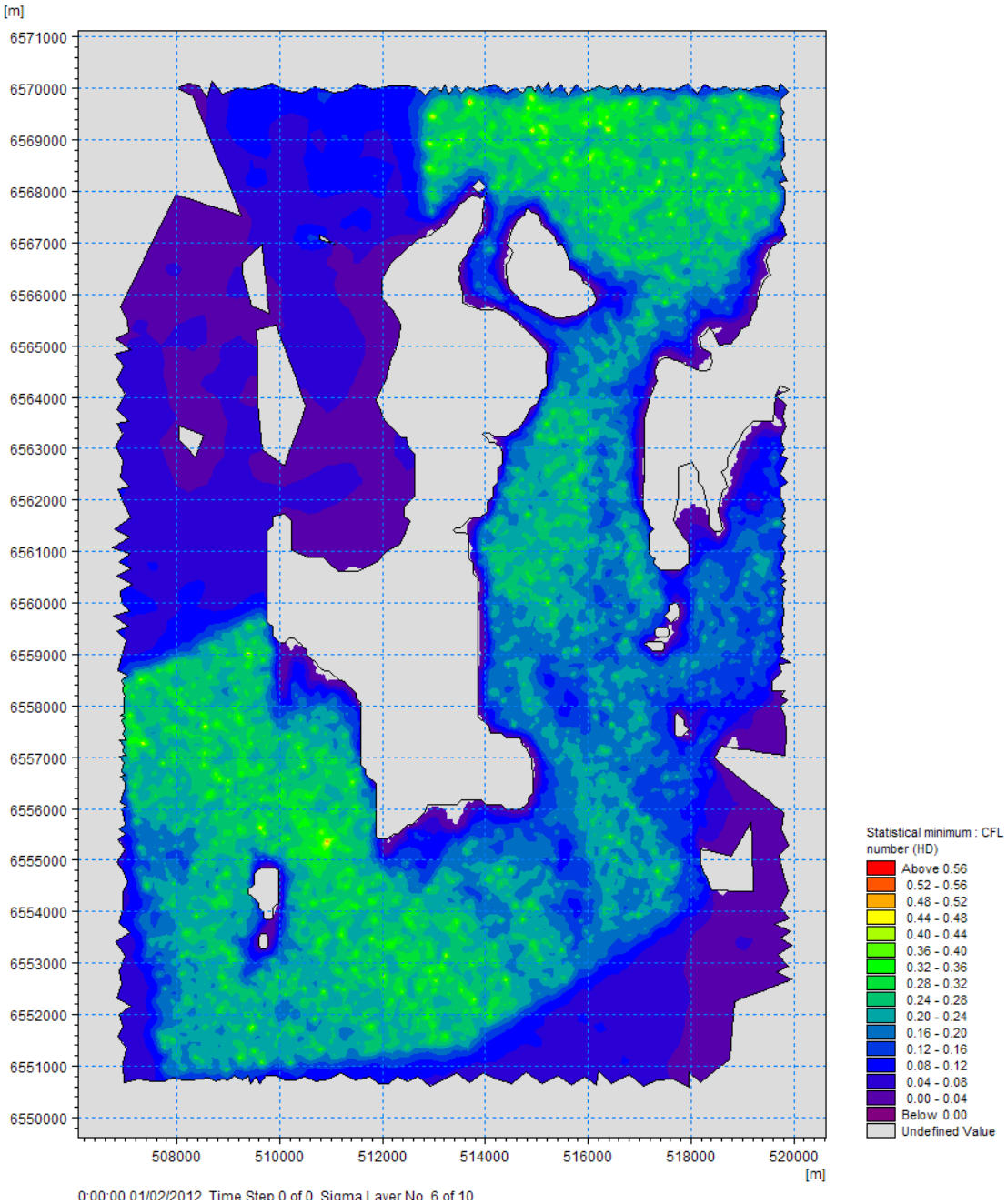

Figure 6.4: *Example plot showing the maximum CFL number that was ever reached by each mesh element of a mid layer during a simulation. Some "hot spots" can be seen in the bottom left and the top of the image.*

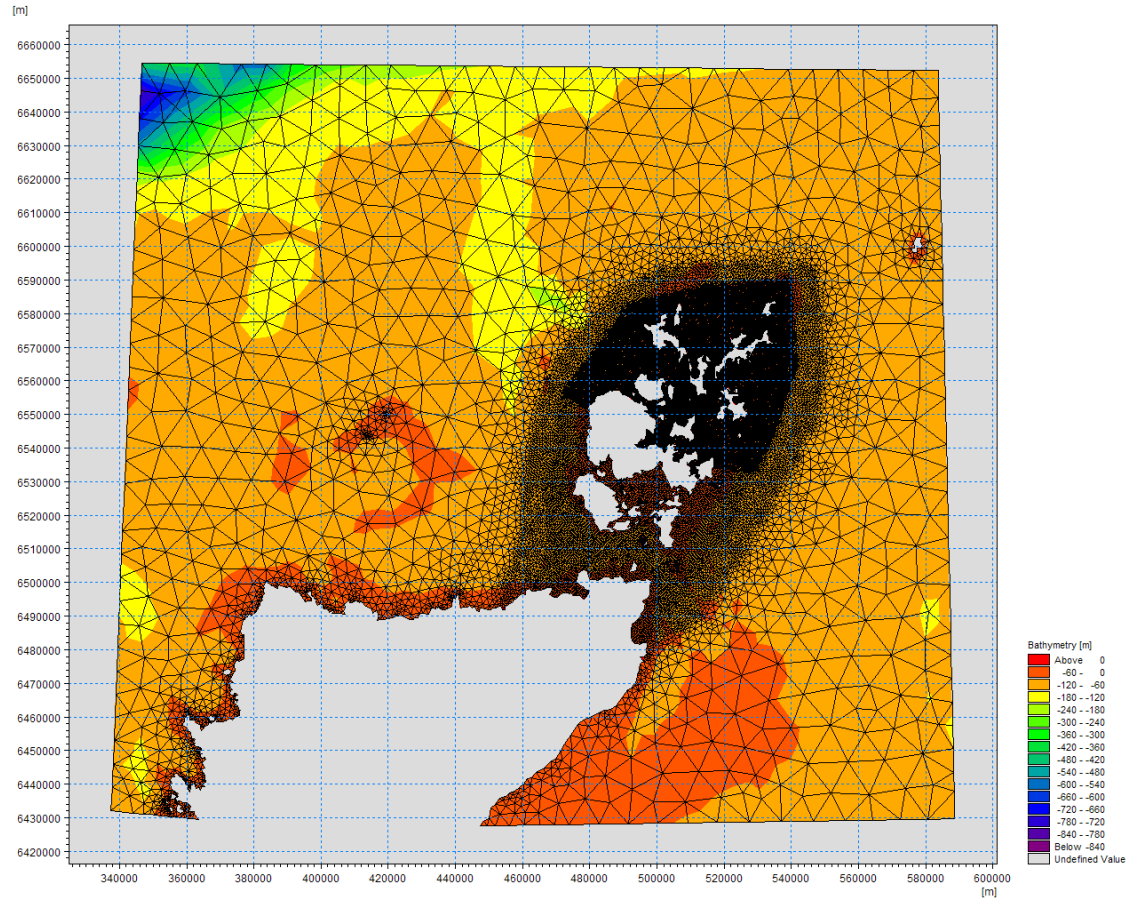

Figure 6.5: *Plot showing the full extent of the final mesh and bathymetry.*

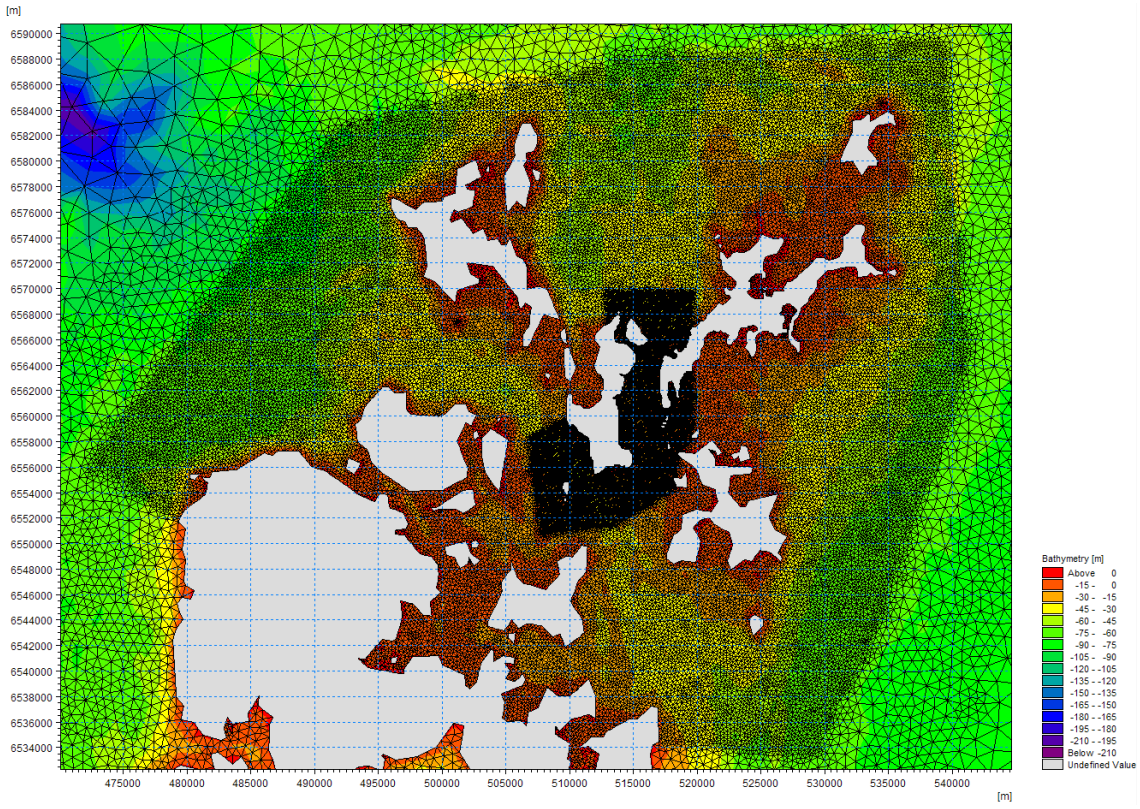

Figure 6.6: *Plot showing a zoomed view of the final mesh and bathymetry around the area of interest.*

Land boundaries were constrained to have zero velocity normal to the boundary, but permitted free slip along the shoreline.

MIKE allows two different methods for specifying seabed resistance. In the simpler one, used in Chapter 3, a quadratic drag coefficient for the seabed (c_f) is specified directly, and the velocity of the bottom layer ($\mathbf{u_b}$) is used with this to calculate the bottom stress $\boldsymbol{\tau_b}$:

$$\frac{\boldsymbol{\tau_b}}{\rho} = c_f \mathbf{u_b}|\mathbf{u_b}| \tag{6.3}$$

where ρ is the density of the water. This approach is limited by taking no account of the changing distance between the centre of the bottom layer and the seabed as the thickness of the model's sigma layers varies over space and time.

The alternative offered is to specify the "hydraulic roughness length" of the seabed, k_s. This roughness length* is translated to a roughness height z_0 thus,

$$z_0 = \frac{k_s}{30} \tag{6.4}$$

and the drag coefficient calculated, on the assumption of a logarithmic velocity profile between the seabed and the middle of the bottom layer, by

$$c_f = \frac{1}{\left(\frac{1}{\kappa}\ln\left(\frac{z_b}{z_0}\right)\right)^2} \tag{6.5}$$

where κ is Von Karman's constant (equal to 0.4), and z_b is the distance above the seabed of the middle of the bottom layer (DHI, 2012b).

This latter method was chosen for use in this chapter, as it takes account of the varying height of z_b. The value of k_s was used as a calibration parameter.

6.3 Calibration and validation

The model was calibrated against ADCP records from the Fall of Warness (marked "FoW ADCP" in Figure 6.9), and validated against records from Lashy Sound. The choice was made to use different locations, rather than different times at the same locations, to ensure confidence in the validation as a measure of the model's skill in the area of interest.

*This is a Nikuradse roughness length, but the usual connection between this number and grain size is unlikely to apply in fast-flowing scenarios such as this, where drag is dominated by bedform rather than skin drag.

Just two days of data (from a four day simulation period, to allow for spinup) was used for calibration. It is acknowledged that the best tuning of the model at a given point in the springs/neaps cycle may not be identical to that at another point, and hence this is a compromise that was made to keep the necessary computation time low while testing different settings.

The seabed roughness parameter k_s was adjusted to obtain the best fit between observations and measurements, considering both a visual assessment of the goodness of fit and statistical measures of the same (see Table 6.3a and Figures 6.7 & 6.8). A small phase shift was observed between observations and measurements, which varied according to the bottom roughness, and minimising this was also taken into account. A value of $k_s = 0.1\,\mathrm{m}$ was chosen. No other parameters were adjusted as calibration.

Post-viva note: When this calibration was carried out, early in my studentship, measurements at all depths contributed to the depth-averaged velocities that were used to compare against model predictions. It was noted at my exam that Figure 6.8 shows some non-tidal flows in the shallowest layers, probably due to wave action, and that it would have been better to remove these layers from measurements and model predictions before performing the comparison. The statistical results after removing these layers are shown in Table 6.3b. Based on this version of the table I might have tested a lesser roughness height (e.g. $0.08\,\mathrm{m}$*). However, the results of visually inspecting Figures 6.7 & 6.8 would have remained unchanged, and so it is likely that I would have still selected* $k_s = 0.1\,\mathrm{m}$ *as the preferred value. If a different value had been chosen, the difference would have been small.*

The model was validated against three ADCP surveys in the area of interest, (marked as "LS ADCPs" in Figure 6.9), using a one-month period in February and March 2012. Comparisons of u and v velocity components were made at three depths corresponding to approximately 20%, 50% and 80% of the water column. Statistical measures of agreement may be viewed in Table 6.4, and visual comparisons in Figures 6.10–6.12.

In Lashy Sound the model provides accurate predictions at most states of the tide. However, it significantly overpredicts the highest current speeds near the surface, especially at Site 1. A "jet" of accelerated flow is predicted downstream of the constriction at the northern end of Lashy Sound — a prediction which can be visually confirmed from the photograph in Figure 6.13. It is possible that the model is incorrectly predicting the width or the strength of this jet. The overprediction may also relate to incorrect simulation of the flow through the subchannel to the west of the Calf of Eday, which meets the main channel close to ADCP Site 1. As this subchannel is shallower than the main channel, its effects would be most apparent

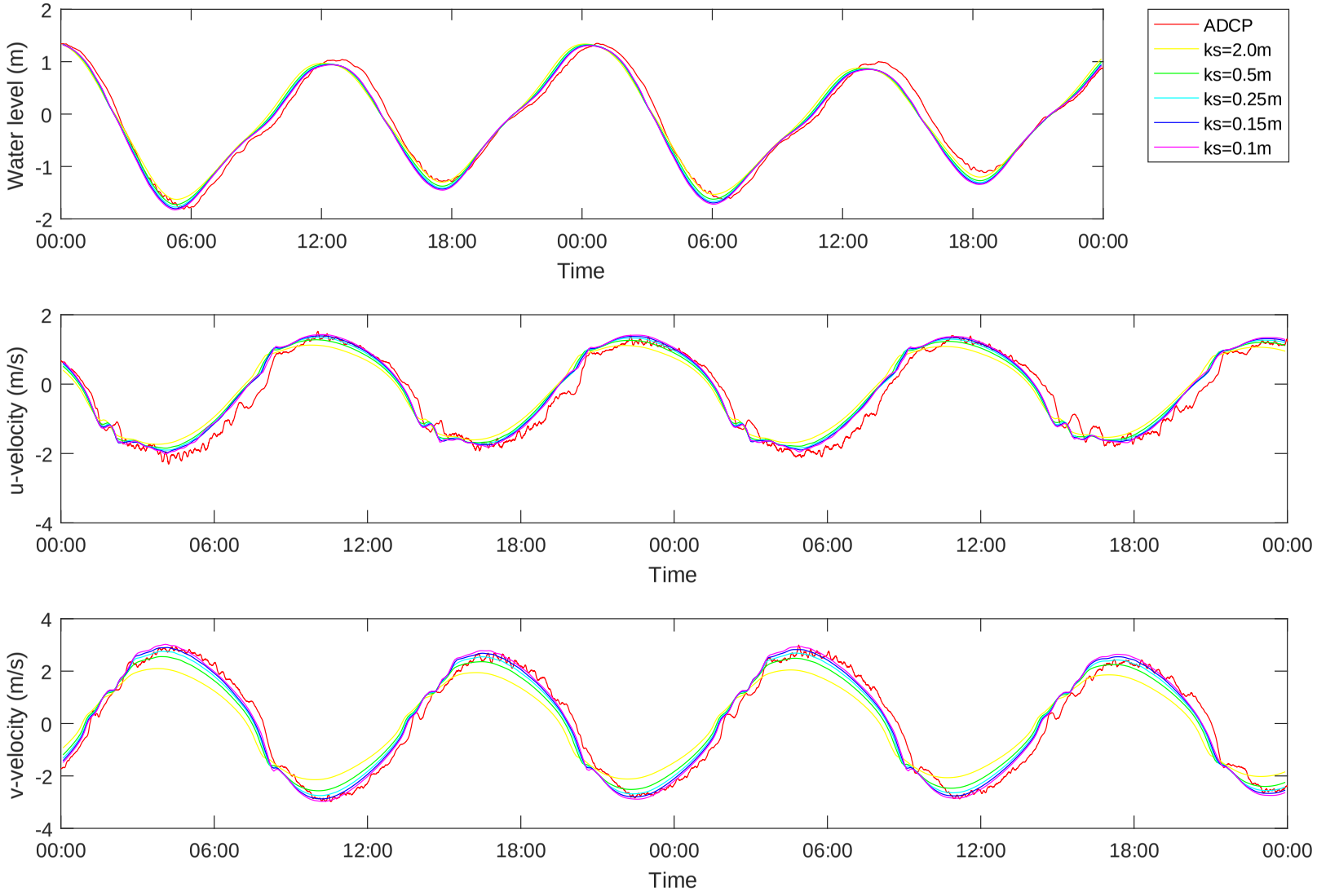

Figure 6.7: *48-hour time series showing calibration runs against Fall of Warness ADCP records.*

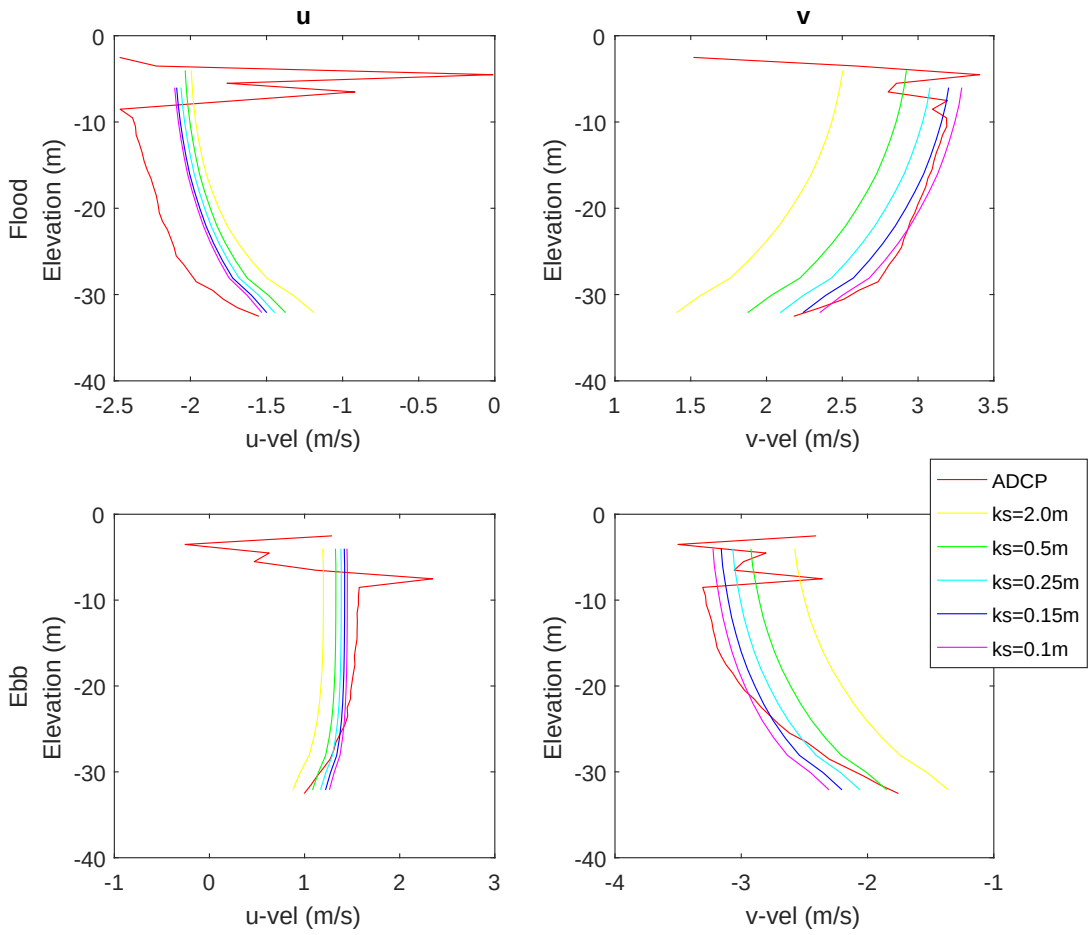

Figure 6.8: *Vertical velocity profiles comparing ADCP measurements at Fall of Warness to model predictions, at two instants, for calibration.*

(a) *Version used for this chapter, including near-surface ADCP bins in measurements.*

k_s (m)	Water level			Depth-averaged u-velocity			Depth-averaged v-velocity		
	RMSE (m)	Bias (m)	Skill	RMSE ($\mathrm{m\,s^{-1}}$)	Bias ($\mathrm{m\,s^{-1}}$)	Skill	RMSE ($\mathrm{m\,s^{-1}}$)	Bias ($\mathrm{m\,s^{-1}}$)	Skill
2.0	0.165	−0.013	—	0.375	−0.086	—	0.713	0.089	—
0.50	0.148	0.021	0.198	0.308	−0.086	0.325	0.469	0.043	0.568
0.25	0.145	0.037	0.230	0.285	−0.089	0.423	0.386	0.022	0.707
0.15	0.145	0.048	0.225	0.274	−0.091	0.464	0.348	0.009	0.761
0.10	0.148	0.057	0.202	0.269	−0.092	0.484	0.332	−0.002	0.782

(b) *Version calculated in retrospect, omitting bins of* <10 m *depth from measurements.*

k_s (m)	Water level			Depth-averaged u-velocity			Depth-averaged v-velocity		
	RMSE (m)	Bias (m)	Skill	RMSE ($\mathrm{m\,s^{-1}}$)	Bias ($\mathrm{m\,s^{-1}}$)	Skill	RMSE ($\mathrm{m\,s^{-1}}$)	Bias ($\mathrm{m\,s^{-1}}$)	Skill
2.0	0.165	−0.013	—	0.390	−0.100	—	0.685	0.100	—
0.50	0.148	0.021	0.198	0.301	−0.099	0.405	0.414	0.058	0.634
0.25	0.145	0.037	0.230	0.267	−0.102	0.532	0.319	0.038	0.783
0.15	0.145	0.048	0.225	0.248	−0.104	0.595	0.275	0.026	0.839
0.10	0.148	0.057	0.202	0.238	−0.105	0.628	0.258	0.015	0.857

Table 6.3: *Statistics used in calibration of Lashy Sound model. All comparisons are between model predictions and Fall of Warness ADCP records over a 48 hour period. Skill scores use the $k_s = 2.0$ model as their baseline.*

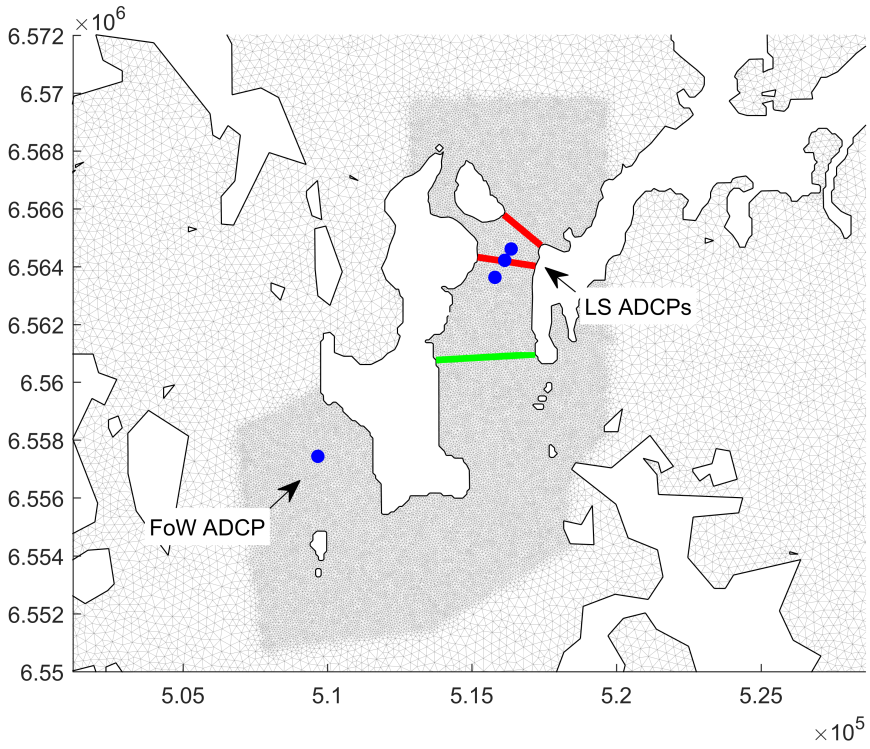

Figure 6.9: *Map showing the inner part of the computational mesh. Red lines show the two transects along which TECs were placed. Green line shows the transect that was used to measure transport from the model. Blue dots show the locations of Fall of Warness (FoW) and Lashy Sound (LS) ADCP surveys used for calibration and validation. LS ADCP points are Site 1, 2 & 3 from north to south. Axis are units of metres, in UTM coordinate system zone 30N.*

		Site 1		Site 2	
		u	v	u	v
RMSE (m/s)	Shallow	0.341	0.298	0.134	0.375
	Mid	0.162	0.294	0.166	0.426
	Deep	0.213	0.260	0.257	0.430
Scatter index	Shallow	0.577	0.304	0.175	0.372
	Mid	0.231	0.256	0.202	0.386
	Deep	0.278	0.206	0.302	0.375
R^2	Shallow	0.980	0.986	0.978	0.982
	Mid	0.983	0.988	0.979	0.983
	Deep	0.983	0.989	0.980	0.984
Bias (m/s)	Shallow	0.077	0.107	0.012	0.040
	Mid	−0.010	0.092	−0.043	0.057
	Deep	−0.117	0.074	−0.092	0.058

Table 6.4: *Validation statistics, comparing predictions of the MIKE 3 model to observations in Lashy Sound over a one month period.*

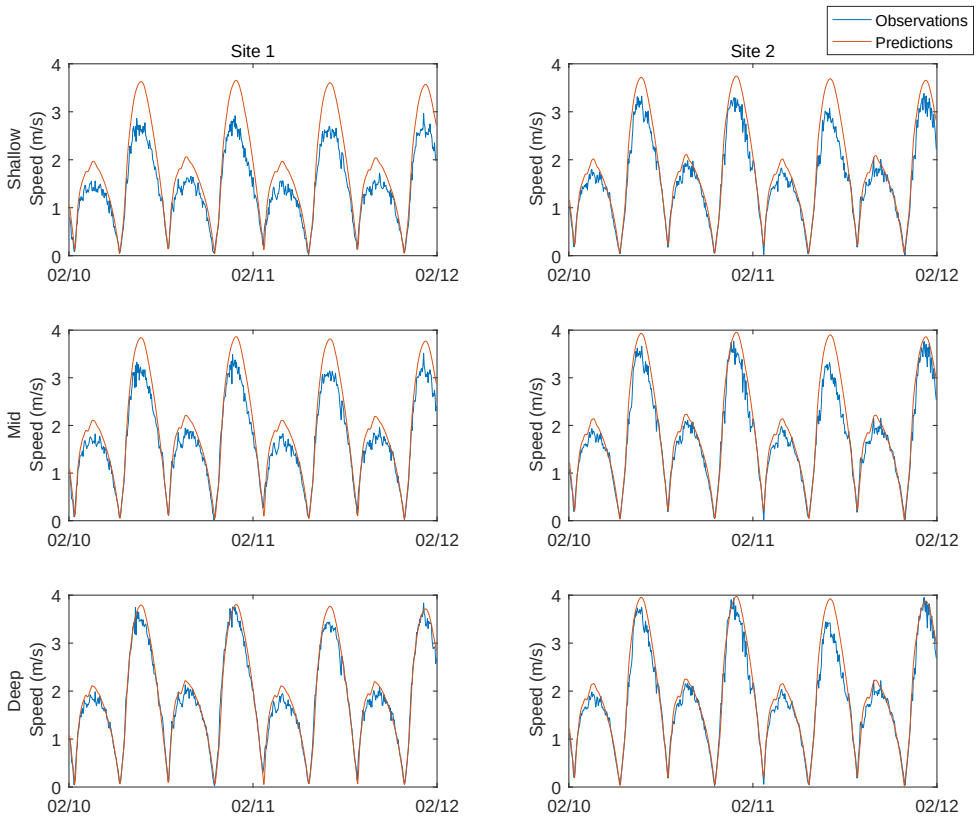

Figure 6.10: *Time series comparison of current speed between model and observations at three depths. For legibility, only 48 hours at spring tides are shown.*

near the surface. These hypotheses are presented as possible explanations for the difference seen, but neither can be tested with the available measurements.

The measured and predicted phases show a good match, and the asymmetry of the flow in the channel is reproduced well. At Site 1 the flow direction is predicted well, but at Site 2 there is a modest discrepancy.

Frequency-domain validation was conducted using the same predictions and measurements, using the `t_tide` software (Pawlowicz *et al.*, 2002). Additionally, a third ADCP survey was made available which was taken at a different time and further south in Lashy Sound. The measured and predicted phases and amplitudes are shown in Table 6.5 and Figure 6.14. All of those at Sites 1 and 2 match within 95% confidence intervals except for M2 amplitudes at Site 2. These M2 amplitudes are underpredicted in the u direction and overpredicted in the v direction, which matches the small discrepancy in flow direction seen in the time-domain analysis.

At Site 3 it was found that the sign of the v-velocities was reversed, and this was corrected. Following this adjustment the phases of model and measurements agree acceptably well, but the amplitudes are quite different; analysis of the ADCP measurements gives M2 and S2 amplitudes that are roughly half of those from the model. Once again, this may relate to the "jet" that forms downstream of the northern constriction. As can be seen in Figure 6.15, the predicted edge of this jet

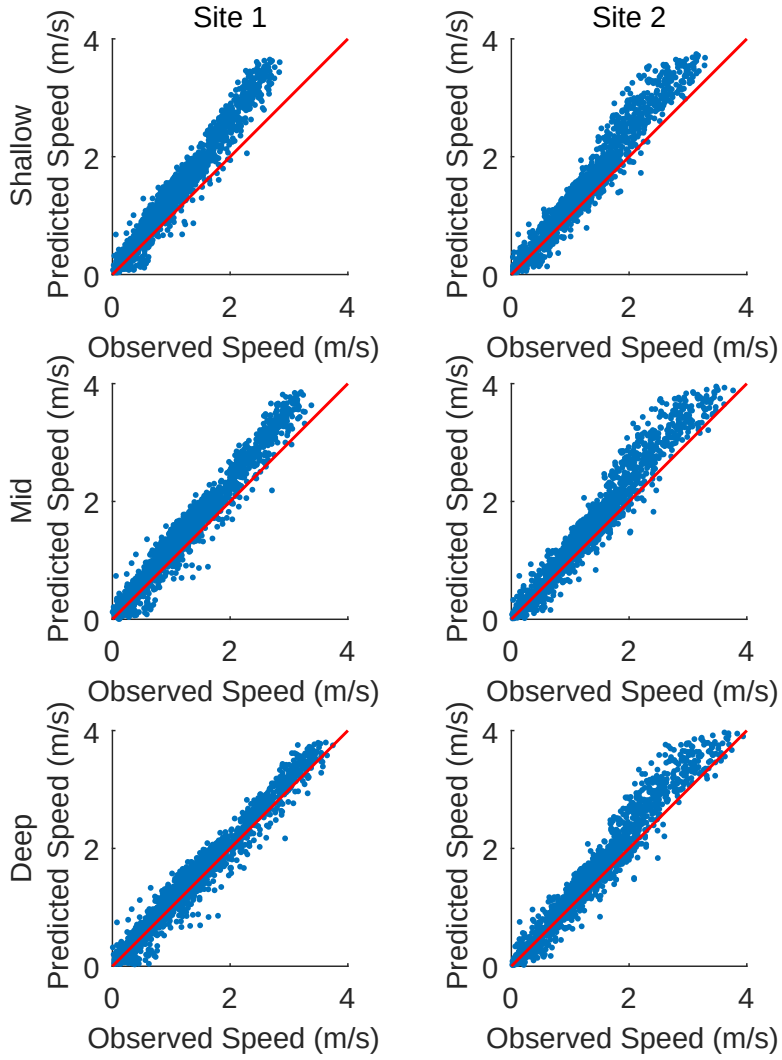

Figure 6.11: *Scatter plots comparing current speed between model and observations at three depths. For legibility, a regular sample of every fifth time step is shown. This results in a plotted time step of 25 minutes, and hence extreme values may be clipped slightly. The red lines represent 1:1 relationships.*

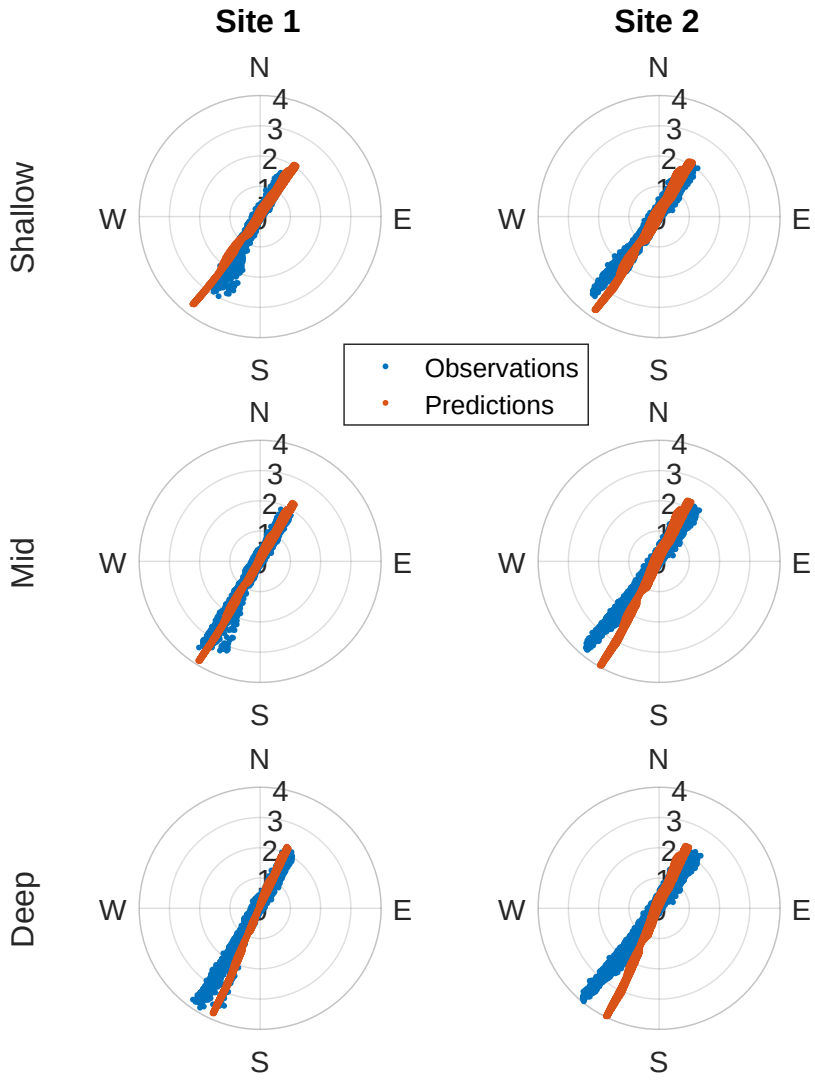

Figure 6.12: *Hodographs comparing measured and predicted velocities at three depths. Direction is that in which the flow is travelling. Radial axis indicates current speed in m/s.*

Figure 6.13: *Ariel photograph looking south into Lashy Sound during a flood tide. Photo: Scotrenewables Ltd.*

		Amplitude (m)		Phase (°)	
		Model	ADCP	Model	ADCP
M2 u	Site 1	1.132	1.064	56.9	59.8
	Site 2	1.040	1.220	59.3	62.3
	Site 3	0.719	0.438	63.5	65.6
M2 v	Site 1	1.881	1.784	55.6	56.9
	Site 2	1.954	1.608	56.5	58.1
	Site 3	1.609	0.646	60.2	62.0
S2 u	Site 1	0.412	0.406	93.5	96.2
	Site 2	0.378	0.461	95.4	96.9
	Site 3	0.262	0.108	98.7	98.8
S2 v	Site 1	0.680	0.691	92.7	93.6
	Site 2	0.709	0.612	93.7	94.7
	Site 3	0.588	0.167	96.5	98.3

Table 6.5: *Comparison of depth-averaged predictions and observations in frequency domain at two ADCP locations in Lashy Sound.*

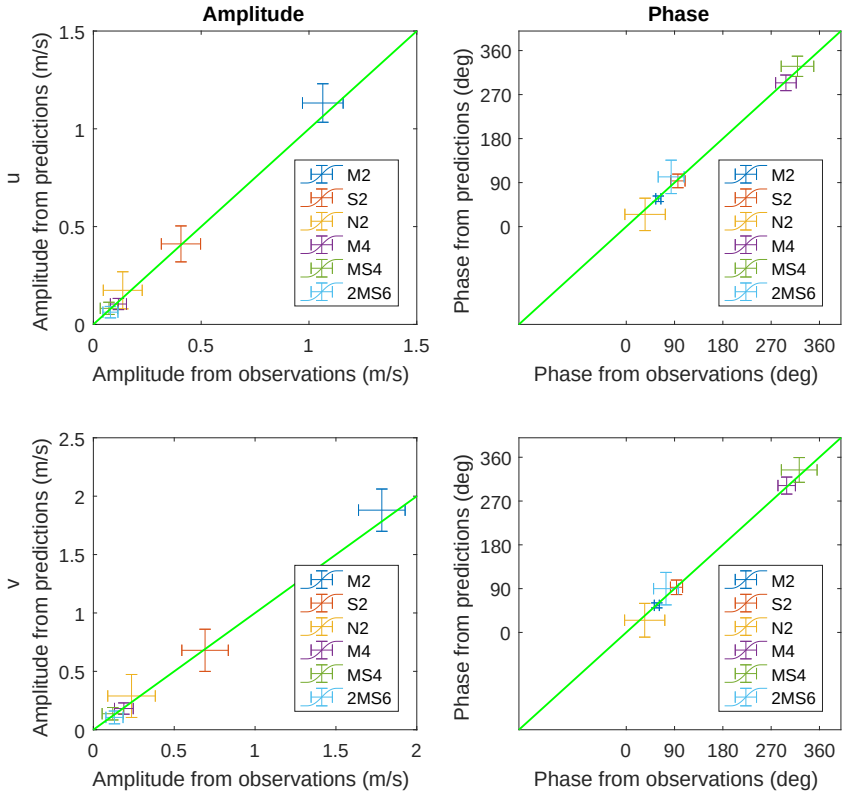

(a) *Site 1*

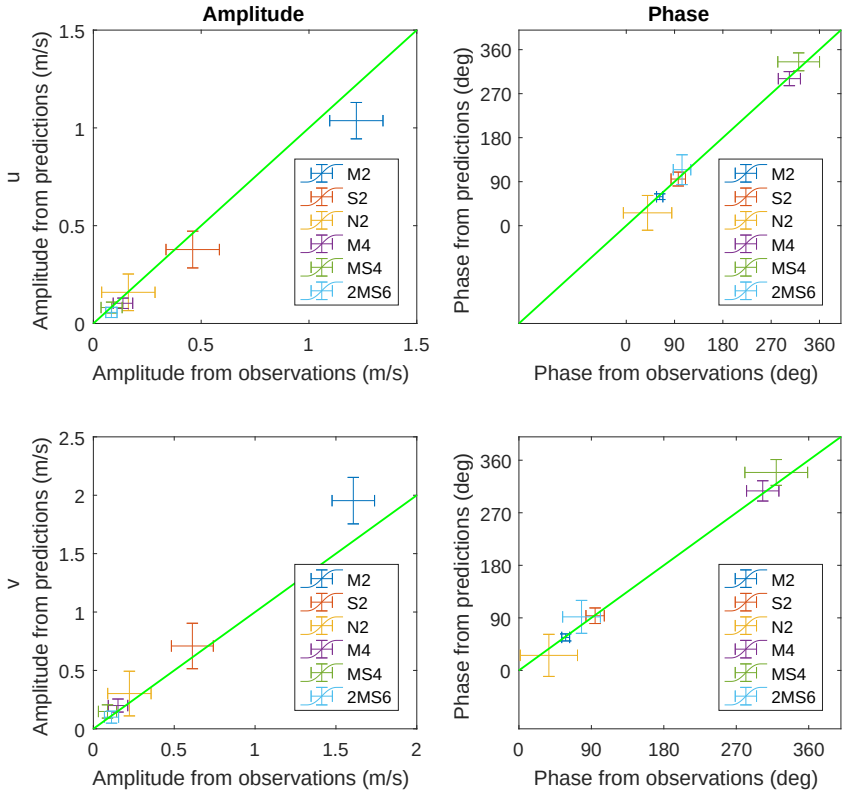

(b) *Site 2*

Figure 6.14: *Graphical representation of frequency-domain validation at three ADCP locations in Lashy Sound (see over for Site 3). Error bars show the 95% confidence intervals given by the t_tide software (Pawlowicz* et al.*, 2002).*

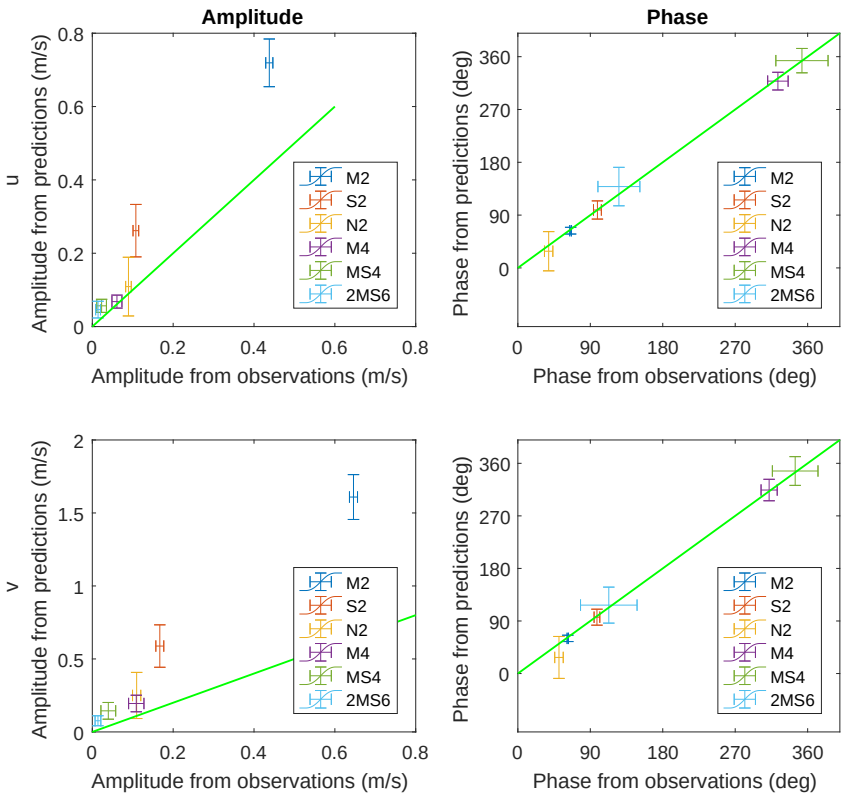

(c) *Site 3*

Figure 6.14: *cont...*

has a sharp edge with a large change in velocity over a short distance, and ADCP Site 3 is close to this edge. If the true edge of the jet is as defined as predicted, and is situated just 100–150 m to the east of where the model predicts it — potentially a matter of a single mesh element — then this could explain the large amplitude discrepancy.

It is interesting to note that harmonic analysis is not able to fully represent the flow in this area, with `t_tide` typically reporting that only 95% of the signal is explained by harmonic constituents. Since this aharmonic flow occurs in the model as well as the measurements, it cannot be attributed to weather effects. It probably relates to the jet of accelerated flow mentioned above, which introduces asymmetry that cannot be represented by sine waves at astronomical frequencies. The inability of harmonic analysis to fully capture shallow water current speeds has previously been noted by Polagye *et al.* (2010).

6.4 Method for predicting maximum power

The aim of this work was not to consider realistic array layouts, but to arrive at a figure for the maximum power obtainable from this channel regardless of engineering or economic considerations. It is known that the most efficient way of extracting energy from a channel is to spread turbines evenly across its whole cross-sectional area to prevent any bypass flow (Garrett and Cummins, 2007; Vennell, 2012). As demonstrated in the Goto Islands, it is necessary to minimise vertical as well as horizontal bypass.

The MIKE software represents tidal energy convertors (TECs) as sub-grid momentum sinks based on actuator disc theory, and requires that they be specified in terms of hub location, diameter, and thrust coefficient. Transects were identified to form "tidal fences" that crossed Lashy Sound at two locations: one at the narrowest point at which it remains a single channel (*i.e.* south of the split around the Calf of Eday; see Figure 6.9), one between the Calf of Eday and Sanday. Turbine locations were placed, evenly spaced, along these lines, in separate model scenarios in the same way as in the previous chapter.

Unlike FVCOM, which allowed the thrust to be spread arbitrarily throughout the water column, MIKE models a circular rotor of a given diameter. The use of a single design of TEC would thus result either in large regions of horizontal bypass flow, at the sides of the channel where the depth was insufficient for the rotor, or — if smaller diameter turbines were used — a great deal of vertical bypass in the middle as flow diverted over and under the rotors. To avoid this bypass flow, the diameter of each turbine was calculated to fit the depth at that location subject to maximum

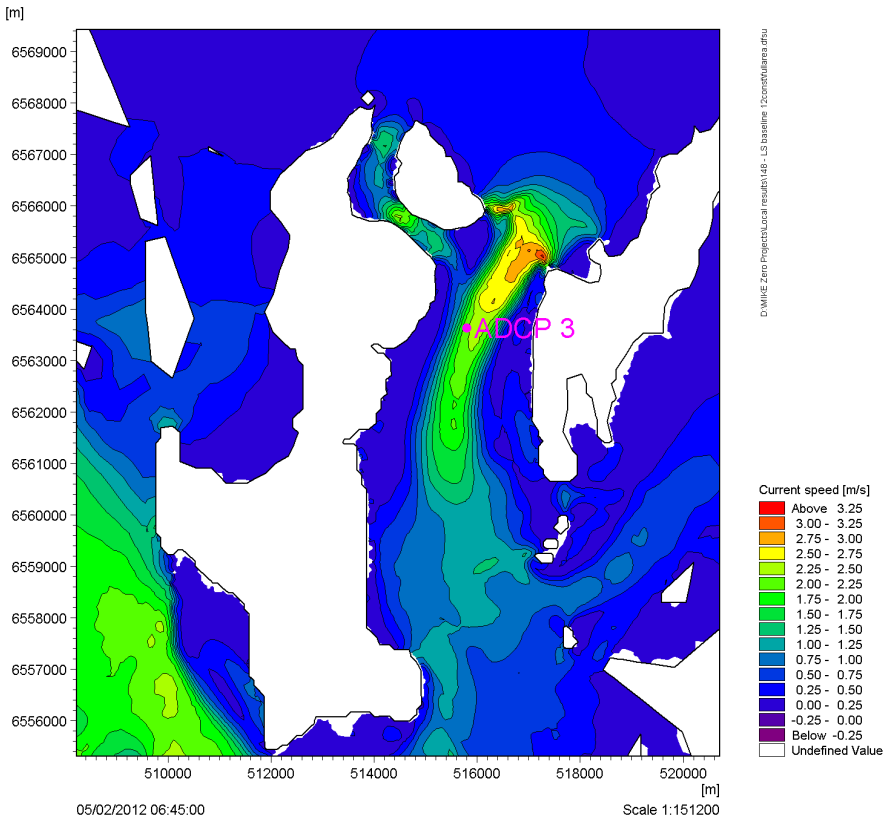

Figure 6.15: *Plot showing predicted depth-averaged speed in Lashy Sound on one timestep near the peak of southbound flow. Pink dot shows location of ADCP Site 3.*

and minimum diameters of 20 m and 4 m respectively, and with a 3 m allowance for bottom clearance and tidal range. However, this change in rotor diameters would have led to evenly spaced turbines having unequal gaps between them, which would have caused changes in local blockage across the channel. To address this, additional rotors were added to each location as necessary to normalise the local blockage ratio to the same as that of the largest turbine (see Figure 6.16). Although clearly not physically realistic at a sub-grid level, at the resolution of the model this is equivalent, in all but the sparsest layouts, to placing the smaller rotors closer together.

A realistic turbine would be expected to have a thrust coefficient that varied as a function of the flow speed. However, as established in the previous chapter, when

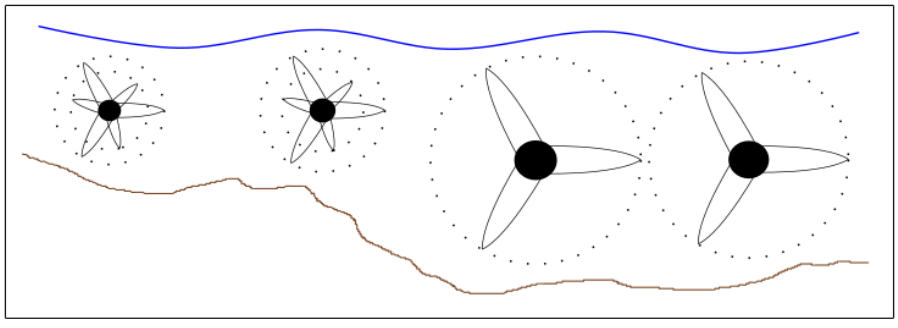

Figure 6.16: *Diagram showing, in section, how additional co-located turbines are added in areas of shallow water to maintain local blockage.*

exploring the maximum potential of a channel this can be problematic, because if the turbines have a cut-in speed they are unable to reduce the flow in the channel below this speed. For this work, therefore, the turbines were given a fixed thrust coefficient of 0.85. For simplicity, no supporting structures were included in the model.

A range of levels of exploitation were simulated, from 10 to 2400 TEC locations. In the more heavily exploited scenarios a single row of turbines is unrealistic, but should be considered as representing a two-dimensional array. Because this single-row layout is unlikely to be optimal, the actual number of TECs should be used only for comparative purposes, and it is not intended that capacity factors or matters of economic viability should be considered.

In order to allow a large number of scenarios to be explored in limited computation time, only the M2 tidal constituent was used. This allows the use of just 12.4 hours of output — a single M2 cycle — as a representative time period. It was determined empirically that the model required 3 days of spinup time before its predictions in Lashy Sound became fully periodic, so each scenario was run for 4 days of model time and the output data taken from the first 12.4 hours of the fourth day.

Power was calculated in the same way as in the previous chapter:

$$F = \tfrac{1}{2}\rho C_T A|\mathbf{u}|\mathbf{u} \tag{6.6}$$

$$P = C_C F|\mathbf{u}| \tag{6.7}$$

with C_C once again set to 0.5.

Volume transport through the channel was recorded for each scenario. This was estimated by taking 200 sample points along a straight line from coast to coast (Figure 6.9), extracting mean depths and depth-averaged velocities normal to this line at each point, and using simple trapezoidal integration.

Parabolic interpolation between the three highest points on each relevant curve of Figure 6.17a was used to estimate the number of TEC locations which would give the greatest mean power for each of the north and the south fence locations. These two scenarios were then simulated using 12 tidal constituents for 29 days (after spinup). It is acknowledged that the optimum number of TEC locations for all constituents may not be identical to that for M2 only, but this approach offers a means of getting close to the correct value at modest computational effort.

6.5 Results

6.5.1 Tidal energy resource

M2 only

Figure 6.17a shows the maximum and mean power output of the various scenarios over a single M2 cycle for both positions of tidal fence. Figure 6.17b relates the maximum output to the maximum reduction in volume transport through the channel.

With both the northern and southern TEC locations there is a near-linear relationship between TEC numbers and output at low levels of exploitation, beyond which the marginal gain in power for each new turbine location decreases as the flow speed through the channel is reduced. This "levelling off" and eventual downturn happens with dramatically different numbers of turbines, with the southern fence achieving maximum yield with approx. three times as many TECs as the northern one. However, both fences offer maximum yield at approximately the same reduction in transport through the channel — around 20%. The northern TEC location appears to offer slightly more power from M2 only, with a maximum and mean powers of 64.0 MW and 25.1 MW respectively compared to 61.6 MW and 23.2 MW from the southern position.

All constituents

The results of the two runs with all constituents are shown in Table 6.6. The two fence locations give broadly similar outputs, although once again, slightly more power appears to be available in the northern location. Achieving these similar outputs requires nearly three times as many turbines in the southern location.

6.5.2 Effects of energy extraction

The effects of energy extraction on the surrounding area were examined in terms of three physical parameters: changes to the depth-averaged current speed, changes to

TEC fence position	# TEC locations	Mean power (MW)	Max power (MW)
North	656	28.1	123.4
South	1749	26.1	117.5

Table 6.6: *Table showing the power available from the "optimum" number of turbines for each fence location, using 12 tidal constituents for 1 month.*

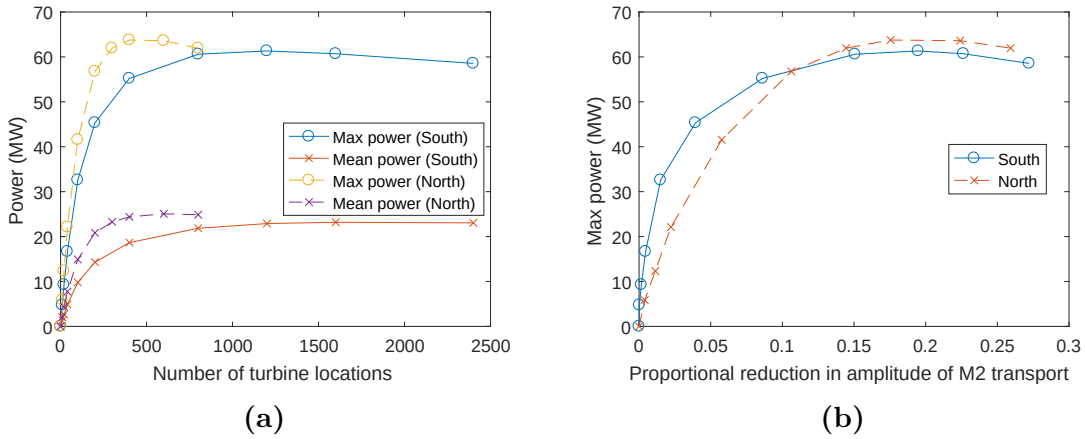

Figure 6.17: *Plots using M2 only, showing (a) the maximum and mean power output of scenarios with varying numbers of TEC locations on the northern (dashed) and southern (solid) fence locations; and (b) the same maximum outputs plotted against the proportional reduction in volume transport through the channel* ($\frac{Q_{\text{old}}-Q_{\text{new}}}{Q_{\text{old}}}$).

the maximum speed in the bottom layer, and changes to maximum and minimum sea level. The first is of interest because of its relevance for navigation and for swimming marine life. The second is similarly relevant to benthic ecology — where the maximum speed is likely to matter more than the mean. The third is important because of potential effects on the intertidal zone and, in the case of changes to maximum sea level, on flood risk.

To allow the consideration of energy extraction scenarios other than the maximum, the M2-only results were used for this analysis. The effects at springs are therefore likely to be slightly greater than those shown, and those at neaps slightly smaller. The predicted effects were similar for the two locations of the tidal fence, so for reasons of brevity only those for the southern fence location are shown here. Two scenarios were considered with this southern location: The first is that of 1200 TEC locations and a peak output of 61 MW which, since it is the most energy that can be extracted, should be the "worst case" for environmental impacts. The second is one with 100 TEC locations and a peak output of 33 MW, which is close to the 30 MW that is planned for Lashy Sound. In each case the flow was compared to that with no TECs.

The effects of energy extraction on mean depth-averaged current speed over an M2 cycle are shown in Figure 6.18. The 61 MW scenario results in a large reduction in speed of up to 0.7 $\mathrm{m\,s^{-1}}$ through the TEC array itself, for the length of Lashy and Eday Sounds, and for some kilometres beyond. Some flow acceleration around the array is also visible, which has arisen because of the lower limit that was placed on the size of a rotor and hence the absence of simulated turbines from water shallower than 7 m.

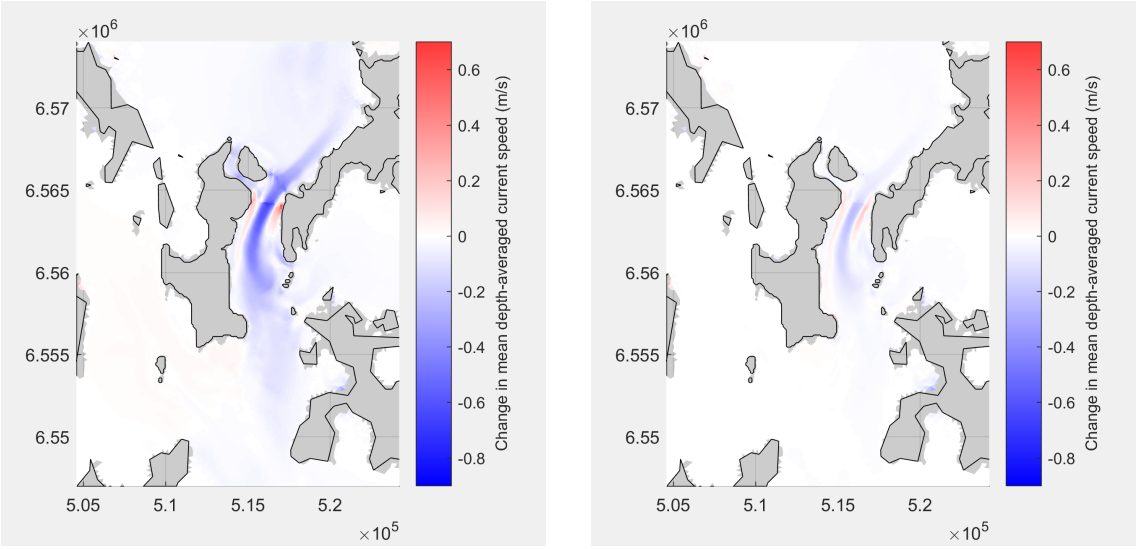

(a) *1200 TEC locations, max* 61 MW. **(b)** *100 TEC locations, max* 33 MW.

Figure 6.18: *Map showing the mean effect on depth-averaged current speed, over a single M2 cycle, of extracting the (a) maximum available power, and (b) approximately the planned power, from Lashy Sound. Speed differences are calculated on a per-timestep basis before the temporal mean is taken. Spatial coordinates are in metres, referring to UTM Zone 30N.*

Outside the immediate area of Lashy and Eday Sounds, effects are small but extant. There is a very small increase in speeds in the Fall of Warness, of up to 5 cm s^{-1}. There are more significant increases in flow along the south coast of Eday (up to 0.2 m s^{-1}) and through the channel between Sanday and Stronsay (up to 0.5 m s^{-1}) at certain stages of the tidal cycle, suggesting that some flow diverts through this route. These changes are not visible in the figure as this only shows a temporal average.

The effects on current speed of the 33 MW scenario are far smaller. A reduction in speed of approx. 0.3 m s^{-1} is predicted through the TEC array, and an increase around it, and the effect is largely confined to Lashy Sound.

Figure 6.19 shows the effects of energy extraction on the maximum bottom layer speed that is reached during an M2 cycle. These effects are similar in character to those on depth-averaged speed, but of greater magnitude: in the 61 MW scenario, a decrease in max bottom speed of up to 1.2 m s^{-1} is predicted through the centre of Lashy Sound, an increase of up to 0.5 m s^{-1} in small areas to either side of the array, and a minor (less than 0.2 m s^{-1}) increase south-east of the Fall of Warness. In the 33 MW scenario effects are once again much smaller and more local, with the only significant change being a reduction of approx. 0.5 m s^{-1} in maximum bottom speed to the south of the TEC array.

Figure 6.20 shows changes in the maximum and minimum water level in each cell. In the 61 MW scenario the line of turbines is very clear because a 15 cm increase

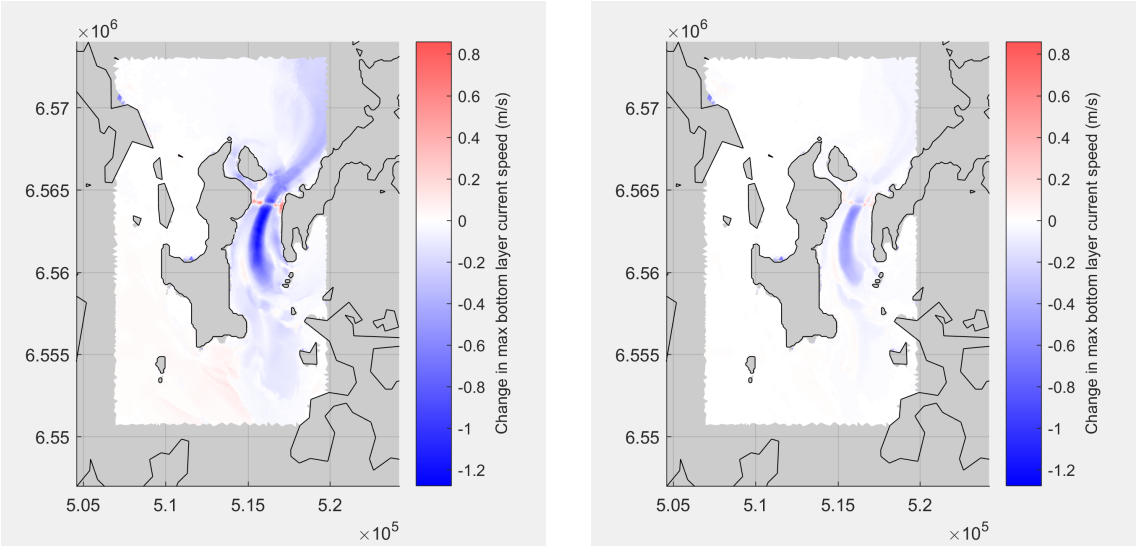

(a) *1200 TEC locations, max* 61 MW. **(b)** *100 TEC locations, max* 33 MW.

Figure 6.19: *Map showing change in the maximum current speed in the bottom layer, over a single M2 cycle, as a result of extracting the (a) maximum available power, and (b) approximately the planned power, from Lashy Sound. Spatial coordinates are in metres, referring to UTM Zone 30N.*

in the amplitude of M2 is produced north of them. This increase in range is not replicated south of the tidal fence; instead, the southern part of Lashy and Eday Sounds show a small increase in both minimum and maximum sea level, with the maximum increasing by up to 7 cm on the coast of Sanday.

Effects on water levels beyond Lashy and Eday sounds are small, even in the maximum-yield scenario, but reductions in tidal range of the order of 1–2 cm are predicted along substantial parts of the Sanday and Stronsay coasts, as well as the south coast of Eday and even parts of Shapinsay, Rousay and the West Mainland (not shown in figure). Mid-channel water levels in the Fall of Warness are affected by a similar amount.

In the 33 MW scenario the effects follow the same pattern, but with greatly reduced magnitude. Within Lashy Sound an increase in maximum sea level at the coasts of up to 2 cm may be expected but impacts beyond Lashy and Eday Sounds, including those on other tidal sites, are predicted to be negligible.

6.6 Discussion

6.6.1 Resource and TEC fence location

The two turbine fence locations are predicted to give similar maximum power yields, with a small advantage to the northern location, but the southern position requires

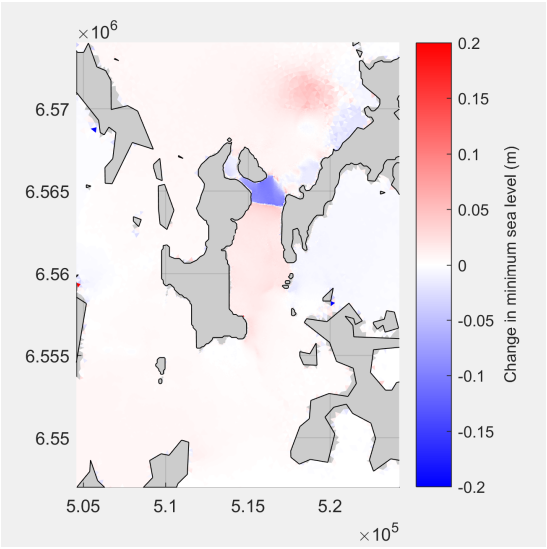

(a) *1200 TECs, change in min sea level*

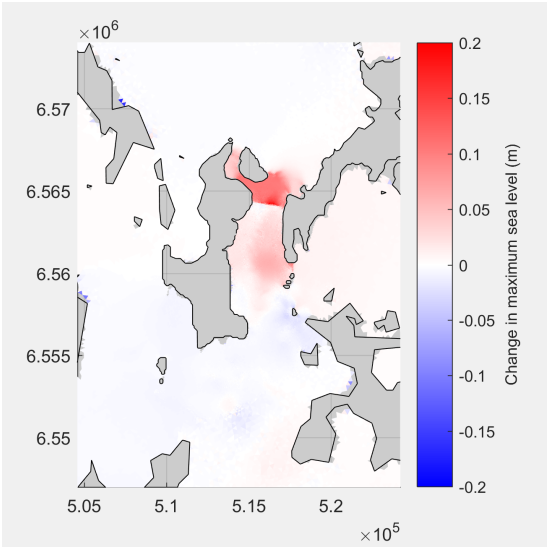

(b) *1200 TECs, change in max sea level*

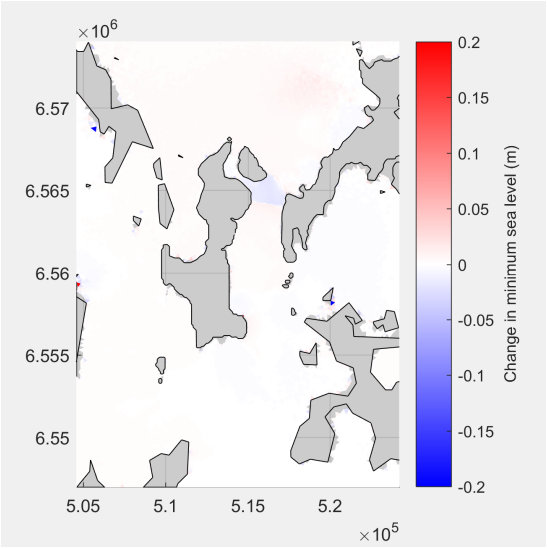

(c) *100 TECs, change in min sea level*

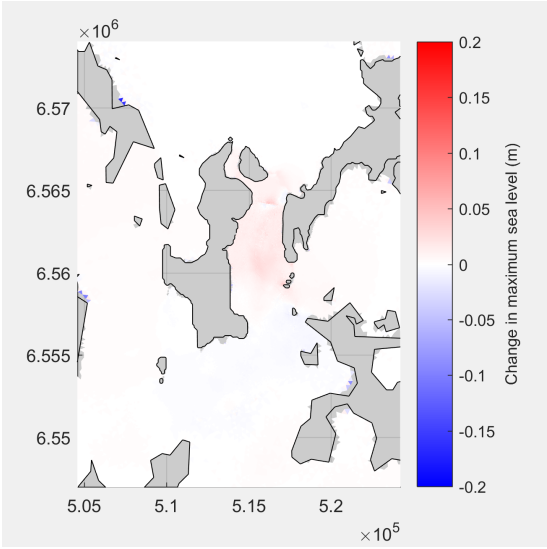

(d) *100 TECs, change in max sea level*

Figure 6.20: *Maps showing the change in the extremes of surface elevation of each cell at any time during an M2 cycle as a result of extracting power from Lashy Sound at the southern TEC fence location. Spatial coordinates are in metres, referring to UTM Zone 30N.*

many more turbines to achieve this (see Figure 6.17a & Table 6.6). The difference in the number of TECs required is unsurprising, because the southern position is wider — hence we expect a greater rotor area to be needed to achieve the same blockage.

The small difference in maximum yield is potentially of interest. From a theoretical perspective the narrower channel and faster flow at the northern location should give a higher power:thrust ratio, and hence a greater maximum yield.* However, the presence of the small channel should permit flow to bypass the tidal fence and thus reduce the yield. It is tempting to conclude that these two effects nearly balance out, giving the similar maximum power values that were found. However, the method adopted for laying out the turbines did not place any in water shallower than 7 m, hence permitting some horizontal bypass at the sides of the channel. Due to differing channel cross-sections at the two locations, the two TEC fences have different amounts of open space at either end, which may have at least as much influence as either of the effects already discussed. It is, then, not possible to make any firm conclusion about the superiority of either location from the perspective of available output — although economic considerations would undoubtedly make the northern one more favourable due to the lower number of TECs required. With hindsight, it would have been better to have no minimum depth for turbines.

The maximum yield of the channel has been identified as approx. 120 MW peak power. While extracting this level of power is very unlikely to be practicable, this does indicate that the planned 30 MW development is likely to be feasible.

In these simulations, the maximum power obtainable from the channel is achieved with a reduction in transport of 20%. This is well outside the range of 29–42% that is given by the simple analytic model of Garrett and Cummins (2005) (hereafter GC05), and substantially below figures that have been identified by numerical modelling for the Goto Islands (Chapter 5) and the Pentland Firth (Draper *et al.*, 2014b; O'Hara Murray and Gallego, 2016).

Part of this discrepancy is due to the presence of bypass flow around the ends of the simulated TEC array where the water is too shallow for the minimum rotor diameter that was specified. Part may also be due to the GC05 model not being fully applicable.

A limitation that Garret and Cummins noted in their model was that it did not allow for the driving head across a channel to change as a result of energy extraction. This is a valid assumption for their scenario of a single channel connecting two large

*This is because the number of TECs that gives maximum yield is determined by the combined thrust of the fence, which varies with the square of the flow speed, while the power available per unit of rotor area varies with the cube of the speed.

basins, but does not hold for the more complex situation studied here. In fact surface elevations near to the northern mouth of Lashy Sound, and within the southern part of Eday Sound, are predicted to change by 2–8 cm at some stages of the tide in the maximum yield scenario. The complexity of the surrounding archipelago may also mean that, even when the model is driven with only the M2 tidal constituent, Lashy Sound itself experiences more complex forcing.

6.6.2 Effects of energy extraction

Roughly doubling the power extracted (from M2 only) from 33 MW to 61 MW involves a 12-fold increase in the area of turbines required in the southern location, with a similarly disproportionate increase in environmental impacts (Figure 6.17a). The difference at the northern fence location is similar. It is clear that reaching the maximum yield of any channel, as well as being impractical from an engineering perspective, is likely to be both environmentally and economically prohibitive.

The environmental changes predicted from the lower 33 MW output scenario in Lashy Sound are small (Figures 6.18b, 6.19b, 6.20c, & 6.20d), and the effect on maximum transport is less than 1.5%. Since a realistic array would spread its thrust less evenly across the channel than the continuous fence arrangement modelled here, it would lose more power to wake mixing (Vennell, 2012). This means that the total power lost from the channel, and hence the impacts predicted here should be seen as lower limits. Nevertheless, this investigation suggests that the environmental impacts of an array of the scale of that which is proposed would be small, and hence probably acceptable to regulators.

6.6.3 Limitations & Further work

Small discrepancies were encountered in validation at Lashy Sound ADCP Site 1, which were thought likely to relate to the output jet of the constriction at the northern mouth of the channel. It would be useful to obtain spatial data, such as could be supplied by a series of transects with a vessel-mounted ADCP, to understand the shape and extent of this jet and test whether MIKE 3 correctly predicts its shape and location. Such a survey might also shed light on the more severe difference between measurements and predictions at Site 3.

With more time and computing resources it might be worthwhile to perform a mesh sensitivity study around this same jet, and additionally in the subchannel to the west of the Calf of Eday. At present this subchannel has very little transport. This may be correct, since it is relatively shallow and very narrow, but it may also be that the

model does not have sufficient resolution to behave realistically in such a small channel. After confidence was gained in the ability of the mesh to model this subchannel, it would be interesting to test the response of the main channel to alterations in the small channel (*e.g.* at the simplest level, blocking or unblocking it). This and the findings in Goto could help to move towards a more general understanding of the interactions of multiple channels and tidal energy extraction.

6.7 Chapter conclusions

In this chapter a new 3D hydrodynamic model of the Pentland Firth and Orkney Waters area was developed to study the area around Lashy Sound. Validation showed good general performance at two out of three sites, although there was an unexplained overprediction of the highest flow speeds. Discrepancies in amplitude were encountered at the third site.

Simulations using only the M2 tidal constituent indicate that the maximum yield available from Lashy Sound, using unrealistically large numbers of turbines that form a nearly complete fence, is a mean power of 23 MW with a peak of 61 MW. This is achieved with a reduction in volume transport of 20%. A mean power of 10 MW and peak of 33 MW, similar to the array that is planned in the strait, can be achieved with a 1.5% reduction in transport. Using all tidal constituents, the unrealistic maximum yield is predicted as approx. 27 MW mean and 120 MW max power.

These powers will be underestimates of the maximum values, because some bypass flow was permitted in shallow water at the sides of the channel. A realistic 30 MW array would lose more energy to wake mixing than the continuous fence arrangement modelled here, and would hence cause a slightly greater reduction in transport for the same power output.

In the 61 MW scenario very small environmental impacts are predicted over a wide area, and increases in maximum sea level of up to 15 cm within Lashy Sound are estimated. We emphasise that this scenario is a hypothetical one which is very unlikely to be realised.

In the 33 MW scenario significant effects do not extend beyond Lashy and Eday Sounds. Changes to the flow patterns within Lashy Sound would have modest effects on bed stress in the area, and an increase in maximum sea level of up to 2 cm is predicted on the coasts of Eday and Sanday close to the development site.

6.8 Further development

The work in this chapter was heavily constrained by the remaining time in the investigator's studentship. The original intention had been, after building the new model, to compare it to a small-domain, high-resolution, quasi-steady-state CFD model that had been made available by Scotrenewables. This would have enabled testing of the MTMC correction against CFD, and would also have permitted investigation of the best methods for using these two types of models together in a complementary fashion. Some very early work towards this goal may be seen in a poster from 2014 (Waldman *et al.*, 2014), but it was never progressed further.

Chapter 7

Discussion & Conclusions

In this final main chapter, selected conclusions from the previous four chapters will be brought together and overall observations made. In many cases only the methods, and not the specific quantitative conclusions, are generally applicable. Therefore, values such as the maximum yield of a specific channel will not be repeated here, and the interested reader should refer to the relevant chapter's conclusions section.

7.1 Modelling practice

The goals of this project, as stated in the introduction, were:

1. To establish whether existing commercial software can be used to predict the regional-scale effects of tidal stream energy extraction, and what the best practice is for using such software for this purpose.
2. To improve upon this state-of-the-art where practicable.
3. To test and demonstrate this best practice, and the improvement made, in a real-world scenario.

Chapters 3, 5 and 6 demonstrated that regional-scale flow modelling can provide valuable insight into both the large-scale energy potential of a channel and the mid- to far-field environmental effects of removing that energy. However, it is clear that models at this scale should not be relied upon for fine-scale detail. More generally, it is evident that all model predictions must be treated with caution: a model necessarily includes errors, and its outputs must be interpreted in line with an understanding of its validation and of the physics that it does and does not include.

The answer to the question in the first goal, then, is "yes": all of the observations in the last paragraph apply to commercial software such as MIKE 3 and Delft3D. At

the time of investigation, MIKE offered better facilities for representing tidal turbines than Delft3D, but both could produce acceptable results for the devices considered here. Delft3D has particular limitations for turbines that yaw, as well as (because of the fixed location of TECs with respect to model layers) for any scenario where the vertical location of energy extraction is particularly important. To the best of my knowledge, no commercial package currently allows floating turbines to be modelled correctly, with realistic vertical positioning throughout the tidal cycle.

The representation of tidal turbines as momentum sinks is effective in three different models that use three different numerical schemes. Some confidence in its accuracy is gained from its agreement with the Garret & Cummins model in Chapter 5. However, no comparison of large-scale energy extraction with full-scale measurements has been possible, to date, because there is no array of sufficient size in the water. The next phase of the Meygen project may have enough scale to start to compare far field effects with models, and it is to be hoped that a measurement programme will be put in place around this array.

The very high variation in current speed that can exist over short distances (Godin, 1983; Polagye and Thomson, 2013) presents a particular challenge for the validation of currents in regions of fast flow; a mis-prediction of the location of a fast current by a matter of tens of metres (*i.e.* just one mesh element) may result in a dramatic difference between predictions and measurements. Given discrepancies between model and measurement in Chapters 3 and 6, it seems likely that MIKE does not simulate "jets" downstream of constrictions correctly; it appears to have a tendency to overpredict their speed, which — given the need for conservation of mass — may indicate that it underpredicts their width. Further investigation of the shape of these jets, using transects of a vessel with a downward-facing ADCP, would help to verify this hypothesis and improve understanding of the hydrodynamics of such flow structures.

It is clear that the use of a single value of bed resistance at every point in a model is incorrect. While attempts have been made in the past to vary the bed resistance according to bottom type, in areas such as the Pentland Firth it is likely to be drag from bedforms, rather than the material surface, that dominates the overall effect (Nash and Moum, 2001; Warner *et al.*, 2013), and with the exceptions of some specific cases such as sandwaves, the effects of bedforms at coastal scale are poorly understood. It seems likely that bedform resistance will vary with the speed and direction of current. A multi-scale research approach, starting from CFD and tank testing, could work towards a better parameterisation that could be used in regional models.

The "MTMC" package developed in Chapter 4 provides an improvement in the

accuracy of thrust in high-resolution shallow water models, fulfilling the second goal above. At present there is no way to obtain turbine power (as opposed to power removed from the flow) from the software, but the theory needed to estimate it is understood. Implementing this calculation, for MIKE or for other models, is a potential avenue for future work. Implementation of a similar correction in FVCOM would be valuable, as would extending the code, if practicable, to allow for more than one turbine per cell.

The development of MTMC fulfills the second goal above. The third goal has been partially completed, in that current best practice has been demonstrated in a number of different models. However, at the time of writing MTMC has not yet been tested in a real-world scenario, due to its inability to handle multiple TECs in a single mesh element.

7.2 Resource assessment & effects of energy extraction

The technique used in Chapters 5 and 6 to estimate the maximum possible yield from a channel works well, and could be accomplished equally well with a two-dimensional model. For evaluation of realistic TEC layouts, however, it has been shown that 3D modelling is required, because 2D models cannot simulate the water diverting above and below the rotors.

This may present a difficulty for commercial use, because 3D modelling is substantially more computationally expensive — and while computing power is cheaper now than at any time in the past, the need to evaluate a number of different array locations or layouts will still make it impractical in many circumstances. It could be useful to investigate whether a theoretical or empirical "rule of thumb" could be developed to allow a 2D model to be used and then corrected to allow for vertical bypass effects.

An interesting result from Chapter 3 is that in some areas of that model, the greatest change in bed stress from energy extraction is found not in line with the tidal array, but where the bypass flow is accelerated. This is of relevance when considering the receptors that may be affected by a development.

7.3 Multi-channel interactions

Chapter 5 highlighted that interactions between multiple channels are not dictated entirely by their relative impedances, but also by their geometry, in particular in relation to the potential gradient created by the hydraulic head. There is scope for further work to understand, in a general sense, how any given set of channels will behave. For example, in a situation such as that in Goto where channels open directly into an ocean, how far apart must their mouths be to avoid significant interactions?

Chapter 6 suggests that tidal flows in Orkney's North Isles are complex, and do not conform to either a single-channel model or one of multiple parallel channels. Further investigation of this region, perhaps using drifters and accurate sea surface elevation measurements to provide ground-truth, would be interesting.

7.4 Policy implications

Although this work has been focused on modelling methods, and is not intended to cover policy with any rigour, two interesting points are raised that have policy implications.

Firstly, when multiple tidal arrays from different companies are likely to be involved in fully exploiting a large channel such as the Pentland Firth, how can these be planned for optimal results? Since the arrays will affect one another, it seems likely that some form of central planning and coordination will be necessary to determine how much energy extraction is installed in what locations. Moreover, one array 'A', built by one company, may only reach its full potential once another array 'B', built by another company, is complete. However, when A's prospective owner must make its investment decision, there is no guarantee that array B will be built at all.

Secondly, at the consenting stage, tidal arrays are authorised for a maximum name-plate capacity (*e.g.* "Company X may build an array in this location with a capacity up to 50 MW"). However, when it comes to environmental impact, and effects on other developments, it is not the electrical generating capacity that is important, but the power that is removed from the flow. It could hence be argued that the wrong thing is being controlled. Water supply companies have authority to remove a certain volume of water from a river per day, but what happens at present with tidal energy is analogous to authorising them to deliver a certain amount *to consumers*, paying no heed to leakage on the way. It would surely be better to authorise a certain rate at which energy could be removed from the channel. However, it is not currently clear

how this could practically be measured, especially in a way that would be sufficiently certain to use in court in the event of a dispute.

7.5 Further work

A number of opportunities for further work have been identified above. Here, they are summarised in a single location.

- Investigation of "jets" in the flow downstream of constrictions, comparing models and vessel-mounted ADCP surveys.
- A "bottom-up" investigation of bedform drag at the scales common at marine energy sites, using high-resolution CFD models of bedforms.
- Further development of the MTMC package to cope with multiple turbines per mesh element, and to provide outputs giving both the power removed at the rotor and the total power removed from the flow. Implementation of the same functionality in FVCOM or other models.
- Investigation into any means of correcting a 2D model to account, perhaps approximately, for the effects of vertical flow diversion, in order to allow accurate results without the computational expense of 3D modelling.
- Further investigation into the effects of channel geometry on inter-channel interactions.
- Further investigation, including measurement, of flows around Orkney's North Isles.
- Consideration, from a policy perspective, of how multiple tidal energy developments may be planned optimally when they will affect one another.
- Consideration of any reliable and practical (although not necessarily precise) means of measuring the power that is removed from the flow by a TEC array.

7.6 Advice for modellers in industry

In this short section I collect useful learning for practical modelling by tidal developers or their consultants, taken from throughout the thesis. These people are of course experienced professionals, but may not have previously applied their skills to predicting tidal resource or the effects of its extraction.

Which models?

All three of the models used in this thesis are capable of acceptably modelling tidal energy extraction at regional scale. MIKE 3 currently has the best facilities and Delft3D the worst, but all will give acceptable results and the choice can reasonably be guided by other factors such as staff familiarity and license availability. There are some caveats to this:

- In the version tested, it was not possible to correctly model a weathervaning turbine (*i.e.* one that yaws to collect power in any direction) in Delft3D. Conversely, it is not currently possible to correctly model a fixed, non-weathervaning, turbine in FVCOM, as the turbine implementation there applies the same thrust to flow from any direction. Either is fine in MIKE 3.
- In the versions tested, none of the models were able to represent floating turbines in their correct vertical positions as the water level rises and falls. In areas with small tidal ranges this will be of limited concern.

Modellers who need to add large numbers of turbines to MIKE 3 may wish to avail themselves of the MATLAB script described in Chapter 3, which has been tested with up to a thousand turbines and is far less tedious than setting them all up in the GUI.

The importance of 3D

Chapter 5 highlighted the importance of using three-dimensional models to estimate tidal resource, especially in scenarios with high blockage. This is because a 2D horizontal model is unable to represent diversion of flow over and under the turbines, and hence will tend to overestimate the extractable power.

Given the computational expense of 3D models, it may be helpful to explore options in 2D and then use 3D for promising candidates.

Open boundaries

Open boundaries should be placed far from the area of interest. While this is true for all models of this type, it is especially important for simulating tidal energy extraction because the aim is to introduce changes in the model that are not present in the global model used to provide the boundary forcing.

The use of radiative or transmissive boundary conditions may reduce the domain size that is necessary.

Grid / mesh resolution for modelling turbines

In general a higher resolution is better, and ideally there should be a maximum of one turbine per cell and one empty cell between any pair of turbines. However, this is rarely practical except for very sparse arrays. If more than one turbine per cell is used, the modeller should bear in mind the likelihood of an overestimate of power and thrust due to the model's inability to account for array effects.

Modellers should also be aware of a "danger zone" in mesh scales smaller than approx. 100 m, where predictions of thrust develop a mesh dependency unless corrected. See Chapter 4 for details and for a correction for MIKE.

Predicting changes in bed stress

One of the important physical parameters when performing modelling in support of an environmetal impact assessment is likely to be changes in bed stress. As noted in Chapter 3, absolute values for bed stress are strongly dependant on the value of bed resistance in the model, and bed resistance is conventionally set through a rather insensitive calibration process. It may therefore be best to avoid reliance on absolute values, but instead to compare the values before and after tidal turbines are added so as to answer the important question of how conditions will change.

Appendix A

MIKE sensitivity study

This Appendix relates initial testing conducted with the MIKE 3 model at an early stage of the studentship. Were it to be repeated now the author would retain depth-resolved information, instead of depth-averaging, to better understand any effects of bed resistance or the number of layers on the vertical velocity profile. This work produces no new scientific insight, but is presented here simply to document the work done and to allow reference to be made from the main text.

An early version of the MIKE model that was later enhanced for use in Lashy Sound was used to test MIKE's sensitivities to various configuration options. The mesh is shown in Figure A.1. Model outputs were evaluated by comparison of water level against the UK Tide Gauge Network tide gauge at Wick, and comparison of depth-averaged current speed predictions against the three ADCPs shown on Figure 3.7.

A.1 Bed resistance

Bed resistance is commonly used as a calibration parameter, and such an approach was explored here. The simulation was run for seven days of model time, and the first three days were discarded as spinup. The current speeds from the model results were modified with a 10-minute centred moving average, to match the ensemble period of the ADCP observations. Both observed and simulated speeds were then depth-averaged.

The root mean square error (RMSE) and mean error (ME) between the predicted and observed values were calculated for each bed resistance value at each site. A graphical plot was made of the data from the final two days (reduced from four days to improve legibility). These results may be seen in Table A.1 and Figure A.2.

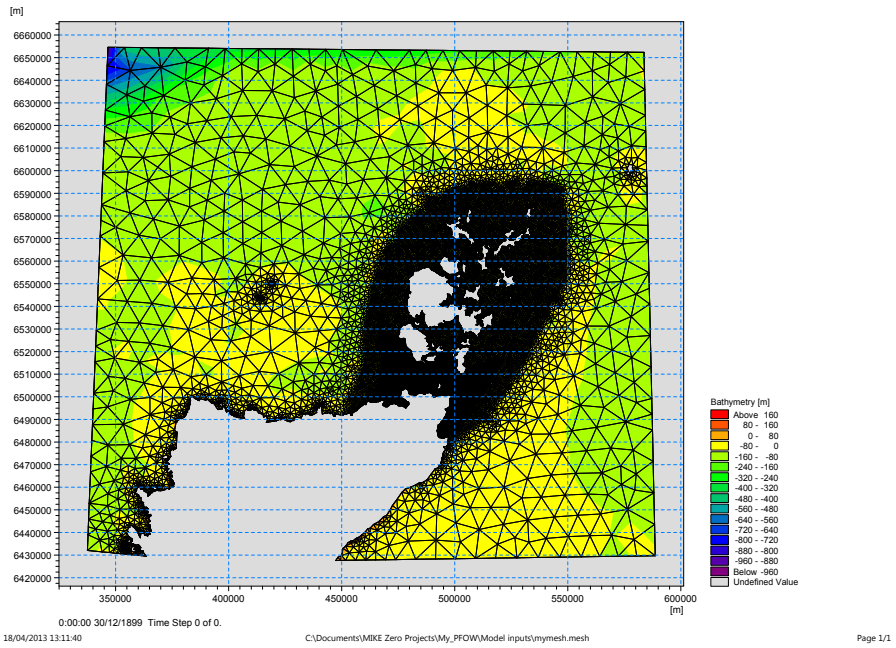

Figure A.1: *Mesh and bathymetry of the PFOW model used for testing.*

k_s value	0.6 m	0.8 m	1.6 m	2.0 m	2.5 m	3.0 m	3.5 m
Site 1 RMSE	0.322	0.297	0.251	0.242	**0.238**	0.239	0.242
Site 1 ME	0.0754	0.0473	**-0.0252**	-0.0502	-0.0761	-0.0981	-0.117
Site 2 RMSE	0.368	0.336	0.278	**0.270**	**0.270**	0.275	0.285
Site 2 ME	0.0991	0.0626	**-0.0341**	-0.0679	-0.1030	-0.1328	-0.159
Site 3 RMSE	0.361	0.343	**0.320**	0.321	0.328	0.337	0.347
Site 3 ME	**-0.0411**	-0.0691	-0.1439	-0.1704	-0.1982	-0.2218	-0.243

Table A.1: *Root Mean Square Error and Mean Error statistics for different bed resistance values. Values closest to zero are highlighted in* ***bold****. All values are in metres per second.*

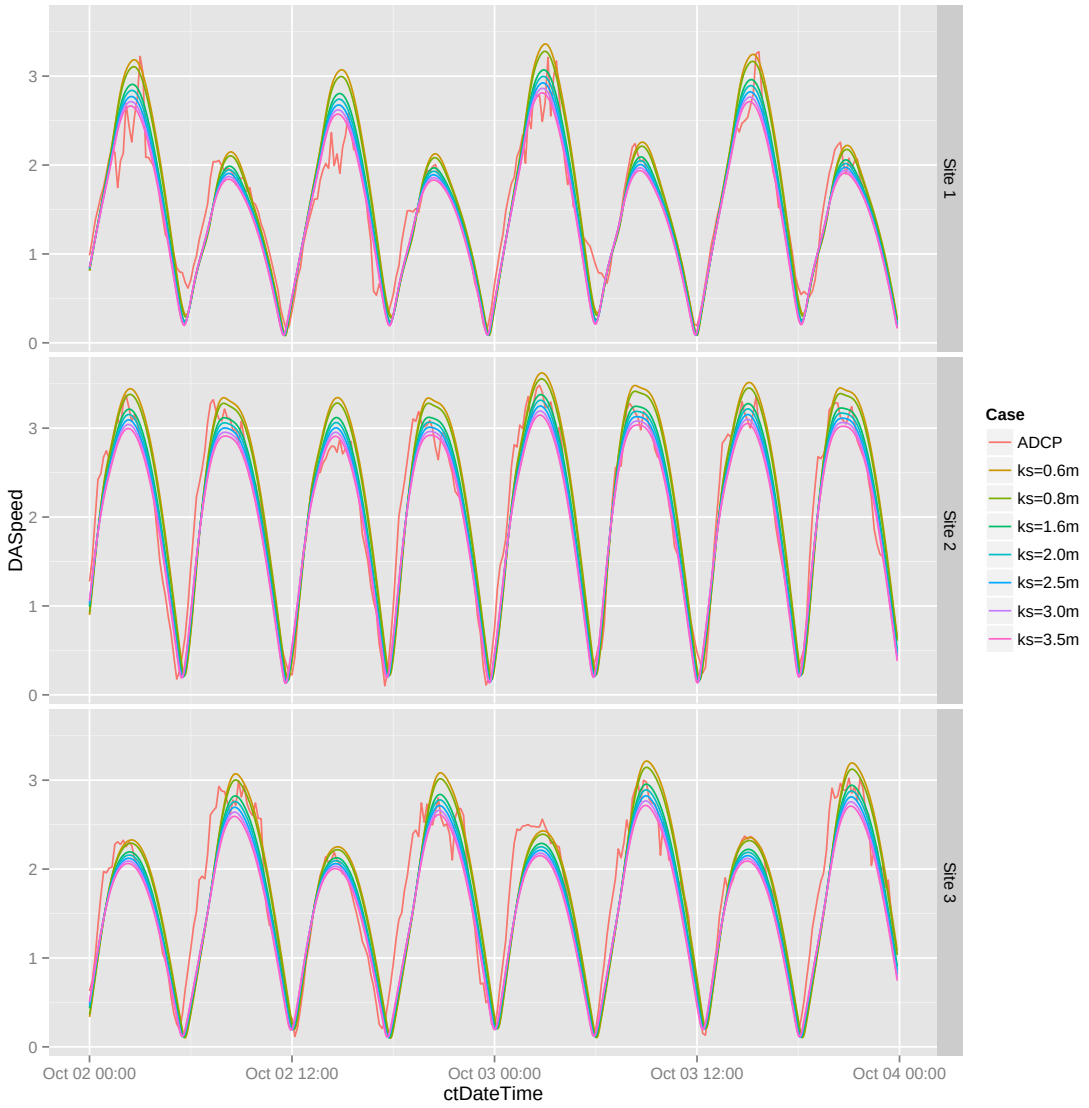

Figure A.2: *Final 2 days of 7-day runs at a range of uniform bed roughness height values, showing depth-averaged current speed over time.*

It is clear that higher bed roughness heights result in lower current speeds, as expected. Based on Table A.1, a value of 1.6–2.5 m would be selected. It is worth noting, however, that different values for bed roughness give the best match to measurements at different locations.

A.2 Other options

The MIKE model was tested for sensitivity to a number of configuration options. The results of this testing informed modelling work in MIKE for the remainder of the project.

A.2.1 Method

The model was run for 7 days, with the first three days discarded for spinup. The timing was chosen so that the remaining four days would include spring tides.

Initially a baseline run was performed, using the settings that had been used in the model up to this point (mostly defaults). Further runs were completed as follows:

'noslip' Land boundary condition: MIKE offers a choice for land boundaries: mesh elements adjacent to the boundary can be set to have zero velocity normal to the boundary but not impede flow parallel to it (the default), or to have zero velocity in all directions ('noslip'). The latter is likely to be more appropriate for very high resolution models, in order to simulate friction from the shore.

The baseline used zero normal velocity, and this run used zero total velocity.

Flooding & drying: For this run, MIKE's flooding and drying module was turned off. To allow this, it was necessary to set a "minimum depth" such that no part of the model dried out. Any depths of less than 2.4 m were automatically increased to 2.4 m This value was derived from the minimum level predicted at Kinlochbervie in the baseline case.

k-ϵ turbulence model: The baseline run used the minimal 'algebraic' turbulence closure system to determine vertical eddy viscosity — *i.e.* no turbulence sub-model, and assumption of a logarithmic shear profile. This run enabled the 'k-ϵ' turbulence model, which solves additional transport equations for turbulent kinetic energy (TKE) and dissipation of TKE. The k-ϵ model has a number of configurable parameters, which were left at their default values.

Vertical layers: The baseline run used ten vertical layers in the mesh. Additional runs were conducted with five and with twenty layers.

Tidal forcing: For small model domains, it is reasonable to assume that the direct gravitational effects of the sun and moon that are experienced by the water in the model are negligible, and that the model can purely be driven by tidal forcing at the boundaries. For larger domains, such as global models or full ocean basins, it is clearly necessary to include direct tidal forcing. Advice from DHI was that the size of this domain was near the threashold of when these effects become significant (personal communication with Suzie Clarke of DHI, 2013).

For the baseline model, no direct tidal forcing was included. For this version, tidal forcing was included using 11 astronomical constituents.

In each case the following measures of agreement were calculated:

- Root mean square error (RMSE)
- Mean error (ME)
- Skill, using the baseline run as the baseline for which Skill = 0 (see Section 2.2.1 for an explanation of this statistic)

A.2.2 Results & discussion

Table A.2 shows the time taken for the model to run in each case. Minor variations in the runtimes are to be expected, as unpredictable background processes will have taken place on the PC. However, the k-ϵ and 5/20 layer runs show significant differences in speed to the base case. This is expected, as the k-ϵ model must solve additional transport equations, and the number of layers in the model has a direct

Model run	Elapsed time (sec)	$\frac{\text{Elapsed time}}{\text{Baseline time}}$
baseline	45 594	—
noslip	43 269	0.95
no flooddry	42 111	0.92
k-ϵ	77 439	1.70
5 layers	22 381	0.49
20 layers	74 944	1.64
tidal forcing	46 519	1.02

Table A.2: *Table of model runtimes for sensitivity testing. All models used identical input paramters except for the changes being tested. All were run on an otherwise unloaded 4-core Intel i7 PC.*

Model run	RMSE (m)	ME (m)	Skill
baseline	0.0589	−0.002 93	—
noslip	0.0585	−0.002 95	0.0110
no flooddry	0.0590	−0.002 94	−0.0054
k-ϵ	0.0585	−0.002 93	0.0133
5 layers	0.0595	−0.002 96	−0.0199
20 layers	0.0587	−0.002 93	0.0056
tidal forcing	0.0590	−0.002 90	−0.0047

Table A.3: *Table of sensitivity testing results for water level*

effect on the scale of the computational problem. Tables A.3 & A.4 show the results of comparing the models' predictions to measurements as described above.

From examining the skill scores, it appears that the model — at least in the areas at which we have measurements to compare against — is insensitive to most of the options tested. The only cases giving skill scores of more than ±0.05 are 'noslip', the choice of turbulence model, and the number of layers.

Caution is required with the 'noslip' result, because the model was known to be overpredicting velocities at the time. Given this, a change that increased the resistance to the flow — in this case at the land boundaries — might be expected to improve the match to measurements regardless of whether it was an appropriate change for the model.

In this test, enabling the k-ϵ turbulence closure model (TCM) gave slightly better matches to observations of water level, but slightly poorer matches for current speed. As such it is difficult to conclude an overall cost or benefit in terms of results. More rigorous testing of the same options in Delft3D by Baston *et al.* (2013) showed that the choice of TCM makes very little difference to current speeds in that model. Were we using a baroclinic model and thus considering the potential for stratification, it may be that the representation of turbulence could have an effect on mixing, but testing this was outside the scope of this work. Since the use of the k-ϵ TCM has little effect and carries a dramatic computational cost, it was disabled for future modelling work.

Using fewer layers gives a very slightly worse match to observations, and using more layers gives a very slightly better match. It is unsurprising that an increase in vertical resolution gives results that better match observations, as the model is able to represent processes in the water column in finer detail. The change seen is small, with a decrease in the Mean Error of less than $0.04\,\mathrm{m\,s^{-1}}$ at all sites. However, it should be remembered that this very brief study has used depth-averaged velocities, which could mask improvements in specific parts of the water column.

Model run	Site 1 RMSE ($m\,s^{-1}$)	Site 1 ME ($m\,s^{-1}$)	Site 1 Skill	Site 2 RMSE ($m\,s^{-1}$)	Site 2 ME ($m\,s^{-1}$)	Site 2 Skill	Site 3 RMSE ($m\,s^{-1}$)	Site 3 ME ($m\,s^{-1}$)	Site 3 Skill
baseline	0.637	0.368	—	0.712	0.452	—	0.607	0.248	—
noslip	0.633	0.365	0.0127	0.664	0.420	0.1315	0.580	0.243	0.0875
no flooddry	0.637	0.367	0.001 75	0.710	0.451	0.005 97	0.607	0.250	0.001 80
k-ϵ	0.656	0.381	−0.0601	0.741	0.483	−0.0820	0.622	0.260	−0.0496
5 layers	0.621	0.381	−0.043 59	0.735	0.472	−0.064 34	0.608	0.249	−0.002 27
20 layers	0.621	0.354	0.052 13	0.695	0.435	0.048 92	0.605	0.247	0.008 78
tidal forcing	0.639	0.365	−0.003 81	0.722	0.448	−0.027 95	0.617	0.246	−0.032 16

Table A.4: *Table of sensitivity testing results for current speed*

Appendix B

Preparing bathymetry for MIKE

Thanks to modern multibeam echo sounder (MBES) surveys, bathymetry data is usually available at a much higher resolution than that of the model grid. Some thought is required on the best way to get from this dense cloud of information to that which is needed for the model.

For a structured grid such as that used by Delft3D (or for MIKE's non-flexible-mesh versions), the best way to prepare the bathymetry is relatively obvious: if one takes the mean of the data points available in each cell, one can reasonably claim to have a representative value for the depth of that cell. With an unstructured mesh for a finite volume model this is less clear. Depths are specified not for the mesh elements (cells) but for the nodes, and so one depth value can influence — but not completely control — a number of elements.

During the process of preparing the mesh it is likely to change a number of times, and hence it is convenient to allow MIKE's built-in interpolation routine to handle the final interpolation onto the mesh nodes. A summary of the technique used by this interpolator is given below. It appears to be a sensible approach for sparse bathymetry. However, when the bathymetric data set is of much higher resolution than the model mesh (e.g. MBES bathymetry at 2 m resolution and a model with element sizes of 100 m or more), it will only consider a very small area around each node — just a few metres in the example given — and thus cannot be considered to be representative of the depth of any of the surrounding triangles.

Therefore, it is desirable to adopt a two-stage process where the quantity of data is reduced first and then supplied to MIKE's built-in routine.

B.1 Summary of MIKE interpolation technique

MIKE uses an interpolation technique known as "Natural Neighbour", first developed by Sibson in the 1980s. A good explanation is given by Ledoux and Gold (2005), but a brief summary follows:

Given a set of points, the Voronoi cell corresponding to a point is the area which is closer to that point than to any other point in the set. A Voronoi diagram (also called a Voronoi tessalation) shows these cells, computed for every point in the set. Consider two Voronoi Diagrams: an initial one for the set of available bathymetric points A, and a second one for the union of that set with the target point for the interpolation p. The "natural neighbours" of point p are the points in A whose Voronoi cells have had area "stolen" by the additional cell when p was added. The weight that should be given to each of the natural neighbours is equal to the proportion of the area of p's cell that was occupied by that neighbour's original cell. This is illustrated by Figure B.1.

It has been shown that natural neighbour interpolation performs better for irregularly distributed data than conventional techniques (see references from Ledoux and Gold (2005)), and this can easily be explained intuitively: In Figure B.1, because the available data are denser to the north-east of the target point than in other directions, a simple inverse distance weighting would have given disproportionate weight to this area. As can be seen, a natural neighbour weighting does not do this. However, the Natural Neighbour algorithm does not look beyond the nearest ring of points, so if it is supplied with a very high resolution data set the area considered in the interpolation will be very small.

B.2 Initial reduction of high-resolution bathymetry

When reducing the full-resolution bathymetry to an intermediate resolution, the objective is that each new data point should be representative of the area around it. An appropriate method for evenly-spaced data is to reduce to a new bathymetric grid where the depth for each cell is the mean of the depths of all points within that cell. Simple tools that sieve or sample from the high-resolution bathymetry, while less demanding to run, carry a risk of providing an unrepresentative output. Care should be taken in areas of uneven point spacing, for the reasons given above, but because the aim here is to reduce very high resolution data to a more manageable density, bias introduced by using a mean across changes in resolution should be confined to a very local area. With datasets where point density and depth are related (*e.g.* if shallower areas have higher resolution) then additional measures may be required to

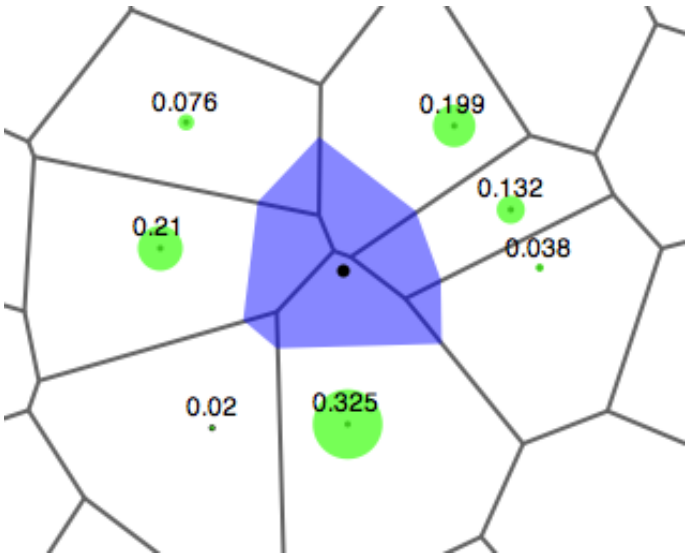

Figure B.1: *Illustration showing the Voronoi Diagram of the original points (black lines) with the "new" cell belonging to the target point superimposed in purple. The numbers and the green circles around each point represent the weight given to each neighbour. Note that these sum to 1.*
Diagram from Wikimedia Commons, user "Markluffel", licensed under Creative Commons Attribution-Share Alike 3.0 Unported Lincese. (Wikipedia, 2013)

avoid a systemiatic bias. This project did not involve such data.

In order not to lose excessive detail in the final interpolation, the bathymetry supplied to MIKE must be at a higher resolution than the mesh itself. However, the resolution supplied to MIKE also determines the extent of the area around each node that is considered when determining that node's depth (see above); the area considered will be approximately equal to the area within the closest ring of bathymetry points around the node. This implies that the intermediate resolution should not be very much more than the resolution of the mesh.

A further limitation is introduced by the maximum number of data points that the MIKE interpolator can handle. The version used for this project used 32-bit code and was unable to process very large numbers of points.

It is unlikely that the number of points required for the resolution of the finest parts of the mesh can be supplied for the whole domain without exceeding the maximum number of points. Additionally, the desired resolution will vary across the domain as the scale of the mesh elements varies.

For both of these reasons it may be necessary to reduce the bathymetry to different resolutions for different parts of the model domain, and there is no single clear answer for the optimum intermediate resolution to use.

Appendix C

Selected peer-reviewed content written during the studentship

During my studentship I was lead author on four peer-reviewed outputs — two journal articles and two conference papers. These are reproduced here. The four papers approximately correspond to the four main chapters of this thesis, and thus there is substantial duplication. The differences between the chapters and the papers are in some cases due to the parts of the work in the papers that were by other authors (which are omitted or summarised in the thesis), and in some cases due to further work that I completed after the papers' acceptance. More information on the correspondence between publications and chapters may be found in Section 1.5. Non-peer-reviewed publications, or those on which I was a minor author, are not included but are listed below.

The four publications included here are,

1. Waldman S, Baston S, Nemalidinne R, Chatzirodou A, Venugopal V, Side J (2017). "Implementation of tidal turbines in MIKE 3 and Delft3D models of Pentland Firth & Orkney Waters". Ocean & Coastal Management. DOI 10.1016/j.ocecoaman.2017.04.015.
   Also included is an erratum to the above, submitted but not yet published.

2. Waldman S, Genet G, Baston S and Side J (2015). "Correcting for mesh size dependency in a regional model's representation of tidal turbines". European Wave & Tidal Energy Conference (EWTEC) 2015.

3. Waldman S, Yamaguchi S, O'Hara Murray R, Woolf D (2017). "Tidal resource and interactions between multiple channels in the Goto Islands, Japan". International Journal of Marine Energy. DOI: 10.1016/j.ijome.2017.09.002

4. Waldman S, Side J, Woolf D (2017). "Numerical investigation of tidal resource

& far field effects in Lashy Sound, Orkney". European Wave & Tidal Energy Conference (EWTEC) 2017.

Other publications in which I have authorship are,

- Baston S, Waldman S, Side J (2014). "Modelling energy extraction in tidal flows"
  Position Paper, output of the TeraWatt UKCMER Grand Challenge project. Rev. 3.1 issued October 2015. (not formally peer reviewed)

- Gallego A, Side J, Baston S, Waldman S, Bell M, James M, Davies I, O'Hara Murray R, Heath M, Sabatino A, McKee D, McCaig C, Karunarathna H, Fairley I, Chatzirodou A, Venugopal V, Nemalidinne R, Yung TZ, Vögler A, McIver R, Burrows M (2016), "Large scale three-dimensional modelling for wave and tidal energy resource and environmental impact: Methodologies for quantifying acceptable thresholds for sustainable exploitation".
  Ocean & Coastal Management. DOI: 10.1016/j.ocecoaman.2016.11.025.

- Neill S, Vögler A, Goward Brown A, Baston S, Lewis M, Gillibrand P, Waldman S, Woolf D (2017), "The wave and tidal resource of Scotland".
  Renewable Energy. DOI: 10.1016/j.renene.2017.03.027.

Ocean & Coastal Management 147 (2017) 21–36

Contents lists available at ScienceDirect

Ocean & Coastal Management

journal homepage: www.elsevier.com/locate/ocecoaman

Implementation of tidal turbines in MIKE 3 and Delft3D models of Pentland Firth & Orkney Waters

S. Waldman [a, *], S. Bastón [a], R. Nemalidinne [b], A. Chatzirodou [c], V. Venugopal [b], J. Side [a]

[a] Heriot-Watt University, Back Road, Stromness, Orkney, KW16 3AW, UK
[b] Institute for Energy Systems, School of Engineering, University of Edinburgh, Edinburgh, EH9 3JL, UK
[c] Energy & Environment Group, Zienkiewicz Centre for Computational Engineering, College of Engineering, Swansea University, Singleton Park, Swansea, SA2 8PP, UK

ARTICLE INFO

Article history:
Received 12 May 2016
Received in revised form
21 April 2017
Accepted 28 April 2017
Available online 7 May 2017

Keywords:
Regional modelling
Energy extraction
MIKE 3
Delft3D

ABSTRACT

As part of the Terawatt project, two regional-scale hydrodynamic models of the Pentland Firth & Orkney waters were developed using unaltered commercially-available software (MIKE 3 and Delft3D), in order to investigate the suitability of such software for predicting the effects of tidal stream energy development. Realistic scenarios for tidal energy extraction were implemented in each, and the predictions of the models with and without turbines compared. Similar predictions were made of depth-averaged current speed (spatial correlation of $R^2 = 0.95$), but bed stress in one model was more than double that in the other due to the use of different values for bed resistance. The effects of energy extraction are consistent between the models at a regional scale but show considerable local differences. We conclude that these model codes are suitable for broad-scale assessment of the effects of energy extraction but that caution, and more detailed survey data, is required at fine scales.

1. Introduction

Tidal energy convertors (TECs) remove energy from the environment, for conversion into electricity. As a consequence, the kinematics of tidal currents will be altered and some change in the hydrodynamics of the local environment is inevitable. Regulatory authorities are required to understand the extent of such effects on specific receptors in order to determine whether they are acceptable, and hence the prediction of these effects is essential to any consenting process that will approve tidal energy developments (Side et al., 2017).

While direct analytical techniques can approximate the hydrodynamics of simple channels with idealised energy extraction (*e.g.* Garrett and Cummins, 2005, 2007), a numerical modelling approach is required to predict the effects of realistic TECs in real-world sea areas such as the Pentland Firth and Orkney Waters (PFOW). Tidal currents have previously been simulated in the North-West European shelf seas using a number of different regional-scale models including SUNTANS, ADCIRC, Fluidity, ROMS, and MIKE (Baston and Harris, 2010; Draper et al., 2013; Martin-Short et al., 2015; Neill et al., 2014; Fairley et al., 2015). A recent review article by Neill et al. (2017) gave a good summary of recent work on the tidal resource of Scotland using the results of models such as these.

The TeraWatt project (Side et al., 2017), of which this work formed a part, aimed to identify best practice methods for predicting the regional-scale effects of tidal energy extraction which could be used by industry and regulators. The project received strong guidance from industrial stakeholders that only unaltered, reputed and well-tested commercial software could be used for this work if the results were to be accepted by investors. We were advised of a perception amongst investors that open source code cannot be trusted unless backed with the reputation of a trusted commercial organization. Many of the academic codes mentioned above were deemed unsuitable on this basis, and based on guidance from industry two three-dimensional modelling suites were selected: MIKE 3 by DHI,[1] and Delft3D-Flow by Deltares.[2] Both of these packages are already in extensive use commercially.

Demonstration models of the PFOW area were developed separately in the two suites by different teams, according to the

* Corresponding author.
E-mail address: simon@simonwaldman.me.uk (S. Waldman).

[1] http://www.mikepoweredbydhi.com/.
[2] https://www.deltares.nl/en/software.

http://dx.doi.org/10.1016/j.ocecoaman.2017.04.015
0964-5691/

capabilities of each. No attempt was made to match parameters between the models, as this approach would be unavailable to a developer or consultancy with access to only one software package. Rather, an emphasis was placed upon evaluating the differences, in both methods and results, between the two systems. Others in TeraWatt are developing methods for predicting changes to benthic ecology, which will be published separately, and time series of current speed and sea bed shear stress predicted by these models were provided to them as input data.

1.1. Overview

The structure of this paper is as follows: First we give a brief description of the area of the study and of the available observational data. Next, the two models are described, their predictions without turbines compared, and the differences discussed. Details are then given of the implementation of tidal turbines in each model, and predictions of the effects of the turbines are examined. Finally, we discuss implications for industry and regulators.

1.2. Description of the area of the study

Orkney is a group of islands separated from the north coast of Scotland by the Pentland Firth. The Pentland Firth is approximately 20 km long and 10–15 km wide (see Fig. 1).

The tides in the area are predominantly semidiurnal, and there is a phase difference of 50–60° from one side of Orkney to the other, equivalent to a time difference of approximately 2 h between high water on the Atlantic and North Sea coasts (Easton et al., 2012). This results in a difference in water level across the archipelago, and thus strong currents in the Pentland Firth and other channels due to hydraulic forcing. In the constrained area between the isles of Stroma and Swona, the current speed regularly exceeds 4.5 m s^{-1} (UK Hydrographic Office, 1986).

In addition to the Pentland Firth, a second channel is of interest: this passes through the North Isles of Orkney and is formed of Westray Sound, the Fall of Warness, and Stronsay Sound.

1.3. Available observational data

Limited observational data is publicly available for the area. Observations from four sources were used for calibration and validation purposes, the locations of which are described in Table 1. The locations of the ADCPs are shown on Fig. 1 (the tide gauges at Wick and Kinlochbervie lie outside the bounds of this map). Tide gauge data was obtained from the Delft3D Dashboard utility (van

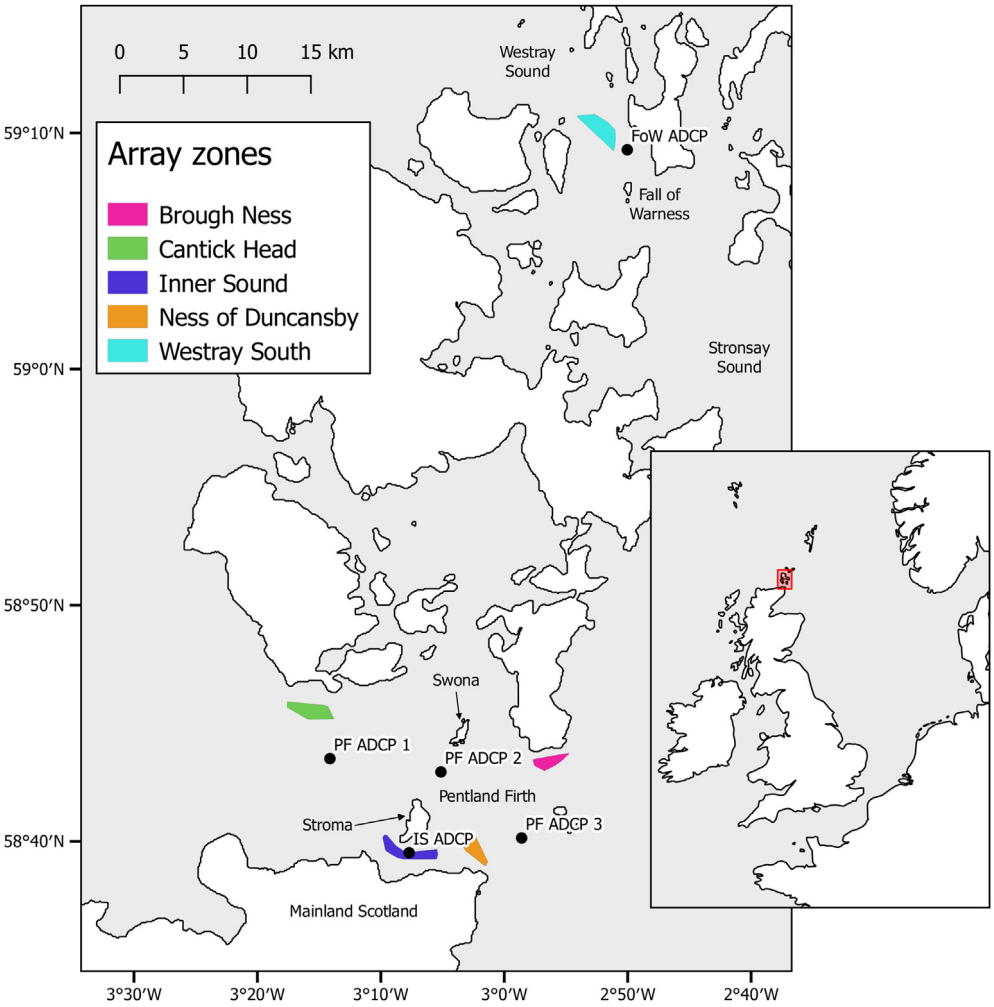

Fig. 1. Map showing part of the Pentland Firth and Orkney Waters. Black points show the locations of the five ADCPs used for calibration & validation: three in the centre of the Pentland Firth (labelled PF), one in the Inner Sound (labelled IS) and one in the Fall of Warness (labelled FoW). Coloured polygons show the areas in which tidal turbines were simulated. Inset map shows location of the area within the North-West Europe region. (For interpretation of the references to colour in this figure legend, the reader is referred to the web version of this article.)

Table 1
Table showing locations of observational data sources used in this work. Further detail may be found in the text of Section 1.3.

Record type	Location	Latitude	Longitude
Tide gauge	Wick	58° 26′28.68″N	3° 5′5.64″W
Tide gauge	Kinlochbervie	58° 27′23.80″N	5° 3′1.30″W
ADCP	PF Site 1 (west)	58° 43′34.00″N	3° 14′11.01″W
ADCP	PF Site 2 (mid)	58° 43′1.02″N	3° 5′9.02″W
ADCP	PF Site 3 (east)	58° 40′13.02″N	2° 58′35.03″W
ADCP	Fall of Warness	59° 9′21.6″N	2° 49′51.6″W
ADCP	Inner Sound	58° 39′35.28″N	3° 7′43.32″W

Koningsveld et al., 2013). Data at the three Pentland Firth ADCP locations was collected by Gardline in 2001 (UK Maritime and Coastguard Agency, 2001). Visual inspection of the envelope of the springs/neaps cycle, as reported by these ADCPs, suggests that velocities at peak springs may be clipped. ADCP data at the Fall of Warness test site was purchased from EMEC. Raw data for the Inner Sound was not availible at the time of writing, but the phases and amplitudes of constituents were sourced from Gillibrand et al. (2016).

2. The models

2.1. MIKE 3 model

The three-dimensional MIKE 3 Flow Model FM (Flexible Mesh) system (2012 version) was used for this study. The MIKE FM modelling suite is based on a cell centred finite volume method, with an unstructured mesh to permit accurate representation of complex coastal areas. The momentum equations used are the incompressible, Reynolds averaged form of the Navier-Stokes equations, using hydrostatic pressure and the Boussinesq assumption as to the representation of turbulence by eddy viscosity. Horizontal eddy viscosity is represented by the Smagorinsky formulation and vertical eddy viscosity is by the standard $k-\varepsilon$ model. The bed resistance is specified as a quadratic drag coefficient. A comprehensive description of the model can be found in Venugopal and Nemalidinne (2014) and DHI (2012).

The model domain, shown in Fig. 2, encompasses the principal high tidal flow regions of the Pentland Firth and the Fall of Warness. It features higher resolution in areas where the kinetic power density is high, and lower resolution in areas where the currents are weaker. The unstructured mesh triangles in coarse areas have a maximum characteristic length of 4000 m; mesh triangles in the finer zones have a characteristic length of 50–200 m. Ten equidistant terrain-following sigma layers are used in the vertical direction. Of the two numerical schemes offered by MIKE, the high order one was selected.

The coastline was defined throughout as an impermeable, zero normal velocity boundary, while the bottom is a no-slip, impermeable boundary with bed resistance specified by a quadratic drag coefficient of 0.01. Bathymetry was interpolated from a proprietary 20 m gridded dataset provided by The Crown Estate. This bathymetry is assembled from publicly available multibeam echo sounder data, described in O'Hara Murray (2015a), where available — which includes the majority of the PFOW area. Gaps in the PFOW area are filled with a commercial bathymetry product purchased from DEFRA. Parts of the model domain outside the immediate PFOW area use bathymetry from Smith and Sandwell (1997). The various data sources were merged, aligned, gridded and quality controlled by ABPmer (ABPmer, 2012) under contract to The Crown Estate.

The open boundaries were specified as clamped time-varying water levels generated using the DHI global tidal model database (Cheng and Andersen, 2010), based on the major diurnal (K1, O1, P1 and Q1) and semi-diurnal (M2, S2, N2 and K2) tidal constituents at a spatial resolution of $0.25 \times 0.25^{\circ}$. This database has been validated against TOPEX/POSEIDON altimetry. The time step was automatically varied according to a target Courant number of 0.8. As there are no significant river discharges in the vicinity of the Pentland Firth, no water sources were included. The simulation was run in barotropic mode without wind forcing or wave radiation stress.

The relatively small size of this domain was necessary in order to match computational effort to the available time and hardware. It is acknowledged that placing the open boundaries further from the area of interest would be preferable. The use of clamped open boundaries is also not ideal, especially on a small domain (Adcock et al., 2011). Both MIKE 3 and Delft3D support more sophisticated radiative/transmissive boundaries, but in both cases they require external velocities, as well as elevations, to be provided. Accurate velocities over large spatial areas are not generally available in coastal areas, and so it would be unhelpful to suggest that commercial modellers should require this information. Some confidence that the model is not compromised by the domain size or the use of clamped boundaries may be gained by the observation that the maximum change in current speed at an open boundary as a result of including energy extraction was approx. 0.02 m s^{-1}, or <2% of the undisturbed value at that time and place.

2.2. Delft3D model

Delft3D-Flow is a finite difference code that solves the Reynolds-averaged Navier-Stokes equations under the assumption of hydrostatic pressure, using terrain-following sigma coordinates. For this work, the open source version of Delft3D with source control tag 3574 was used.

Horizontal spatial discretization is on a structured rectangular Arakawa-C grid. This is a staggered grid in which water levels are computed at grid cell centres and flow velocity components are defined at the mid-points of the cell faces to which they are perpendicular. For full details, see Deltares (2014).

Two computational grids were bidirectionally coupled: a) a coarse grid covering the North of Scotland with a domain of 254×226 km and a horizontal resolution of 1×1 km; and b) a smaller grid covering the PFOW at a higher resolution of 200×200 m (see Fig. 3). The size of the domain was chosen to minimise the chance that any numerical instability that might arise at the boundaries would affect the area of interest. Bathymetry was interpolated from the same 20 m gridded dataset, provided by The Crown Estate, as was used for MIKE.

In order to reduce computation times, the outer domain was simulated in two dimensions and the inner in three. The model displayed low sensitivity to the number of vertical layers used for the inner grid; ten layers were used in this study. Horizontal eddy viscosity is provided by a large eddy simulation approach. Vertical eddy viscosity uses the $k-\varepsilon$ method, although a previous study showed that this model is not sensitive to the choice of vertical turbulence scheme (Baston et al., 2013).

The open boundaries are driven by clamped time-varying surface elevation conditions, provided by the TPXO 7.2 Global Inverse Tidal Model (Egbert et al., 1994; Egbert and Erofeeva, 2002) including 13 tidal constituents at a spatial resolution of 1/12°. The model was run with a fixed time step of 25 s, which provides for a Courant number of less than 1.

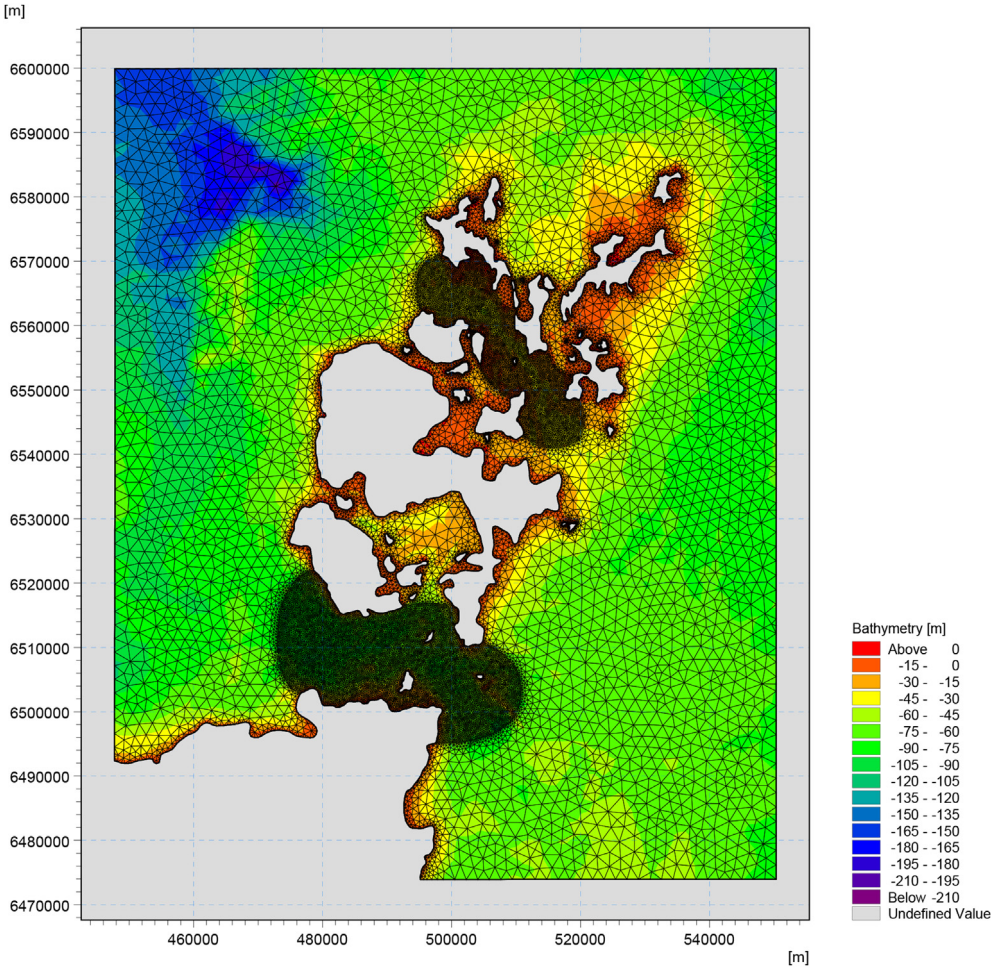

(a)

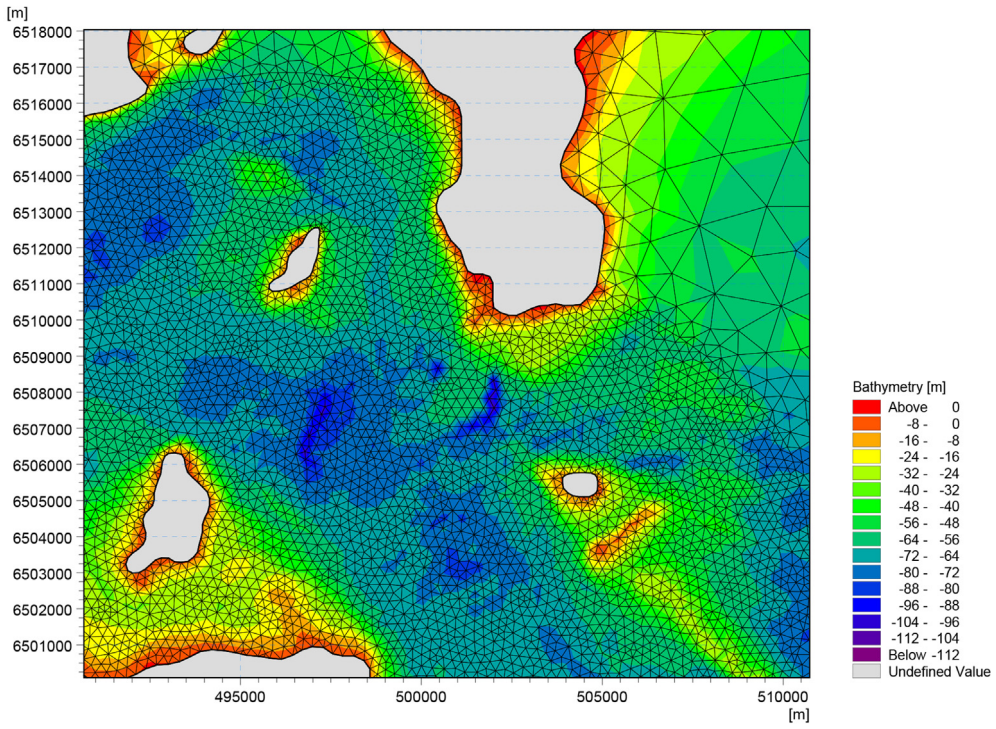

(b)

Fig. 2. (a) Complete computational domain, mesh and bathymetry for MIKE 3 model; (b) detail showing Eastern part of Pentland Firth. Coordinates are in metres, referring to the UTM coordinate system zone 30N.

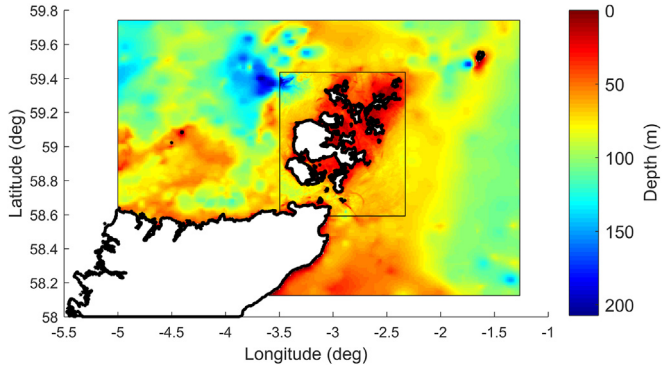

Fig. 3. Map showing the Delft3D model domain. The outer grid (full coloured area) has a resolution of 1 × 1 km, while the inner PFOW grid (inner black box) has a resolution of 200 × 200 m. Colours show the model bathymetry. (For interpretation of the references to colour in this figure legend, the reader is referred to the web version of this article.)

As with the MIKE model no river sources were defined, and the model was run in barotropic mode without wind or wave forcing.

2.3. Calibration & validation

The outer grid of the Delft3D model was tested against tide gauge records. No water level comparison was performed between the tide gauges and the MIKE model, because the smaller domain of this model results in the gauges location being either excluded or very close to open boundaries.

The inner Delft3D model was calibrated against ADCP records at the Fall of Warness, and the MIKE model against three ADCPs in the Pentland Firth. In both cases the bottom friction was adjusted to achieve the best match between predictions and measurements.

The use of different data sets for calibration presents a difficulty in displaying comparable validation statistics. In this section both models will be compared against the Pentland Firth ADCPs in the time domain for the period 21/09/2001–04/10/2001. It is acknowledged that for the MIKE model the same data are being used for calibration and validation, so the skill of the model in the area of these measurements does not necessarily imply equal skill in other areas; however, it is in this area that most of the areas of interest for tidal energy extraction are situated, and hence it is still a useful comparison to make.

In order to provide an additional check on both models, they were compared in the frequency domain with the phases and amplitudes of tidal constituents measured in the Inner Sound and published by Gillibrand et al. (2016).

See Fig. 1 and Table 1 for the locations of all the ADCPs described.

2.3.1. Time domain

The original ADCP observation campaign recorded 4 m depth bins throughout the water column (UK Maritime and Coastguard Agency, 2001). However, observations at only three depths (different at each site) were available to this project. A 10-min ensemble period was used in the observations. For the purposes of comparison, for each ADCP observation a mean was taken of all the model predictions that were closer in time to that observation than any other — in effect, a centred moving average.

A sensitivity analysis on the Delft3D model showed that the water levels in the inner domain were not significantly affected by the level of bed resistance in the outer domain. Bed resistance for the outer domain was therefore specified as a Chezy parameter of $65 m^{1/2}\ s^{-1}$, which is approximately equivalent to a "standard" classical quadratic drag coefficient of 0.0025 (Davies and Xing, 1995). Predicted water levels from the outer grid were compared with tidal gauge data from Wick, Kinlochbervie and three points from the International Hydrographic Organization (IHO) at the shelf edge, obtained using Delft Dashboard (van Koningsveld et al.,

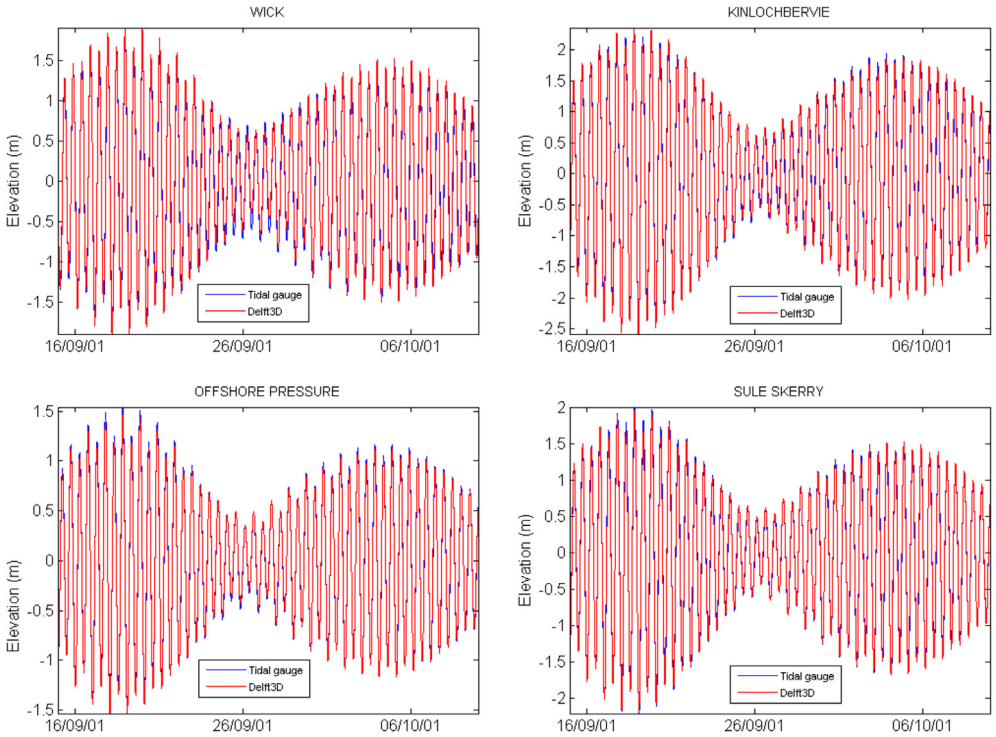

Fig. 4. Comparison of water level time series for four locations on the outer (shelf) grid in Delft3D.

Table 2
Validation statistics in time domain, comparing the MIKE 3 model to observations in the Pentland Firth over a two week period in 2001. Scatter Index (SI) is defined as the RMSE divided by the mean of the observed values.

		Site 1		Site 2		Site 3	
		u	v	u	v	u	v
RMSE (m/s)	Depth 1	0.650	0.379	0.400	0.267	0.254	0.196
	Depth 2	0.386	0.284	0.324	0.247	0.214	0.174
	Depth 3	0.339	0.402	0.258	0.339	0.199	0.321
SI (%)	Depth 1	55.4	142	33.0	113	27.6	90.4
	Depth 2	22.4	41.1	19.9	38.1	21.1	47.0
	Depth 3	31.9	36.1	26.2	33.1	26.9	43.6
R^2	Depth 1	0.917	0.082	0.948	0.367	0.939	0.475
	Depth 2	0.978	0.949	0.976	0.936	0.967	0.915
	Depth 3	0.946	0.949	0.956	0.951	0.946	0.892
Bias (m/s)	Depth 1	0.177	−0.183	0.050	−0.218	−0.012	−0.124
	Depth 2	0.107	−0.049	0.112	0.016	0.034	0.038
	Depth 3	0.008	0.567	0.018	0.448	−0.007	0.213

Table 3
Validation statistics in time domain, comparing the Delft3D model to observations in the Pentland Firth over a two week period in 2001. Scatter Index (SI) is defined as the RMSE divided by the mean of the observed values.

		Site 1		Site 2		Site 3	
		u	v	u	v	u	v
RMSE (m/s)	Depth 1	0.638	0.388	0.435	0.300	0.393	0.231
	Depth 2	0.422	0.306	0.360	0.255	0.226	0.155
	Depth 3	0.370	0.481	0.360	0.359	0.325	0.341
SI (%)	Depth 1	53.5	146	35.8	123	42.6	107
	Depth 2	24.5	44.2	22.2	39.3	22.3	41.6
	Depth 3	34.8	43.1	36.6	35.0	43.9	46.3
R^2	Depth 1	0.860	0.219	0.906	0.329	0.874	0.313
	Depth 2	0.973	0.935	0.973	0.923	0.969	0.926
	Depth 3	0.934	0.921	0.944	0.921	0.930	0.858
Bias (m/s)	Depth 1	−0.003	−0.181	−0.091	−0.242	−0.064	−0.164
	Depth 2	0.004	−0.027	0.037	0.069	−0.029	−0.001
	Depth 3	0.186	0.622	0.151	0.461	0.026	0.237

2013). Fig. 4 shows comparisons of the predictions of the outer model with the water level series at four measurement sites. A good match between model output and data was found.

Validation statistics from the time-domain comparison of current velocities in both models are shown in Tables 2 and 3. For reasons of space, only the magnitudes of current speeds have been illustrated in Figs. 5 and 6.

A number of observations may be made on these statistics:

- In general there is a good match between predictions and observations, especially at Sites 2 and 3. The match at Site 1 is poorer in both models, especially in the shallow layer. As the month of the ADCP survey included heavy weather,[3] this may relate to wind and wave effects near the surface.
- There is poor correlation between predictions and observations of *v*-velocities at all three sites with both models, in the shallow layer only. The depth-dependence of this discrepancy suggests that it may also relate to the effects of weather, although we are unable to verify this.
- Both models overpredict the highest current speeds, especially at Sites 1 & 3. This is especially evident at the shallow layer, and may relate to the to the jet that is formed downstream of the constriction between Stroma and Swona. Alternatively, the observational data may be at fault; as noted in Section 1.3, there is evidence that these ADCPs experienced "knockdown" at times of peak flow.

[3] according to ECMWF interim reanalysis data there were four periods during the survey in which wind speeds exceeded 14 m s^{-1} and significant wave heights exceeded 4 m.

2.3.2. Frequency domain

Time series of one month duration were extracted from the outputs of both models to show *u*- and *v*-velocities at the same location and similar depths to those reported by Gillibrand et al. (2016) for their Inner Sound ADCP. The t_tide package (Pawlowicz et al., 2002) was used to perform harmonic analysis, and the amplitudes and phases of the M2 and S2 constituents were compared to those of the observations. This comparison is shown in detail in Table 4 and illustrated in Fig. 7.

At the Inner Sound location, *u*-velocities are given the correct amplitude by Delft3D and are somewhat underpredicted by MIKE 3. Conversely, their phase in MIKE is close to the observations, while in Delft3D, M2 is 71° (or nearly 2.5 h) ahead. This is surprising because, while some phase difference in this direction is visible in the results for the main channel of the Pentland Firth (Fig. 5), it is not of this magnitude. The lower amplitudes predicted by MIKE here — especially in the deepest layer — are also interesting, since in Fig. 6 the opposite is seen.

Less importance was placed on the *v*-velocities because they are small in the Inner Sound. Both models underpredicted the amplitudes, while once again MIKE agreed well with observations as to the phases and Delft3D did not.

3. Method for calculating bed stress

As noted by Soulsby and Clarke (2005), there is little consensus on the best method for estimating bed shear stress (τ_b) from predictions of velocity. Wilcock (1996) identifies three approaches that are feasible, all of which make use of the Law Of the Wall:

$$\frac{u_z}{u_*} = \frac{1}{\kappa}\ln\left(\frac{z}{z_0}\right) \quad (1)$$

where u_z is the flow velocity at a distance z above the seabed, $u_* = \sqrt{\tau_b/\rho}$ where ρ is the density of seawater, κ is Von Karman's constant (equal to 0.4), and z_0 is the hydraulic roughness length of the seabed. This formulation makes the assumption that the vertical variation in velocity follows a logarithmic profile.

The three approaches mentioned by Wilcock are:

1. Use a single value of u at the deepest available vertical location to estimate τ_b. This has the advantage that it only assumes a logarithmic vertical profile for the part of the water column between this location and the seabed.
2. Use the depth-averaged velocity. This is the only method available for 2D models, but it requires the assumption of a logarithmic vertical profile for the entire water column.
3. The Law of the Wall can be rearranged into the form of an equation of a straight line. Consequently u_*, and hence τ_b, can be estimated by plotting $\ln(z)$ against u and finding the gradient of the line of best fit. This method assumes a logarithmic vertical profile, but also offers a means of assessing the validity of this assumption by looking at the quality of the fit. Unlike the other two methods, it does not require knowledge of z_0 (which is related to the intercept of the line of best fit).

A test of all three methods was performed using a short set of MIKE 3 output data in three different locations. It was found that method 1 consistently gave the lowest values of bed stress, followed by method 2 and finally method 3. The difference in absolute

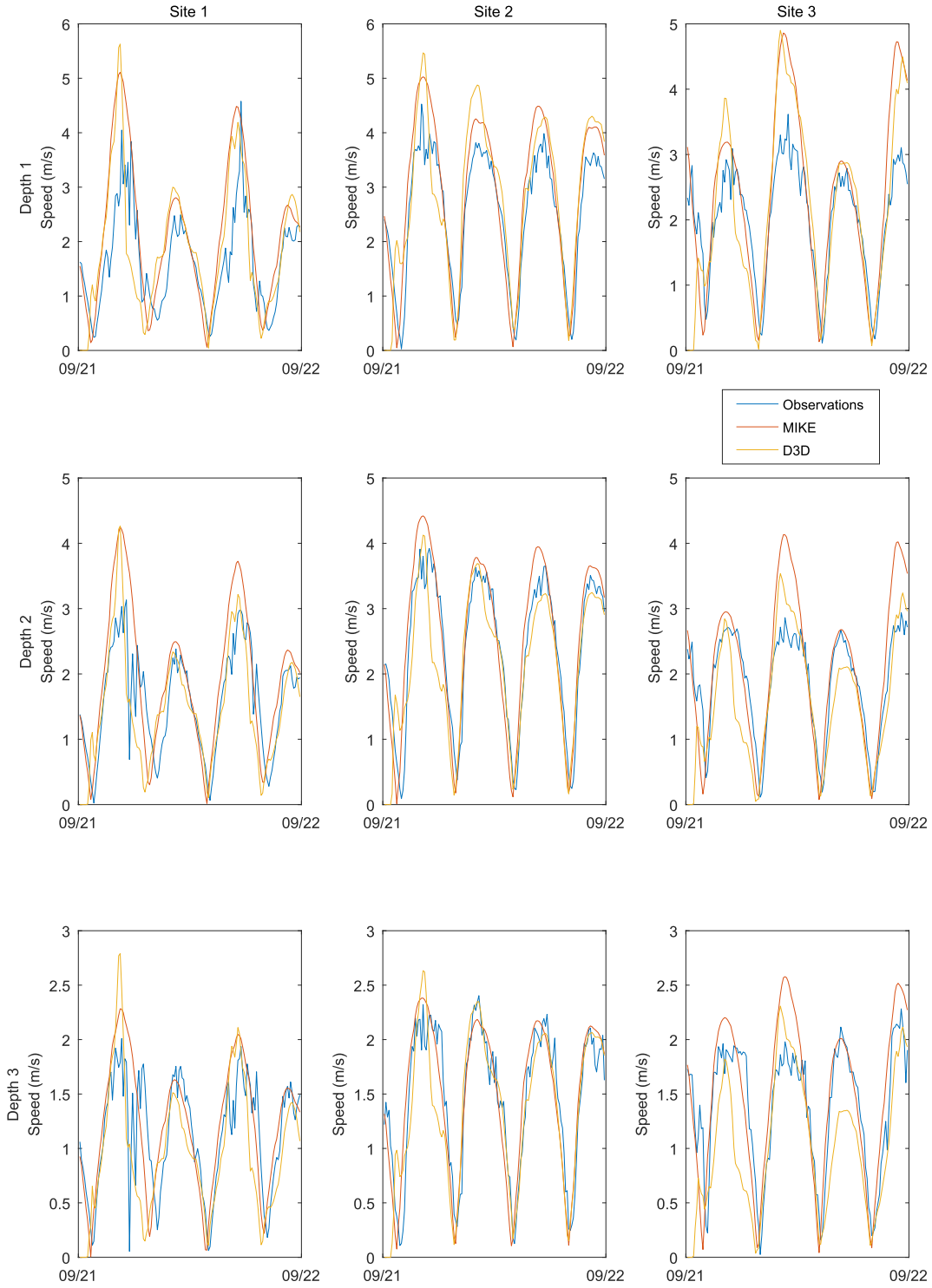

Fig. 5. Time series plots of current speed, showing 24 h at spring tides at three Pentland Firth ADCP locations at three depths. Depth 1 (top) is the shallowest and Depth 3 (bottom) the deepest.

values was up to a factor of three, but the proportional variation across the spatial domain was approximately constant regardless of the method used. Without any known values to compare against, we cannot judge which method produces more accurate results for bed stress; however, all appear to be similarly good for understanding its variation.

The R^2-value for the line of best fit in method 3 was usually above 0.98 (except for short periods around slack water), which suggests that the assumption of a logarithmic vertical profile in the model outputs is a good one. However, method 3 proved to be impractical for use beyond this short test, due to the computational effort required to perform a least-squares fit for every cell at every

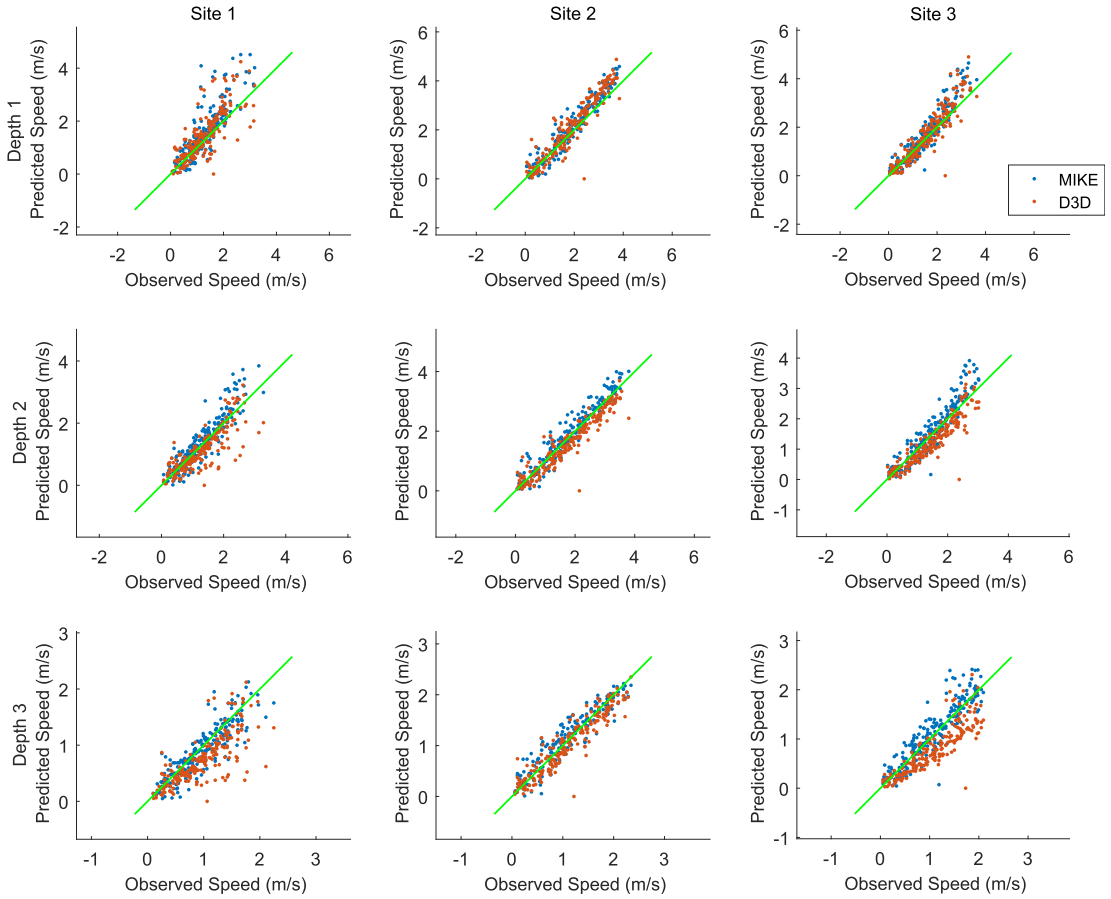

Fig. 6. Scatter plots showing comparisons of both models' predictions of current speed against observations at three Pentland Firth ADCP locations, at three depths, over a two week period in 2001. To improve legibility every tenth data point is plotted. Depth 1 (top) is the shallowest and Depth 3 (bottom) the deepest. Green lines show a 1:1 relationship. (For interpretation of the references to colour in this figure legend, the reader is referred to the web version of this article.)

timestep. Method 1, while appealing in that it fully uses the three-dimensional capabilities of the models, has the disadvantage that the distance from the seabed at which the velocity is read varies spatially and temporally, as the vertical position of the centre of the bottom layer changes. Consequently, method 2 was adopted for the remainder of this work.

Bed stress $\overrightarrow{\tau_b}$ can be calculated by (from Soulsby (1997)),

$$\overrightarrow{\tau_b} = \rho \overrightarrow{U} \left| \overrightarrow{U} \right| \left(\frac{0.4}{1 + \ln(z_0/h)} \right)^2 \tag{2}$$

where $\overrightarrow{U}$ is the depth-averaged velocity and h is the water depth. This formulation can be applied to the output from both models once z_0 is known, but the method of finding z_0 is different for each model due to the different ways in which they define bed resistance.

In the MIKE 3 model, bed resistance is specified as a constant quadratic drag coefficient c_f that is applied to the bottom layer. z_0 can be derived as follows:

$$z_0 = \frac{z_b}{\exp\left(\frac{\kappa}{\sqrt{c_f}}\right)} \tag{3}$$

where z_b is the distance from the seabed to the centre of the bottom layer.

In the Delft3D model, bed resistance is specified as a constant Chezy value C_{3D}, defined as:

$$C_{3D} = \frac{\sqrt{g}}{\kappa} \ln\left(1 + \frac{z_b}{z_0}\right) \tag{4}$$

z_0 can therefore be found by,

Table 4
Comparison of measurements and observations in frequency domain, comparing both models to observations in the Inner Sound. Observations are from Gillibrand et al. (2016). Phases are relative to UTC. Depth 1 is the shallowest and Depth 3 the deepest.

		Amplitude (m)			Phase (°)		
		MIKE 3	Delft3D	Obs	MIKE 3	Delft3D	Obs
M2 *u*	Depth 1	2.75	3.09	3.16	229	307	236
	Depth 2	2.33	2.96	2.97	229	307	236
	Depth 3	1.65	2.56	2.47	230	307	236
S2 *u*	Depth 1	1.10	1.18	1.28	268	272	271
	Depth 2	0.93	1.14	1.18	268	272	272
	Depth 3	0.66	0.98	0.97	269	272	271
M2 *v*	Depth 1	0.17	0.09	0.27	212	160	222
	Depth 2	0.27	0.05	0.42	220	223	225
	Depth 3	0.25	0.12	0.58	222	284	226
S2 *v*	Depth 1	0.07	0.02	0.15	256	135	255
	Depth 2	0.12	0.02	0.20	262	226	259
	Depth 3	0.10	0.05	0.25	262	260	261

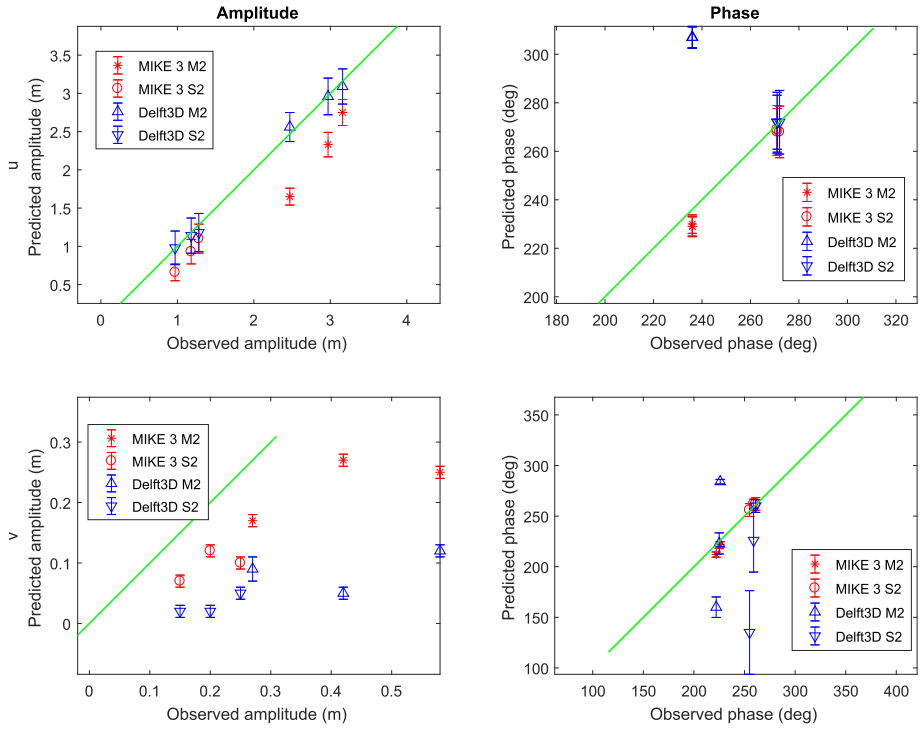

Fig. 7. Plots comparing amplitude and phase of M2 and S2 constituents of *u* (top) and *v* (bottom) velocities between observations and predictions. Error bars show 95% confidence intervals on the harmonic analyses of the predictions; error information is not available for observations. Green lines show 1:1 relationship. (For interpretation of the references to colour in this figure legend, the reader is referred to the web version of this article.)

$$z_0 = \frac{z_b}{\exp\left(\frac{\kappa C_{3D}}{\sqrt{g}}\right) - 1} \tag{5}$$

3.1. Difference in bed resistance

Using Equations (3) and (5) we can compare the values of bed resistance in the two models. c_f is set to 0.01 in MIKE. In the range of values used here, $c_f \simeq g/C_{3D}^2$ (an approximation also provided by Soulsby (1997)). Using the value of $C_{3D} = 50\ \mathrm{m}^{1/2}\ \mathrm{s}^{-1}$ set in Delft3D, this evaluates to $c_f = 0.004$, showing that the Delft3D model uses just under half the quadratic bed resistance of the MIKE one.

4. Predictions without turbines

Each model was run for a period of 32 days starting from 01/02/2012. Output from the first four days was discarded to allow for model spinup, leaving 28 days of predictions for use.

For each parameter of interest, mean predictions over this period were plotted to provide a qualitative visual comparison. These mean predictions from both models were then interpolated onto a common 100 m square grid covering the area of the inner Delft3D domain (see Fig. 3), and the comparison between models for each parameter shown as a scatter plot. These plots are shown in in Figs. 8 and 9.

It is evident that there is an excellent match between the two models on the spatial variation of each parameter across the domain, even in areas that were not used for calibration. The magnitudes of the predictions are well-matched for depth-averaged current speed. Delft3D predicts slightly faster current speeds in the bottom layer, and dramatically lower bed stress (approximately half), than MIKE.

4.1. Discussion

The two models, developed independently by different teams, using different software and different sources for open boundary conditions, predicted very similar relative change in values across the spatial domain in all of the parameters of interest.

Similar absolute magnitudes were predicted for depth-averaged current speed. This is as expected, because the models were calibrated using this measurement. This agreement was achieved by the use of dissimilar levels of bed resistance. Other researchers doing comparisons between models have also found it necessary to use different values for bed resistance with different software (Rahman and Venugopal, 2015).

The use of bed resistance as a tuning parameter in calibration means that its value embodies not only the actual seabed resistance, but also a correction representing all physical processes that are not explicitly modelled, as well as any inaccuracies introduced by the numerical methods used (Green and McCave, 1995). As such, it is difficult to ascribe the difference in calibrated bed resistance values to a specific cause.

The difference in bed resistance affects the vertical velocity profiles predicted by the models, hence the bottom layer speeds, and also the bed stresses. The magnitudes of these parameters differ between the models in ways that are consistent with the difference in bed resistance.

Due to the limited availability of velocity data close to the seabed, we cannot determine whether either model's predictions of these parameters is accurate. However, for the purposes of the environmental modelling in the TeraWatt project, it is spatial variation rather than absolute magnitudes that is important. On this matter the close match between MIKE 3 and Delft3D offers some confidence.

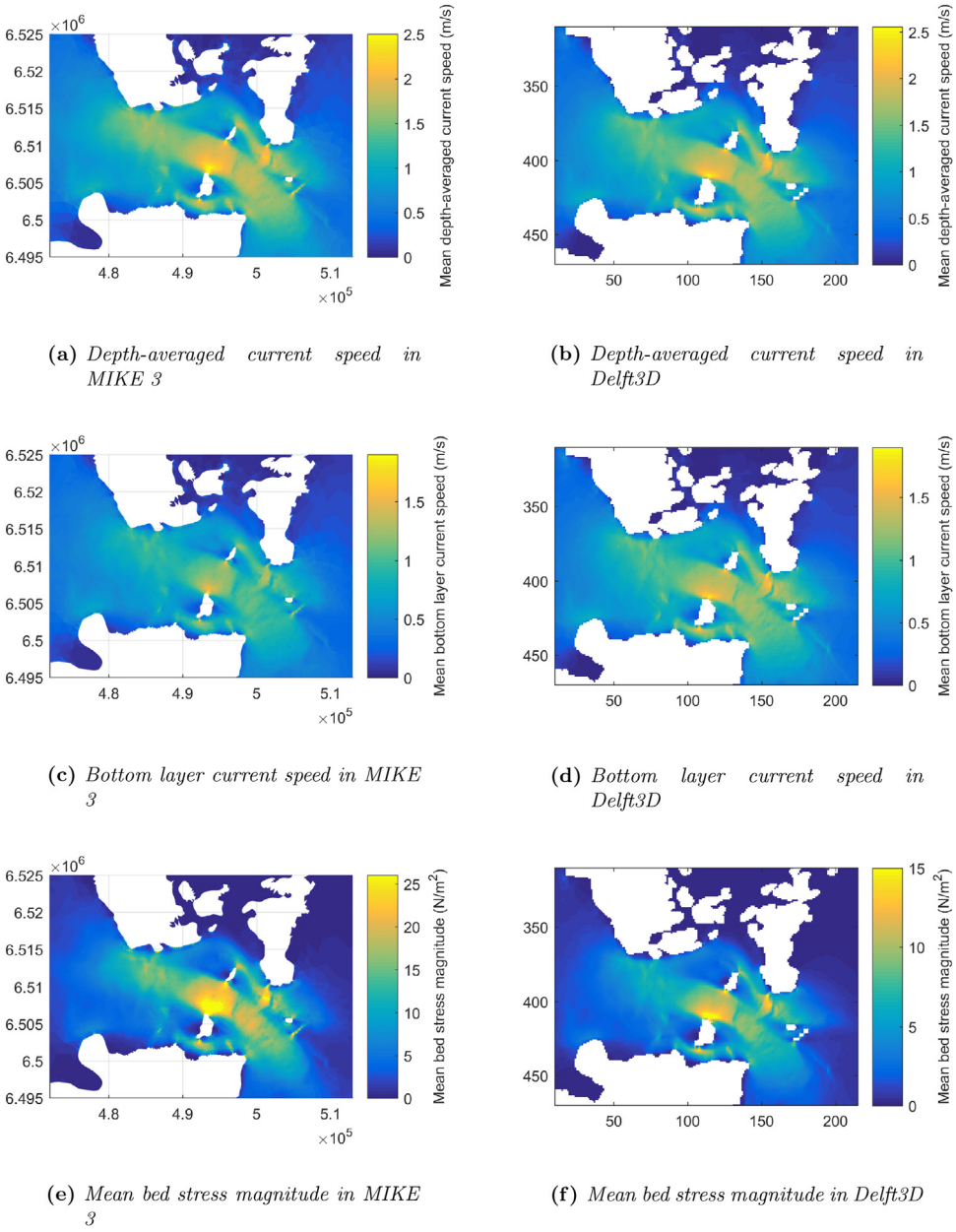

(a) *Depth-averaged current speed in MIKE 3*

(b) *Depth-averaged current speed in Delft3D*

(c) *Bottom layer current speed in MIKE 3*

(d) *Bottom layer current speed in Delft3D*

(e) *Mean bed stress magnitude in MIKE 3*

(f) *Mean bed stress magnitude in Delft3D*

Fig. 8. Comparison of mean depth-averaged current speed, bottom layer current speed, and bed stress magnitude, over 28 days, predicted by the MIKE 3 and Delft3D models without turbines. Note the different colour scales between subfigures (e) & (f). Different scales are used to show the similarity in relative spatial variation. (For interpretation of the references to colour in this figure legend, the reader is referred to the web version of this article.)

5. Implementation of energy extraction

5.1. Turbine parameters & array layouts

At a workshop for wave and tidal energy developers, hosted by Marine Scotland Science, parameters were agreed for a generic tidal turbine that is plausible for use in the Pentland Firth. The agreed device has a 20 m diameter rotor, a cut-in speed of 1 m s^{-1}, a rated speed of 2.5 m s^{-1}, and a cut-out speed of 4 m s^{-1}. Its thrust coefficient curve[4] is as shown in Fig. 10, and the turbine would be rated at approximately 1 MW.

Realistic array layouts were developed by Marine Scotland Science from Environmental Statements submitted by developers. Five tidal array areas were identified from The Crown Estate round 1 lease zones (see Fig. 1). Within these zones, turbines were arranged in rows aligned normal to the prevailing directions of flow, in positions with sufficient depth and with the highest undisturbed velocities (based on the MIKE 3 model without turbines). At the Brough Ness site, twin-rotor devices of 1 MW per rotor are planned, so each rotor was treated as one generic device. For the detailed methodology used for the array layouts see O'Hara Murray (2015b).

A brief investigation was made into the frequency distribution of tidal speeds and directions in each of the array areas, based on the depth-averaged predictions of the MIKE 3 model. Tidal roses showing the outcome of this work are shown in Fig. 11. Note that

[4] The thrust coefficient C_T determines the relationship between the axial flow speed and the thrust of the turbine (the retarding force that it exerts on the water), so that $F \propto C_T u^2$.

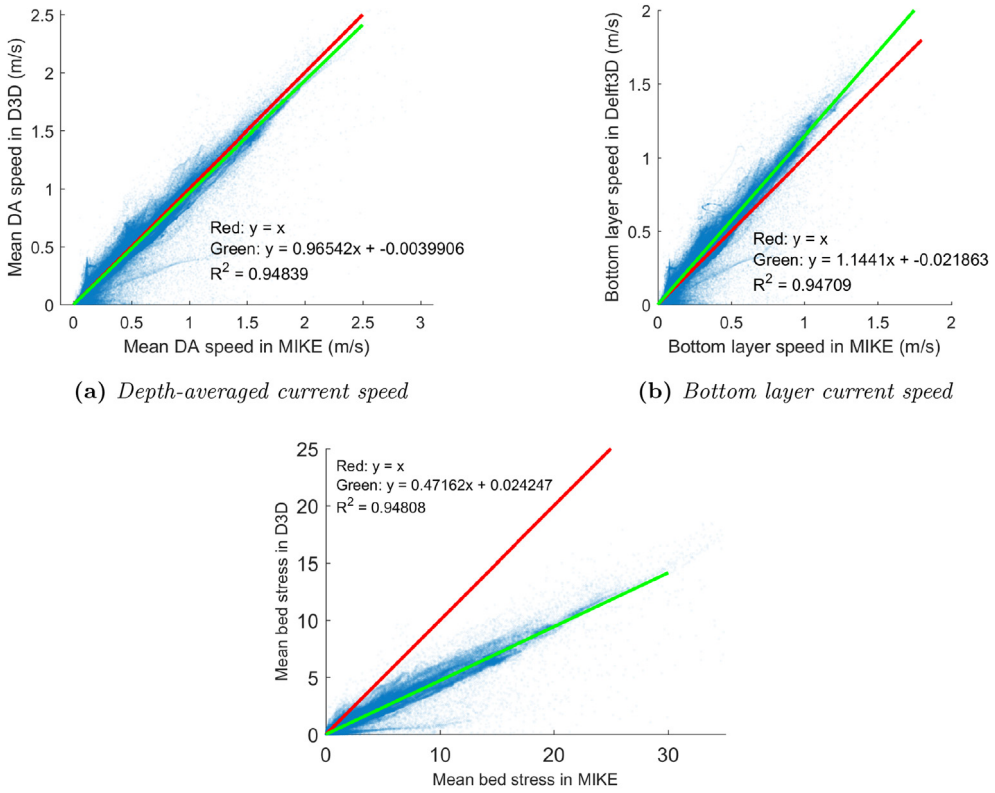

(a) *Depth-averaged current speed*

(b) *Bottom layer current speed*

(c) *Bed stress magnitude*

Fig. 9. Scatter plots comparing mean predictions of three parameters, over 28 days, by the two models without turbines. Plots include points from the area covered by the inner domain of the Delft3D model. Points are partially transparent to emphasise regions of high point density. Red lines indicate 1:1 relationships, while green lines show lines of best fit. (For interpretation of the references to colour in this figure legend, the reader is referred to the web version of this article.)

while Westray South and Cantick Head have flows which reverse direction by 180°, the other sites have more complex cycles where the ebb does not exactly reciprocate the flood. Parts of the Brough Ness site, including the point from which the rose was generated, are affected by an eddy that causes them to experience strong tidal flow in only one direction.

5.2. Implementation in MIKE 3

MIKE 3 provides a built-in structure type called “Turbine”. This represents a horizontal axis tidal turbine as a sub-grid object via a simple actuator disc model (DHI, 2012). The thrust coefficient C_T is expressed as a function of current speed using a user-defined look-up table. The software allows the thrust coefficient and the resulting force to be split into components parallel and orthogonal to the turbine's axis (described by DHI as drag and lift coefficients). This facility was not used for this work; except where stated otherwise it was assumed that the turbines in MIKE yaw to face the flow at all times, and thus $C_{\text{drag}} = C_T$ and $C_{\text{lift}} = 0$.

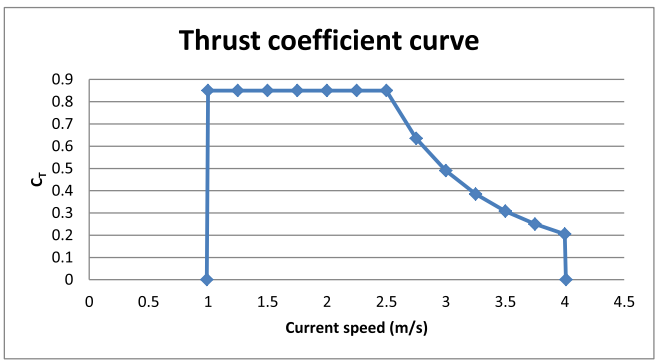

Fig. 10. Generic tidal turbine thrust curve agreed with developers.

Inserting tidal turbines into MIKE is simply a matter of inputting the parameters of the turbines, together with their locations, in the GUI. This process is very slow for a large number of turbines, so the task was automated using a MATLAB script (available in the TeraWatt/EcoWatt2050 code repository; see Section 8).

Supporting structures were represented as circular monopiles of 2.5 m diameter, extending from the seabed to the hub height. These were implemented using MIKE's built-in “Pier” structure, which is designed for bridge supports but does not require the pier to occupy the entire water column.

Strictly speaking, the value for flow velocity that MIKE uses to calculate thrust should be the “free-stream velocity”, which is the velocity that the water has upstream, before it begins to feel the effects of the turbine. This value is not known to MIKE, and so instead the modelled velocity for that cell is used. The cell velocity will be lower than the free-stream velocity because of the retarding effect of the turbine, so the predicted effects of the turbine will be underestimated. This effect is negligible with large cell sizes, but becomes significant when the length of a triangle face in the mesh is below approx. 150–200 m. Further detail on this effect is given by Kramer and Piggott (2016), and a correction that applies to simple idealised scenarios is available in Waldman et al. (2015).

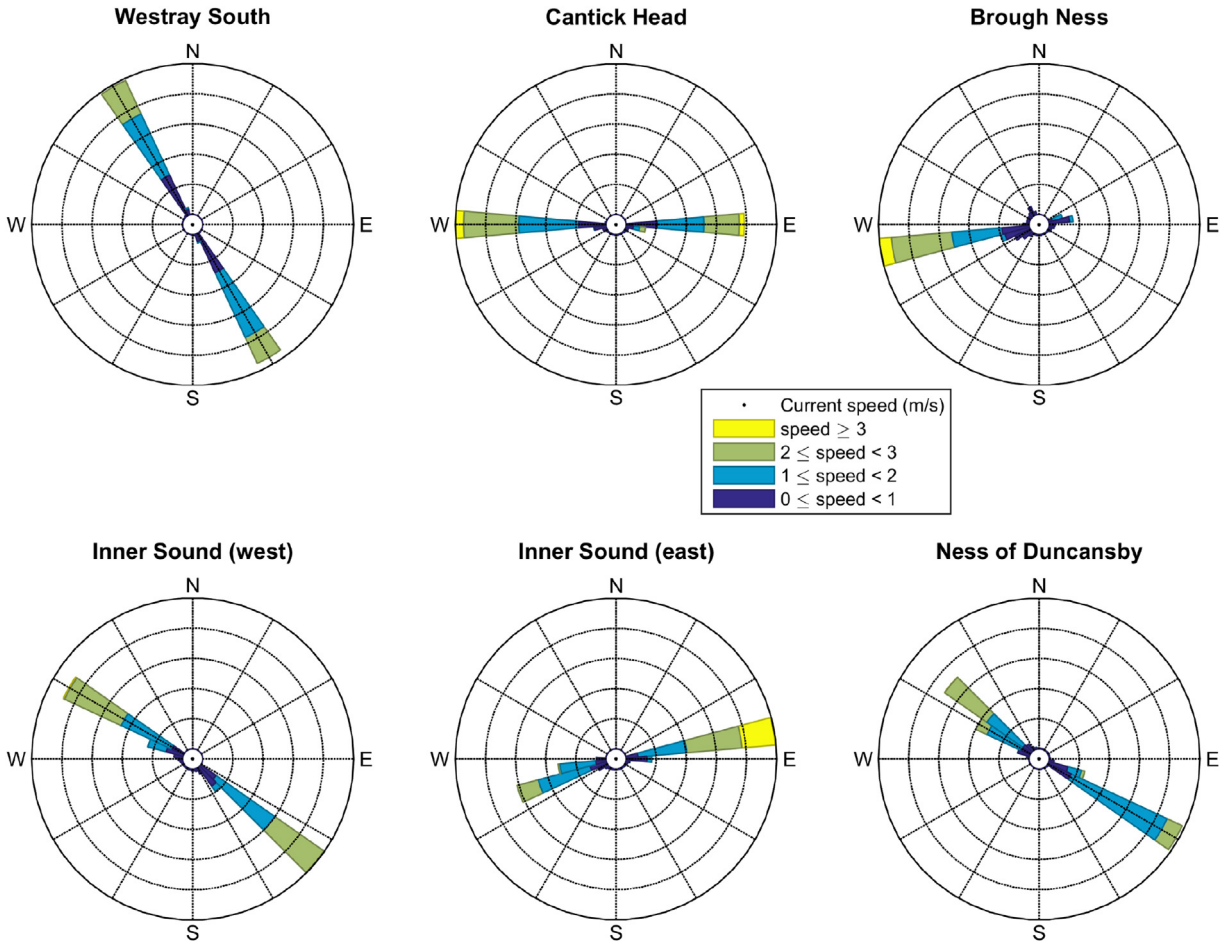

Fig. 11. Tidal roses as predicted by the MIKE model from the central areas of the arrays, using depth-averaged velocities over 28 days. The distance that sectors extend from the centre of each circle indicates the frequency of flow in that direction, while colours indicate the distribution of current speed in that direction. Two roses are shown for the Inner Sound array as there is a significant change in the flow direction within the exploited area. (For interpretation of the references to colour in this figure legend, the reader is referred to the web version of this article.)

5.3. Implementation in Delft3D

The current version of Delft3D does not include any dedicated provision for tidal turbines. Other studies have modified the code of Delft3D to incorporate TECs as momentum sinks (*e.g.* Ramos et al., 2013, 2014; Sánchez et al., 2014). We were advised by commercial stakeholders that investors and regulators typically require the use of well-known software as released by its vendors, without modifications or improvements. For this work, therefore, turbines were modelled by introducing a series of porous plates into the model using the unmodified code (Fig. 12b). The porous plates apply a retarding force on the flow based on a parameter c_{loss}, which is a quadratic drag coefficient applied to the layers that the porous plate occupies.

Porous plates in Delft3D may only lie along the grid axes or at 45° to them. In order to simulate turbines at arbitrary angles we created two porous plates, at right angles to each other, for each cell containing turbines, and decomposed the required force into components in the u and v directions before calculating the necessary porosities. The drag of each plate was determined by (taking as an example the one parallel to the v axis),

$$c_{loss-u} = \frac{C_T A_u}{2\Delta y \Delta z n} \tag{6}$$

$$A_u = \sum A_t |\sin\theta| \tag{7}$$

where C_T is the thrust coefficient for the turbine(s), Δy is the distance between grid points along the v axis, Δz is the height of a vertical layer, and n is the number of layers that the porous plate covers. A_u represents the total area of rotor in that cell that would be visible to an observer looking along the u direction; hence A_t is the area of a turbine rotor, the sum is over all turbines in the cell, and θ is the angle between the u direction and the turbine's axis.

A MATLAB script was developed to calculate the appropriate porous plate positions and porosities, and this is available in the project code repository (see Section 8). Full details, including derivation of the formula for c_{loss} with and without a correction for free-stream velocity, may be found in Baston et al. (2015).

The porous plate approach in Delft3D introduces a number of limitations:

- The vertical positions of porous plates are specified in terms of the model layers that they occupy. Because the model uses 'sigma' layers, the layers intersected by a turbine rotor will change between timesteps. Delft3D does not allow porous plates to move during a simulation, so it was necessary to fix the plate as occupying the layers that are intersected by the turbine at mean sea level.

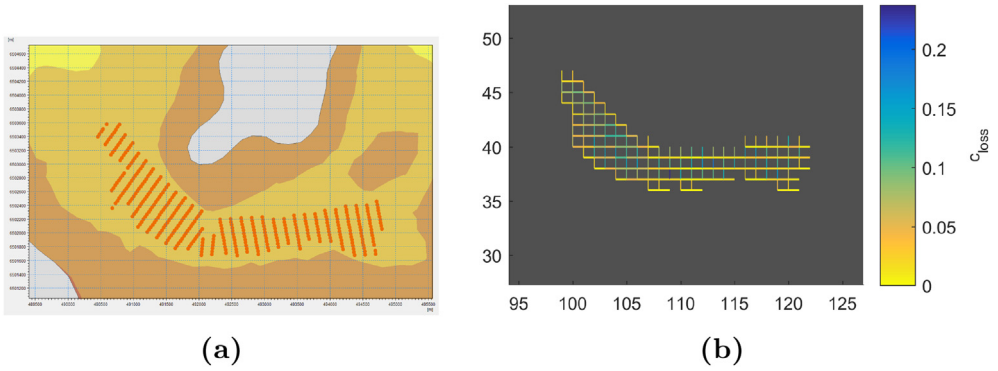

Fig. 12. (a) 400 turbines in the Inner Sound, viewed through the MIKE Zero GUI; (b) The same 400 turbines represented as porous plates for Delft3D. Higher values of the c_{loss} parameter, shown by bluer colours, indicate plates with higher drag. (For interpretation of the references to colour in this figure legend, the reader is referred to the web version of this article.)

- The porosity of a porous plate cannot change over time. It is therefore not possible to realistically model turbines with variable thrust coefficients. Instead, the thrust coefficient at the rated current speed ($C_T = 0.85$) was fixed as a constant.
- Our method of representing arbitrary turbine orientations, together with the point above, means that turbines in Delft3D cannot yaw to follow the flow; they must instead be fixed at a single orientation. In commercial practice, a site developer would supply their modeller with orientation as well as position information. For the purposes of this work, the orientation of each turbine was fixed at the direction of the fastest undisturbed flow during a tidal cycle.

Supporting structures are not currently represented in the Delft3D model.

6. Predictions with turbines

Each model was run with and without turbines. The predictions with turbines were subtracted from those without on a per-element, per-timestep basis, to produce maps of the change that results from energy extraction.

The models show similar general features in the effect of turbines in depth-averaged current speed (Fig. 13a and b). There is a decrease in speed in line with TEC arrays, and an increase in speed to either side as flow diverts around the impedance of the turbines. These effects are particularly strong in the Inner Sound, where the largest array is positioned and where the flow is constrained by land boundaries on both sides. Current speeds in regions of the Pentland Firth without energy extraction are affected slightly (< 0.1 m s^{-1}), but in some areas the models disagree on whether this is a slight increase or a slight decrease.

At the Cantick Head and Westray South sites,[5] the magnitude of the effect of energy extraction is greater in Delft3D than MIKE. In regions distant from energy extraction, the more general effects on the flow are also greater in Delft3D. The opposite is true for the Inner Sound, Ness of Duncansby and Brough Ness sites, with a greater mean change in current speed in MIKE than in Delft3D. Additionally, at these sites there is a clear difference between the models in the spatial areas affected.

The predicted effects of energy extraction on bottom layer current speed (Fig. 13c and d) are similar to those on depth averaged speed, although slightly smaller in magnitude.

[5] See Fig. 1 for site names; Westray South not shown in Figs. 13–15.

Because of the difference between the models in the absolute predicted values of bed stress without turbines, there is little benefit in plotting the absolute changes resulting from energy extraction. Instead, Fig. 14 shows the effect of adding turbines on bed stress as a proportion of the bed stress without turbines. Viewed in this way, the effects are similar to those for depth-averaged speed. Increases in speed cause more of a difference in bed stress than decreases in speed, because of the square relationship between current speed and bed stress. The changes to bed stress are substantial; decreases of 45% and increases of up to 100% are predicted in some areas.

6.1. Discussion

The greater effect of turbines in Delft3D over most of the domain is consistent with the lower bed resistance used in the Delft3D model: since the natural resistance of the channel is lower, the additional resistance of the turbines is a greater proportionate change in the overall impedance in that area.

Of greater interest are the three sites (Inner Sound, Brough Ness and Ness of Duncansby) where not only lesser, but spatially distinct, effects are observed in Delft3D. It was initially thought that this could be related to the inclusion of supporting structures in MIKE but not in Delft3D. However, removing the supports from the MIKE model in a test made little difference to the effects of the turbines.

The difference may, instead, be related to differences in the treatment of turbine yaw. As noted in Sections 2.1 & 2.2, the MIKE 3 model assumes that turbines yaw to face into the flow at all times, while the Delft3D model requires that turbines have a fixed orientation. As noted in Section 5.1, the direction of the ebb at these sites is not the reciprocal of the flood, although the differences are small. Thus, in the Delft3D model, if the turbine is oriented correctly for the flood then the ebb must reach it slightly off-axis, and hence experience a lesser force from it.

To test this hypothesis, directional turbines similar to those in Delft3D were implemented in MIKE 3 and tested in a short 24 h simulation. The resulting predictions (Fig. 15a) show a similar magnitude of velocity deficit in line with the turbines in the Inner Sound, but still do not exhibit the same spatial variation as those of a similar 24 h Delft3D run (Fig. 15b). In the areas of these remaining differences, both models predict eddies at a scale which can only just be resolved by the meshes used. It is possible, therefore, that the different computational meshes in the two models are simulating these eddies in slightly different locations, such that they affect the turbines differently in the two models.

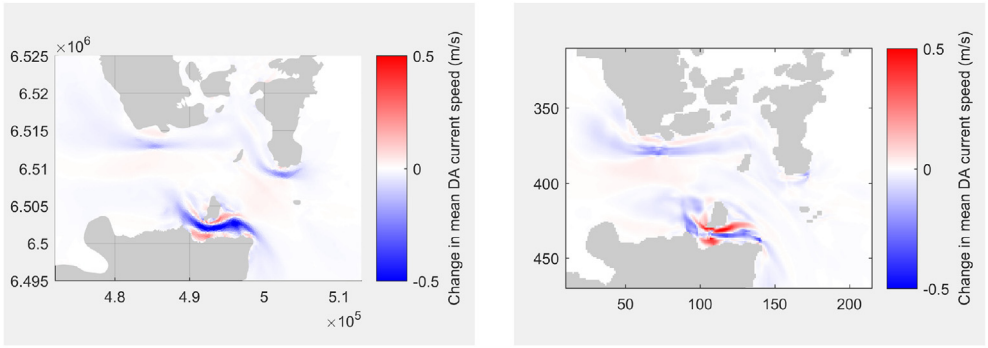

(a) *Depth-averaged current speed in MIKE*

(b) *Depth-averaged current speed in Delft3D*

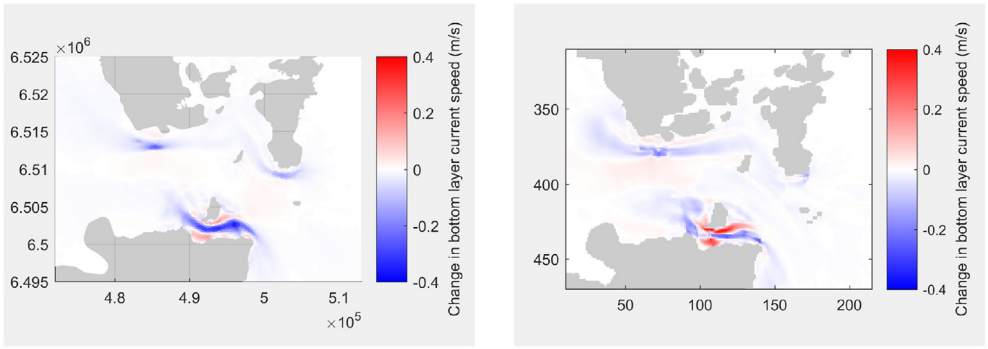

(c) *Bottom layer current speed in MIKE*

(d) *Bottom layer current speed in Delft3D*

Fig. 13. Changes in mean current speeds over 28 days as a result of adding turbines.

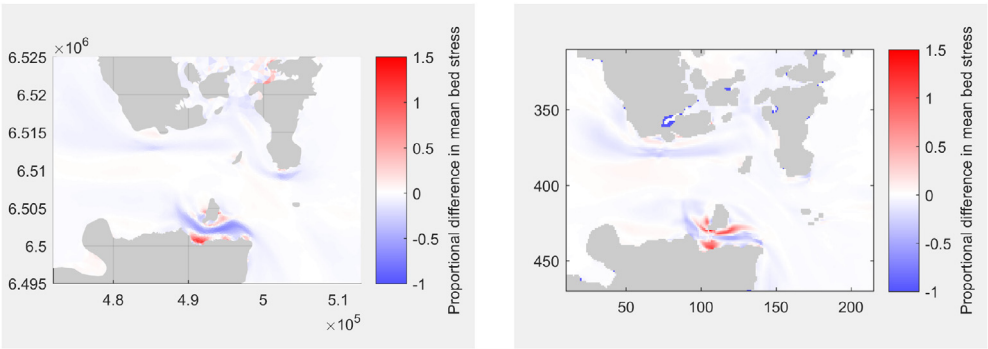

(a) *MIKE*

(b) *Delft3D*

Fig. 14. Change in mean bed stress magnitude over 28 days as a result of adding turbines, expressed as a proportion of the value without turbines.

Without velocity data in these areas, it is not possible to know which model is more accurate.

7. Further discussion & conclusions

For discussion of the results of these specific models without and with turbines, see Sections 4.1 and 6.1 respectively. The aim of this work was not to develop the best possible tidal energy extraction models of the region of interest, but to determine how to best use existing industry-standard tools for this purpose, given their capabilities and limitations. Therefore, the emphasis of this final section is not on the specific models that were developed, but on observations of a broader scope.

7.1. Observations on model capabilities

MIKE 3's unstructured mesh offers greater flexibility than Delft3D's structured grid in varying the mesh density for areas of complex flow. However, this comes at a cost in computation time, for while the mesh can be sparse in outer areas, the maximum time step will tend to be set by the smallest cells. In Delft3D, higher performance has been achieved by running the outer model in two dimensions. Within the high-resolution three-dimensional area, Delft3D also runs faster.

At the time of writing, it is clear that MIKE 3 offers superior facilities for representing horizontal-axis tidal turbines. The porous plate approach used in Delft3D has been shown to be a good

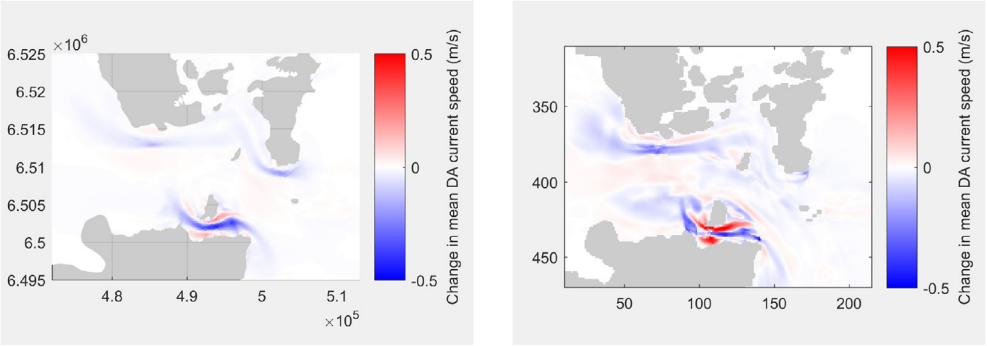

(a) *MIKE with directional turbines* (b) *Delft3D*

Fig. 15. Change in mean depth averaged current speed over 24 h as a result of adding turbines. The turbines in MIKE have been specified to have a fixed orientation, resembling as closely as possible the ones in Delft3D.

approximation, but requires that turbines are represented with a constant thrust coefficient and a constant orientation, and causes their vertical position to vary over time in an unrealistic way.

Since this work was conducted both DHI and Deltares have released new versions of their respective software suites. Delft3D now offers an unstructured mesh, and it is believed that a dedicated tidal turbine module is planned soon.

For some users it will be notable that MIKE is a commercial software package that must be licensed at considerable cost, while Delft3D is open source and available without payment. However, given the perception of open source software mentioned in Section 1, if a user is aiming to satisfy an investor that the model code is trustworthy it is probable that they will use the commercial version of Delft3D, which attracts a license fee. This version uses the same underlying model code as the open source one, but benefits from the full support of Deltares.

Both models, operating as they do at a regional scale where the turbine is unresolved, can only deal in terms of the power removed from the flow by TECs. This will be greater than the power available for conversion to electricity, due to energy that is lost in mixing turbulence between the turbine wakes and the surrounding flow (Vennell, 2010). The power removed from the flow is the correct quantity to study when interested in environmental impacts, but it is interesting to note this discrepancy between the quantity being studied and the quantity that is controlled by the consenting process.

7.2. Observations on model predictions

Models were developed independently in MIKE 3 and Delft3D, using the facilities available in each. Following calibration the two made similar predictions of depth-averaged current speed across all areas of the model (including those not used for calibration), with an R^2 value of 0.95 when comparing the two models' predictions at each point of a common interpolated grid, and a ratio of Delft3D predictions to MIKE 3 predictions of 0.97 (see Fig. 9). Achieving this calibration required the seabed resistance, which was used as a tuning parameter, to be set to markedly different values in the two models, resulting in the prediction of different absolute values for bed stress between the two models; the mean bed stress predicted by Delft3D was 47% of that predicted by MIKE 3. The spatial distribution of bed stress is highly correlated between the models.

The models predict broadly similar effects from energy extraction, and it is reasonable to conclude that their results may be used to inform policy as to regional-scale effects. There is some small disagreement on the magnitude of the effects on velocities, which is likely to be largely due to the difference in bed resistance mentioned above. There are significant differences in the models' predictions at a finer scale, which indicate that a model of this type should not be used for studying the effects of turbines within an array or at specific fine-scale locations elsewhere. For applications where such predictions are important, validation data should be collected at the points of interest. In some cases the use of a finer-scale model, backed up by this data, may be warranted. In the case of changes in bed stress, where different absolute magnitudes are predicted, the spatial variation — which is a measure of interest for the prediction of environmental impact within the TeraWatt project — was similar between the models.

The differences between our models, and the differences in model performance in different locations evident in Section 2.3, underline the importance of developing methods of setting model bed resistance from theory or measurement, rather than using it as an empirical tuning parameter, and this should be a focus for future work. It may be of benefit to vary the bed resistance spatially, if that variation is based on physics or measurement. However, the use of spatial variation without such justification must be treated with caution. By fitting to data with sufficient local freedom, nearly any model could be made to match nearly any measurements without retaining predictive power for locations or time periods other than those measured — a situation that has been described as "over-calibration" (Gerritsen et al., 1995).

Given the sensitivity of model predictions to calibration parameters, and given that errors in parameters of interest will often have square or cubic relationships to errors in current speeds (Neill et al., 2014; Filipot et al., 2014), there is a need for careful and rigorous standards for validation. This requires velocity data for the area(s) of interest which, while it may have been collected by developers, is often not publicly available.

One result of this square relationship between velocity and bed stress — which means that increases in velocity have a stronger effect on bed stress than decreases do — is that the greatest changes in bed stress may be found not from the slowed flow through the turbines, but in areas of increased current speed to either side, especially where the channel is tightly constrained. This finding may be of relevance to environmental impact assessments.

8. Code availability

The MATLAB scripts mentioned in this paper are available for inspection and use at https://github.com/TeraWatt-EcoWatt2050. These automate the insertion of tidal turbines into MIKE 3 models, automate the calculation of equivalent porous plates for turbines in Delft3D models, and provide an experimental correction for the

error noted in Section 5.2. We hope that they are helpful to other users of MIKE and Delft3D.

Acknowledgements

This work was funded by EPSRC grant EP/J010170/1. We thank the other members of the TeraWatt consortium for advice and feedback, and The Crown Estate and the UK Hydrographic Office for the provision of data for the project. The advice of industry representatives, in workshops and on the Steering Group, is gratefully acknowledged, as is the assistance of the Marine Alliance for Science & Technology for Scotland (supported by Scottish Funding Council grant ref. HR09011) and Marine Scotland Science for coordinating these events. We thank David Woolf for his comments on a draft.

References

UK Maritime and Coastguard Agency, 2001. Gardline Surveys, 'Pentland Firth - Tidal Stream Observations'. Technical Report Contract NBSA5B/2959.

ABPmer, 2012. Pentland Firth and Orkney Waters Strategic Area : Preparation of Bathymetry to Support Modelling Studies. Technical Report R. 1963.

Adcock, T.A.A., Borthwick, A.G.L., Houlsby, G.T., 2011. The open boundary problem in tidal basin modelling with energy extraction. In: Proceedings of the 9th European Wave and Tidal Energy Conference. Southampton, UK. URL. http://www.see.ed.ac.uk/~shs/EWTEC%202011%20full/papers/315.pdf.

Baston, S., Harris, R.E., 2010. Modelling the hydrodynamic characteristics of tidal flow in the Pentland Firth. In: 9th European Wave & Tidal Enegy Conference.

Baston, S., Harris, R., Woolf, D.K., Hiley, R.A., Side, J., 2013. Sensitivity analysis of the turbulence closure models in the assessment of tidal energy resource in Orkney. In: Proceedings of the 10th Wave & Tidal Energy Conference, Aalborg.

Baston, S., Waldman, S., Side, J., 2015. Modelling energy extraction in tidal flows, rev 3.1. In: TeraWatt Position Papers. MASTS, pp. 75–107. URL: http://www.masts.ac.uk/media/166596/position_papers_terawatt_e-book.pdf.

Cheng, Y., Andersen, O.B., 2010. Improvement of global ocean tide models in shallow water regions. In: Altimetry for Oceans & Hydrology OST-ST Meeting. URL, Lisbon. http://www.space.dtu.dk/english/~/media/Institutter/Space/English/scientific_data_and_models/global_ocean_tide_model/yongcuncheng_no_sv_1_68_45.ashx.

Davies, A.M., Xing, J., 1995. An intercomparison and validation of a range of turbulence closure schemes used in three dimensional tidal models. In: Lynch, D.R., Davies, A.M. (Eds.), Quantitative Skill Assessment for Coastal Ocean Models. American Geophysical Union, Washington DC, pp. 71–95 volume 47 of Coastal and Estuarine studies.

Deltares, 2014. Delft3D-FLOW User Manual, Hydro-morphodynamics, Version 3.15.34158. Technical Report. URL: http://content.oss.deltares.nl/delft3d/manuals/Delft3D-FLOW_User_Manual.pdf.

DHI, 2012. MIKE 3 Flow Model FM Hydrodynamic Module User Guide.

Draper, S., Adcock, T.A., Borthwick, A.G., Houlsby, G.T., 2013. Estimate of the tidal stream power resource of the Pentland Firth. Renew. Energy 63, 650–657. http://dx.doi.org/10.1016/j.renene.2013.10.015.

Easton, M.C., Woolf, D.K., Bowyer, P.A., 2012. The dynamics of an energetic tidal channel, the Pentland Firth, Scotland. Cont. Shelf Res. 48, 50–60. http://dx.doi.org/10.1016/j.csr.2012.08.009.

Egbert, G.D., Erofeeva, S.Y., 2002. Efficient inverse modeling of barotropic ocean tides. J. Atmos. Ocean. Technol. 19, 183–204. http://dx.doi.org/10.1175/1520-0426(2002)019<0183:EIMOBO>2.0.CO;2.

Egbert, G.D., Bennett, A.F., Foreman, M.G.G., 1994. TOPEX/POSEIDON tides estimated using a global inverse model. J. Geophys. Res. 99, 24821–24852. http://dx.doi.org/10.1029/94JC01894.

Fairley, I., Masters, I., Karunarathna, H., 2015. The cumulative impact of tidal stream turbine arrays on sediment transport in the Pentland Firth. Renew. Energy 80, 755–769. http://dx.doi.org/10.1016/j.renene.2015.03.004.

Filipot, J.F., Delafosse, C., Marzin, T., Baston, S., 2014. On the modelling errors in the tidal power assessment. In: 5th International Conference on Ocean Energy (ICOE), Halifax. URL: http://archimer.ifremer.fr/doc/00230/34114/32569.pdf.

Garrett, C., Cummins, P., 2005. The power potential of tidal currents in channels. Proc. Royal Soc. A. Math. Phys. Eng. Sci. 461, 2563–2572. http://dx.doi.org/10.1098/rspa.2005.1494.

Garrett, C., Cummins, P., 2007. The efficiency of a turbine in a tidal channel. J. Fluid Mech. 588 http://dx.doi.org/10.1017/S0022112007007781.

Gerritsen, H., de Vries, H., Philippart, M., 1995. The Dutch continental shelf model. In: Lynch, D.R., Davies, A.M. (Eds.), Quantitative Skill Assessment for Coastal Ocean Models. American Geophysical Union, Washington DC, pp. 425–467 volume 47 of Coastal and Estuarine Studies.

Gillibrand, P.A., Walters, R.A., McIlvenny, J., 2016. Numerical simulations of the effects of a tidal turbine array on near-bed velocity and local bed shear stress. Energies 9, 852. http://dx.doi.org/10.3390/en9100852.

Green, M.O., McCave, I.N., 1995. Seabed drag coefficient under tidal currents in the eastern Irish Sea. J. Geophys. Res. 100, 16057. http://dx.doi.org/10.1029/95JC01381.

Kramer, S.C., Piggott, M.D., 2016. A correction to the enhanced bottom drag parameterisation of tidal turbines. Renew. Energy 92, 385–396. http://dx.doi.org/10.1016/j.renene.2016.02.022.

Martin-Short, R., Hill, J., Kramer, S., Avdis, A., Allison, P., Piggott, M., 2015. Tidal resource extraction in the Pentland Firth, UK: potential impacts on flow regime and sediment transport in the Inner Sound of Stroma. Renew. Energy 76, 596–607. http://dx.doi.org/10.1016/j.renene.2014.11.079.

Neill, S.P., Hashemi, M.R., Lewis, M.J., 2014. The role of tidal asymmetry in characterizing the tidal energy resource of Orkney. Renew. Energy 68, 337–350. http://dx.doi.org/10.1016/j.renene.2014.01.052.

Neill, S.P., Vgler, A., Goward-Brown, A.J., Baston, S., Lewis, M.J., Gillibrand, P.A., Waldman, S., Woolf, D.K., 2017. The wave and tidal resource of Scotland. Renew. Energy. http://dx.doi.org/10.1016/j.renene.2017.03.027.

O'Hara Murray, R.B., 2015a. Data acquisition and processing for TeraWatt, rev 1.1. In: TeraWatt Position Papers. MASTS, pp. 9–29. URL: http://www.masts.ac.uk/media/166596/position_papers_terawatt_e-book.pdf.

O'Hara Murray, R.B., 2015b. Tidal stream and wave energy array scenarios for the Pentland Firth and Orkney Waters strategic area, Rev. 2.2. In: TeraWatt Position Papers. MASTS, pp. 31–47. URL: http://www.masts.ac.uk/media/166596/position_papers_terawatt_e-book.pdf.

Pawlowicz, R., Beardsley, B., Lentz, S., 2002. Classical tidal harmonic analysis including error estimates in MATLAB using T_tide. Comput. Geosci. 28, 929–937. http://dx.doi.org/10.1016/S0098-3004(02)00013-4.

Rahman, A., Venugopal, V., 2015. Inter-comparison of 3D tidal flow models applied to Orkney islands and Pentland Firth. In: Proceedings of the 11th European Wave & Tidal Energy Conference (EWTEC), Nantes, France.

Ramos, V., Carballo, R., Álvarez, M., Sánchez, M., Iglesias, G., 2013. Assessment of the impacts of tidal stream energy through high-resolution numerical modeling. Energy. http://dx.doi.org/10.1016/j.energy.2013.08.051.

Ramos, V., Carballo, R., Sanchez, M., Veigas, M., Iglesias, G., 2014. Tidal stream energy impacts on estuarine circulation. Energy Convers. Manag. 80, 137–149. http://dx.doi.org/10.1016/j.enconman.2014.01.027.

Sánchez, M., Carballo, R., Ramos, V., Iglesias, G., 2014. Tidal stream energy impact on the transient and residual flow in an estuary: a 3d analysis. Appl. Energy 116, 167–177. http://dx.doi.org/10.1016/j.apenergy.2013.11.052.

Side, J., Gallego, A., James, M., Davies, I., Heath, M., Karunathra, H., Venugopal, V., Vögler, A., Burrows, M., 2017. Developing methodologies for large scale wave and tidal stream marine renewable energy extraction and its environmental impact: an overview of the TeraWatt project. J. Ocean Coast. Manag. 147, 1–5. http://dx.doi.org/10.1016/j.ocecoaman.2016.11.015.

Smith, W., Sandwell, D., 1997. Measured and Estimated Seafloor Topography. Technical Report Research Publication RP-1. In: World Data Center-A for Marine Geology and Geophysics. URL: http://gcmd.nasa.gov/records/GCMD_SIO_NOAA_SEAFLOORTOPO.html.

Soulsby, R., 1997. Dynamics of Marine Sands: a Manual for Practical Applications. Thomas Telford.

Soulsby, R., Clarke, S., 2005. Bed Shear-stresses under Combined Waves and Currents on Smooth and Rough Beds. Technical Report TR137 rev 1.0. HR Wallingford.

UK Hydrographic Office, 1986. Admiralty Tidal Stream Atlas NP209 : Orkney and Shetland Islands.

van Koningsveld, M., Damsma, T., van der Hout, R., van Wiechen, J., de Boer, G., 2013. Openearth: a knowledge management workflow for dredging projects. Terra Aqua 131, 3–14.

Vennell, R., 2010. Tuning turbines in a tidal channel. J. Fluid Mech. 663, 253–267. http://dx.doi.org/10.1017/S0022112010003502.

Venugopal, V., Nemalidinne, R., 2014. Marine energy resource assessment for Orkney and Pentland waters with a coupled wave and tidal flow model. In: International Conference on Ocean, Offshore & Arctic Engineering (OMAE) 2014. http://dx.doi.org/10.1115/OMAE2014-24027.

Waldman, S., Genet, G., Baston, S., Side, J., 2015. Correcting for mesh size dependency in a regional model's representation of tidal turbines. In: Proceedings of the 11th European Wave & Tidal Energy Conference (EWTEC), Nantes, France.

Wilcock, P.R., 1996. Estimating local bed shear stress from velocity observations. Water Resour. Res. 32, 3361–3366. http://dx.doi.org/10.1029/96WR02277.

Erratum correcting previous work: Implementation of tidal turbines in MIKE 3 and Delft3D models of Pentland Firth & Orkney Waters

S Waldman[a,*], S Bastón[a], R Nemalidinne[b], A Chatzirodou[c], V Venugopal[b], J Side[a]

[a] *Heriot-Watt University, Back Road, Stromness, Orkney, KW16 3AW, UK*
[b] *Institute for Energy Systems, School of Engineering, University of Edinburgh, Edinburgh, EH9 3JL, UK*
[c] *Energy & Environment Group, Zienkiewicz Centre for Computational Engineering, College of Engineering, Swansea University, Singleton Park, Swansea, SA2 8PP, UK*

In our article in this journal last year (Waldman et al., 2017), a mistake relating to coordinate handling was present in the MATLAB code used to introduce tidal turbines into Delft3D as porous plates. While the plates were positioned in the correct horizontal locations, their depths and their drag coefficients were wrong. This resulted in incorrect predictions for the effects of tidal turbines in Delft3D. The predictions without turbines are unaffected, as are those from the MIKE 3 model. The overall conclusions of the article remain valid.

Presented here are replacements for Figures 12, 13 and 14 of the original paper, showing the corrected results. Figure 15 is also incorrect, and should be disregarded (see below).

Much of Section 6 of the original paper, discussing the effects of tidal energy extraction, was concerned with the differences that were present between the predictions of the two models. Now that Delft3D's predictions are corrected, most of these differences no longer exist. Delft3D now predicts greater effects from energy extraction than MIKE 3 in all parts of the domain. This is consistent with the lower bed resistance used in Delft3D. As may be seen from the new figures, although some small differences remain between the effects of turbines in the two models, these are of much lesser magnitude than originally reported.

A small study was described in Section 6 of the original paper, investigating yawing and fixed-axis turbine representations to see whether this would explain the discrepancy that was noted. As this discrepancy no longer exists, this small study is no longer required. Figure 15 of the original paper, showing the results of this work, should be disregarded.

The authors apologise for any inconvenience caused to other researchers by this error. The version of the code that is publicly available at `https://github.com/TeraWatt-EcoWatt2050` has been corrected, and anybody using

*Corresponding author. email: s.waldman@hw.ac.uk

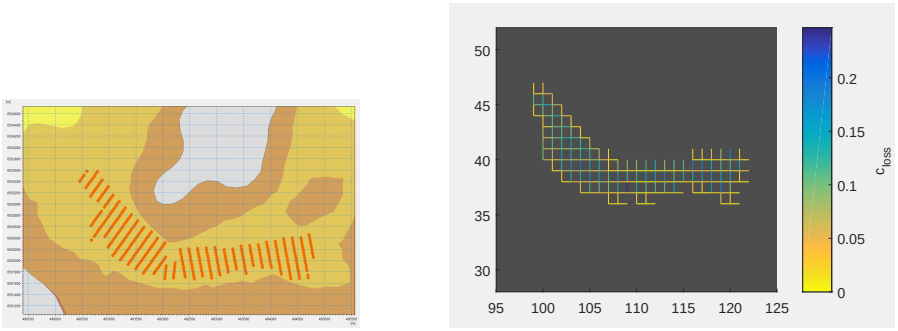

(a) **(b)**

Figure 12: *(a) 400 turbines in the Inner Sound, viewed through the MIKE Zero GUI; (b) The same 400 turbines represented as porous plates for Delft3D. Higher values of the c_{loss} parameter, shown by bluer colours, indicate plates with higher drag.*

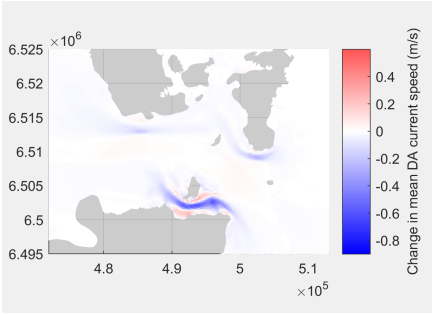

(a) *Depth-averaged current speed in MIKE*

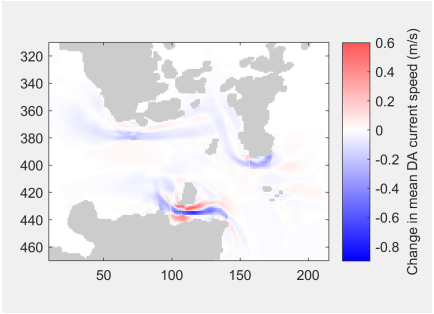

(b) *Depth-averaged current speed in Delft3D*

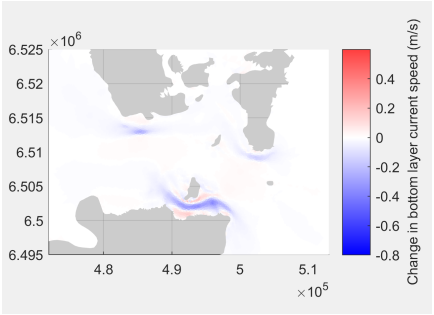

(c) *Bottom layer current speed in MIKE*

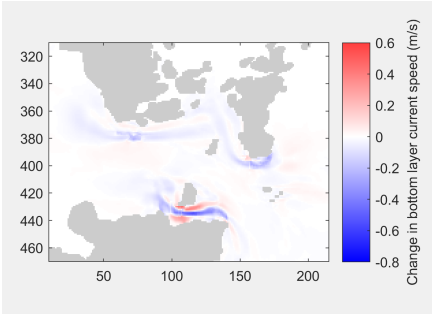

(d) *Bottom layer current speed in Delft3D*

Figure 13: *Changes in mean current speeds over 28 days as a result of adding turbines.*

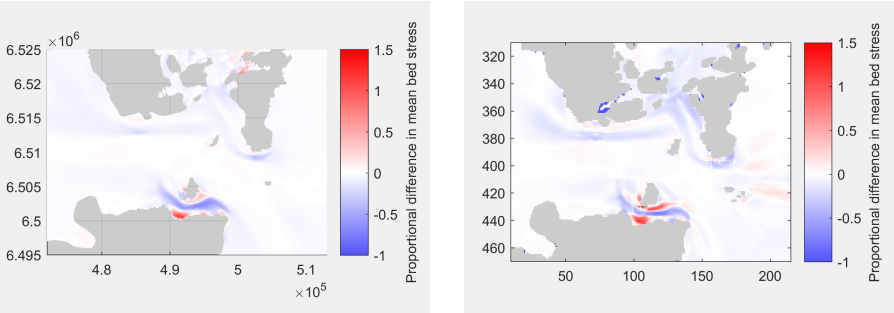

(a) *MIKE* **(b)** *Delft3D*

Figure 14: *Change in mean bed stress magnitude over 28 days as a result of adding turbines, expressed as a proportion of the value without turbines.*

this for their own work is urged to download the latest version.

References

Waldman, S., Bastón, S., Nemalidinne, R., Chatzirodou, A., Venugopal, V., Side, J., 2017. Implementation of tidal turbines in MIKE 3 and Delft3D models of Pentland Firth & Orkney Waters. Ocean & Coastal Management 147, 21–36. doi:10.1016/j.ocecoaman.2017.04.015.

Correcting for mesh size dependency in a regional model's representation of tidal turbines

Simon Waldman
ICIT, Heriot-Watt University
Orkney, UK
smw13@hw.ac.uk

Guillaume Genet
Institut National des Science Appliquées
Strasbourg, France
guillaume.genet@insa-strasbourg.fr

Susana Bastón
ICIT, Heriot-Watt University
Orkney, UK
s.baston@hw.ac.uk

Jonathan Side
ICIT, Heriot-Watt University
Orkney, UK
j.c.side@hw.ac.uk

***Abstract*—When regional-scale hydrodynamic models use fine mesh sizes, such that the cross-section of a cell approaches that of a turbine, an error emerges in the calculation of turbine thrust. This error can be corrected using a method derived from actuator disk theory. We demonstrate this error, explain its source, and then present and test a new MATLAB package to correct for it. Although some minor mesh dependency remains after the correction, its effect is reduced by an order of magnitude.**

***Keywords*—numerical modelling, marine renewable energy, tidal energy, energy extraction, MIKE 3**

I. Introduction

Regional-scale hydrodynamic modelling has emerged as an essential tool for predicting both the potential performance of tidal stream energy installations [1], [2], and the environmental impacts that they may have [3]. A number of modelling systems now have the facility to represent tidal turbines and their effect on the flow.

Historically, regional hydrodynamic models have used cell sizes that are much larger than the diameter of a tidal turbine. In recent years, for applications related to tidal energy, the resolution of these models has increased such that the cross-sectional area of a cell in the model approaches that of a turbine rotor (*e.g.* [4], [5]). This increase in resolution is desirable as it permits more accurate representation of a channel and/or turbine array, which can make a significant difference to predicted current speeds [6]. However, at these high resolutions a mesh dependency emerges that can cause the effect of tidal turbines to be underestimated. This effect was recently demonstrated for a two-dimensional MIKE21 model, and a correction proposed, by Kramer *et al.* [7]. In this work we have adapted that correction to operate appropriately with a 3D model using a triangular mesh, and we have developed a MATLAB package to perform the correction for MIKE. Our work uses the flexible mesh (FM) version of MIKE 3 by DHI, but a similar error is likely to exist in other model codes that use the same approach to energy extraction and do not include a correction.

MIKE by DHI is a commercial hydrodynamic modelling suite commonly used in industry. The MIKE 3 Flow Model FM module solves the three-dimensional incompressible Reynolds-averaged Navier-Stokes equations under Boussinesq and hydrostatic pressure assumptions, using a cell-centred finite volume method [8]. Horizontal spatial discretization is on a flexible (unstructured) mesh. Vertical discretization uses σ layers, *i.e.* a constant number of equally-spaced terrain-following layers that change their thickness according to the depth of the water column. The "2012" version of MIKE was used for this work, with the latest available service packs. A later "2014" edition of MIKE has been released, but was unavailable for this project.

The structure of this paper is as follows: Section II explains the reason that the mesh dependency arises, and Section III demonstrates it. Section IV explains a correction for the error, and Section V describes the MATLAB package that was developed to perform this correction for MIKE models. Section VI presents tests of this package, and Section VII discusses conclusions.

II. Source of the Error

MIKE 3 represents a tidal turbine as a sub-grid object. It calculates the retarding force that is exerted on the flow as a function of the flow velocity, the turbine's thrust coefficient, and the area of the rotor:

$$F = \frac{1}{2}\rho\alpha C_T A u^2 \tag{1}$$

where ρ is the density of the water, C_T is the thrust coefficient, A is the area of the rotor, u is the flow speed and α is a user-defined correction factor that is equal to 1 by default (simplified from [9], assuming that the turbine axis is aligned with the flow*). This force is applied in the horizontal mesh element that contains the turbine centre, and is equally split between vertical elements that intersect the rotor, but cannot be localised any further than that.

As water approaches a tidal turbine, it slows from its upstream speed u_0 (which is the "free stream" speed of the flow before it has begun to feel the effects of the turbine) to the speed at the turbine u_t.

By convention, the thrust coefficient is defined in terms of the free-stream velocity u_0. Therefore, it is u_0 that should be used

*MIKE actually allows for turbines that are not oriented into the flow by splitting the thrust coefficient into what the manual describes as drag and lift coefficients, to refer to axial and orthogonal components respectively. For the purposes of this work we make the assumption that the turbine is aligned with the flow, and thus replace C_D with the more commonly used C_T and assume that $C_L = 0$.

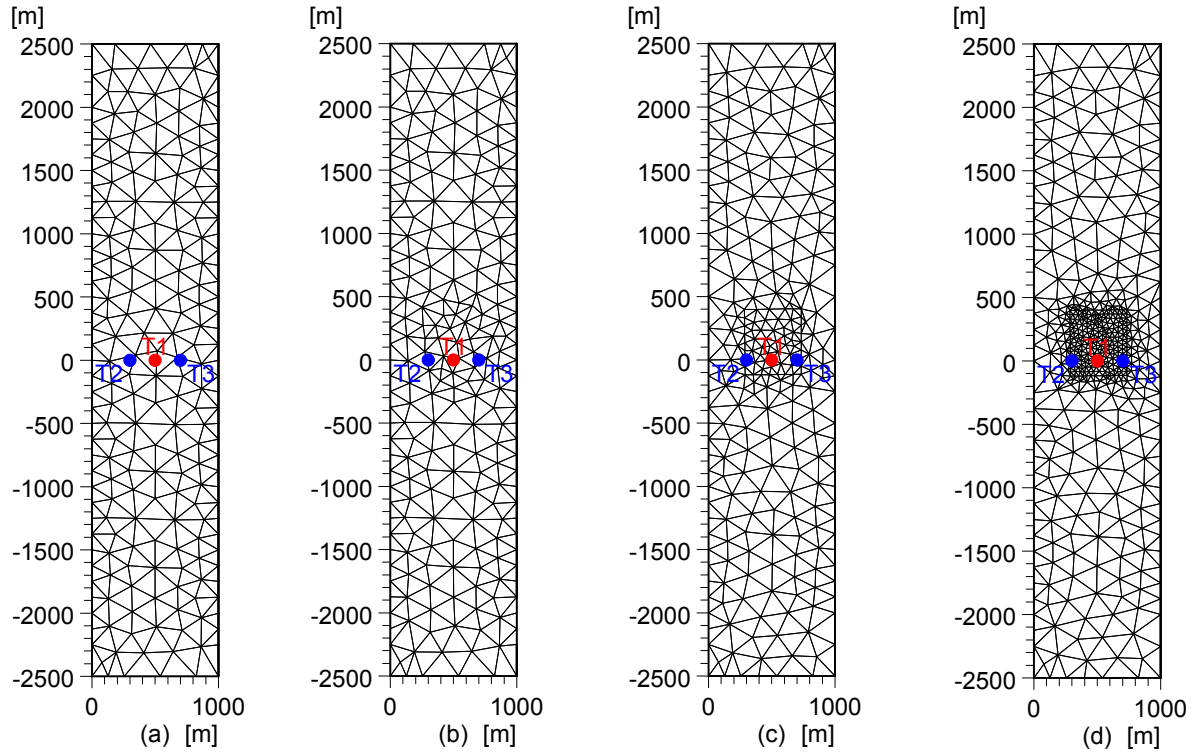

Fig. 1. The four meshes used for testing purposes. Target triangle face lengths were (a) 250 m, (b) 150 m, (c) 100 m, and (d) 50 m. Turbine position T1, described in Section III, is shown in red. Turbine positions T2 & T3, described in Section VI, are shown in blue. The direction of current flow is from the bottom to the top of the figure.

in (1) when calculating the thrust. However, the free-stream velocity is not known in the model.

High-resolution CFD simulations can use actuator disc theory to calculate the free-stream velocity from the velocity at the turbine u_t (see Section IV), but this option is not directly available to a regional-scale model as it does not have sufficient resolution to determine u_t. Instead, it only has access to the velocity u_{cell} that represents the cell as a whole, and this is the value used to calculate the thrust in (1).

When the cell is large compared to the turbine, most of the cell is unobstructed and $u_{cell} \simeq u_0$, so a reasonably accurate result will be obtained. However, as the size of the cell is reduced to approach the scale of the turbine, an increasingly large proportion of its cross-section is occupied by the rotor. This means that the reduction in speed due to the turbine has a significant effect on the cell as a whole, and so $u_{cell} < u_0$. This results in an underestimate of the force applied by the turbine to the flow, which will lead to an error in any prediction of either the energy that can be harvested by the turbine or the environmental effects of its energy extraction.

III. Demonstration of the Error

A. Method

To demonstrate this effect, four simple models were built in MIKE 3, identical except for their meshes. The scenario chosen was a channel 5 km in length and 1 km in width, with a rectangular cross-section and a constant depth of 50 m. Bed roughness height was set to a constant value of $k_s = 0.05$ m and vertical eddy viscosity was by a simple log law formulation. Two open boundaries were specified at the ends of the channel, and were given clamped elevations so that there was a difference in water level of 0.083 m (an arbitrary value) from one end of the channel to the other, resulting in a steady undisturbed flow of 2.1 ms^{-1}.

All four meshes used ten equally spaced vertical layers. The MIKE Mesh Generator tool was used to create a computational mesh with a target triangle face length of approximately 250 m. The same base mesh was used for all four models, but for three of them an area of approximately 500 m square was refined to higher resolution, as shown in Figure 1.

For each mesh the model was run for 25 hours, which was more than sufficient for a steady flow to be reached. Initially they were run without any turbines in place, in order to test for any mesh sensitivity unrelated to the turbine implementation.

A single turbine was then added at the centre of each channel, close to the upstream end of the refined mesh region (position T1 in Figure 1) and oriented to face into the direction of

TABLE I
PREDICTED FLOW SPEEDS IN THE FOUR MESHES WITHOUT AND WITH A TURBINE.

Triangle face length (m)	Speed without turbine (m/s)	Speed with turbine (m/s)	Force on turbine (kN)
250	2.109	1.897	514
150	2.109	1.876	502
100	2.109	1.815	470
50	2.109	1.756	440

flow. The diameter of the turbine was set to 20 m, and its hub elevation to −37 m*. A constant thrust coefficient of 0.9 was specified. The force experienced by the turbine on the final time step was recorded and plotted against the width of the mesh element in Figure 2.

B. Result & discussion

In the test without turbines, all four meshes predicted the same flow speed at the planned turbine location to four significant figures (see Table I). Thus, it is reasonable to conclude that the model is insensitive to mesh size when there are no turbines present.

With the turbine included, it can be clearly seen in Table I and Figure 2 that the force experienced by the turbine decreases with the size of the cell, indicating that the result depends on the mesh. The loss of apparent force from the coarsest to the finest mesh trialled was approx. 14%.

This result qualitatively matches those presented by Kramer *et al.* from larger, but two-dimensional, models in both MIKE21 and Fluidity [7].

IV. CORRECTING FOR THE ERROR

A. Princples

The problem facing us is that the value used for u in (1) is u_{cell}, where it should be u_0. MIKE 3 allows for an arbitrary coefficient α in (1), which we can use to perform a correction. What is needed, then, is a way to find the appropriate value for α so that

$$\alpha = \frac{u_0^2}{u_{cell}^2} \tag{2}$$

There are a number of possible approaches to this. The most straightforward, in our simple case of one turbine in a regular channel, would be to take the velocity from some distance upstream of the turbine. However, it is not obvious what upstream point should be used if the turbine is in the second or later row of an array, or otherwise in non-uniform flow, which would limit the practical utility of this method for real-world models. Instead, the approach adopted here is to use the relationship between α and C_T that is given by actuator disc theory. More sophisticated theoretical models of turbine performance (*e.g.* [11]) could be used in a similar manner.

*A 20 m diameter was chosen following feedback from developers that this a probable rotor size for the Round 1 Pentland Firth developments [10, Appendix A]. We note that the vertical position used is unlikely to be practicable for real turbines due to its proximity to the seabed. However, the aim of this work is to examine mesh size dependency and not to make realistic predictions.

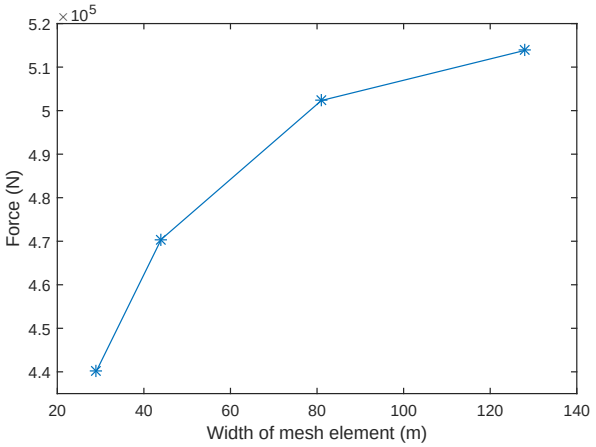

Fig. 2. Initial results, demonstrating the existence of the hypothesised mesh dependency. The definition of 'width' used here is explained in Section IV and shown in Figure 3.

It is a well-known result from actuator disc theory [12] that

$$C_T = 4a(1-a) \tag{3}$$

where a is the axial induction factor $a = 1 - \frac{u_t}{u_0}$. Solving the quadratic for a, substituting in the definition of a, and then squaring both sides gives

$$u_0^2 = \frac{4}{\left(1+\sqrt{1-C_T}\right)^2} u_t^2 \tag{4}$$

In (4), C_T can be thought of as representing the proportion of the momentum passing through the rotor that is removed. If we define an analogous coefficient ν for the whole cell, we can say that,

$$u_0^2 = \frac{4}{\left(1+\sqrt{1-\nu}\right)^2} u_{cell}^2 \tag{5}$$

where ν is equal to the turbine's thrust coefficient, scaled by the proportion of the cross-sectional area of the cell that the turbine occupies. In a three-dimensional model, where the rotor may intersect more than one vertical layer and where (as in MIKE 3) the thrust is split equally between all such layers,

$$\nu = C_T \frac{A_e/n}{\Delta x \Delta z} \tag{6}$$

where A_e is the effective area of the rotor, n is the number of vertical layers intersected, and $\Delta x \Delta z$ is the cross-sectional area of the cell. Note that in the two-dimensional case $\nu = C_T \frac{A_e}{\Delta x H}$, where H is water depth, as given in [7].

In (6), Δx represents the width of the cell or mesh element. In a triangular horizontal mesh, it is not obvious how the 'width' of a triangle sould be defined. The approach that we have adopted is to use the horizontal distance between two faces of the triangle along a horizontal line that passes through the centroid of the triangle and is perpendicular to the direction of current flow (see Figure 3).

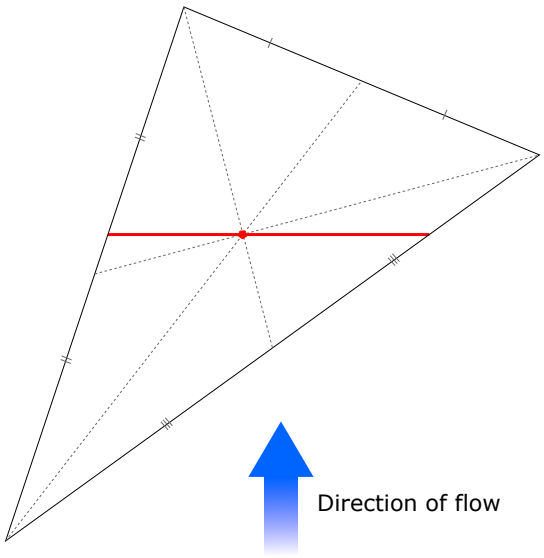

Fig. 3. Illustration of the definition of the width of a triangular mesh element used for this work. The red dot is its centroid, and the length of the heavy red line is the 'width'. Note that the red line is perpendicular to the direction of flow.

B. Practicalities & implementation

In the simplest of modelling arrangements, this calculation might be made once and a correction implemented. However, in realistic scenarios the speed and direction of flow in a mesh element may change on each time step, as may the water level. C_T (a function of speed) and Δx (a function of direction) may therefore change from time step to another, as may both the value of Δz and the number of layers that the rotor intersects, due to the use of sigma coordinates in the vertical. Therefore, it is necessary to calculate α once for each turbine, for each time step.

Furthermore, when a realistic turbine is being modelled, the thrust coefficient and the current speed will both depend upon each other. It may therefore be necessary to iterate new correction factors back into the model a number of times until an acceptable covergence is attained.

Clearly, in any but the simplest cases, it is impractical to carry out these corrections by hand, and an automated approach is required. Consequently a MATLAB package was developed to perform the corrections with a minimum of human input.

V. The MATLAB package

A. Approach, inputs & ouputs

The MATLAB package built to perform this correction was named 'MTMC', for 'MIKE Turbine Mesh Correction'. The primary design intent was to minimise the amount of human intervention that was required, in order to allow its use as part of a practical workflow. To this end, all of the required input data is parsed from various MIKE model files. Three outputs are produced in the filesystem:

- A new data file containing a time series of correction factors for each turbine.
- Modification of the "Turbines" section of the model definition file to instruct MIKE to apply the correction factors given in the new data file.
- A MATLAB (`.mat`) data file that is used to pass information from one iteration of this function to the next. This makes it unnecessary to repeat time-consuming operations on mesh geometry after the first time that it is run, and makes it easy for the user, by reading this file, to track convergence of force or correction factor over multiple iterations.

The flow of information and calculations is described visually in Figure 4.

B. Versions and prerequisites

The MTMC package was developed in MATLAB version 2014b. The following additional packages are required:

- MATLAB Mapping Toolbox.
- DHI MATLAB Toolbox (available from [13]). The 2012 edition was used for this work, but the 2014 version has also been tested. Note that this must be modified, as described below.
- Either MIKE Zero (the MIKE pre/postprocessing suite, included with MIKE 3 licenses), or the MIKE SDK (available without license from DHI). One of these must be present on the system to enable the DHI Toolbox to read MIKE binary files. The 2012 edition of MIKE Zero was used for this work.

If the user is in a country that uses '/' rather than '-' as a date separator, a modification must be made to the DHI MATLAB toolbox to reflect this. In the file `mbin\@dfsTSO\private\parseDatetimeString.m`, hyphens must be changed to slashes in lines 7 and 11 (line numbers from toolbox 2012 edition). This is because MIKE Zero respects locale settings when producing `.dfs0` files, but the Toolbox does not do the same when reading them.

C. Usage

The main `MTMC.MakeCorrection` function takes five arguments, all of which are filenames:

- The filename of the model definition file.
- The filename of the MATLAB data file that will be generated to pass information between iterations.
- A cell array containing the filenames of one or more turbine output files, generated from a prior model run.
- The filename of the mesh file.
- The base filename that should be used for the data file that will be created with correction factors.

It provides no returns within MATLAB.

The sequence of usage is as follows:

1) Set up the model, giving the turbines a fixed correction factor of 1 as per default. The model must use Cartesian coordinates; spherical coordinates are not currently supported. The thrust curve should be specified as the 'drag coefficient' identically for all angles using the "Tabulated drag and lift coefficient" option, and the 'lift coefficient'

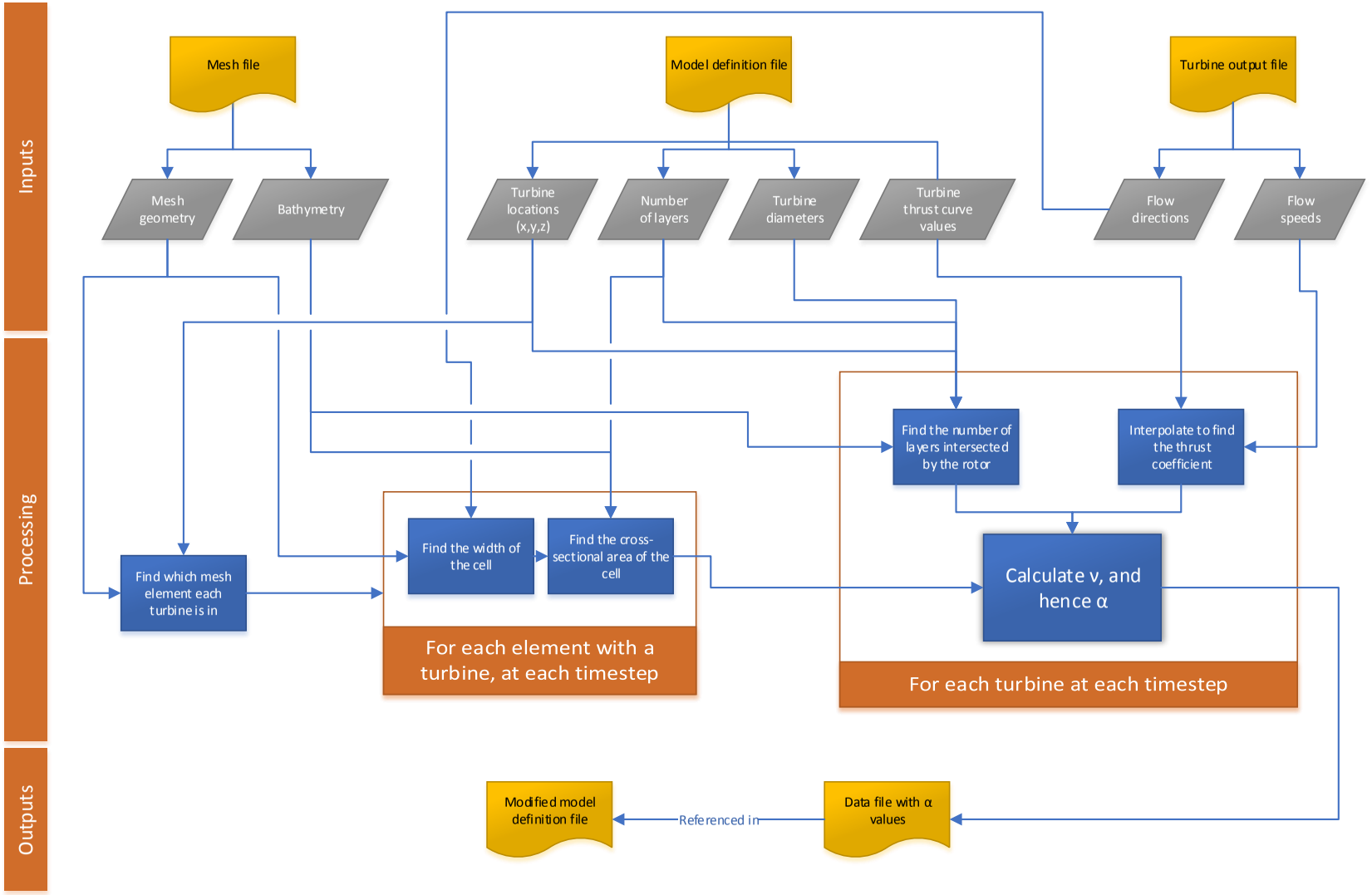

Fig. 4. Flow of information & calculations in the MATLAB package.

set to zero for all angles. This represents a turbine that is always aligned with the oncoming flow. The current version of this script does not support turbines that are not aligned with the flow. Ensure that there is a maximum of one turbine in any mesh element.

2) Run the model. This will provide current speed and direction information for the script.
3) Run `MTMC.MakeCorrection` for the first time. This will automatically modify the model definition file to assign time-varying correction factors to the turbines.
4) Run the model again. If a fixed thrust coefficient is being used, this may provide stable predictions.
5) If a variable thrust coefficient is being used, run the model and then `MTMC.MakeCorrection` as many times as necessary to obtain acceptable convergence. At any time after the first run of the function, the contents of the `.mat` file can be inspected to view the sequence of correction factors and predicted forces until that point.

D. Limitations

The current version of the package has a number of limitations that must be borne in mind:

- No account is currently taken of changing surface elevations; it is assumed that the surface elevation is always equal to mean sea level. This is a reasonable assumption when testing with steady flows, but it may cause significant inaccuracies with real tidal conditions, especially in shallow areas, because a change in surface elevation implies a change in Δz for a model cell.
- Off-axis turbines are not yet supported. This precludes the use of this script for turbines that do not 'weathervane' to face into the flow, unless they are used in a perfectly bidirectional tidal environment.
- There is no support for having multiple turbines in one mesh element. In practice, if the mesh scale is large enough for this to be an issue for well-spaced turbines, then the error that this correction addresses will be small. If the mesh is small and turbines are very tightly packed, then errors due to array effects are likely to be greater than those due to mesh size.

E. Availability

The package is still undergoing testing and improvement, but will be made publicly available at `https://github.com/TeraWatt-EcoWatt2050/MTMC` by the time of this paper's presentation. Improvements are welcomed from the community.

VI. Testing the Correction

The proposed correction was initially applied 'by hand' to the simple scenario described in Section III. The region of each mesh around the turbine was printed at a large scale, and the geometry of the mesh element containing the turbine was measured and scaled. The appropriate correction for each version of the mesh was calculated, and was applied as a constant correction factor in a second iteration of the model.

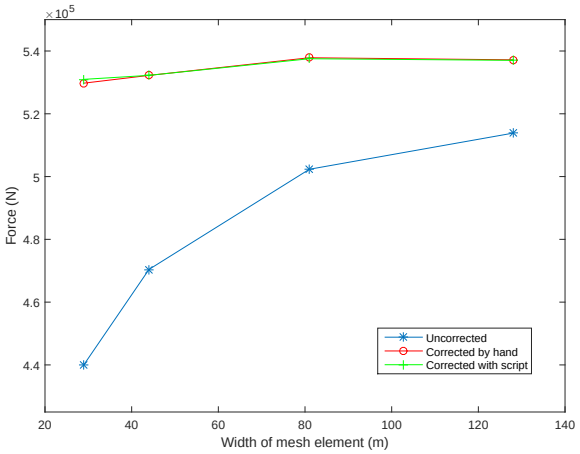

Fig. 5. Force experienced by turbine according width of mesh element. The blue (lower) line is uncorrected; the red line is corrected by hand measurement and calculation, and the green by the MATLAB script. The latter two lines are superimposed and difficult to discern.

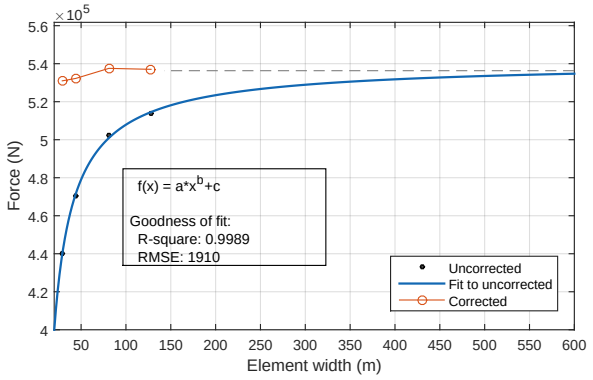

Fig. 6. The corrected and uncorrected values shown in Figure 5 are reproduced here, with a curve fitted to the uncorrected values and the x-axis extended to extrapolate to its assymptotic value. As illustrated by the dashed line, this is close to the corrected values.

Once the MATLAB script for the correction had been completed, this was run against the same simple scenario. As may be seen in Figure 5, the results were very similar, which provides confidence that the intended calculation was correctly implemented. Runtime for the script was less than half a second for this single-turbine scenario.

If a curve is fitted to the uncorrected values using a power law, then its extension to large element width approaches an assymptote (see Figure 6). This is expected, as the assymptote represents the limit where $u_{cell} = u_0$ at large mesh scales. The uncorrected force predicted at these large mesh scales is similar to the corrected predictions at small mesh scales. This is evidence not only that the intended calculation was implemented without error, but that it was the correct calculation to perform.

The result of this correction is not perfect mesh-independence, since there is still some variance in force with mesh size. However, the range in forces amongst the four

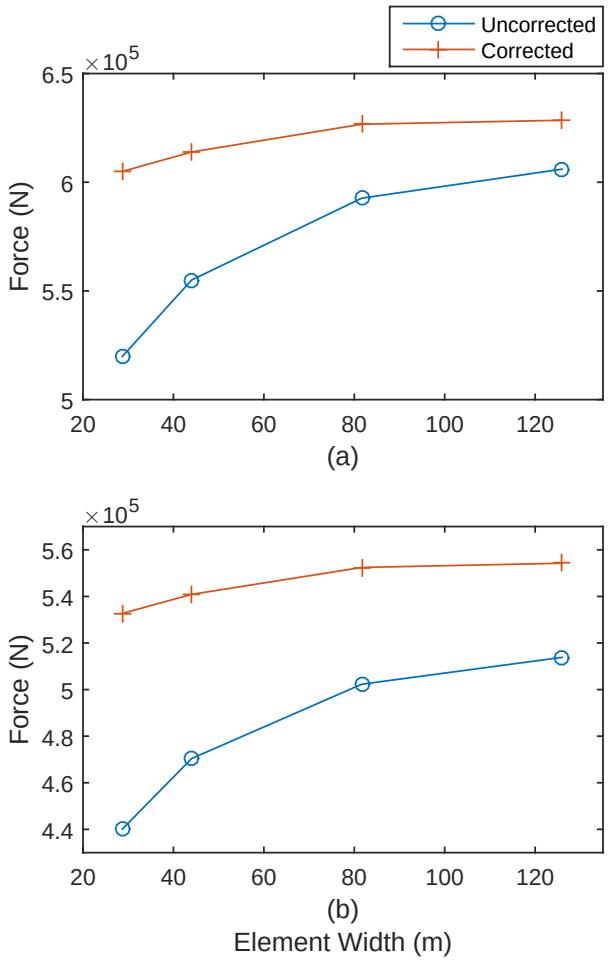

Fig. 7. Correction applied to a turbine at the same horizontal location (T1), at depths (a) 25m, (b) 37m.

meshes tested was reduced from 14% of the maximum to just 1%, which suggests an improvement.

In order to give further confidence in its correct evaluation of mesh geometry, the script was used to correct a turbine at a number of different depths and horizontal locations (positions T2 & T3 in Figure 1). To avoid any risk of interactions, which might confuse matters at this stage, only one turbine was modelled, and its location changed for each set of simulations.

For different depths in the same horizontal location (Figure 7), while the absolute force values vary with depth due to vertical shear, the change in force with mesh size is near-identical. This is as expected, because the same horizontal triangle on each mesh hosts the turbine at any depth. When the turbine is placed in different horizontal locations (Figure 8), we observe that in each case the corrected result shows a reduction in sensitivity to mesh size when compared to the uncorrected result, but that some mesh dependency clearly remains, and that this varies in magnitude between different locations on the mesh.

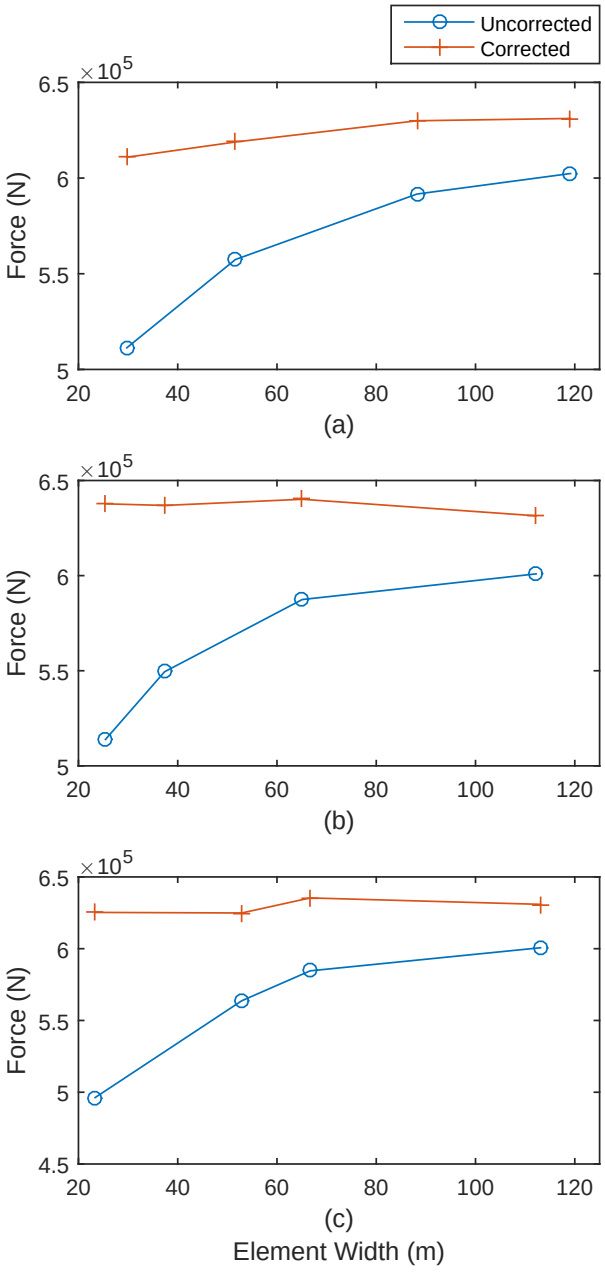

Fig. 8. Correction applied to a turbine at the three horizontal locations (a) T1, (b) T2, (c) T3, shown in Figure 1. In each case the turbine was at 26m depth.

VII. Conclusions

This work is a step towards being able to use high mesh resolutions in regional-scale models, such as MIKE 3, without suffering from the mesh dependency that is illustrated. It is possible that future versions of MIKE may make this correction internally, but in the meantime, the use of this script allows greater accuracy to be attained in predictions of energy resource and of environmental impact.

We have demonstrated that there is no significant mesh dependency in the simulation before turbines are added (Ta-

ble I). We have shown that a mesh dependency does develop in the presence of a turbine, and that the effects of this vary in a manner consistent with theory, including approaching an asymptote for very coarse meshes (Figure 6). We have presented a correction that reduces this effect by an order of magnitude, automated this correction through MATLAB and performed initial testing of it in a simple model.

The corrections made are not perfect, in that some sensitivity to the mesh still remains. This may be due to limitations in the theory used (*e.g.* the one-dimensional nature of actuator disc theory, or the assumption that all drag due to a turbine happens at the rotor, thus ignoring wake mixing losses), or it may be due to limitations in the current implementation of the correction (*e.g.* in the definition of the width of a triangle).

Further work will focus on testing this script further, improving the correction, and then applying it to more realistic tidal model scenarios. Comparison with measurements and/or high-resolution CFD simulation will provide validation of the results obtained.

ACKNOWLEDGMENTS

This work has been conducted under the auspices of TeraWatt, an EPSRC-funded research project. We thank David Woolf for his comments on a draft of this paper.

REFERENCES

[1] A. Cornett, M. Toupin, S. Baker, S. Piche, and I. Nistor, "Appraisal of IEC standards for wave and tidal energy resource assessment," in *International Conference on Ocean Energy (ICOE) 2014*, Halifax, Canada, Nov. 2014. [Online]. Available: http://www.icoe2014canada.org/wp-content/uploads/2014/11/2-CornettAndrewARTICLE_9-3.pdf

[2] EMEC and C. Legrand, "Assessment of tidal energy resource," 2009. [Online]. Available: http://www.emec.org.uk/assessment-of-tidal-energy-resource/

[3] M. A. Shields, D. K. Woolf, E. P. Grist, S. A. Kerr, A. Jackson, R. E. Harris, M. C. Bell, R. Beharie, A. Want, E. Osalusi, S. W. Gibb, and J. Side, "Marine renewable energy: The ecological implications of altering the hydrodynamics of the marine environment," *Ocean & Coastal Management*, vol. 54, no. 1, pp. 2–9, Jan. 2011.

[4] V. Ramos, R. Carballo, M. lvarez, M. Snchez, and G. Iglesias, "Assessment of the impacts of tidal stream energy through high-resolution numerical modeling," *Energy*, Sep. 2013.

[5] R. Martin-Short, J. Hill, S. Kramer, A. Avdis, P. Allison, and M. Piggott, "Tidal resource extraction in the Pentland Firth, UK: Potential impacts on flow regime and sediment transport in the inner sound of stroma," *Renewable Energy*, vol. 76, pp. 596–607, Apr. 2015.

[6] J. Culina and R. Karsten, "Comparison of different resolution models and observed current profiles in the Bay of Fundy, Canada using turbine-relevant metrics," in *Proceedings of the 9th European Wave and Tidal Energy Conference.*, Southampton, 2011.

[7] S. Kramer, M. Piggott, J. Hill, L. Kregting, D. Pritchard, and B. Elsaesser, "The modelling of tidal turbine farms using multi-scale, unstructured mesh models," in *Proceedings of the 2nd International Conference on Environmental Interactions of Marine Renewable Energy Technologies*, Stornoway, 2014.

[8] DHI, "MIKE 21 & MIKE 3 flow model FM hydrodynamic & transport module scientific documentation," 2012.

[9] DHI, "MIKE 3 Flow Model FM Hydrodynamic Module user guide," 2012.

[10] S. Baston, S. Waldman, and J. Side, "Modelling energy extraction in tidal flows," TeraWatt position paper, May 2015. [Online]. Available: http://www.masts.ac.uk/about/masts-publications/terawatt-publications/

[11] J. Whelan, J. Graham, and J. Peir, "A free-surface and blockage correction for tidal turbines," *Journal of Fluid Mechanics*, vol. 624, pp. 281–291, 2009, 281.

[12] J. F. Manwell, *Wind energy explained: theory, design and application*, 2nd ed. Chichester, U.K: Wiley, 2009.

[13] DHI, "DHI Matlab toolbox." [Online]. Available: http://www.mikepoweredbydhi.com/download/mike-by-dhi-tools/coastandseatools/dhi-matlab-toolbox

International Journal of Marine Energy 19 (2017) 332–344

Contents lists available at ScienceDirect

International Journal of Marine Energy

journal homepage: www.elsevier.com/locate/ijome

Tidal resource and interactions between multiple channels in the Goto Islands, Japan

S. Waldman [a,*], S. Yamaguchi [b], R. O'Hara Murray [c], D. Woolf [a]

[a] Heriot-Watt University, Back Road, Stromness, Orkney KW16 3AW, UK
[b] Department of Earth System Science and Technology, Kyushu University, Fukuoka, Japan
[c] Marine Scotland Science, Scottish Government, 375 Victoria Road, Aberdeen AB11 9DB, UK

ARTICLE INFO

Article history:
Received 17 March 2017
Revised 6 September 2017
Accepted 19 September 2017
Available online 30 September 2017

Keywords:
FVCOM
Numerical modelling
Goto Islands
Tidal energy
Split channels

ABSTRACT

The Goto Islands in Nagasaki Prefecture, Japan, contain three parallel channels that are suitable for tidal energy development and are the planned location for a tidal energy test centre. Energy extraction is added to a 3D numerical hydrodynamic model of the region, using a sub-grid momentum sink approach, to predict the effects of tidal development.

The available resource with first-generation turbines is estimated at 50–107 MW peak output. Spreading turbine thrust across the whole cross-section to prevent bypass flow results in a 64% increase in peak power in one channel, highlighting the importance of 3D over 2D modelling.

The energy available for extraction in each strait appears to be independent of the level of extraction in other straits. This contrasts with theoretical and numerical studies of other multi-channel systems. The weak interactions found in this study can be traced to the hydraulic effects of energy extraction not extending to neighbouring channels due to their geometry.

1. Introduction

1.1. Background

In 2010 nuclear power provided 25% of Japan's electricity [1], making Japan the third-largest producer of nuclear energy in the world [2]. Following the tsunami of 2011 and the subsequent events at the Fukushima Daiichi nuclear power plant this figure dropped to less than 2% (in 2012) as the nation's reactors were taken off-line, and most of the shortfall was replaced by fossil fuels. Lacking substantial fossil resources of its own, by 2015 Japan had become one of the world's greatest importers of fossil fuels, and in addition to the environmental implications this represents a significant drain on economic resources [2]. While there has been some limited resumption of nuclear generation, this is deeply unpopular with sections of the public [3]. As part of a strategy to increase domestic energy supply, the Japanese government plans for 22–24% of electricity to be generated by renewables in 2030 [4]. Work is in progress to set up a marine energy test centre, similar to the European Marine Energy Centre in Scotland, in the Goto Islands of Nagasaki Prefecture [5].

* Corresponding author.
E-mail address: simon@simonwaldman.me.uk (S. Waldman).

https://doi.org/10.1016/j.ijome.2017.09.002
2214-1669/

1.2. Geographic & hydrodynamic situation

The Goto Islands are an archipelago approximately 80 km to the west of Nagasaki city and, at their closest point, separated from the Japanese mainland by approximately 20 km of sea (Fig. 1a). To the north is the Korea Strait, the main southern entrance to the Sea of Japan, while to the south lies part of the East China Sea and the Pacific Ocean. A portion of flow between these large bodies of water must pass through or around the archipelago.

Within the islands there are four channels running from north-west to south-east, three of which are approximately parallel and of similar dimensions: 7–8 km in length, 1–3 km in width, and 50–60 m deep in mid-channel. These are the Tanoura, Naru and Takigawara Straits (Fig. 1b). The first two have been designated by the Japanese government as an area for tidal energy development, and the first tidal energy convertor (TEC) is due to be installed by OpenHydro in the Naru Strait in 2018 [6]. The fourth channel, the Wakamatsu Strait, is less than 30 m deep for most of its length and is hence unsuitable for the TEC design considered here.

The region experiences mixed diurnal/ semi-diurnal tides. When compared to European seas, less of the energy is to be found in the M2 constituent and a greater proportion (approx. 15% of the total) is in K1 and O1. Table 1 shows the most important constituents.

1.3. Theoretical background & prior work

To extract tidal stream (or "hydrokinetic") energy, a porous obstruction is placed in the flow in the form of a TEC. A proportion of the kinetic energy passing through the TEC is removed for conversion to electricity and a retarding force is applied to the flow, usually resulting in a reduction in its speed. For a given array in a given channel a there exists an optimum proportion of energy removed, beyond which the flow is retarded to such an extent that the available power diminishes.

Garrett and Cummins [8] described a theoretical model of a channel between two large bodies of water, and used this to derive an approximate formula for the power lost to a channel as a result of energy extraction at optimum yield. Their model assumes that the extraction of energy in the channel cannot influence the elevation difference across the channel, which may be thought of as the "head" available to the turbines.

The exportable power available from the turbines cannot exceed the power extracted from the flow, and will usually be less. Losses include drag from the TECs' supporting structures, turbulence generated at the turbine blades, and inefficiencies in the conversion to electrical energy. Where the array does not fill the cross-section of a channel, some flow will divert around it. The kinetic energy of this bypass flow is clearly not available for conversion, but some of it will still be lost from the channel in turbulent mixing when the bypass flow meets the slower wake behind the turbine [9]. Thus, so long as financial limitations on the number of turbines do not apply, a tidal stream array occupying the entire cross-section of a channel will always be optimal. This was demonstrated with theoretical models by Garrett and Cummins [10] and Houlsby et al. [11].

The behaviour of multiple channels has been studied from a theoretical perspective by Atwater and Lawrence [12], who considered the available power in terms of head loss, and Cummins [13], who used the analogy of an electrical circuit.

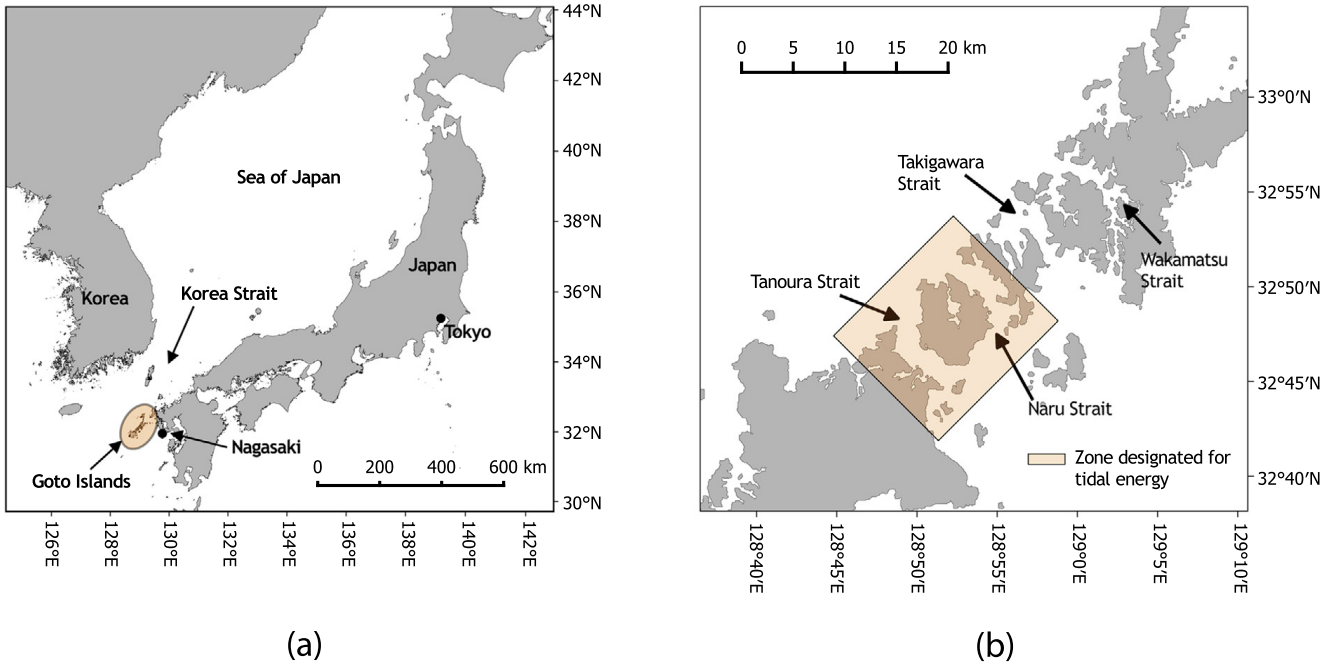

Fig. 1. Maps showing (a) the situation of the Goto Islands with respect to Japan, and (b) the four channels running through the middle of the archipelago.

Table 1
Table showing the five most energetic tidal constituents, based on a 29 day time series of surface elevation from a combined pressure sensor and ADCP deployment in the Naru Strait [7]. Harmonic analysis conducted using the U-Tide software.

Constituent	Proportion of total energy (%)
M2	65.2
S2	13.2
K1	9.2
O1	6.0
N2	2.7

Practical modelling investigations of the multiple channels in the Pentland Firth, Scotland, have been conducted by Draper et al. [14] (in two dimensions), Goward Brown et al. [15] (in three dimensions), and O'Hara Murray and Gallego [16] (in three dimensions, with the same software used here). In all of these studies, where there are parallel sub-channels, there is a tendency for exploitation of one channel to cause flow to be diverted into unexploited sub-channels, reducing the yield.

The authors are unaware of any prior resource assessments of the Goto Islands that account for the effects of energy extraction, and hence the estimates offered by this paper may be the first available.

1.4. Outline of this paper

The work described in this paper has two goals: Firstly, to provide an initial tidal resource assessment for the Goto Islands, and secondly to explore the behavior of the parallel channels when energy is extracted.

Section 2 describes the numerical model that was used. Sections 3–5 relate simulations using realistic TEC representations, aimed at estimating the available resource. In Section 6 we put aside the realistic TEC parameters in an effort to explore the maximum possible extractable power in one of the channels and its effect on the other straits. Section 7 discusses our findings and compares the behavior of the Goto Islands to that of the well-studied Pentland Firth.

2. Description of the model

Numerical simulations were conducted using the free surface three-dimensional Finite Volume Community Ocean Model (FVCOM) [17]. The model used in this work was developed by others at Kyushu University in collaboration with the second author. It will be summarised here, but is described more fully in [7].

The computational domain, shown in Fig. 2, consists of non-overlapping unstructured triangular mesh elements (Fig. 3). The use of an unstructured mesh is efficient in allowing coverage of a large area with fine scale detail in areas of interest. A typical element size of 50 m was adopted around the three narrow channels in the Goto Islands, gradually increasing to 5000 m toward the open boundary. Vertical discretization is provided by 20 equally-spaced sigma layers.

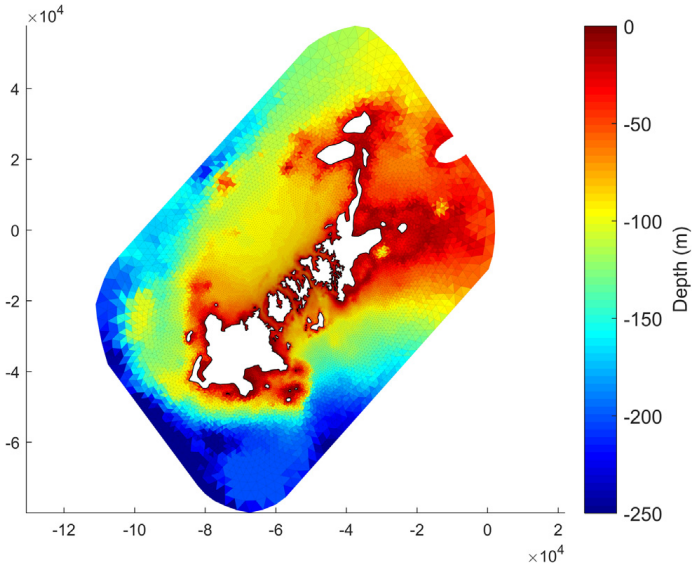

Fig. 2. Plot showing the model domain and bathymetry. The spatial coordinates are in metres, referring to the "Japan Plane Rectangular" coordinate system zone CS1, EPSG ref 2443.

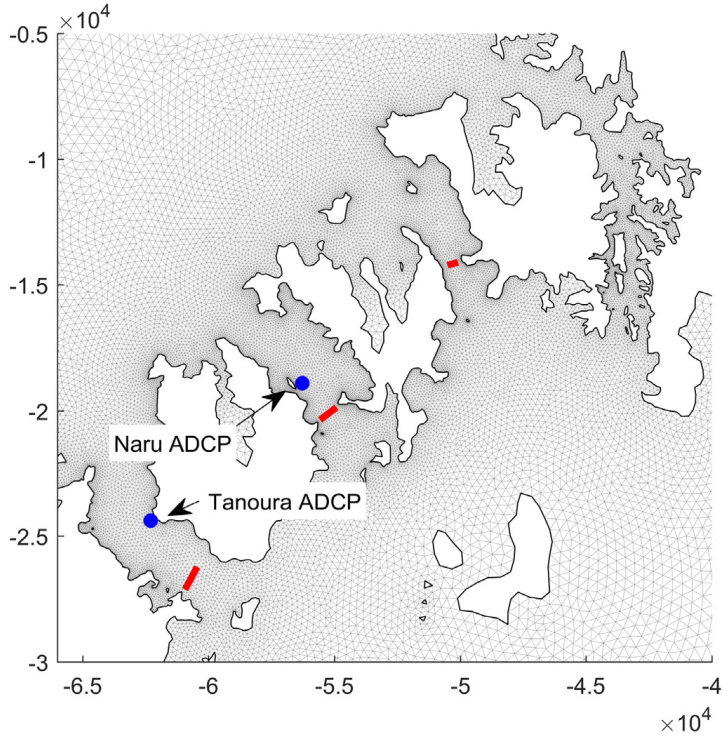

Fig. 3. Plot showing the inner part of the computational mesh. Thick red lines show the locations used for tidal turbines, as described in Section 3. Blue points show the locations of ADCP surveys used for validation. Spatial coordinates are in metres, referring to the "Japan Plane Rectangular" coordinate system zone CS1, EPSG ref 2443.

The horizontal velocity components (u, v) are calculated at the centroid of each triangle while elevations are calculated at the vertices. FVCOM is closed mathematically using a modified Mellor and Yamada level 2.5 turbulence closure scheme [18] for vertical eddy mixing and the Smagorinsky parameterization [19] for horizontal eddy viscosity.

The model bathymetry (Fig. 2) was produced from data supplied by the Hydrographic and Oceanographic Department, Japan Coast Guard. Eight major tidal constituents (M2, S2, K2, N2, K1, O1, P1, Q1) were forced at open boundary nodes using amplitudes and phases based on the NAO.99Jb regional tide model [20]. The phases of these forcing constituents were then adjusted as part of the calibration procedure to improve the agreement with measurements in the tidal straits. The model was run in barotropic mode with no freshwater inputs or meteorological effects.

The model was validated by comparison of velocities at two locations (see Fig. 3) between ADCP measurements and model predictions over a two-week period. Error and correlation statistics are reproduced in Table 2 and show an excellent match in the Tanoura strait. In the Naru strait the correlation is poorer for the u-velocity, but since the flow in this location is dominated by the north–south axis this was considered acceptable. A harmonic analysis of surface elevation at a tide gauge station was also conducted, and the comparison between these measurements and predictions is shown graphically in Fig. 4.

2.1. Energy extraction

The code used to represent energy extraction was that of O'Hara Murray and Gallego [16], which follows the approach of Yang et al. [21] and incorporates tidal stream energy extraction into FVCOM using a sub-grid scale momentum sink method. This approach represents the horizontal retarding force, applied by tidal stream turbines on the flow, as additional terms in the 3D momentum equations. The retarding force can be applied at any vertical layer, or combination of layers. Assuming a tidal turbine is always orientated to face the current, *i.e.* it weathervanes to face the flow, the retarding force can be expressed as a quadratic drag law

$$F = \frac{1}{2}\rho C_T A|\mathbf{u}|\mathbf{u} \tag{1}$$

Table 2
Table showing RMSE and R^2 statistics for comparison of depth-averaged velocities between observations and predictions at two locations (see map in Fig. 3).

Location	u-Velocity		v-Velocity	
	RMSE (ms^{-1})	R^2	RMSE (ms^{-1})	R^2
Tanoura Strait	0.18	0.94	0.31	0.92
Naru Strait	0.26	0.79	0.24	0.93

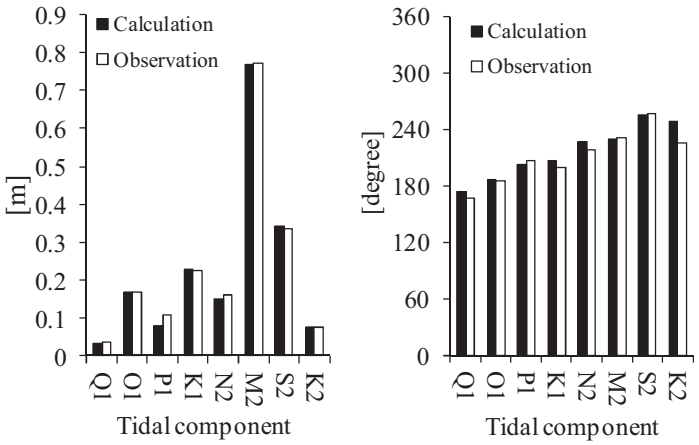

Fig. 4. Chart comparing predicted and observed amplitudes (left) and phases (right) of eight tidal constituents at the location of a tide gauge in Fukue City. This location is a short distance beyond the southern edge of Fig. 3, at 32.7°N, 128.85°E. Note that phases at the open boundaries were adjusted during calibration.

where ρ is the water density, C_T is the thrust coefficient of the turbine, A is the flow facing area of the turbine, and $\mathbf{u}$ is the flow velocity vector. For simplicity, no supporting structures were included in the model.

FVCOM uses a mode splitting method in order to solve the 2D, depth averaged, barotropic equations, and the 3D baroclinic equations, with different time steps [17]. Therefore, additional terms were added to both the 2D and 3D momentum equations. In order to allow for the turbines to span multiple vertical layers a parameter K, expressing the fraction of A occupied by the turbine in each layer was included. Thus, equations for the retarding force exerted by N turbines on the fluid for any model element, i, and for the 2D and 3D equations respectively, are

$$F_{2D}(i) = \frac{1}{2}\rho N(i) C_T(i) A(i) \sum_{j=1}^{n} K(i,j)|\mathbf{u}(i,j)|\mathbf{u}(i,j) \tag{2}$$

$$F_{3D}(i,j) = \frac{1}{2}\rho N(i) C_T(i) A(i) K(i,j)|\mathbf{u}(i,j)|\mathbf{u}(i,j) \tag{3}$$

where j is the depth layer, and n is the total number of depth layers. $N(i)$, $C_T(i)$, $A(i)$,and $K(i,j)$ can all potentially vary between mesh elements, *i.e.* depending on the water depth and the number and type of turbines deployed in each element. $C_T(i)$ may be expressed as a function of $u(i)$ using a lookup table and linear interpolation, to allow for the representation of realistic thrust curves. A full description of the energy extraction implementation can be found in [16].

The simulated TEC was based on the OpenHydro device that has been proposed for the Naru Strait. This is a seabed-mounted design with a diameter of 16 m, a hub height of 19 m above the seabed, and a rated capacity of 2 MW (OpenHydro, personal communication with SY). A realistic thrust curve was applied, based on that given by Baston et al. [22] but scaled to use a cut-in speed of 1 ms^{-1} and a rated speed of 3 ms^{-1}. This rated speed was adopted because it is a speed that is regularly encountered during spring tides in the area of interest; the turbine's rated capacity of 2 MW would imply a rated speed of over 3.5 ms^{-1}, but it is unlikely that this would ever be reached. The thrust coefficient between the cut-in and rated speeds is 0.85, while above the rated speed it is scaled to provide a constant power output.

Two limitations of the current implementation of energy extraction are the assumption that TECs always face the flow (which is unlikely to be the case with the OpenHydro design, which does not yaw) and the definition of the vertical position of the momentum sink in terms of sigma layers, causing the simulated TECs to move up and down with the rise and fall of the tide.

2.2. Calculation of power

Electrical power was calculated from simulated current speeds as a post-processing step. Initially, thrust was determined using (1). Power was then estimated using

$$P = C_C F|\mathbf{u}| \tag{4}$$

where C_C is a coefficient that represents the conversion losses between kinetic energy in the flow and electricity. It is acknowledged that some inaccuracy is inherent in using the same value of $|\mathbf{u}|$, representing an entire mesh element, in both of the equations above (more correctly, the velocity in (1) should be the free-stream velocity and that in (4) should be the velocity at the turbine, but neither of these values is known to the model), and correction for this is implicitly included in the value of C_C. A value of 0.5 was assigned to C_C based on experimental results with a Schottel turbine reported by Jeffcoate

et al. [23]. This two-stage approach is equivalent, below the rated speed, to a power coefficient of 0.425, which is within the range shown by Bahaj et al. [24] from tank testing.

3. Single-channel scenarios

A transect across each strait between the 30 m depth contours was identified to hold TECs. This depth limitation allowed for the full height of the TEC (27 m from base to blade tip) to remain submerged throughout the tidal cycle. Simulated turbines were placed, evenly spaced, along these lines, and the number of turbines lying inside each intersected mesh element was provided to the FVCOM model. The transects were located by inspection of the areas of highest speeds without turbines on both flood and ebb, which were usually at or near to the narrowest parts of the channels. Their locations can be seen in Fig. 3.

A wide range of turbine numbers was tested in each channel, from the conservative to the implausible. In the more heavily exploited scenarios a single row of turbines is unrealistic, as they would be placed very close together and even overlap and collide. However, this approach allowed the level of energy extraction in a channel to be reduced to a single parameter, which is convenient and, in the event of performing an optimisation across multiple channels, reduces the number of degrees of freedom. Since the purpose of this work was not to study realistic array layouts but to examine the behaviour of the channel as a whole, this was judged to be acceptable.

In order to minimise computation time, initial simulations were driven only by the M2 tidal constituent. This allows the use of just 12.4 h of output – a single M2 cycle – as a representative time period. It was determined empirically that the model required 3 days of spinup time before its output became fully periodic, so each scenario was run for 4 days of model time and the output data taken from the final 12.4 h.

Fig. 5 shows the maximum and mean power output for each channel with scenarios between 5 and 1000 turbines. The use of M2 only means that results in this section show unrealistically low levels of power, so limited attention should be paid to the absolute power levels; of interest instead are the differences in output between different scenarios. It is clear that even with modest numbers of TECs, additional machines offer diminishing returns. The mean power available in each strait peaks at implausibly high levels of exploitation, ranging from 270 to 446 TECs; beyond this point, adding additional turbines gives a negative marginal return. The maximum power also peaks in each channel, but at even higher numbers of TECs than the mean.

O'Hara Murray and Gallego [16] noted that when simulating turbines in their correct vertical locations, as done here, a portion of the flow would divert over and under the turbine rotors instead of passing through them (although in reality, or in a more detailed simulation, some of the flow under the rotor would be impeded by the device's base structure). This behavior appears to be replicated in the Goto channels, as suggested by Fig. 6. Vertical diversion limits the power output that can be achieved, but is unavoidable while using bottom-mounted turbines and while, in some areas, preserving clear water above for navigation.

The use of realistic TEC arrangements will be continued for the next two sections to arrive at realistic resource estimates. In Section 6 the TEC description will be modified to explore the maximum power that can be extracted without engineering or navigational constraints.

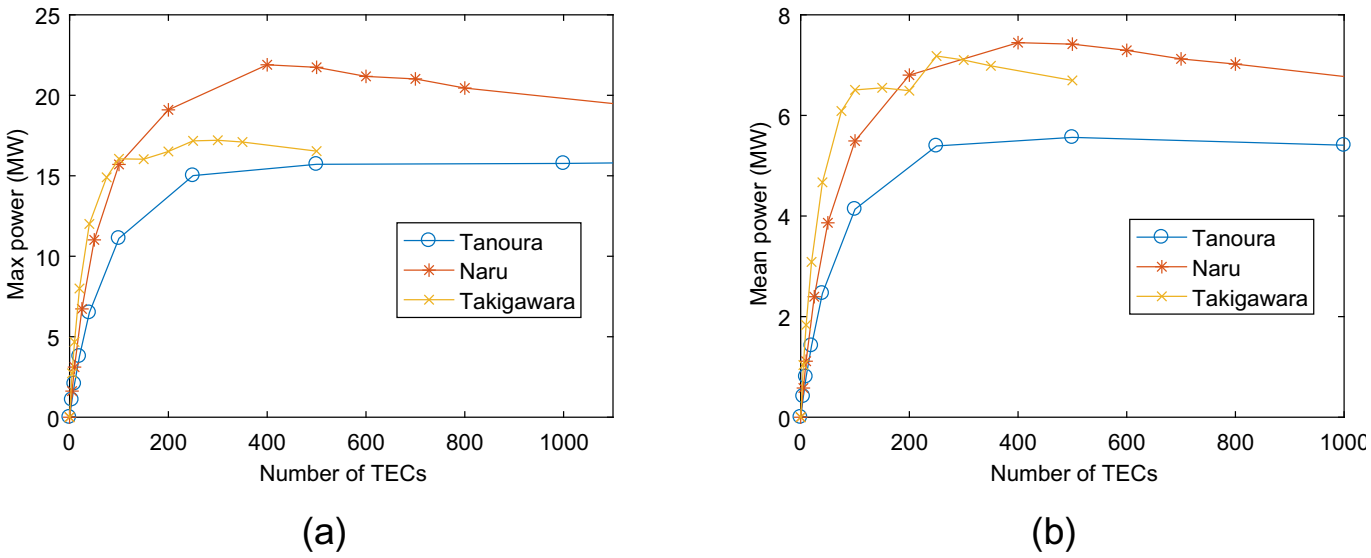

Fig. 5. Plots showing (a) maximum and (b) mean power output from the three channels with varying numbers of realistic TECs. The maximum power in the Tanoura strait peaks at approximately 2400 TECs, beyond the limits of this plot.

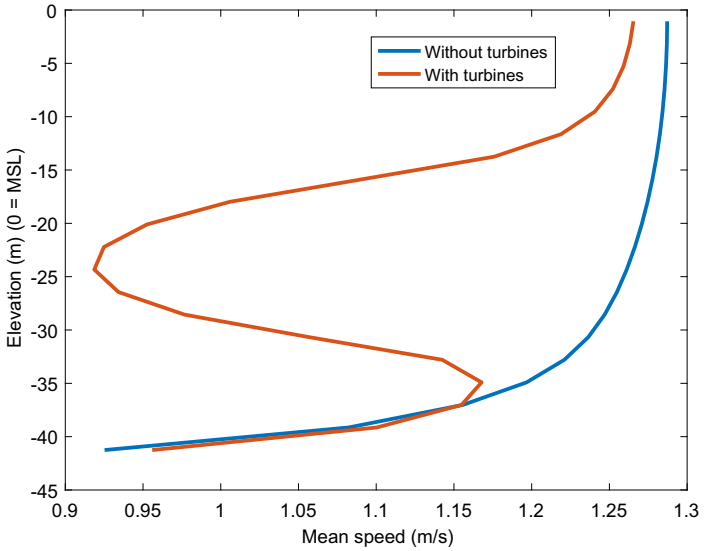

Fig. 6. Vertical speed profiles showing mean current speed over 24 h with and without TECs. The scenario used for "with turbines" is that of 100 TECs in the Naru strait, and the mesh element used is that with the greatest number of TECs in this scenario.

4. Interactions between channels

Fig. 7 shows the effect on mean depth-averaged current speeds of placing 100 TECs in the Naru Strait. A reduction in mean speed of up to 0.15 ms^{-1} through the TECs is seen, as expected, and an increase of 0.1 ms^{-1} occurs at the sides of the channel around the array. Adding impedance to the Naru Strait has only small effects on the other channels; mean speeds in the Tanoura Strait are affected by less than 0.02 ms^{-1}, and those in the Takigawara Strait by slightly more.

There are substantial areas of change to the north and south of the islands. These appear to be caused by changes in the positions of eddy structures that form at the downstream ends of the channels.

The equivalent maps for the other two channels are not shown, but the qualitative results are similar: reductions in mean speed in the exploited channel, but only small changes in other channels.

In order to provide a quantitative perspective on inter-channel effects a series of simulations was conducted, using only the M2 constituent, with 60 TECs in each channel and in each combination of channels. Comparisons were made between the maximum and mean power outputs of these channels, and in particular between the power provided by a scenario with two

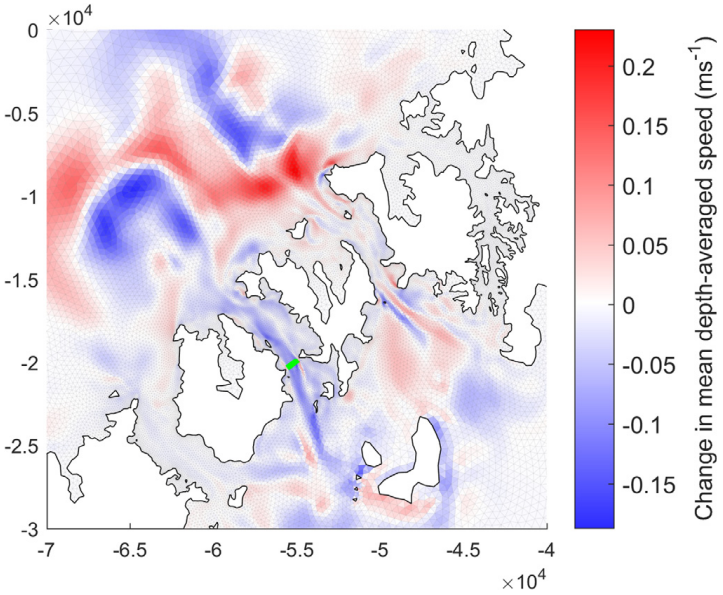

Fig. 7. Map showing the change in mean current speed over an M2 cycle in each mesh element as a result of adding 100 TECs to the Naru Strait. Green line shows location of turbines. Spatial coordinates are in metres in the "Japan Plane Rectangular" coordinate system zone CS1, EPSG ref 2443.

Table 3
Table showing mean and maximum outputs from different combinations of channels. 60 turbines were used in the exploited channels. Sums are on a per-timestep basis. The models were forced with M2 only, so the power estimates will be unrealistically low.

Channels exploited	Mean power (MW)	Max power (MW)
Tanoura alone	3.2	8.4
Naru alone	4.3	12.3
Takigawara alone	5.6	13.8
Sum of Tanoura & Naru separately	7.4	20.3
Tanoura & Naru together	7.5	20.5
Sum of Naru & Takigawara separately	9.9	25.2
Naru & Takigawara together	10.0	25.2
Sum of all 3 separately	13.1	32.7
All 3 together	13.2	32.3

or three channels together and the sum of the powers provided by each of those channels alone; interactions between the channels would result in differences between these values.

The results of these simulations are shown in Table 3, and show an increase in mean power of the order of 1% from using two channels together, indicating that some interaction does exist but that it is weak. The reason that "all 3 together" has a lower maximum power, but a higher mean power, than the sum of 3 separately, is unclear. It may relate to slight phase differences in the progress of the tide through the channels.

The low level of interaction between channels in Goto contrasts with the findings of Draper et al. [14] in the Pentland Firth, where the power available in each subchannel depended markedly upon the level of exploitation in the others.

5. Estimating the resource

Thus far simulations have been driven only by the M2 constituent in order to minimise computation time. However, only 65% of tidal energy in this region is in M2 (see Table 1), and so this does not give a useful estimate of the available power.

Four "candidate scenarios" were identified to be run for 28 days (plus spinup) with eight constituents. Three corresponded to low, medium and high levels of development, where for each scenario the turbines of each channel had the same capacity factor. This was intended to represent a similar level of return on investment in each channel. The actual values of the capacity factors are not meaningful due to both the unrealistic array layouts and the use of M2 only, and so are not reported here. In the fourth scenario, termed "optimum", each channel had the number of turbines that corresponded to the greatest mean power output attainable over an M2 cycle. This "optimum" number of TECs may be different with more constituents than with M2 only, and indeed may change with improved array layouts, but the number established here is used as an approximation that is available while keeping computing times low. The optimum number of TECs was calculated using simple parabolic interpolation between the highest-power scenario in Section 3 and the two either side of it.

It should be noted that this approach, where each channel is optimised independently and then the indicated level of deployment for each combined in a single model, is not generally applicable; it is appropriate in situations such as this one where the channels do not interact significantly with one another, and avoids the need for a more difficult simultaneous optimisation of all channels.

Each of the four scenarios was simulated with all three channels active and with turbines in the Takigawara Strait removed, thus including only the channels currently designated for development. Table 4 shows the mean and maximum power outputs of each scenario, as well as the ratio of mean to maximum power output.

Table 4
Table showing the number of turbines allocated to each channel in each scenario, and the predicted power outputs. Scenarios marked "A" use only the two channels designated for tidal development, while those marked "B" use all three.

Level of development	Number of turbines				Power (MW)		Mean/Max
	Tanoura	Naru	Takigawara	Total	Mean	Max	
Low (A)	5	42	0	47	4.70	23.50	20%
Medium (A)	46	88	0	134	9.67	48.38	20%
High (A)	130	190	0	320	14.08	69.01	20%
Optimum (A)	414	446	0	860	16.25	79.30	20%
Low (B)	5	42	73	120	11.93	49.49	24%
Medium (B)	46	88	112	246	17.73	75.16	24%
High (B)	130	190	182	502	22.34	97.35	23%
Optimum (B)	414	446	270	1130	24.53	106.78	23%

It is notable that at low levels of exploitation, the Takigawara Strait is predicted to give the most power at a given capacity factor, offering more than the other two channels combined in the "Low" scenario. At higher levels of development the Naru strait has more potential, matching the M2-only predictions in Fig. 5. In all scenarios, the ratio of mean:max power is higher when the Takigawara Strait is included than when it is not.

6. Exploring the maximum power in the Naru Strait

In earlier sections a realistic representation of a bottom-mounted TEC was used. As noted in Section 3, this only occupies a portion of the water column and allows the flow to divert over and under the rotor. Additionally, the limitation of not placing TECs in water shallower than 30 m allows large regions of horizontal diversion in some channels. In this section these restrictions are discarded in an effort to maximise the energy available in one channel – the Naru Strait – and look for any response in the other channels.

Three changes were made from earlier scenarios:

1. Instead of extracting momentum from the vertical layers intersected by the rotor, the same thrust was applied evenly across all layers. This simulates the way that energy extraction would appear in a two-dimensional model, and approximates a possible future scenario where a large number of smaller TECs, with lower individual thrust, are deployed at different depths throughout the water column. Such a deployment might be possible through designs such as the Triton device [25] that is planned for deployment in the Bay of Fundy. The same approach of "smearing" thrust throughout the water column was used by O'Hara Murray and Gallego [16] for some scenarios in their modelling of the Pentland Firth.
2. Instead of placing turbines along a line between the 30 m contours, the line was extended to run from coast to coast. This is unrealistic with a natural coastline, but could be achieved through civil engineering works to provide a minimum depth.
3. The thrust curve, previously a function of the current speed, was changed to a constant value of $C_T = 0.85$. This is because the presence of a cut-in speed would otherwise set a limit on how far the TECs could reduce the transport through the channel. This constant thrust coefficient is probably unrealistic, but it is certainly possible that future TECs will have cut-in speeds below the 1 ms^{-1} that was used to this point.

The M2-only simulations of the Naru Strait were repeated with these modifications. Additionally, transport through the northern mouth of the strait was recorded for each scenario. This was calculated by taking 200 sample points along a straight line from coast to coast, extracting mean depths and depth-averaged velocities normal to this line at each point, and using simple trapezoidal integration. The number of TECs was increased far beyond commercially realistic levels until a maximum power output was found past which the marginal change in power for extra TECs was negative. Fig. 8 shows the power output as a function of the number of turbines, and Fig. 9 relates it to the reduction in transport through the channel.

The maximum power available from the Naru Strait (M2 only) under these artificial conditions is predicted as approximately 36 MW, with between 600 and 800 turbines. This maximum occurs when transport through the channel is reduced by 36%; additional impedance, and further reductions in transport, beyond this point result in decreased power output.

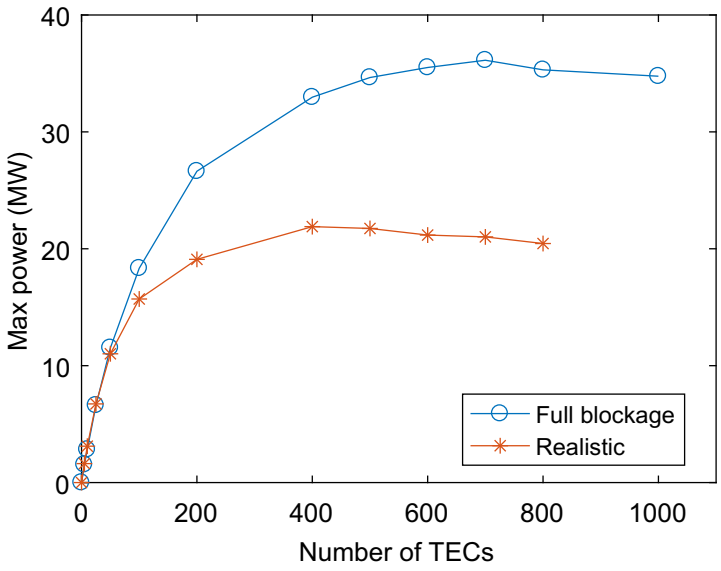

Fig. 8. Maximum output during a tidal cycle from M2 only with turbines evenly spread across full channel height and width, with no cut-in speed, compared to the realistic circumstances of Section 3.

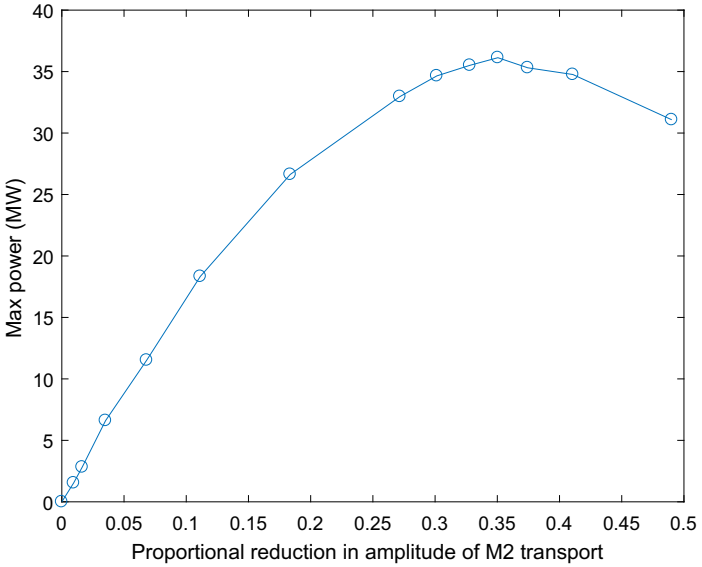

Fig. 9. Maximum power output during a tidal cycle from M2 only with turbines evenly spread across full channel height and width, with no cut-in speed, plotted against proportional reduction in the maximum transport.

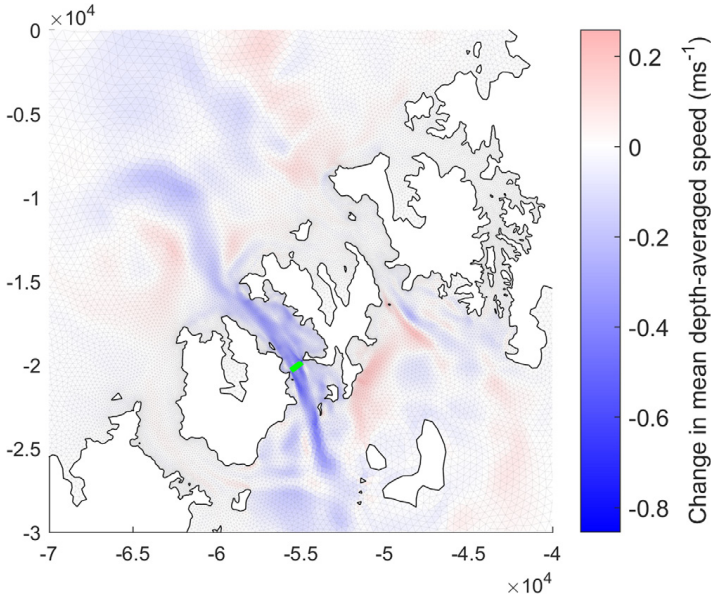

Fig. 10. Map showing the change in mean current speed over an M2 cycle in each mesh element as a result of adding 700 TECs to the Naru Strait, covering the full cross-section of the channel. Green line shows the location of turbines. Spatial coordinates are in metres in the "Japan Plane Rectangular" coordinate system zone CS1, EPSG ref 2443.

Fig. 10 shows the effect on mean current speeds of 700 turbines across the full height and width of the Naru Strait. The effects in the exploited strait are unsurprisingly much greater than those with 100 turbines in Fig. 7. Once again, it is clear that there is minimal effect on the other channels through the archipelago.

7. Discussion

7.1. Capacity of Naru Strait

When pushing the simulated Naru Strait to its limit of available power, through unrealistic array layouts and turbine parameters, maximum power (36 MW) was predicted with a reduction in transport through the channel of 36%. This may be compared against similar values found in modelling the Pentland Firth of 38% [16] and 42% [14], and is within the range of 29–42% that is given from theory by Garrett and Cummins [8].

The maximum power that can be removed from this channel can be compared to that predicted by the Garrett & Cummins model:

$$P_{lost} = \gamma \rho g a Q_{\max} \tag{5}$$

where γ is set to 0.20 based on a phase lag between head and transport, measured from the model, of 24°. Using values for $Q_{\max}$ and a from the model, this predicts a maximum power of 65 MW.

Garrett and Cummins noted that an assumption in their model was that there was no "back effect", *i.e.* the height difference between the ends of the channel is not increased by the imposition of the turbines. As shown in Fig. 11, there is a small but noticeable back effect in the case of the Naru Strait at optimal yield, which should cause an increase in both flow and yield. Our calculation of power includes an efficiency factor of 0.5 in (4), and once this is taken into account our value of 36 MW is indeed slightly greater than that suggested by the simple model. We find the level of agreement between these values encouraging.

Comparison with the realistic turbine setup used in earlier sections (Fig. 8) shows, as mentioned with respect to theory in Section 1.3, that spreading a given thrust evenly across a channel will maximise the available power. While this is difficult to realise with bottom-mounted TECs, and while allowing room for navigation, it is possible to design tidal energy projects to get as close to this ideal as possible given the available technology and constraints. It is likely that some of the benefit of filling the channel cross-section with TECs could be realised by using a lesser quantity of TECs and reducing the channel cross-section, or increasing the impedance of bypass areas, with passive civil engineering measures. However, we have not modelled this option and it may have severe environmental impacts.

The difference between the realistic and non-realistic scenarios, in terms of the vertical distribution of thrust, highlights the importance of using three-dimensional models for resource assessment work – a conclusion also reached by Goward Brown et al. [15].

7.2. Interaction between channels

In the Pentland Firth, Scotland, Draper et al. [14] found strong connections between subchannels; exploiting one led to flow diversion into others, and exploiting all together gave more power than the sum of each channel alone. This does not appear to be the case in the Goto Islands. While in some respects the channel systems of the Goto Islands and the Pentland Firth are quite similar, there are notable differences in the connectivity between their channels.

Both the Pentland Firth and the Goto channels run between large bodies of water that are strongly connected by other routes, and hence whose surface elevations cannot be altered by changes to the transport through the channels in question (although local changes around the channel mouth(s) are possible). Thus the head over the archipelago as a whole is approximately fixed, but the distribution of the head loss within the isles may be altered by the addition of TECs.

In the Pentland Firth, the three sub-channels merge at either end into a single main channel. If a single channel is exploited, then (assuming low impedance in unexploited channels) the maximum head available for generation is slightly greater than the undisturbed elevation change over the length of the divided subchannel. This is because once the head reaches this level it also affects the other subchannels and causes flow to divert into them, resulting in the strong interactions that are predicted in that region. The full potential of the elevation difference between the Atlantic and the North Sea is thus only available if all three subchannels are exploited together.

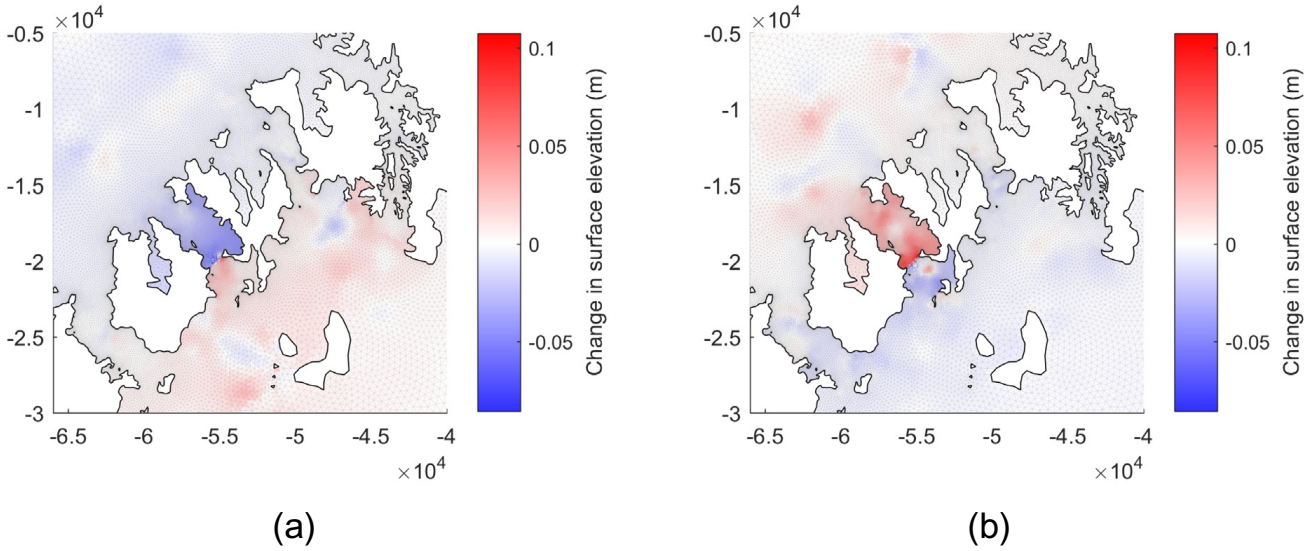

Fig. 11. Maps showing the change in surface elevations at single timesteps during (a) flood and (b) ebb, as a result of adding 700 turbines to the Naru Strait with full horizontal and vertical blockage.

In Goto, by contrast, the three main channels are almost entirely distinct, opening directly into the large bodies of water that they link without an intervening combined channel. As a result the full potential drop across the islands is available for energy extraction in any or all of the channels independently. Because there is no combined channel, and because the channel mouths are separated by significant distances, local elevation changes at one channel mouth are greatly diminished before they reach other channels. This results in very weak interactions between the straits.

Fig. 11 shows the changes in surface elevations as a result of adding 700 turbines to the Naru Strait. It is clear that the elevation gradient of that channel is dramatically altered – with water level upstream of the TECs increased and that downstream decreased, and most of the potential drop concentrated on the line of turbines. This effect does propagate weakly beyond the ends of the channel, in particular to the south, and this is probably because the bay-like shape of the archipelago here acts as a buffer between the Naru Strait and the South China Sea. However, this wider effect is small (generally < 1 cm) and there is almost no change in the elevation drop across the other straits.

While there seems to be a satisfactory explanation for the behaviors of the two locations mentioned here, it would be beneficial to establish a more general description of the interactions of parallel channels.

7.3. Resource estimation

Estimating resource in the channels of Goto is more straightforward than in some areas because the channels do not significantly affect one another. In other areas it would be necessary to perform a difficult optimisation with at least as many degrees of freedom as there are channels, but in Goto one can simply arrive at a resource estimate for each channel and sum them.

In this case the number of turbines required to obtain the greatest possible mean output from each channel is very high, and unlikely to be commercially viable. Therefore, in addition to optimising for mean power, we have selected three arbitrary scenarios which have equal capacity factors (CF) in each channel. These scenarios were each run for 28 days with eight tidal constituents, and we report a maximum (peak) and mean (time-averaged) power for each scenario. The total available power from the three channels reaches maxima of 49.5, 75.2, and 97.4 MW at low, medium and high levels of exploitation respectively. The mean power in each scenario is consistently 23–24% of the maximum. There is a greater difference between mean and maximum here than is common in European waters, which may make development slightly less economically attractive. The relatively high variation in this study area can be attributed to its mixed diurnal and semidiurnal tides.

The maximum available resource in just the Tanoura and Naru straits, which are those designated for tidal energy development, is 23.5, 48.4, or 69.0 MW for the three scenarios. It is interesting to note that the channel with the greatest output in the low deployment scenario (probably the most economically attractive scenario) is the Takigawara Strait, which is not within the designated development area. Omitting the Takigawara Strait also reduces the Mean:Max power ratio to 20%.

The Wakamatsu Strait has been excluded from this study due to its shallow depth. However, future generations of TEC design may be able to operate in a wider range of speeds and water depths [26], and hence may open this additional channel to exploitation as well as increasing the power available from the other straits due to lower cut-in speeds.

The relatively modest capacities of these channels means that, even at quite low levels of development, TECs' performances within any single channel will not be independent of one another. This will have implications for the management of the planned marine energy test centre, where a number of device developers might be testing different technologies within the same channel and may be affected by each others' activities.

8. Conclusions

In this work, numerical modelling has been used to predict the effects of tidal energy extraction from the Tanoura, Naru and Takigawara Straits in the Goto Islands using tidal energy converters (TECs) of the type planned by OpenHydro for deployment in the region. We estimate that between 24 and 79 MW of power is available, depending on the level of development, from the designated tidal energy zone, and that between 50 and 107 MW is available from all three channels together, using the currently proposed bottom-mounted turbines (Table 4). We note that the channel with the greatest potential at early stages of development (the Takigawara Strait) is not in the designated area.

As the level of energy extraction increases the marginal gain from adding additional turbines decreases, both because of a reduction in transport through the channel as a result of the increased impedance and because flow tends to divert over and under the rotors. TECs occupying more of the water column can use the same total rotor area more efficiently, which may be achievable in future using a larger number of smaller rotors.

Because modest levels of exploitation have noticeable effects on transport, managers and clients of the planned tidal energy test centre will need to be aware that the performance of a given device or array may be influenced by other test activities occurring in the same channel.

The maximum power that could, in principle, be generated from the Naru strait from M2 only is estimated to be 36 MW, in contrast with 22 MW using realistic technology. The necessary conditions for this higher output are unrealistic and undoubtedly uneconomical, but it is possible that civil engineering works to modify the channel, together with different designs of TEC, could permit a closer approach to this maximum. We have not studied the environmental consequences of such works.

There is little interaction between the channels in the Goto Islands, meaning that any or all of them can be exploited independently of the others. This may increase the attractiveness of the area for development, as – unlike Scotland's Pentland Firth – it is not necessary to develop all channels to realise the full potential of one. The interaction of parallel channels is sensitive to their geometry, and it would be useful to understand this more fully.

Acknowledgements

This work was made possible by a research exchange to Kyushu University, Japan. Travel funding was received from the MASTS pooling initiative (the Marine Alliance for Science and Technology for Scotland) and their support is gratefully acknowledged. MASTS is funded by the Scottish Funding Council (grant reference HR09011) and contributing institutions. We thank Kyushu University, and in particular Prof. Changhong Hu, for hosting the exchange and providing office space and computing time. The participation of David Woolf was enabled by the UK Engineering and Physical Sciences Research Council (EPSRC) through the EcoWatt2050 project (EP/K012851/1). The Ministry of Environment of Japan is gratefully acknowledged for permission to use observation data, which were obtained through the project for "Promotion of Realization of Tidal Current Power Generation", supported by the Ministry, in 2014 and 2015. The FVCOM model of the Goto Islands was originally developed and validated by Dr. Huihui Sun, and FVCOM itself is by Dr. Changsheng Chen. The first author thanks Dr. Patxi Novo Garcia for both technical assistance and friendship during his time in Japan.

References

[1] Statistics Japan, Japan Statistical Yearbook 2015, Table 11–14 "Electrical power generated", http://www.stat.go.jp/english/data/nenkan/65nenkan/1431-11.htm, accessed 2016-11-07, 2016.
[2] US Energy Information Administration, Japan: International energy data and analysis, https://www.eia.gov/beta/international/analysisincludes/countrieslong/Japan/japan.Pdf, accessed 2016-11-07, 2015.
[3] J.D. Bricker, M. Esteban, H. Takagi, V. Roeber, Economic feasibility of tidal stream and wave power in post-Fukushima Japan, Renewable Energy, ISSN 0960-1481. doi:https://doi.org/10.1016/j.renene.2016.06.049.
[4] World Nuclear Association, Nuclear Power in Japan, http://www.world-nuclear.org/information-library/country-profiles/countries-g-n/japan-nuclear-power.aspx, accessed 2016-11-07, 2016.
[5] M. Iwata, Nagasaki plans asia first major testing site for marine energy, Wall Street J. http://blogs.wsj.com/japanrealtime/2015/04/01/nagasaki-plans-asias-first-major-testing-site-for-marine-energy/, accessed 2016-11-07.
[6] OpenHydro, OpenHydro secures Japanese tidal turbine contract (press release), http://www.openhydro.com/OpenHydro/media/Documents/News accessed 2016-11-17, 2016.
[7] H. Sun, Y. Kyozuka, T. Yamashiro, Tidal current power potential in Goto Islands by observations and simulations, in: 2nd Asian Wave & Tidal Energy Conference (AWTEC), Tokyo, 2014.
[8] C. Garrett, P. Cummins, The power potential of tidal currents in channels, Proc. R. Soc. A: Math. Phys. Eng. Sci. 461 (2060) (2005) 2563–2572, https://doi.org/10.1098/rspa.2005.1494.
[9] R. Vennell, The energetics of large tidal turbine arrays, Renewable Energy 48 (2012) 210–219, https://doi.org/10.1016/j.renene.2012.04.018, 210–219, ISSN 09601481.
[10] C. Garrett, P. Cummins, The efficiency of a turbine in a tidal channel, J. Fluid Mech. 588, 1469–7645, ISSN 0022-1120. doi:https://doi.org/10.1017/S0022112007007781 .
[11] G.T. Houlsby, S. Draper, M.L.G. Oldfield, Application of linear momentum actuator disc theory to open channel flow, Tech. Rep. OUEL 2296/08, University of Oxford, Oxford, http://www.eng.ox.ac.uk/civil/publications/reports-1/ouel229608.pdf, 2008.
[12] J.F. Atwater, G.A. Lawrence, Power potential of a split tidal channel, Renewable Energy 35 (2) (2010) 329–332, https://doi.org/10.1016/j.renene.2009.06.023, ISSN 0960-1481.
[13] P.F. Cummins, The extractable power from a split tidal channel: an equivalent circuit analysis, Renewable Energy 50 (2013) 395–401, https://doi.org/10.1016/j.renene.2012.07.002, ISSN 0960–1481.
[14] S. Draper, T.A. Adcock, A.G. Borthwick, G.T. Houlsby, Estimate of the tidal stream power resource of the Pentland Firth, Renewable Energy 63 (2014) 650–657, https://doi.org/10.1016/j.renene.2013.10.015, ISSN 09601481.
[15] A.J. Goward Brown, S.P. Neill, M.J. Lewis, Tidal energy extraction in three-dimensional ocean models, Renewable Energy, ISSN 0960-1481. doi: https://doi.org/10.1016/j.renene.2017.04.032.
[16] R. O'Hara Murray, A. Gallego, A modelling study of the tidal stream resource of the Pentland Firth, Scotland, Renewable Energy, ISSN 0960-1481. doi: https://doi.org/10.1016/j.renene.2016.10.053.
[17] C. Chen, H. Liu, R.C. Beardsley, An unstructured grid, finite-volume, three-dimensional, primitive equations ocean model: application to coastal ocean and estuaries, J. Atmos. Oceanic Technol. 20 (1) (2003) 159–186, ISSN 0739-0572, doi: 10.1175/1520-0426(2003) 0200159:AUGFVT2.0.CO;2..
[18] G.L. Mellor, T. Yamada, Development of a turbulence closure model for geophysical fluid problems, Rev. Geophys. 20 (4) (1982) 851–875, https://doi.org/10.1029/RG020i004p0085, ISSN 1944-9208.
[19] J. Smagorinsky, General circulation experiments with the primitive equations, Monthly Weather Rev. 91 (3) (1963) 99–164, ISSN 0027–0644, doi: 10.1175/1520-0493(1963)0910099:GCEWTP2.3.CO;2..
[20] K. Matsumoto, T. Takanezawa, M. Ooe, Ocean tide models developed by assimilating TOPEX, POSEIDON altimeter data into hydrodynamical model: a global model and a regional model around Japan, J. Oceanogr. 56 (5) (2000) 567–581, https://doi.org/10.1023/A:1011157212596, ISSN 0916-8370, 1573-868X.
[21] Z. Yang, T. Wang, A.E. Copping, Modeling tidal stream energy extraction and its effects on transport processes in a tidal channel and bay system using a three-dimensional coastal ocean model, Renewable Energy 50 (2013) 605–613, https://doi.org/10.1016/j.renene.2012.07.024, ISSN 2214-1669.
[22] S. Baston, S. Waldman, J. Side, Modelling energy extraction in tidal flows, revision 3.1, in: TeraWatt Position Papers, MASTS, 75–107, ISBN 978-0-9934256-1-5, http://www.masts.ac.uk/media/166596/positionpapersterawatte-book.pdf, 2015.
[23] P. Jeffcoate, R. Starzmann, B. Elsaesser, S. Scholl, S. Bischoff, Field measurements of a full scale tidal turbine, Int. J. Marine Energy, ISSN 2214-1669. doi: https://doi.org/10.1016/j.ijome.2015.04.002.
[24] A. Bahaj, A. Molland, J. Chaplin, W. Batten, Power and thrust measurements of marine current turbines under various hydrodynamic flow conditions in a cavitation tunnel and a towing tank, Renewable Energy 32 (3) (2007) 407–426, https://doi.org/10.1016/j.renene.2006.01.01, ISSN 09601481.
[25] Black Rock Tidal Power, Technology, http://www.blackrocktidalpower.com/technology/, accessed 2016-11-10, n.d.
[26] M. Lewis, S.P. Neill, P.E. Robins, M.R. Hashemi, Resource assessment for future generations of tidal-stream energy arrays, Energy, ISSN 0360-5442. doi: https://doi.org/10.1016/j.energy.2015.02.038.

Numerical investigation of tidal resource & far field effects of energy extraction in Lashy Sound, Orkney

Simon Waldman[1], Jonathan Side[2], David Woolf[3]
International Centre for Island Technology
Heriot-Watt University
Back Road, Stromness
Orkney, KW16 3BA, UK
[1]smw13@hw.ac.uk; [2]j.c.side@hw.ac.uk; [3]d.k.woolf@hw.ac.uk

***Abstract*—Lashy Sound is a small channel in Orkney, Scotland, where a tidal stream energy development is planned. This study uses numerical modelling to investigate the energy resource of the Sound and the effects on the flow of removing this power. A new 3D regional-scale hydrodynamic model of the area was built using the MIKE software and was used to study Lashy Sound. A standard momentum sink approach was used to represent tidal energy converters. It is estimated that the maximum possible yield from this channel from the M2 tidal constituent alone is 23 MW mean and 61 MW peak power, although this would require an unrealistic and uneconomic arrangement of tidal turbines. The 30 MW capacity that is planned is predicted to be feasible, and the environmental effects of both large and small arrays are discussed.**

***Keywords*—MIKE, hydrodynamics, resource assessment, environmental impact**

I. Introduction

The Orkney archipelago in northern Scotland (Figure 1) contains a complex network of inter-island channels of which many, like the Pentland Firth to the south, experience rapid tidal flows and are hence of interest for tidal stream energy development. The strength of tidal activity in the region is due to the time taken for the M2 tidal wave to propagate around Scotland, and the resulting phase difference between the Atlantic and North Sea sides of Orkney [1].

Much research effort has been put into studying the Pentland Firth, which promises a great deal of tidal energy (e.g. [1]–[5]), and the large northern channel that includes the Fall of Warness, which is the location of the European Marine Energy Centre (EMEC) tidal test site (e.g. [6], [7]). Relatively little attention has been paid to the smaller channels within Orkney, what power may be available from them, and whether their exploitation could affect the major sites. In this work we use numerical modelling to examine one of these smaller channels, Lashy Sound, which has tidal energy development planned but has been largely uncovered in the academic literature.

In this paper we describe a new three-dimensional numerical hydrodynamic model of the Pentland Firth and Orkney Waters (PFOW) area that was developed to study Lashy Sound and its surroundings. We relate validation of this model, and describe early work on using the model to address two questions:

1) How much power is available from Lashy Sound?

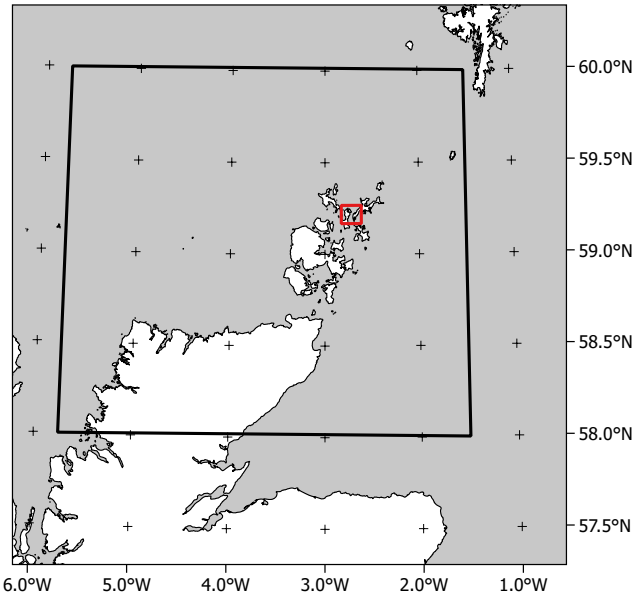

Fig. 1. Situation of Lashy Sound with respect to the Orkney archipeligo and the north of Scotland. The black box shows the extent of the model domain, and the red box highlights the location of Lashy Sound.

2) What effect would exploitation of Lashy Sound have on other channels?

II. The channel

Lashy Sound lies in the northern part of the Orkney archipeligo, situated between the isles of Eday to the west and Sanday to the east. At the southern end it becomes Eday Sound, which links to the large channel through Orkney that includes the Fall of Warness. Eday Sound also has a shallow and partially-obstructed exit to the east which sustains rapid flows at some states of the tide. To the north, Lashy Sound opens into open sea. For a labelled map of these channels, see Figure 2.

It is notable that Lashy Sound has a north-south orientation, while the dominant tidal flow across the archipeligo as a whole is between east and west. Strong currents in Lashy Sound must, therefore, stem not directly from the hydraulic forcing between

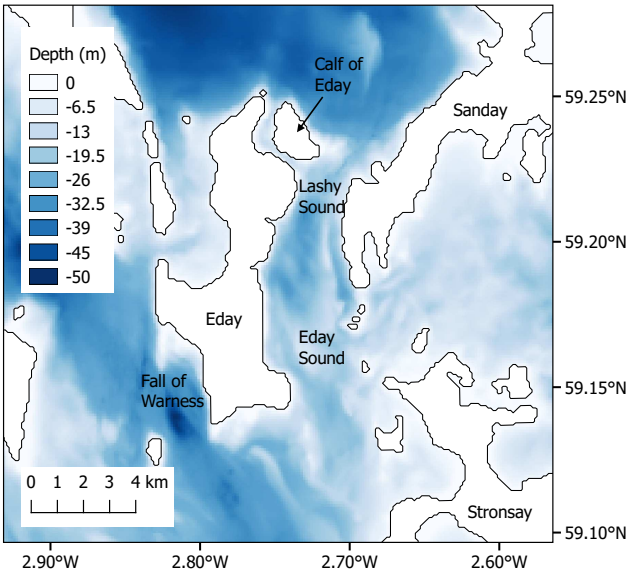

Fig. 2. Map showing the layout of Lashy Sound and the surrounding islands and channels. Colours show bathymetry with respect to mean sea level.

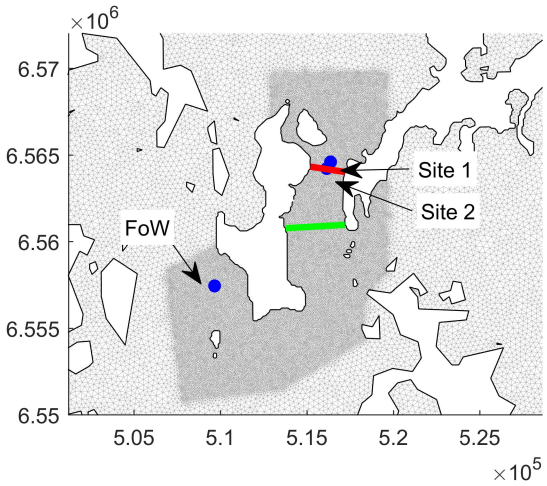

Fig. 3. Map showing the computational mesh for a part of the model. Blue points show the locations of ADCP surveys in the Fall of Warness (FoW) and Lashy Sound (Sites 1 & 2). The red line shows the transect used to place TECs, and the green line the transect used to measure transport through the channel. Spatial coordinates are in metres, referring to UTM Zone 30N.

the Atlantic and the North Sea, but from these links to other channels.

Lashy Sound itself is approximately $5\,\mathrm{km}$ long (measuring to the southern end of Sanday), between 3.5 and $1.5\,\mathrm{km}$ in width, and between 10 and $30\,\mathrm{m}$ deep. At the northern end a smaller subchannel of $<0.5\,\mathrm{km}$ width and approx. $10\,\mathrm{m}$ depth branches off the main stream and passes to the other side of a small island known as the Calf of Eday. Between the Calf of Eday and Sanday, which is the narrowest part of the main channel, is a narrow constriction in the deep channel with shallow water to either side.

Lashy Sound is of interest for commercial tidal energy generation, and developer Scotrenewables Ltd. has received an "agreement for lease" from The Crown Estate for a project of up to $30\,\mathrm{MW}$ capacity [8].

III. The Model

A. Description

MIKE by DHI is a commercial hydrodynamic modelling suite commonly used in industry. For this work the 2012 version of the 3D Flexible Mesh Hydrodynamic Module (MIKE 3 FM HD) was used. This uses an element-centred finite volume approach to solve the three-dimensional incompressible Reynolds-averaged Navier-Stokes equations under an assumption of hydrostatic pressure [9]. Turbulence is represented by eddy viscosity, which in this case was determined in the horizontal by the Smagorinsky formulation and in the vertical by a simple log law. Horizontal spatial discretization is on an unstructured mesh, while vertical discretization uses sigma layers. The simulation was run in barotropic mode without wind forcing.

Open boundaries were specified as clamped time-varying water levels, generated using the DHI global tidal model database [10]. This database is derived from TOPEX/POSEIDON altimetry and provides twelve tidal constituents at a spatial resolution of $0.125°$. Land boundaries were constrained to have zero velocity normal to the boundary, but permitted free slip along the shoreline. The seabed resistance was represented by a hydraulic roughness length, which was used as a calibration parameter.

The typical node spacing of the computational mesh was 80–$120\,\mathrm{m}$ in the area of interest around Lashy Sound and the Fall of Warness, increasing in stages to $8\,\mathrm{km}$ at the edges of the domain. Due to practical limits on computation time, finer meshes were not investigated. Bathymetric data within Lashy Sound was provided by Scotrenewables, while for the rest of the PFOW area a $20\,\mathrm{m}$ gridded dataset was provided by The Crown Estate (described in [11]). For the outer regions of the domain not covered by these sources, further bathymetry was supplied by SeaZone [12] on a grid of 6" resolution. The full extent of the model may be seen in Figure 1, and a part of the mesh in Figure 3.

B. Calibration & validation

The model was calibrated against ADCP records from the Fall of Warness, and validated against records from Lashy Sound. The choice was made to use different locations, rather than different times at the same locations, to ensure confidence in the validation as a measure of the model's skill in the area of interest.

Calibration was conducted by adjusting the seabed roughness parameter k_s to achieve the best possible match of current speed between measurements and predictions. A value of $k_s = 0.1\mathrm{m}$ was chosen.

The model was validated against two ADCP surveys in the area of interest, (marked Site 1 & Site 2 in Figure 3), using a one-month period in February and March 2012. Comparisons

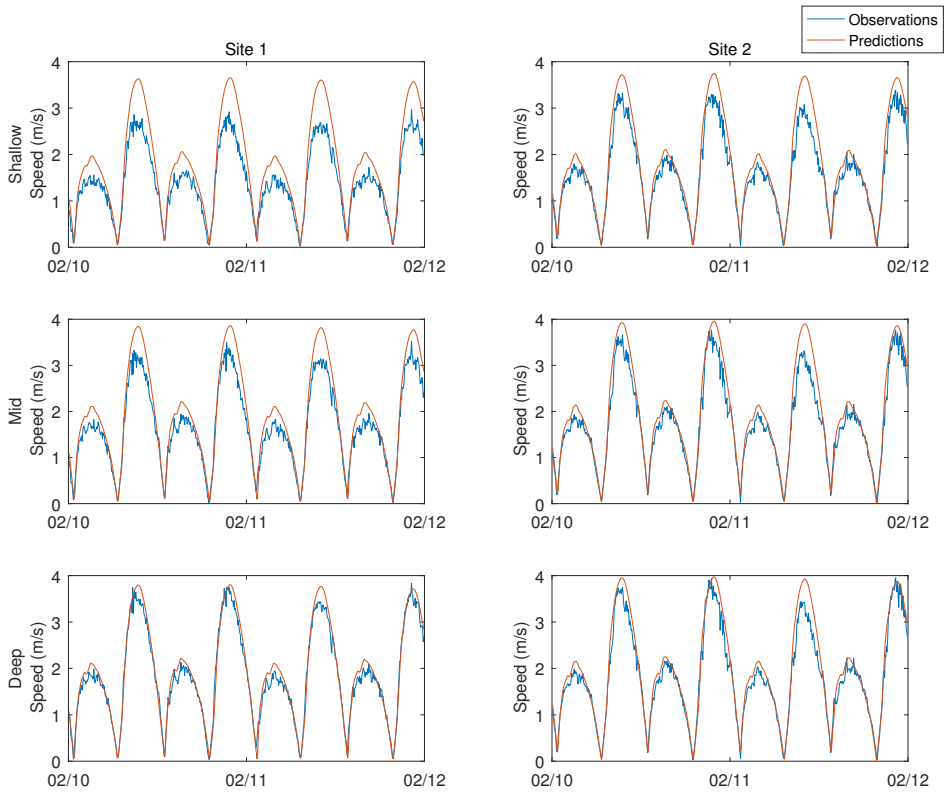

Fig. 4. Time series comparison of current speed between model and observations at three depths. For legibility, only 48 hours at spring tides are shown.

TABLE I
VALIDATION STATISTICS, COMPARING PREDICTIONS OF THE MIKE 3 MODEL TO OBSERVATIONS IN LASHY SOUND OVER A ONE MONTH PERIOD.

		Site 1		Site 2	
		u	v	u	v
RMSE (m/s)	Shallow	0.341	0.298	0.134	0.375
	Mid	0.162	0.294	0.166	0.426
	Deep	0.213	0.260	0.257	0.430
Scatter index	Shallow	0.577	0.304	0.175	0.372
	Mid	0.231	0.256	0.202	0.386
	Deep	0.278	0.206	0.302	0.375
R^2	Shallow	0.980	0.986	0.978	0.982
	Mid	0.983	0.988	0.979	0.983
	Deep	0.983	0.989	0.980	0.984
Bias (m/s)	Shallow	0.077	0.107	0.012	0.040
	Mid	−0.010	0.092	−0.043	0.057
	Deep	−0.117	0.074	−0.092	0.058

of u and v velocity components were made at three depths corresponding to approximately 20%, 50% and 80% of the water column. Statistical measures of agreement may be viewed in Table I, and visual comparisons in Figures 4–6.

In Lashy Sound the model provides accurate predictions at most states of the tide. However, it significantly overpredicts the highest current speeds near the surface, especially at Site 1. A "jet" of accelerated flow is predicted downstream of the constriction at the northern end of Lashy Sound, and it is possible that the model is incorrectly predicting the width or the strength of this jet. The overprediction may also relate to incorrect simulation of the flow through the subchannel to the west of the Calf of Eday, which meets the main channel close to ADCP Site 1. As this subchannel is shallower than the main channel, its effects would be most apparent near the surface. These hypotheses are presented as possible explanations for the difference seen, but neither can be tested with the available measurements.

The measured and predicted phases show a good match, and the asymmetry of the flow in the channel is reproduced well. At Site 1 the flow direction is predicted well, but at Site 2 there is a modest discrepancy.

Frequency-domain validation was conducted using the same predictions and measurements. For reasons of space it is only shown here in textual, depth-averaged, form (Table II). Phases and amplitudes of the major constituents, as given by `t_tide` [13], all match within 95% confidence intervals except for M2 amplitudes at Site 2. These M2 amplitudes are underpredicted in the u direction and overpredicted in the v direction, which matches the small discrepancy in flow direction seen in the time-domain analysis. It is interesting to note that harmonic analysis is not able to fully represent the flow in this area, with `t_tide` typically reporting that only 95% of the signal is explained by harmonic constituents. Since this aharmonic flow occurs in the model as well as the measurements, it cannot be attributed to weather effects. It probably relates to the jet of accelerated flow

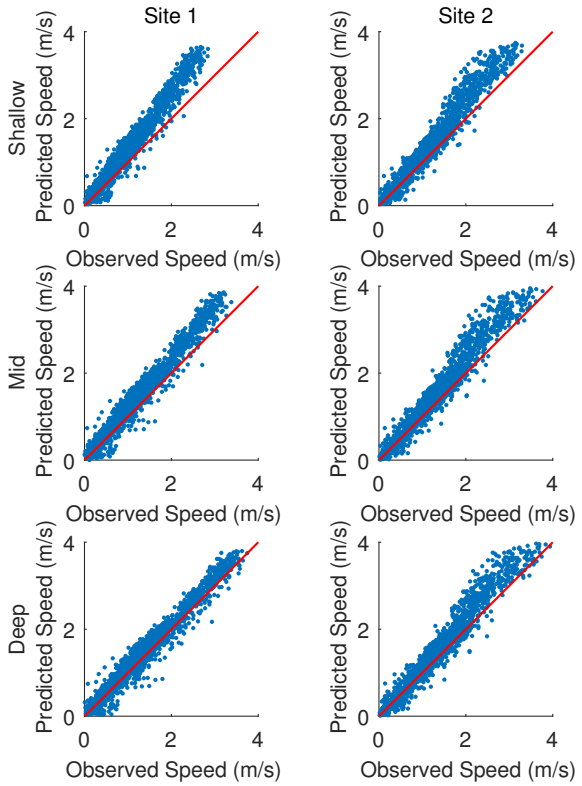

Fig. 5. Scatter plots comparing current speed between model and observations at three depths. For legibility, a regular sample of every fifth time step is shown. This results in a plotted time step of 25 minutes, and hence extreme values may be clipped slightly. The red lines represent 1:1 relationships.

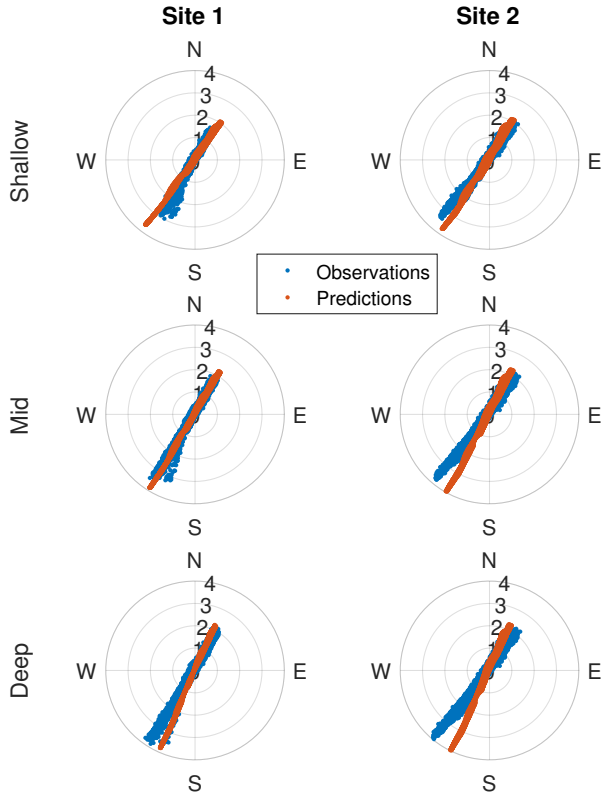

Fig. 6. Hodographs comparing measured and predicted velocities at three depths. Direction is that in which the flow is travelling. Radial axis indicates current speed in m/s.

TABLE II
COMPARISON OF DEPTH-AVERAGED PREDICTIONS AND OBSERVATIONS IN FREQUENCY DOMAIN AT TWO ADCP LOCATIONS IN LASHY SOUND.

		Amplitude (m)		Phase (°)	
		Model	ADCP	Model	ADCP
M2 u	Site 1	1.132	1.064	56.9	59.8
	Site 2	1.040	1.220	59.3	62.3
M2 v	Site 1	1.881	1.784	55.6	56.9
	Site 2	1.954	1.608	56.5	58.1
S2 u	Site 1	0.412	0.406	93.5	96.2
	Site 2	0.378	0.461	95.4	96.9
S2 v	Site 1	0.680	0.691	92.7	93.6
	Site 2	0.709	0.612	93.7	94.7

mentioned above, which introduces asymmetry that cannot be represented by sine waves at astronomical frequencies.

IV. ESTIMATING RESOURCE

A. Method

The approach taken in this work was not to consider realistic array layouts, but to arrive at a figure for the maximum power obtainable from this channel regardless of engineering or economic considerations. It is known that the most efficient way of extracting energy from a channel is to spread turbines evenly across its whole cross-sectional area to prevent any bypass flow [14], [15].

The MIKE software represents tidal energy convertors (TECs) as sub-grid momentum sinks based on actuator disc theory, and requires that they be specified in terms of hub location, diameter, and thrust coefficient. A transect was identified that crossed Lashy Sound at the narrowest point at which it remains a single channel (i.e. south of the split around the Calf of Eday; see Figure 3), and turbine locations were placed, evenly spaced, along this line.

The use of a single design of TEC would result either in large regions of horizontal bypass flow, at the sides of the channel where the depth was insufficient for the rotor, or — if smaller diameter turbines were used — a great deal of vertical bypass in the middle as flow diverted over and under the rotors. To avoid this bypass flow, the diameter of each turbine was calculated to fit the depth at that location subject to maximum and minimum diameters of $20\,\mathrm{m}$ and $4\,\mathrm{m}$ respectively, and with a $3\,\mathrm{m}$ allowance for bottom clearance and tidal range. However, this change in rotor diameters would have led to evenly spaced turbines having unequal gaps between them, which would have caused changes in local blockage across the channel. To address this, additional rotors were added to each location as necessary to normalise the local blockage ratio

to the same as that of the largest turbine. Although clearly not physically realistic at a sub-grid level, at the resolution of the model this is equivalent, in all but the sparsest layouts, to placing the smaller rotors closer together.

A realistic turbine would be expected to have a thrust coefficient that varied as a function of the flow speed. However, when exploring the maximum potential of a channel this can be problematic, because if the turbines have a cut-in speed they are unable to reduce the flow in the channel below this speed. For this work, therefore, the turbines were given a fixed thrust coefficient of 0.85. For simplicity, no supporting structures were included in the model.

A range of levels of exploitation were simulated, from 10 to 2400 TEC locations. In the more heavily exploited scenarios a single row of turbines is unrealistic, but should be considered as representing a two-dimensional array. Because this single-row layout is unlikely to be optimal, the actual number of TECs should be used only for comparative purposes, and it is not intended that capacity factors or matters of economic viability should be considered.

In order to allow a large number of scenarios to be explored in limited computation time, only the M2 tidal constituent was used. This allows the use of just 12.4 hours of output — a single M2 cycle — as a representative time period. It was determined empirically that the model required 3 days of spinup time before its predictions in Lashy Sound became fully periodic, so each scenario was run for 4 days of model time and the output data taken from the first 12.4 hours of the fourth day.

Rotor thrust is reported by the MIKE software on a per-turbine basis by

$$F = \tfrac{1}{2}\rho C_T A|\boldsymbol{u}|\boldsymbol{u} \tag{1}$$

where F is thrust, ρ is the density of the water, C_T is the thrust coefficient, A is the area of the rotor and $\boldsymbol{u}$ is the flow velocity. In this work it was assumed that all rotors face into the flow at all times. Power produced was estimated as a post-processing step using

$$P = C_C F|\boldsymbol{u}| \tag{2}$$

where C_C is a coefficient that represents the conversion losses between kinetic energy in the flow and electricity. A value of 0.5 was assigned to C_C based on experimental results reported by Jeffcoate *et al.* [16]. The chosen values of $C_T = 0.85$ and $C_C = 0.5$ are equivalent to a power coefficient of $C_P = 0.425$.

It is acknowledged that some inaccuracy is inherent in using the same value of $|\boldsymbol{u}|$, representing an entire mesh element, in both of the equations above. More correctly, the velocity in (1) should be the free-stream velocity and that in (2) should be the velocity at the turbine, neither of which is known to the model [17], [18]. We plan to address this discrepancy in future work.

Transport through the channel was recorded for each scenario. This was calculated by taking 200 sample points along a straight line from coast to coast (Figure 3), extracting mean depths and depth-averaged velocities normal to this line at each point, and using simple trapezoidal integration.

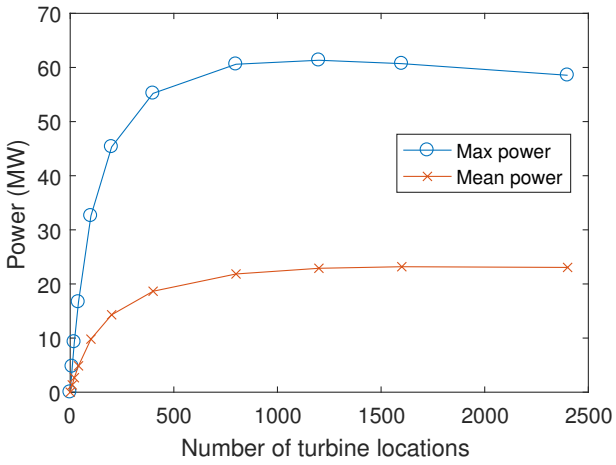

Fig. 7. Mean and maximum output over a M2 tidal cycle, with respect to the number of TEC locations.

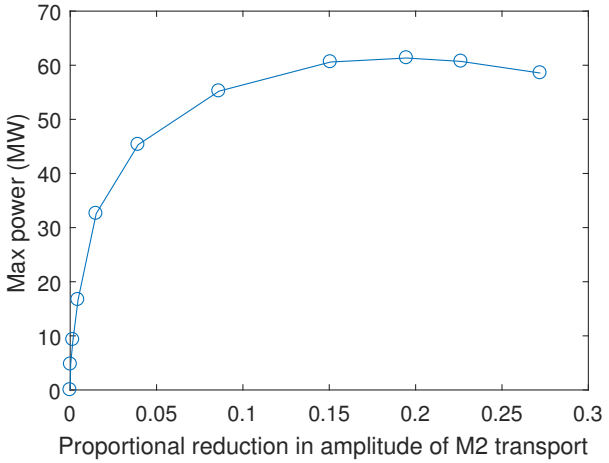

Fig. 8. Maximum output over a M2 tidal cycle, with respect to proportional reduction in volume transport through the channel.

B. Results

Figure 7 shows the maximum and mean power output of the various scenarios over a single M2 cycle. Figure 8 relates the maximum output to the maximum reduction in volume transport through the channel. There is a near-linear relationship between TEC numbers and output at low levels of exploitation, beyond which the marginal gain in power for each new turbine location decreases as the flow speed through the channel is reduced. At approximately 1200 TEC locations the marginal gain from additional turbines turns negative, as the reduction in power from the loss of flow speed outweighs the effect of adding more generating capacity. This point therefore represents the maximum yield available from the channel, and corresponds to mean and maximum outputs of 23 MW and 61 MW respectively. This is achieved with a reduction in transport of approximately 20%.

V. Far field effects

Two scenarios were studied: The first is that identified above with 1200 TEC locations and a peak output of 61 MW which, since it is the most energy that can be extracted, should be the "worst case" for environmental impacts. The second is one with 100 TEC locations and a peak output of 33 MW, which is close to the 30 MW that is planned for Lashy Sound. In each case the flow was compared to that with no TECs, and the effects on mean depth-averaged current speed are shown in Figure 9.

The 61 MW scenario results in a large reduction in mean current speed through the TEC array itself, for the length of Lashy and Eday Sounds, and for some kilometres beyond. Some flow acceleration around the array is also visible, which has arisen because of the lower limit that was placed on the size of a rotor and hence the absence of simulated turbines from water shallower than 7 m.

Outside the immediate flow of Lashy Sound, effects are small but extant. There is a very small increase in speeds in the Fall of Warness, of up to $5\,\mathrm{cm\,s^{-1}}$. There are more significant increases in flow along the south coast of Eday (up to $0.2\,\mathrm{m\,s^{-1}}$) and through the channel between Sanday and Stronsay (up to $0.5\,\mathrm{m\,s^{-1}}$) at certain stages of the tidal cycle. These changes are not visible in the figure as this only shows a temporal average.

Figure 10 shows changes in the maximum and minimum water level in each cell in the 61 MW scenario. The line of turbines is very clear in these maps because a 15 cm increase in the amplitude of M2 is produced north of them. This increase in range is not replicated south of the tidal fence; instead, the southern part of Lashy and Eday Sounds show a small increase in both minimum and maximum sea level, with the maximum increasing by up to 7 cm on the coast of Sanday.

Effects on water levels beyond Lashy and Eday sounds are small, but reductions in tidal range of the order of 1–2 cm are predicted along substantial parts of the Sanday and Stronsay coasts, as well as the south coast of Eday and even parts of Shapinsay, Rousay and the West Mainland (not shown in figure). Mid-channel water levels in the Fall of Warness are affected by a similar amount.

In the 33 MW scenario the magnitude of the effects is lower and impacts beyond Lashy and Eday Sounds, including those on other tidal sites, are predicted to be negligible. Within Lashy Sound an increase in maximum sea level at the coasts of up to 2 cm may be expected (not shown), and the reduction in mean current speed in line with the array is approximately $0.3\,\mathrm{m\,s^{-1}}$ in mid-channel (see Figure 9b).

VI. Discussion

In these simulations, the maximum power obtainable from the channel is achieved with a reduction in transport of 20%. This is well outside the range of 29–42% that is given by the simple analytic model of Garrett and Cummins [19] (hereafter GC05), and substantially below figures that have been identified for the Pentland Firth by numerical modelling [4], [5].

Part of this discrepancy is due to the presence of bypass flow around the ends of the simulated TEC array where the water is too shallow for the minimum rotor diameter that was specified. Part may also be due to the GC05 model not being fully applicable.

A limitation that Garret and Cummins noted in their model was that it did not allow for the driving head across a channel to change as a result of energy extraction. This is a valid assumption for their scenario of a single channel connecting two large basins, but does not hold for the more complex situation studied here. In fact surface elevations near to the northern mouth of Lashy Sound, and within the southern part of Eday Sound, are predicted to change by 2–8 cm at some stages of the tide in the maximum yield scenario. The complexity of the surrounding archipeligo may also mean that, even when the model is driven with only the M2 tidal constituent, Lashy Sound itself experiences more complex forcing. Further study of the dynamics of this channel, with and without energy extraction, is planned for the future.

The agreement to lease that has been granted by The Crown Estate for this area permits development of a tidal array with output capacity of 30 MW. Our work indicates that this is feasible from a physical perspective. Since 30 MW of maximum power is reached in the near-linear part of Figure 7 it is likely to be attainable with a modest number of TECs, contributing to a high capacity factor, which is a favourable contribution to any study of the economic viability of the site. However, the asymmetry of current velocities in this channel leads to a relatively low ratio of mean to maximum power output, even with M2 only, of around 30%, and this will act to reduce the capacity factor. A more detailed study, using realistic array layouts and more tidal constituents, would of course be required to establish an accurate figure.

In the simulation with maximum yield, hence that with the greatest environmental impacts, energy extraction results in changes to the flow over a moderate area, including the waters south of Eday and those between Sanday and Stronsay. It appears that this path acts as an alternate route into which a proportion of the flow diverts when Lashy Sound is obstructed. In this "worst case" scenario maximum water levels on the Eday and Sanday coasts are increased by up to 15 cm. This change could have implications for intertidal habitats and perhaps for human activities, but such effects are outside the scope of this study. Smaller effects, unlikely to be of any importance, are predicted as far afield as the West Mainland of Orkney.

In the more realistic scenario approximating the planned 30 MW of peak power, the increase in maximum water level is reduced to 2 cm along the coasts of the northern part Lashy Sound, and no significant effects are predicted beyond this area. As with any tidal stream development, changes to the flow pattern within the Sound would have modest effects on bed stress, and hence potentially on benthic ecology. These effects on bed stress would need to be investigated as part of the environmental impact assessment for any development.

It is important to note that roughly doubling the power extracted from 33 MW to 61 MW involves a 12-fold increase

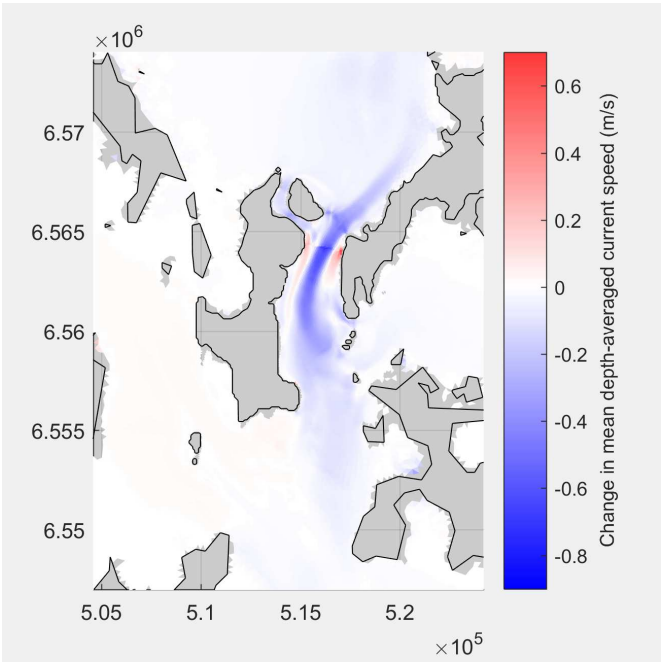

(a) 1200 TEC locations, max 61 MW.

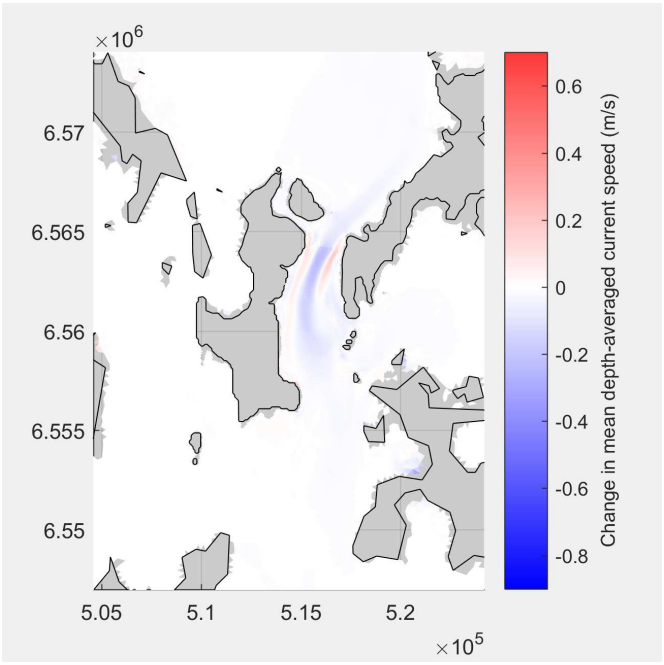

(b) 100 TEC locations, max 33 MW.

Fig. 9. Map showing the mean effect on depth-averaged current speed, over a single M2 cycle, of extracting the (a) maximum available power, and (b) approximately the planned power, from Lashy Sound. Speed differences are calculated on a per-timestep basis before the temporal mean is taken. Spatial coordinates are in metres, referring to UTM Zone 30N.

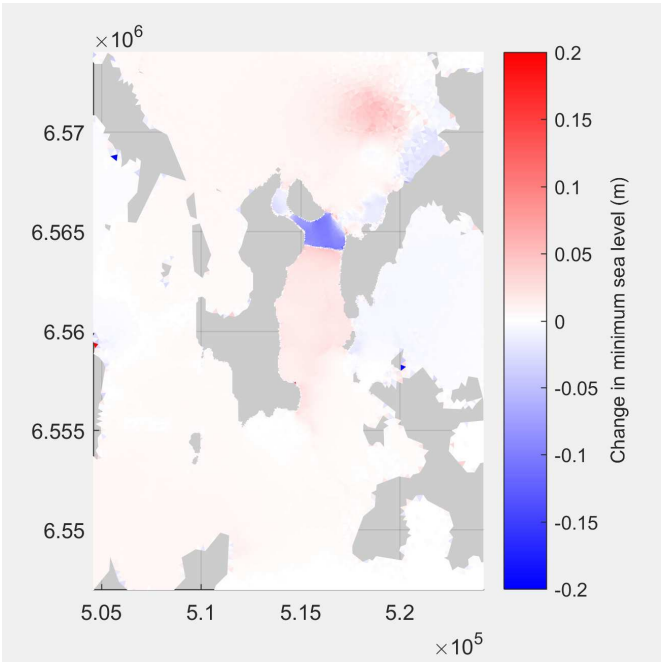

(a)

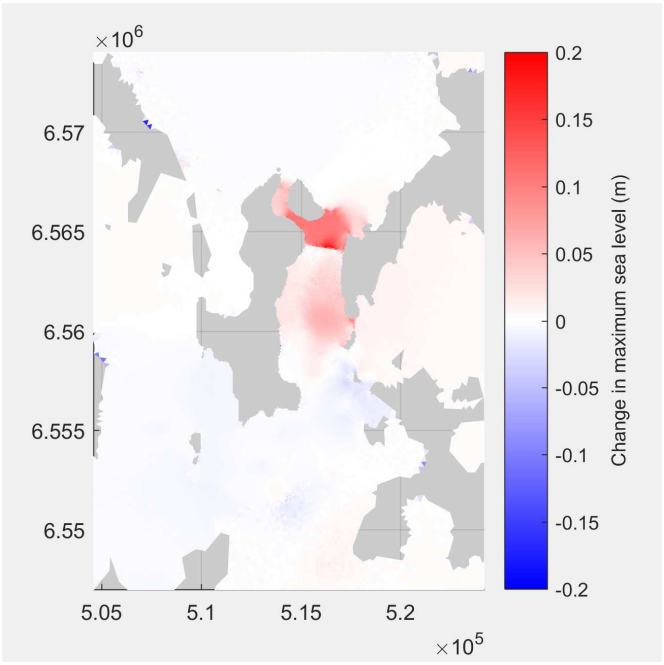

(b)

Fig. 10. Maps showing the change in the (a) minimum and (b) maximum surface elevation of each cell at any time during an M2 cycle as a result of extracting the maximum available power (peak 61 MW) from Lashy Sound. Spatial coordinates are in metres, referring to UTM Zone 30N. Note that both of these plots correspond to the scenario shown in Fig. 9a; the effects on elevation of the second scenario, which are small, are not shown for space reasons.

in the area of turbines and a similarly disproportionate increase in environmental impacts. Although this study was not intended to address economic matters, it is clear that reaching the higher level of exploitation — the maximum physically possible in the channel — would be economically prohibitive and hence is extremely unlikely to ever occur.

Since a realistic array would spread its thrust less evenly across the channel than the continuous fence arrangement modelled here, it would lose more power to wake mixing [15]. This means that the total power lost from the channel, and hence the resulting environmental effects, might be greater than those shown here for the same electrical output. However, since the effect on maximum transport predicted here for a 33 MW output is less than 1.5%, the far-field effects of a well-designed array are still likely to be small.

VII. Conclusions

In this work a new 3D hydrodynamic model of the Pentland Firth and Orkney Waters area was developed to study the area around Lashy Sound. Validation showed good general performance, although there was an unexplained overprediction of the highest flow speeds.

Simulations using only the M2 tidal constituent indicate that the maximum yield available from Lashy Sound, using unrealistically large numbers of turbines that form a nearly complete fence, is a mean power of 23 MW with a peak of 61 MW. This is achieved with a reduction in volume transport of 20%. A mean power of 10 MW and peak of 33 MW, similar to the array that is planned in the strait, can be achieved with a 1.5% reduction in transport.

These powers will be underestimates of the true values, because only the M2 tidal constituent was simulated and because some bypass flow was permitted in shallow water at the sides of the channel. A realistic 30 MW array would lose more energy to wake mixing than the continuous fence arrangement modelled here, and would hence cause a slightly greater reduction in transport for the same power output.

In the 61 MW scenario very small environmental impacts are predicted over a wide area, and increases in maximum sea level of up to 15 cm within Lashy Sound are estimated. We emphasise that this scenario is a hypothetical one which is very unlikely to be realised.

In the 33 MW scenario significant effects do not extend beyond Lashy and Eday Sounds. Changes to the flow patterns within Lashy Sound would have modest effects on bed stress in the area, and an increase in maximum sea level of up to 2 cm is predicted on the coasts of Eday and Sanday close to the development site.

Acknowledgments

We are grateful to Scotrenewables Ltd. for bathymetry and coastline data for Lashy Sound and for the ADCP records used for validation. Neither the specification of turbines nor any of the layouts used herein are intended to represent Scotrenewables' technology or their plans for the area. We thank The Crown Estate for access to their gridded bathymetry for the region, and the UK Hydrographic Office for access to the VORF dataset. Support was provided by the EPSRC-funded TeraWatt and EcoWatt2050 UKCMER Grand Challenge projects (grant numbers EP/J010170/1 & EP/K012851/1 respectively).

References

[1] M. C. Easton, D. K. Woolf, and P. A. Bowyer, "The dynamics of an energetic tidal channel, the Pentland Firth, Scotland," *Continental Shelf Research*, vol. 48, pp. 50–60, Oct. 2012. [Online]. Available: http://www.sciencedirect.com/science/article/pii/S0278434312002233

[2] S. Baston and R. E. Harris, "Modelling the Hydrodynamic Characteristics of Tidal Flow in the Pentland Firth," in *9th European Wave & Tidal Enegy Conference*, 2010.

[3] T. A. A. Adcock, S. Draper, G. T. Houlsby, A. G. L. Borthwick, and S. Serhadlioglu, "The available power from tidal stream turbines in the Pentland Firth," *Proceedings of the Royal Society A: Mathematical, Physical and Engineering Sciences*, vol. 469, no. 2157, pp. 20 130 072–20 130 072, Jul. 2013. [Online]. Available: http://rspa.royalsocietypublishing.org/cgi/doi/10.1098/rspa.2013.0072

[4] S. Draper, T. A. Adcock, A. G. Borthwick, and G. T. Houlsby, "Estimate of the tidal stream power resource of the Pentland Firth," *Renewable Energy*, vol. 63, pp. 650–657, 2014. [Online]. Available: http://linkinghub.elsevier.com/retrieve/pii/S0960148113005466

[5] R. O'Hara Murray and A. Gallego, "A modelling study of the tidal stream resource of the Pentland Firth, Scotland," *Renewable Energy*, 2016. [Online]. Available: http://www.sciencedirect.com/science/article/pii/S0960148116309181

[6] J. Lawrence, H. Kofoed-Hansen, and C. Chevalier, "High-resolution metocean modelling at EMEC's (UK) marine energy test sites," in *Proc. of the 8th European Wave and Tidal Energy Conference*, vol. 7, 2009. [Online]. Available: http://mhk.pnnl.gov/wiki/images/e/e7/Lawrence_2009.pdf

[7] S. P. Neill, M. R. Hashemi, and M. J. Lewis, "The role of tidal asymmetry in characterizing the tidal energy resource of Orkney," *Renewable Energy*, vol. 68, pp. 337–350, Aug. 2014. [Online]. Available: http://www.sciencedirect.com/science/article/pii/S0960148114000998

[8] Scotrenewables, "Award of 'Agreement for Lease' for Lashy Sound Demonstrator Project and SR250 Reaches and Exceeds Rated Power," Nov. 2012. [Online]. Available: http://www.scotrenewables.com/news/57-award-of-agreement-for-lease-for-lashy-sound-demonstrator-project-and-sr250-reaches-and-exceeds-rated-power-november-2012

[9] DHI, "MIKE 21 & MIKE 3 Flow Model FM Hydrodynamic & Transport Module Scientific Documentation," 2012.

[10] Y. Cheng and O. B. Andersen, "Improvement of global ocean tide models in shallow water regions," in *Altimetry for Oceans & Hydrology OST-ST Meeting*, vol. Poster, SV.1-68 45, Lisbon, 2010. [Online]. Available: http://www.space.dtu.dk/english/~/media/Institutter/Space/English/scientific_data_and_models/global_ocean_tide_model/yongcuncheng_no_sv_1_68_45.ashx

[11] R. B. O'Hara Murray and A. Gallego, "Data review and the development of realistic tidal and wave energy scenarios for numerical modelling of Orkney Islands waters, Scotland," *Ocean & Coastal Management*, 2017. [Online]. Available: http://www.sciencedirect.com/science/article/pii/S0964569117302405

[12] SeaZone Solutions Ltd., obtained via EDINA Marine Digimap Service, "Hydrospatial bathymetry, 6" resolution, Tiles: NW25800020/40/60," 2008. [Online]. Available: http://edina.ac.uk/digimap

[13] R. Pawlowicz, B. Beardsley, and S. Lentz, "Classical tidal harmonic analysis including error estimates in MATLAB using T_tide," *Computers & Geosciences*, vol. 28, no. 8, pp. 929–937, Oct. 2002.

[14] C. Garrett and P. Cummins, "The efficiency of a turbine in a tidal channel," *Journal of Fluid Mechanics*, vol. 588, Sep. 2007. [Online]. Available: https://www.cambridge.org/core/journals/journal-of-fluid-mechanics/article/efficiency-of-a-turbine-in-a-tidal-channel/0B669CAB1CC61009F51577A774F3C9DD

[15] R. Vennell, "The energetics of large tidal turbine arrays," *Renewable Energy*, vol. 48, pp. 210–219, Dec. 2012. [Online]. Available: https://www.sciencedirect.com/science/article/pii/S0960148112002595

[16] P. Jeffcoate, R. Starzmann, B. Elsaesser, S. Scholl, and S. Bischoff, "Field measurements of a full scale tidal turbine," *International Journal of Marine Energy*, 2015. [Online]. Available: http://www.sciencedirect.com/science/article/pii/S221416691500017X

[17] S. C. Kramer and M. D. Piggott, "A correction to the enhanced bottom drag parameterisation of tidal turbines," *Renewable Energy*, vol. 92, pp. 385–396, Jul. 2016. [Online]. Available: http://linkinghub.elsevier.com/retrieve/pii/S0960148116301239

[18] S. Waldman, G. Genet, S. Baston, and J. Side, "Correcting for mesh size dependency in a regional model's representation of tidal turbines," in *Proceedings of the 11th European Wave & Tidal Energy Conference (EWTEC) 2015*, Nantes, France, Sep. 2015.

[19] C. Garrett and P. Cummins, "The power potential of tidal currents in channels," *Proceedings of the Royal Society A: Mathematical, Physical and Engineering Sciences*, vol. 461, no. 2060, pp. 2563–2572, Aug. 2005. [Online]. Available: http://rspa.royalsocietypublishing.org/cgi/doi/10.1098/rspa.2005.1494

References

ABP Mer (2007). *Quantification of Exploitable Tidal Energy Resources in UK Waters*. Tech. rep. ABP Mer. URL: http://www.abpmer.co.uk/allnews1623.asp.

– (2008). *Atlas of UK Marine Renewable Energy Resources*. Tech. rep. URL: http://www.renewables-atlas.info/.

– (2012). *Pentland Firth and Orkney Waters Hydrodynamic Modelling: Model Calibration*. Tech. rep. R1935.

ABPmer (Aug. 2012). *Pentland Firth and Orkney Waters Strategic Area : Preparation of bathymetry to support modelling studies*. R. 1963.

Adcock, T. A. A., Borthwick, A. G. L. and Houlsby, G. T. (2011). "The Open Boundary Problem in Tidal Basin Modelling with Energy Extraction". In: *Proceedings of the 9th European Wave and Tidal Energy Conference. Southampton, UK*. URL: http://www.see.ed.ac.uk/~shs/EWTEC%202011%20full/papers/315.pdf (visited on 09/07/2013).

Adcock, T. A. A., Draper, S., Houlsby, G. T., Borthwick, A. G. L. and Serhadlioglu, S. (July 2013). "The available power from tidal stream turbines in the Pentland Firth". In: *Proceedings of the Royal Society A: Mathematical, Physical and Engineering Sciences* 469.2157. ISSN: 1364-5021, 1471-2946. DOI: 10.1098/rspa.2013.0072.

Ahmadian, R., Falconer, R. and Bockelmann-Evans, B. (Feb. 2012). "Far-field modelling of the hydro-environmental impact of tidal stream turbines". In: *Renewable Energy* 38.1, pp. 107–116. ISSN: 0960-1481. DOI: 10.1016/j.renene.2011.07.005.

ASME (2009). *Standard for Verification and Validation in Computational Fluid Dynamics and Heat Transfer*. URL: http://gnssn.iaea.org/RTWS/general/Shared%20Documents/Waste%20Management/Apr%202012%20WG%20on%20developing%20DPCSC%20guidance%20document/IP15%20ASMEVV20-2009.pdf (visited on 30/09/2013).

Atwater, J. F. and Lawrence, G. A. (Feb. 2010). "Power potential of a split tidal channel". In: *Renewable Energy* 35.2, pp. 329–332. ISSN: 0960-1481. DOI: 10.1016/j.renene.2009.06.023.

Autodesk (28th Dec. 2015). *Finite Element vs Finite Volume*. Autodesk Knowledge Network. URL: https://knowledge.autodesk.com/support/cfd/learn-explore/caas/CloudHelp/cloudhelp/2014/ENU/SimCFD/files/GUID-12A9AED8-2047-4D3A-BC80-82BE9CF47517-htm.html (visited on 31/03/2018).

Bahaj, A., Molland, A., Chaplin, J. and Batten, W. (Mar. 2007). "Power and thrust measurements of marine current turbines under various hydrodynamic flow conditions in a cavitation tunnel and a towing tank". In: *Renewable Energy* 32.3, pp. 407–426. ISSN: 09601481. DOI: 10.1016/j.renene.2006.01.012.

Bahaj, A. and Myers, L. (Oct. 2004). "Analytical estimates of the energy yield potential from the Alderney Race (Channel Islands) using marine current energy converters". In: *Renewable Energy* 29.12, pp. 1931–1945. ISSN: 0960-1481. DOI: 10.1016/j.renene.2004.02.013.

Bakker, A. (2006a). "Lecture 10 : Turbulence models". Lectures on applied CFD. URL: http://www.bakker.org/dartmouth06/engs150/10-rans.pdf (visited on 16/07/2017).

– (2006b). "Lecture 9 :: Kolmogorov's Theory". Lectures on applied CFD. URL: http://www.bakker.org/dartmouth06/engs150/10-rans.pdf (visited on 16/07/2017).

Baston, S., Harris, R., Woolf, D. K., Hiley, R. A. and Side, J. (Sept. 2013). "Sensitivity Analysis of the Turbulence Closure Models in the Assessment of Tidal Energy Resource in Orkney". In: EWTEC 2013. Aalborg.

Baston, S., Waldman, S. and Side, J. (2015). "Modelling energy extraction in tidal flows, revision 3.1". In: *TeraWatt Position Papers*. MASTS, pp. 75–107. ISBN: 978-0-9934256-1-5. URL: http://www.masts.ac.uk/media/166596/position_papers_terawatt_e-book.pdf (visited on 20/10/2015).

Benjamins, S., DALE, A. C., HASTIE, G., Waggitt, J. J., Lea, M. A., Scott, B. and Wilson, B. (July 2015). "Confusion reigns? A review of marine megafauna interactions with tidal-stream environments". In: *Oceanography and Marine Biology: An Annual Review*. Ed. by R. N. Hughes, D. J. Hughes, I. P. Smith and A. C. Dale. Vol. 53. CRC Press, pp. 1–54. ISBN: 978-1-4987-0546-2.

Black & Veatch (2005). *Phase 2 UK Tidal Stream Energy Resource Assessment*. URL: http://www.carbontrust.co.uk/SiteCollectionDocuments/Various/Emerging%20technologies/Technology%20Directory/Marine/Other%20topics/PhaseIITidalStreamResourceReport.pdf.

Black Rock Tidal Power (n.d.). *Technology*. Accessed 2016-11-10. URL: http://www.blackrocktidalpower.com/technology/.

Blanchfield, J., Garrett, C., Wild, P. and Rowe, A. (May 2008). "The extractable power from a channel linking a bay to the open ocean". en. In: *Proceedings of the Institution of Mechanical Engineers, Part A: Journal of Power and Energy* 222.3, pp. 289–297. ISSN: 0957-6509, 2041-2967. DOI: 10.1243/09576509JPE524.

Blayo, E. and Debreu, L. (2005). "Revisiting open boundary conditions from the point of view of characteristic variables".

In: *Ocean Modelling* 9.3, pp. 231–252. ISSN: 1463-5003.
DOI: 10.1016/j.ocemod.2004.07.001.

Boon, J. D. (2004). *Secrets of the Tide*. Horwood. ISBN: 1-904275-17-6.

Box, G. E. P. (1979). "Robustness in the Strategy of Scientific Model Building".
In: *Robustness in Statistics*. Ed. by R. L. Launer and G. N. Wilkinson. Academic Press, pp. 201–236. ISBN: 978-0-12-438150-6. DOI: 10.1016/B978-0-12-438150-6.50018-2.

Bricker, J. D., Esteban, M., Takagi, H. and Roeber, V. (2016).
"Economic feasibility of tidal stream and wave power in post-Fukushima Japan".
In: *Renewable Energy*. ISSN: 0960-1481. DOI: 10.1016/j.renene.2016.06.049.

Brière, C., Abadie, S., Bretel, P. and Lang, P. (Apr. 2007). "Assessment of TELEMAC system performances, a hydrodynamic case study of Anglet, France".
In: *Coastal Engineering* 54.4, pp. 345–356. ISSN: 03783839.
DOI: 10.1016/j.coastaleng.2006.10.006.

Bryden, I. G. and Couch, S. J. (Feb. 2006).
"ME1—marine energy extraction: tidal resource analysis".
In: *Renewable Energy* 31.2, pp. 133–139. ISSN: 0960-1481.
DOI: 10.1016/j.renene.2005.08.012.

Carter, G. S. and Merrifield, M. A. (2007).
"Open boundary conditions for regional tidal simulations".
In: *Ocean Modelling* 18.3–4, pp. 194–209. ISSN: 1463-5003.
DOI: 10.1016/j.ocemod.2007.04.003.

Chen, C., Liu, H. and Beardsley, R. C. (Jan. 2003).
"An unstructured grid, finite-volume, three-dimensional, primitive equations ocean model: Application to coastal ocean and estuaries".
In: *Journal of Atmospheric and Oceanic Technology* 20.1, pp. 159–186. ISSN: 0739-0572.
DOI: 10.1175/1520-0426(2003)020<0159:AUGFVT>2.0.CO;2.

Cheng, Y. and Andersen, O. B. (2010).
"Improvement of global ocean tide models in shallow water regions". en.
In: *Altimetry for Oceans & Hydrology OST-ST Meeting*. Vol. Poster, SV.1-68 45. Lisbon.
URL: http://www.space.dtu.dk/english/~/media/Institutter/Space/English/scientific_data_and_models/global_ocean_tide_model/yongcuncheng_no_sv_1_68_45.ashx (visited on 18/03/2014).

Clay Mathematics Institute (2000). *Millennium Problems*.
URL: http://www.claymath.org/millennium-problems (visited on 27/07/2017).

Cooke, S., Willden, R., Byrne, B., Stallard, T. and Olczak, A. (Sept. 2015). "Experimental investigation of thrust and power on a partial fence array of tidal turbines".
In: *Proceedings of the 11th European Wave & Tidal Energy Conference (EWTEC)*. EWTEC 2015. Nantes, France.

Couch, S. J. and Bryden, I. (1st Dec. 2006).
"Tidal current energy extraction: Hydrodynamic resource characteristics".
In: *Proceedings of the Institution of Mechanical Engineers, Part M: Journal of*

Engineering for the Maritime Environment 220.4, pp. 185–194. ISSN: 1475-0902, 2041-3084. DOI: 10.1243/14750902JEME50.

Crammond, S., Caljouw, R., Jones, I., Wells, A., Hamill, I. and Petersen, O. (Sept. 2013). "MeyGen Tidal Energy Project: Numerical Modelling of Tidal Turbine Wake Interactions". In: EWTEC 2013. Aalborg.

Culina, J. and Karsten, R. (2011). "Comparison of Different Resolution Models and Observed Current Profiles in the Bay of Fundy, Canada Using Turbine-Relevant Metrics". In: *Proceedings of the 9th European Wave and Tidal Energy Conference*. EWTEC 2011. Southampton. URL: http://www.see.ed.ac.uk/~shs/EWTEC%202011%20full/papers/94.pdf (visited on 04/06/2013).

Cummins, P. F. (Feb. 2013). "The extractable power from a split tidal channel: An equivalent circuit analysis". In: *Renewable Energy* 50, pp. 395–401. ISSN: 0960-1481. DOI: 10.1016/j.renene.2012.07.002.

Cushman-Roisin, B. and Beckers, J.-M. (2011). *Introduction to geophysical fluid dynamics: physical and numerical aspects*. 2nd ed. International geophysics series v. 101. Waltham, MA: Academic Press. 828 pp. ISBN: 978-0-12-088759-0.

Davies, A. M. and Gerritsen, H. (1994). "An intercomparison of three-dimensional tidal hydrodynamic models of the Irish Sea". en. In: *Tellus A* 46.2, 200–221. ISSN: 1600-0870. DOI: 10.1034/j.1600-0870.1994.t01-1-00008.x.

De Dominicis, M., O'Hara Murray, R. and Wolf, J. (2017). "Multi-scale ocean response to a large tidal stream turbine array". In: *Renewable Energy*. ISSN: 0960-1481. DOI: 10.1016/j.renene.2017.07.058.

Dee, D. P. (1995). "A Pragmatic Approach to Model Validation". In: *Quantitative Skill Assessment for Coastal Ocean Models*. Ed. by D. R. Lynch and A. M. Davies. Vol. 47. Coastal and Estuarine Studies. Washington DC: American Geophysical Union, pp. 1–13. ISBN: 0-87590-261-8.

Defne, Z., Haas, K. A. and Fritz, H. M. (Dec. 2011). "Numerical modeling of tidal currents and the effects of power extraction on estuarine hydrodynamics along the Georgia coast, USA". In: *Renewable Energy* 36.12, pp. 3461–3471. ISSN: 0960-1481. DOI: 10.1016/j.renene.2011.05.027.

Deltares (May 2014). *Delft3D-FLOW User Manual, Hydro-Morphodynamics, Version 3.15.34158*. Tech. rep., p. 710. URL: http://content.oss.deltares.nl/delft3d/manuals/Delft3D-FLOW_User_Manual.pdf (visited on 28/05/2014).

DHI (2012a). *MIKE 21 & MIKE 3 Flow Model FM Hydrodynamic & Transport Module Scientific Documentation*.

– (2012b). *MIKE 21 & MIKE 3 Flow Model FM Hydrodynamic & Transport Module Scientific Documentation*.

DHI (2012c). *MIKE 3 Flow Model FM Hydrodynamic Module User Guide*.

Dix, J. K., Lambkin, D. O. and Cazenave, P. W. (2007).
Development of a regional sediment mobility model for submerged archaeological sites.
Tech. rep. English Heritage ALSF project no 5524.
School of Ocean & Earth Science, University of Southampton, p. 156. URL:
http://archaeologydataservice.ac.uk/archiveDS/archiveDownload?t=arch-977-1/dissemination/pdf/Sediment_Mobility_Modelling.pdf (visited on 06/06/2014).

Draper, S., Houlsby, G., Oldfield, M. and Borthwick, A. (2010).
"Modelling tidal energy extraction in a depth-averaged coastal domain".
In: *IET Renewable Power Generation* 4.6, p. 545. ISSN: 17521416.
DOI: 10.1049/iet-rpg.2009.0196.

Draper, S., Stallard, T., Stansby, P., Way, S. and Adcock, T. A. A. (Sept. 2013).
"Laboratory scale experiments and preliminary modelling to investigate basin scale tidal stream energy extraction". In: EWTEC 2013. Aalborg.

Draper, S., Adcock, T. A. A., Borthwick, A. G. L. and Houlsby, G. T. (Jan. 2014a).
"An electrical analogy for the Pentland Firth tidal stream power resource". en.
In: *Proceedings of the Royal Society A: Mathematical, Physical and Engineering Science* 470.2161, p. 20130207. ISSN: 1364-5021, 1471-2946. DOI: 10.1098/rspa.2013.0207.

Draper, S., Adcock, T. A., Borthwick, A. G. and Houlsby, G. T. (2014b).
"Estimate of the tidal stream power resource of the Pentland Firth".
In: *Renewable Energy* 63, pp. 650–657. ISSN: 09601481.
DOI: 10.1016/j.renene.2013.10.015.

Durran, D. R. (2010).
Numerical methods for fluid dynamics: with applications to geophysics. 2nd ed.
Texts in applied mathematics 32. New York: Springer. 516 pp. ISBN: 978-1-4419-6411-3.

Easton, M. C. and Woolf, D. K. (Sept. 2013). "The influence of non-linear turbine dynamics on the environmental stress of tidal stream arrays". In: EWTEC 2013. Aalborg.

Easton, M. C., Woolf, D. K. and Bowyer, P. A. (Oct. 2012).
"The dynamics of an energetic tidal channel, the Pentland Firth, Scotland".
In: *Continental Shelf Research* 48, pp. 50–60. ISSN: 0278-4343.
DOI: 10.1016/j.csr.2012.08.009.

EMEC (2009). *Assessment of Tidal Energy Resource*.
URL: http://www.emec.org.uk/assessment-of-tidal-energy-resource/ (visited on 25/04/2013).

EPSRC (2012). *Details of Grant : TeraWatt*. en.
URL: http://gow.epsrc.ac.uk/NGBOViewGrant.aspx?GrantRef=EP/J010170/1 (visited on 25/05/2017).

– (2014). *Details of Grant : EcoWatt2050*. en.
URL: http://gow.epsrc.ac.uk/NGBOViewGrant.aspx?GrantRef=EP/K012851/1 (visited on 25/05/2017).

ETSU (2003). *Tidal Stream Energy Review*. Tech. rep. ETSU.

European Commission (1996).
JOULE II : The exploitation of tidal marine currents (ref. EUR 16683 EN). Tech. rep. European Commission.
URL: http://bookshop.europa.eu/is-bin/INTERSHOP.enfinity/WFS/EU-Bookshop-Site/en_GB/-/EUR/ViewPublication-Start?PublicationKey=CGNA16683.

Fairley, I., Masters, I. and Karunarathna, H. (Sept. 2015). "Sediment transport in the Pentland Firth and impacts of tidal stream energy extraction".
In: *Proceedings of the 11th European Wave & Tidal Energy Conference (EWTEC)*. EWTEC 2015. Nantes, France.

Flather, R. A. (1976). "A tidal model of the northwest European continental shelf".
In: *Mem. Soc. R. Sci. Liege* 10.6, pp. 141–164. URL: http://www.citeulike.org/group/2200/article/1116673 (visited on 27/05/2014).

Flather, R. (1987). "A tidal model of the northeast pacific".
In: *Atmosphere-Ocean* 25.1, pp. 22–45. ISSN: 0705-5900.
DOI: 10.1080/07055900.1987.9649262.

Gallego, A. *et al.* (2016). "Large scale three-dimensional modelling for wave and tidal energy resource and environmental impact: Methodologies for quantifying acceptable thresholds for sustainable exploitation". In: *Ocean & Coastal Management*.
ISSN: 0964-5691. DOI: 10.1016/j.ocecoaman.2016.11.025. (Visited on 11/12/2016).

Garrett, C. and Cummins, P. (2004). "Generating Power from Tidal Currents".
In: *Journal of Waterway, Port, Coastal, and Ocean Engineering* 130.3, pp. 114–118.
DOI: 10.1061/(ASCE)0733-950X(2004)130:3(114).

– (Aug. 2005). "The power potential of tidal currents in channels".
In: *Proceedings of the Royal Society A: Mathematical, Physical and Engineering Sciences* 461.2060, pp. 2563–2572. DOI: 10.1098/rspa.2005.1494.

– (Sept. 2007). "The efficiency of a turbine in a tidal channel".
In: *Journal of Fluid Mechanics* 588. ISSN: 0022-1120, 1469-7645.
DOI: 10.1017/S0022112007007781.

– (2013). "Maximum power from a turbine farm in shallow water".
In: *Journal of Fluid Mechanics* 714, pp. 634–643. DOI: 10.1017/jfm.2012.515.

Garrett, C. and Greenberg, D. A. (Mar. 1977).
"Predicting Changes in Tidal Regime : The Open Boundary Problem".
In: *Journal of Physical Oceanography*.

Gerritsen, H., de Vries, H. and Philippart, M. (1995).
"The Dutch Continental Shelf Model".
In: *Quantitative Skill Assessment for Coastal Ocean Models*.
Ed. by D. R. Lynch and A. M. Davies. Vol. 47. Coastal and Estuarine Studies.
Washington DC: American Geophysical Union, pp. 425–467. ISBN: 0-87590-261-8.

Gill, A. B. (Aug. 2005). "Offshore renewable energy: ecological implications of generating electricity in the coastal zone: Ecology and offshore renewable energy". en.
In: *Journal of Applied Ecology* 42.4, pp. 605–615. ISSN: 00218901, 13652664.
DOI: 10.1111/j.1365-2664.2005.01060.x.

Gillibrand, P. A., Walters, R. A. and McIlvenny, J. (Oct. 2016).
"Numerical Simulations of the Effects of a Tidal Turbine array on Near-Bed Velocity and Local Bed Shear Stress". en. In: *Energies* 9.10, p. 852. DOI: 10.3390/en9100852.

Godin, G. (Jan. 1983). "On the Predictability of Currents".
In: *The International Hydrographic Review* 60.1. ISSN: 0020-6946.
URL: https://journals.lib.unb.ca/index.php/ihr/article/view/23537 (visited on 28/01/2016).

Green, M. O. and McCave, I. N. (1995).
"Seabed drag coefficient under tidal currents in the eastern Irish Sea".
In: *Journal of Geophysical Research* 100.C8, p. 16057. ISSN: 0148-0227.
DOI: 10.1029/95JC01381.

Gunn, K. and Stock-Williams, C. (Sept. 2013).
"On Validating Numerical Hydrodynamic Models of Complex Tidal Flow". In: Aalborg.

Hackett, B., Røed, L. P., Gjevik, B., Eide, L. I. and Martinsen, E. A. (1995). "A Review of the Metocean Modelling Project (MOMOP) Part 2: Model Validation Study".
In: *Quantitative Skill Assessment for Coastal Ocean Models*.
Ed. by D. R. Lynch and A. M. Davies. Vol. 47. Coastal and Estuarine Studies.
Washington DC: American Geophysical Union, pp. 307–327. ISBN: 0-87590-261-8.

Hasegawa, D., Sheng, J., Greenberg, D. A. and Thompson, K. R. (Nov. 2011).
"Far-field effects of tidal energy extraction in the Minas Passage on tidal circulation in the Bay of Fundy and Gulf of Maine using a nested-grid coastal circulation model". en.
In: *Ocean Dynamics* 61.11, pp. 1845–1868. ISSN: 1616-7341, 1616-7228.
DOI: 10.1007/s10236-011-0481-9.

Haverson, D., Bacon, J., Smith, H., Venugopal, V. and Xiao, Q. (Sept. 2015).
"Cumulative impact assessment of tidal energy in the Irish Sea".
In: *Proceedings of the 11th European Wave & Tidal Energy Conference (EWTEC)*.
Nantes, France.

Hennequin, G. (2016). *Hydro, Tidal and Wave Energy in Japan*. Tech. rep.
EU-Japan Centre for Industrial Cooperation. URL:
http://cdnsite.eu-japan.eu/sites/default/files/publications/docs/2016-10-hydro_and_marine_energy_japan_guillaume_hennequin_min.pdf (visited on 02/11/2016).

Hodges, J. S. and Dewar, J. A. (1992).
Is it You Or Your Model Talking?: A Framework for Model Validation.
Santa Monica, CA: Rand.
URL: http://www.rand.org/content/dam/rand/pubs/reports/2006/R4114.pdf.

Horlock, J. H. (1978). *Actuator disk theory: discontinuities in thermo-fluid dynamics*.
London; New York: McGraw-Hill. ISBN: 0-07-030360-6.

Houlsby, G. T., Draper, S. and Oldfield, M. L. G. (2008).
Application of linear momentum actuator disc theory to open channel flow.
Tech. rep. OUEL 2296/08. Oxford: University of Oxford. URL:
http://www.eng.ox.ac.uk/civil/publications/reports-1/ouel_2296_08.pdf (visited on 07/11/2013).

Houlsby, G. T. and Vogel, C. R. (May 2016).
"The power available to tidal turbines in an open channel flow".
In: *Proceedings of the Institution of Civil Engineers - Energy*, pp. 1–10. ISSN: 1751-4223. DOI: 10.1680/jener.15.00035.

IEA (2016). *CO2 emissions from fuel combustion highlight statistics (2016 edition).*
Tech. rep. International Energy Agency.
URL: https://www.iea.org/publications/freepublications/publication/co2-emissions-from-fuel-combustion-highlights-2016.html.

IEC (May 2013). *Marine energy - Wave, tidal and other water current converters - Part 200: Electricity producing tidal energy converters - Power performance assessment.*
Technical Specification IEC/TS 62600-200 Ed 1.0.
International Electrotechnical Commission.
URL: https://bsol.bsigroup.com/Download/SubscriptionPdfDocument?materialNumber=00000000030207230&documentNumber=PD%20IEC%2FTS%2062600-200%3A2013 (visited on 21/09/2015).

IEC Technical Committee PEL/114 (2015). *Marine energy — Wave, tidal and other water current converters; Part 201: Tidal energy resource assessment and characterization.*
Technical Specification TS 62600-201:2015. ISBN 978-2-8322-2591-2.
International Electrotechnical Commission.
URL: https://bsol.bsigroup.com/Bibliographic/BibliographicInfoData/000000000030267208 (visited on 27/08/2015).

IPCC (2014).
Climate change 2014: synthesis report. Contribution of Working Groups I, II and III to the Fifth Assessment Report of the Intergovernmental Panel on Climate Change.
Ed. by R. K. Pachauri and L. Mayer. OCLC: 914851124. Geneva, Switzerland: IPCC. 151 pp. ISBN: 978-92-9169-143-2. URL: https://www.ipcc.ch/report/ar5/syr/.

Iwata, M. (Apr. 2015).
"Nagasaki Plans Asia's First Major Testing Site for Marine Energy". English.
In: *Wall Street Journal*. Accessed 2016-11-07.
URL: http://blogs.wsj.com/japanrealtime/2015/04/01/nagasaki-plans-asias-first-major-testing-site-for-marine-energy/.

Japanese Ministry of Economy, Trade and Industry (July 2015).
Long-term energy supply and demand outlook.
URL: http://www.meti.go.jp/english/press/2015/pdf/0716_01a.pdf (visited on 05/12/2017).

Jeffcoate, P., Starzmann, R., Elsaesser, B., Scholl, S. and Bischoff, S. (2015).
"Field measurements of a full scale tidal turbine".
In: *International Journal of Marine Energy*. ISSN: 2214-1669.
DOI: 10.1016/j.ijome.2015.04.002.

Von Karman, T. (Mar. 1931). *Mechanical Similitude and Turbulence.*
Technical Memorandum NACA-TM 611.
Washington DC: National Advisory Committee for Aeronautics. URL:

http://ntrs.nasa.gov/archive/nasa/casi.ntrs.nasa.gov/19930094805.pdf (visited on 24/11/2015).

Karsten, R. H., McMillan, J. M., Lickley, M. J. and Haynes, R. D. (Aug. 2008). "Assessment of tidal current energy in the Minas Passage, Bay of Fundy". en. In: *Proceedings of the Institution of Mechanical Engineers, Part A: Journal of Power and Energy* 222.5, pp. 493–507. ISSN: 0957-6509, 2041-2967. DOI: 10.1243/09576509JPE555.

Kawase, M. and Gedney, M. (Sept. 2013). "Tidal Energy Extraction in an Idealized Ocean-Fjord Tidal Model with Astronomical Forcing". In: *Proceedings of the 10th European Wave & Tidal Energy Conference (EWTEC)*. EWTEC 2013. Aalborg.

Kinoshita, T. (Sept. 2012). *The Potential of Marine Energy*. English. URL: http://www.nippon.com/en/in-depth/a01203/ (visited on 06/08/2017).

Kramer, S. C., Funke, S. W. and Piggott, M. D. (Sept. 2015). "A continuous approach for the optimisation of tidal turbine farms". In: *Proceedings of the 11th European Wave & Tidal Energy Conference (EWTEC)*. EWTEC 2015. Nantes, France.

Kramer, S. C. and Piggott, M. D. (July 2016). "A correction to the enhanced bottom drag parameterisation of tidal turbines". In: *Renewable Energy* 92, pp. 385–396. ISSN: 09601481. DOI: 10.1016/j.renene.2016.02.022.

Kramer, S., Piggott, M., Hill, J., Kregting, L., Pritchard, D. and Elsaesser, B. (2014). "The modelling of tidal turbine farms using multi-scale, unstructured mesh models". In: *Proceedings of the 2nd International Conference on Environmental Interactions of Marine Renewable Energy Technologies*. Stornoway.

Kurniawan, A., Ooi, S., Gerritsen, H. and Twigt, D. (2010). "Tidal Calibration of the Singapore Regional Model Using OpenDA". In: Tianjin, China. URL: https://publicwiki.deltares.nl/download/attachments/8684038/FEWS_UserMeeting4Nov2010_CalibrationDelft3DApplicationsUsingOpenDA.pdf?version=1&modificationDate=1289300800000 (visited on 07/05/2013).

Kutney, T., Karsten, R. and Polagye, B. (Sept. 2013). "Priorities for Reducing Tidal Energy Resource Uncertainty". In: EWTEC 2013. Aalborg.

Launder, B. E. and Spalding, D. B. (Mar. 1974). "The numerical computation of turbulent flows". In: *Computer Methods in Applied Mechanics and Engineering* 3.2, pp. 269–289. ISSN: 0045-7825. DOI: 10.1016/0045-7825(74)90029-2.

Ledoux, H. and Gold, C. (1st Jan. 2005). "An Efficient Natural Neighbour Interpolation Algorithm for Geoscientific Modelling". In: *Developments in Spatial Data Handling*. Springer Berlin Heidelberg, pp. 97–108. ISBN: 978-3-540-22610-9 978-3-540-26772-0. URL: http://link.springer.com/chapter/10.1007/3-540-26772-7_8.

Lesieur, M. and Metais, O. (1996).
"New Trends in Large-Eddy Simulations of Turbulence".
In: *Annual Review of Fluid Mechanics* 28.1, pp. 45–82.
DOI: 10.1146/annurev.fl.28.010196.000401.

Li, X., Li, M., McLelland, S. J., Jordan, L.-B., Simmons, S. M., Amoudry, L. O., Ramirez-Mendoza, R. and Thorne, P. D. (2017). "Modelling tidal stream turbines in a three-dimensional wave-current fully coupled oceanographic model".
In: *Renewable Energy*. ISSN: 0960-1481. DOI: 10.1016/j.renene.2017.02.033.

Manwell, J. F. (2009). *Wind energy explained: theory, design and application*.
In collab. with J. G. McGowan and A. L. Rogers. 2nd ed. Chichester, U.K: Wiley.
689 pp. ISBN: 978-0-470-01500-1.

Martin-Short, R., Hill, J., Kramer, S., Avdis, A., Allison, P. and Piggott, M. (Apr. 2015).
"Tidal resource extraction in the Pentland Firth, UK: Potential impacts on flow regime and sediment transport in the Inner Sound of Stroma".
In: *Renewable Energy* 76, pp. 596–607. ISSN: 09601481.
DOI: 10.1016/j.renene.2014.11.079.

MASTS (2015). *TeraWatt Position Papers*. MASTS. ISBN: 978-0-9934256-1-5. URL: http://www.masts.ac.uk/about/masts-publications/terawatt-publications/ (visited on 25/05/2017).

Matsumoto, K., Takanezawa, T. and Ooe, M. (Oct. 2000).
"Ocean tide models developed by assimilating TOPEX/POSEIDON altimeter data into hydrodynamical model: A global model and a regional model around Japan". en.
In: *Journal of Oceanography* 56.5, pp. 567–581. ISSN: 0916-8370, 1573-868X.
DOI: 10.1023/A:1011157212596.

McMillan, J. M., Hay, A. E., Karsten, R. and Trowse, G. (Sept. 2013).
"Comprehensive Tidal Energy Resource Assessment in the lower Bay of Fundy, Canada".
In: EWTEC 2013. Aalborg.

Mellor, G. L. and Yamada, T. (1st Nov. 1982).
"Development of a turbulence closure model for geophysical fluid problems".
In: *Reviews of Geophysics* 20.4, pp. 851–875. ISSN: 1944-9208.
DOI: 10.1029/RG020i004p00851.

Moin, P. and Mahesh, K. (1998).
"Direct numerical simulation: A Tool in Turbulence Research".
In: *Annual Review of Fluid Mechanics* 30.1, pp. 539–578.
DOI: 10.1146/annurev.fluid.30.1.539.

Munk, W. and Wunsch, C. (1998).
"Abyssal recipes II: energetics of tidal and wind mixing".
In: *Deep-Sea Research Part I* 45.12, pp. 1977–2010.
DOI: 10.1016/S0967-0637(98)00070-3.

Murphy, A. H. (Dec. 1992). "Climatology, Persistence, and Their Linear Combination as Standards of Reference in Skill Scores". In: *Weather and Forecasting* 7.4, pp. 692–698.
ISSN: 0882-8156, 1520-0434.
DOI: 10.1175/1520-0434(1992)007<0692:CPATLC>2.0.CO;2.

Myers, L. and Bahaj, A. (Jan. 2012). "An experimental investigation simulating flow effects in first generation marine current energy converter arrays". In: *Renewable Energy* 37.1, pp. 28–36. ISSN: 0960-1481. DOI: 10.1016/j.renene.2011.03.043.

Nash, J. D. and Moum, J. N. (2001). "Internal hydraulic flows on the continental shelf: High drag states over a small bank". In: *Journal of Geophysical Research: Oceans (1978–2012)* 106 (C3), pp. 4593–4611. URL: http://onlinelibrary.wiley.com/doi/10.1029/1999JC000183/full (visited on 05/07/2013).

NEDO (Feb. 2014). "Chapter 6 : Ocean Energy". Japanese. In: *Renewable Energy Technology white paper, 2nd edition*. 2nd. URL: http://www.nedo.go.jp/content/100544821.pdf (visited on 06/08/2017).

Neill, S. P., Litt, E. J., Couch, S. J. and Davies, A. G. (Dec. 2009). "The impact of tidal stream turbines on large-scale sediment dynamics". In: *Renewable Energy* 34.12, pp. 2803–2812. ISSN: 0960-1481. DOI: 10.1016/j.renene.2009.06.015.

Nishino, T. and Willden, R. H. J. (Oct. 2012a). "Effects of 3-D channel blockage and turbulent wake mixing on the limit of power extraction by tidal turbines". In: *International Journal of Heat and Fluid Flow* 37, pp. 123–135. ISSN: 0142-727X. DOI: 10.1016/j.ijheatfluidflow.2012.05.002.

– (Oct. 2012b). "The efficiency of an array of tidal turbines partially blocking a wide channel". In: *Journal of Fluid Mechanics* 708, pp. 596–606. ISSN: 1469-7645. DOI: 10.1017/jfm.2012.349.

NOAA (Oct. 2003). *NOS Standards for evaluating operational nowcast and forecast hydrodynamic model systems*. NOAA Technical Report NOS CS 17. URL: http://www.nauticalcharts.noaa.gov/csdl/docs/RD_standards_Hess_etal.pdf (visited on 30/09/2013).

O'Hara Murray, R. B. (2015). "Tidal stream and wave energy array scenarios for the Pentland Firth and Orkney Waters strategic area, Rev. 2.2". In: *TeraWatt Position Papers*. MASTS, pp. 31–47. ISBN: 978-0-9934256-1-5. URL: http://www.masts.ac.uk/media/35656/position_papers_terawatt_e-book.pdf (visited on 20/10/2015).

O'Hara Murray, R. B. and Gallego, A. (2017). "Data review and the development of realistic tidal and wave energy scenarios for numerical modelling of Orkney Islands waters, Scotland". In: *Ocean & Coastal Management*. ISSN: 0964-5691. DOI: 10.1016/j.ocecoaman.2017.03.011.

O'Hara Murray, R. and Gallego, A. (2016). "A modelling study of the tidal stream resource of the Pentland Firth, Scotland". In: *Renewable Energy*. ISSN: 0960-1481. DOI: 10.1016/j.renene.2016.10.053.

Oke, P. R. *et al.* (2002). "A modeling study of the three-dimensional continental shelf circulation off Oregon. Part I: Model-data comparisons".

In: *Journal of Physical Oceanography* 32.5, pp. 1360–1382.
URL: http://journals.ametsoc.org/doi/abs/10.1175/1520-0485(2002)032%3C1360%3AAMSOTT%3E2.0.CO%3B2 (visited on 30/09/2013).

OpenHydro (July 2016). *OpenHydro secures Japanese tidal turbine contract (press release)*. Accessed 2016-11-17.
URL: http://www.openhydro.com/OpenHydro/media/Documents/News%20PDFs/26-July-2016.pdf.

Owen, A. and Bryden, I. (2007). "Energy extraction implications of structurally significant velocity variation in tidal currents". In: *OCEANS 2007 - Europe*.
OCEANS 2007 - Europe, pp. 1–5. DOI: 10.1109/OCEANSE.2007.4302409.

Pawlowicz, R., Beardsley, B. and Lentz, S. (Oct. 2002).
"Classical tidal harmonic analysis including error estimates in MATLAB using T_TIDE".
In: *Computers & Geosciences* 28.8, pp. 929–937. ISSN: 0098-3004.
DOI: 10.1016/S0098-3004(02)00013-4.

Pérez-Ortiz, A., Borthwick, A. G., McNaughton, J., Smith, H. C. and Xiao, Q. (Apr. 2017).
"Resource characterization of sites in the vicinity of an island near a landmass".
In: *Renewable Energy* 103, pp. 265–276. ISSN: 09601481.
DOI: 10.1016/j.renene.2016.10.086.

Plew, D. R. and Stevens, C. L. (Sept. 2013). "Numerical modelling of the effect of turbines on currents in a tidal channel – Tory Channel, New Zealand".
In: *Renewable Energy* 57, pp. 269–282. ISSN: 0960-1481.
DOI: 10.1016/j.renene.2013.02.001.

Pointwise (June 2012). *Accuracy, Convergence and Mesh Quality*.
URL: http://www.pointwise.com/ (visited on 03/07/2017).

Polagye, B., Malte, P., Kawase, M. and Durran, D. (1st Aug. 2008).
"Effect of large-scale kinetic power extraction on time-dependent estuaries".
In: *Proceedings of the Institution of Mechanical Engineers, Part A: Journal of Power and Energy* 222.5, pp. 471–484. ISSN: 0957-6509, 2041-2967.
DOI: 10.1243/09576509JPE519.

Polagye, B. and Thomson, J. (1st May 2013). "Tidal energy resource characterization: methodology and field study in Admiralty Inlet, Puget Sound, WA (USA)".
In: *Proceedings of the Institution of Mechanical Engineers, Part A: Journal of Power and Energy* 227.3, pp. 352–367. ISSN: 0957-6509, 2041-2967.
DOI: 10.1177/0957650912470081.

Polagye, B., Epler, J. and Thomson, J. (Sept. 2010).
"Limits to the predictability of tidal current energy". In: *OCEANS 2010*. OCEANS 2010, pp. 1–9. DOI: 10.1109/OCEANS.2010.5664588.

Post, D. E. and Votta, L. G. (2005). "Computational science demands a new paradigm".
In: *Physics today* 58.1, 35–41. URL: http://www.climateknowledge.org/figures/Rood_Climate_Change_AOSS480_Documents/Model_validation/Post_Computational_Science_Demands_PhysToday_2005.pdf (visited on 25/04/2013).

Ramos, V., Carballo, R., Álvarez, M., Sánchez, M. and Iglesias, G. (Sept. 2013). "Assessment of the impacts of tidal stream energy through high-resolution numerical modeling". In: *Energy*. ISSN: 0360-5442. DOI: 10.1016/j.energy.2013.08.051.

Ramos, V., Carballo, R., Sanchez, M., Veigas, M. and Iglesias, G. (Apr. 2014). "Tidal stream energy impacts on estuarine circulation". In: *Energy Conversion and Management* 80, pp. 137–149. ISSN: 0196-8904. DOI: 10.1016/j.enconman.2014.01.027.

Roc, T., Conley, D. C. and Greaves, D. (Mar. 2013). "Methodology for tidal turbine representation in ocean circulation model". In: *Renewable Energy* 51, pp. 448–464. ISSN: 09601481. DOI: 10.1016/j.renene.2012.09.039. (Visited on 02/07/2013).

Roc, T., Greaves, D., Conley, D. C. and Leybourne, M. (Sept. 2013). "Optimising commercial-scale TEC arrays: genetic algorithm, Fractal & Eco-mimicry". In: EWTEC 2013. Aalborg.

Roc, T., Greaves, D., Thyng, K. M. and Conley, D. C. (Jan. 2014). "Tidal turbine representation in an ocean circulation model: Towards realistic applications". In: *Ocean Engineering*. ISSN: 00298018. DOI: 10.1016/j.oceaneng.2013.11.010.

Scotrenewables (Nov. 2012). *Award of 'Agreement for Lease' for Lashy Sound Demonstrator Project and SR250 Reaches and Exceeds Rated Power*. URL: http://www.scotrenewables.com/news/57-award-of-agreement-for-lease-for-lashy-sound-demonstrator-project-and-sr250-reaches-and-exceeds-rated-power-november-2012 (visited on 24/04/2017).

SeaZone Solutions Ltd., obtained via EDINA Marine Digimap Service (2008). *Hydrospatial bathymetry, 6" resolution, Tiles: NW25800020/40/60*. URL: http://edina.ac.uk/digimap.

Sentchev, A. and Thiébaut, M. (Sept. 2015). "Mapping tidal energy resources by high frequency radar: Application to resource characterization around the Ushant Island (W. Brittany coast)". In: *Proceedings of the 11th European Wave & Tidal Energy Conference (EWTEC)*. EWTEC 2015. Nantes, France.

Shields, M. A. *et al.* (Jan. 2011). "Marine renewable energy: The ecological implications of altering the hydrodynamics of the marine environment". In: *Ocean & Coastal Management* 54.1, pp. 2–9. ISSN: 0964-5691. DOI: 10.1016/j.ocecoaman.2010.10.036.

Shives, M. and Crawford, C. (Sept. 2015). "Validation of a practical CFD method for predicting hydrokinetic turbine performance in wake shadow". In: *Proceedings of the 11th European Wave & Tidal Energy Conference (EWTEC)*. EWTEC 2015. Nantes, France.

Shives, M., Crawford, C., Hiles, C. and Walters, R. (Sept. 2013). "Combining Numerical Methods for Basin and Turbine Scales for Improved Modelling of in-situ Turbine Arrays". In: *Proceedings of the 10th European Wave and Tidal Energy Conference*. EWTEC 2013. Aalborg.

Smagorinsky, J. (1st Mar. 1963).
"General circulation experiments with the primitive equations".
In: *Monthly Weather Review* 91.3, pp. 99–164. ISSN: 0027-0644.
DOI: 10.1175/1520-0493(1963)091<0099:GCEWTP>2.3.CO;2.

Soulsby, R. and Clarke, S. (Aug. 2005).
Bed shear-stresses under combined waves and currents on smooth and rough beds.
Tech. rep. TR137 rev 1.0. HR Wallingford.

Soulsby, R. (1st Jan. 1997).
Dynamics of Marine Sands: A Manual for Practical Applications. Thomas Telford.
280 pp. ISBN: 978-0-7277-2584-4.

Stallard, T., Collings, R., Feng, T. and Whelan, J. (Feb. 2013). "Interactions between tidal turbine wakes: experimental study of a group of three-bladed rotors". en.
In: *Phil. Trans. R. Soc. A* 371.1985, p. 20120159. ISSN: 1364-503X, 1471-2962.
DOI: 10.1098/rsta.2012.0159.

Statistics Japan (2016).
Japan Statistical Yearbook 2015, Table 11-14 "Electrical power generated".
Accessed 2016-11-07.
URL: http://www.stat.go.jp/english/data/nenkan/65nenkan/1431-11.htm.

Stewart, R. H. (2008). *Introduction To Physical Oceanography.* Texas A&M University.

Sun, H., Kyozuka, Y. and Yamashiro, T. (July 2014).
"Tidal current power potential in Goto islands by observations and simulations".
In: *2nd Asian Wave & Tidal Energy Conference (AWTEC).* Tokyo.

Sutherland, D. R., Sellar, B. G., Harding, S. and Bryden, I. (2013). "Initial Flow Characterisation Utilising Turbine and Seabed Installed Acoustic Sensor Arrays". In: EWTEC 2013. Aalborg.

Sutherland, G., Foreman, M. and Garrett, C. (Mar. 2007).
"Tidal current energy assessment for Johnstone Strait, Vancouver Island". en.
In: *Proceedings of the Institution of Mechanical Engineers, Part A: Journal of Power and Energy* 221.2, pp. 147–157. ISSN: 0957-6509, 2041-2967.
DOI: 10.1243/09576509JPE338.

Sutherland, J., Peet, A. and Soulsby, R. (Oct. 2004).
"Evaluating the performance of morphological models".
In: *Coastal Engineering* 51.8–9, pp. 917–939. ISSN: 0378-3839.
DOI: 10.1016/j.coastaleng.2004.07.015.

Sutherland, J., Walstra, D., Chesher, T., van Rijn, L. and Southgate, H. (Apr. 2004).
"Evaluation of coastal area modelling systems at an estuary mouth".
In: *Coastal Engineering* 51.2, pp. 119–142. ISSN: 0378-3839.
DOI: 10.1016/j.coastaleng.2003.12.003.

Taylor, K. E. (2001).
"Summarizing multiple aspects of model performance in a single diagram".
In: *Journal of Geophysical Research: Atmospheres* 106 (D7), pp. 7183–7192.
ISSN: 2156-2202. DOI: 10.1029/2000JD900719.

Teledyne RD Instruments (Jan. 2011).
Acoustic Doppler Current Profiler - Principles of Operation - A Practical Primer.
Tech. rep. P/N 951-6069-00.
URL: http://www.rdinstruments.com/mm_papers.aspx (visited on 29/08/2013).

University College London (26th May 2012). *Vertical Offshore Reference Frames (VORF)*.
URL: https://www.ucl.ac.uk/vorf (visited on 11/09/2017).

US Energy Information Administration (2015).
Japan : International energy data and analysis. Accessed 2016-11-07.
URL: https://www.eia.gov/beta/international/analysis_includes/countries_long/Japan/japan.Pdf.

Vennell, R. (Oct. 2010). "Tuning turbines in a tidal channel".
In: *Journal of Fluid Mechanics* 663, pp. 253–267. DOI: 10.1017/S0022112010003502.

– (Mar. 2011). "Tuning tidal turbines in-concert to maximise farm efficiency".
In: *Journal of Fluid Mechanics* 671, pp. 587–604. DOI: 10.1017/S0022112010006191.

– (Dec. 2012). "The energetics of large tidal turbine arrays". en.
In: *Renewable Energy* 48, pp. 210–219. ISSN: 09601481.
DOI: 10.1016/j.renene.2012.04.018.

– (July 2013). "Exceeding the Betz limit with tidal turbines".
In: *Renewable Energy* 55, pp. 277–285. ISSN: 0960-1481.
DOI: 10.1016/j.renene.2012.12.016.

Vennell, R., Funke, S. W., Draper, S., Stevens, C. and Divett, T. (Jan. 2015).
"Designing large arrays of tidal turbines: A synthesis and review". en.
In: *Renewable and Sustainable Energy Reviews* 41, pp. 454–472. ISSN: 13640321.
DOI: 10.1016/j.rser.2014.08.022.

Venugopal, V. and Nemalidinne, R. (8th June 2014).
"Marine Energy Resource Assessment for Orkney and Pentland Waters With a Coupled Wave and Tidal Flow Model".
In: *International Conference on Ocean, Offshore & Arctic Engineering (OMAE) 2014*.
OMAE 2014. DOI: 10.1115/OMAE2014-24027.
URL: http://dx.doi.org/10.1115/OMAE2014-24027 (visited on 03/06/2015).

Vested, H. J., Nielsen, J. W., Jensen, H. R. and Kristensen, K. B. (1995).
"Skill Assessment of an Operational Hydrodynamic Forecast System for the North Sea and Danish Belts". In: *Quantitative Skill Assessment for Coastal Ocean Models*.
Ed. by D. R. Lynch and A. M. Davies. Vol. 47. Coastal and Estuarine Studies.
Washington DC: American Geophysical Union, pp. 373–396. ISBN: 0-87590-261-8.

Vogel, C., Houlsby, G. and Willden, R. (Apr. 2016). "Effect of free surface deformation on the extractable power of a finite width turbine array". en.
In: *Renewable Energy* 88, pp. 317–324. ISSN: 09601481.
DOI: 10.1016/j.renene.2015.11.050.

Vogel, C., Willden, R. H. and Houlsby, G. T. (Sept. 2013).
"A Correction for Depth-Averaged Simulations of Tidal Turbine Arrays". In:
EWTEC 2013. Aalborg.

Waldman, S., Bastón, S., Nemalidinne, R., Chatzirodou, A., Venugopal, V. and Side, J. (2017). "Implementation of tidal turbines in MIKE 3 and Delft3D models of Pentland Firth & Orkney Waters". In: *Ocean & Coastal Management*. ISSN: 0964-5691. DOI: 10.1016/j.ocecoaman.2017.04.015.

Waldman, S., Yamaguchi, S., O'Hara Murray, R. and Woolf, D. (1st Sept. 2017). "Tidal resource and interactions between multiple channels in the Goto Islands, Japan". In: *International Journal of Marine Energy* 19 (Supplement C), pp. 332–344. ISSN: 2214-1669. DOI: 10.1016/j.ijome.2017.09.002.

Waldman, S., Genet, G., Baston, S. and Side, J. (Sept. 2015). "Correcting for mesh size dependency in a regional model's representation of tidal turbines". In: *Proceedings of the 11th European Wave & Tidal Energy Conference (EWTEC 2015)*. EWTEC 2015. Nantes, France.

Waldman, S., Miller, C., Baston, S. and Side, J. (May 2014). "Comparison of two hydrodynamic models for investigating energy extraction from tidal flows". In: *Poster presented at the 2nd conference on Environmental Interactions of Marine Energy*. EIMR 2014. Stornoway. URL: https://www.simonwaldman.me.uk/static/publications/2014/EIMR_Waldman_et_al_2014.pdf.

Waldman, S., Side, J. and Woolf, D. (Aug. 2017). "Numerical investigation of tidal resource & far field effects of energy extraction in Lashy Sound, Orkney". In: *Proceedings of the 12th European Wave & Tidal Energy Conference (EWTEC 2017)*. 12th European Wave & Tidal Energy Conference (EWTEC 2017). Cork, Ireland.

Walkington, I. A. (2014). "Changing the Tides". In: *Proceedings of the 2nd International Conference on Environmental Interations of Marine Renewable Energy Technologies*. EIMR 2014. Stornoway.

Wan, D., Klymak, J. M., Foreman, M. G. G. and Cross, S. F. (2015). "Barotropic tidal dynamics in a frictional subsidiary channel". In: *Continental Shelf Research*. ISSN: 0278-4343. DOI: 10.1016/j.csr.2015.05.011.

Warner, J. C., Geyer, W. R. and Lerczak, J. A. (2005). "Numerical modeling of an estuary: A comprehensive skill assessment". en. In: *Journal of Geophysical Research: Oceans* 110.C5, n/a–n/a. ISSN: 2156-2202. DOI: 10.1029/2004JC002691.

Warner, S. J., MacCready, P., Moum, J. N. and Nash, J. D. (June 2013). "Measurement of Tidal Form Drag Using Seafloor Pressure Sensors". In: *Journal of Physical Oceanography* 43.6, pp. 1150–1172. ISSN: 0022-3670, 1520-0485. DOI: 10.1175/JPO-D-12-0163.1.

Wessel, P. and Smith, W. H. F. (10th Apr. 1996). "A global, self-consistent, hierarchical, high-resolution shoreline database". In: *Journal of Geophysical Research: Solid Earth* 101 (B4), pp. 8741–8743. ISSN: 2156-2202. DOI: 10.1029/96JB00104.

Whelan, J., Graham, J. and Peiró, J. (2009). "A free-surface and blockage correction for tidal turbines". English. In: *Journal of Fluid Mechanics* 624. 281, pp. 281–291. ISSN: 00221120. DOI: 10.1017/S0022112009005916.

Wikipedia (2013). *Natural Neighbor interpolation*. In: *Wikipedia*. URL: https://en.wikipedia.org/w/index.php?title=Natural_neighbor&oldid=544783582 (visited on 29/03/2013).

Wilcock, P. R. (Nov. 1996). "Estimating local bed shear stress from velocity observations". en. In: *Water Resources Research* 32.11, pp. 3361–3366. ISSN: 1944-7973. DOI: 10.1029/96WR02277.

Willmott, C. J. (1981). "On the validation of models". In: *Physical geography* 2.2, 184–194. URL: http://www.tandfonline.com/doi/abs/10.1080/02723646.1981.10642213 (visited on 07/09/2013).

Wolf, J., Yates, N., Brereton, A., Buckland, H., De Dominicis, M., Gallego, A. and O'Hara Murray, R. (2016). "The Scottish Shelf Model. Part 1: Shelf-Wide Domain". In: *Scottish Marine and Freshwater Science* 7.3. DOI: 10.7489/1692-1.

Woolf, D. (Sept. 2013). "The Strength and Phase of the Tidal Stream". In: EWTEC 2013. Aalborg.

Yang, Z. and Wang, T. (2013). "Modeling the Effects of Tidal Energy Extraction on Estuarine Hydrodynamics in a Stratified Estuary". In: *Estuaries and Coasts*, pp. 1–16. ISSN: 1559-2723, 1559-2731. DOI: 10.1007/s12237-013-9684-2.

Yang, Z., Wang, T. and Copping, A. E. (Feb. 2013). "Modeling tidal stream energy extraction and its effects on transport processes in a tidal channel and bay system using a three-dimensional coastal ocean model". In: *Renewable Energy* 50, pp. 605–613. ISSN: 0960-1481. DOI: 10.1016/j.renene.2012.07.024.

Yang, Z., Wang, T., Copping, A. and Geerlofs, S. (Sept. 2013). "Modeling In-stream Tidal Energy Extraction and Its Potential Environmental Impacts". In: *Proceedings of the 10th European Wave & Tidal Energy Conference (EWTEC)*. EWTEC 2013. Aalborg.

Ziebart, M. and Iliffe, J. (27th Oct. 2009). "VORF: Concept and Current Status". Hydrography and Marine Spatial Infrastructure. Bradfield College. URL: http://www.ths.org.uk/documents/ths.org.uk/downloads/3_-_marek_ziebart_-_ucla_-_vorf_concept_&_status.pdf (visited on 11/09/2017).